Design of an Economically Optimum PWR Reload Core for a 36-Month Cycle

by

Luis García-Delgado
Ingeniero Industrial, Universidad Politécnica de Madrid (1996)
Ingénieur, Ecole Centrale Paris (1996)

Submitted to the Department of Nuclear Engineering in partial fulfillment of the requirements for the degrees of Nuclear Engineer and Master of Science in Nuclear Engineering

at the

MASSACHUSETTS INSTITUTE OF TECHNOLOGY

May 7th, 1998
[June 1998]

Author .....
Department of Nuclear Engineering
May 7th, 1998

Certified by .....
N.E. Todreas, Professor of Nuclear Engineering
Thesis Co-Supervisor

Certified by .....
M.J. Driscoll, Professor Emeritus of Nuclear Engineering
Thesis Co-Supervisor

Certified by .....
J.E. Meyer, Professor of Nuclear Engineering
Thesis Co-Supervisor

Accepted by .....
L. Lidsky, Professor of Nuclear Engineering
Chairman, Dept. Committee on Graduate Students

Design of an Economically Optimum PWR Reload Core for a 36-Month Cycle

by

Luis García-Delgado

Submitted to the Department of Nuclear Engineering on May 7, 1998, in partial fulfillment of the requirements for the degrees of Nuclear Engineer and Master of Science in Nuclear Engineering

Abstract

The goal of making nuclear plants more economically competitive with other sources of electricity has motivated research on extended operating cycles. By increasing cycle length in currently operating PWRs, the outage frequency is reduced, and the capacity factor is improved, providing an economic benefit. On the other hand, fuel with higher enrichment is required, and the fuel fabrication costs go up. A single-batch strategy is required if the current burnup licensing limit (60 GWD/MTU) is to be maintained. Previous work has shown the technical feasibility of single-batch cycles up to 44 calendar months in PWRs. Parametric studies indicated that the economically optimum length for a PWR, single-batch core is about 36 calendar months.

The goal of this thesis is to design a PWR reload core for a 36-month cycle ready for implementation in current reactors and capable of appealing to utility managers. The core design includes physics, fuel performance and economics analysis. For the neutronics study, the core is modeled in 3 dimensions and in the steady-state using the codes CASMO-3/SIMULATE-3. Several steps are considered in the design process. First, the fuel enrichment required for the cycle and the most suitable burnable absorber are selected. Then, an optimum design is obtained for the peripheral assemblies that minimizes fuel costs. Finally, axial blankets that reduce neutron leakage are analyzed, as well as the benefits of axially grading the poison loading. The fuel performance --key to the technical feasibility of the core-- is analyzed with the code FROSSTEY-2, and simple models are developed for cladding corrosion and fission gas release. Core costs are calculated and the influence of operational and economics parameters is studied.

A PWR reload core is presented that meets current physics and fuel performance design limits for a cycle of 33.9 EFPM or 36 calendar months when operating at a capacity factor of 94.1%. Fuel is enriched to 6.5% U-235 and selected pins use gadolinia as burnable absorber mixed with UO_2. By including pins with two different concentrations of gadolinia in the asssemblies, very good reactivity control is obtained, and the power is evenly distributed over a broad region of the core. Fuel costs are optimized by loading the core periphery with reused assemblies. The rest of the assemblies are discharged after one cycle in the core. The design criteria for peak pin exposure, axial enthalpy rise hot channel factor, and total peaking factors are met.

The fuel performance analysis indicates that fuel centerline temperature, rod internal pressure, cladding oxide thickness, clad surface temperature and fission gas release are within

acceptable limits, although in general slightly larger than for a contemporary reference 18-month cycle multibatch loading strategy.

The 36-month core is economically competitive with an 18-month reference core under certain operational conditions. Considering a refueling outage of 30 days and 3% forced outage rate, the 36-month core is about $5M/yr more expensive than an 18-month reference core. However, if the outage length increases to 42 days, costs are similar for both cores. Furthermore, the reduction in enrichment costs expected with the development of AVLIS technology will make the 36-month cycle more economically attractive and potentially cost competitive with the 18-month reference cycle.

Thesis Co-Supervisor: Michael J. Driscoll
Title: Prof. Emeritus of Nuclear Engineering

Thesis Co-Supervisor: John E. Meyer
Title: Prof. of Nuclear Engineering

Thesis Co-Supervisor: Neil E. Todreas
Title: Prof. of Nuclear Engineering

Acknowledgments

I am very grateful to Professors N.E. Todreas, M.J. Driscoll, and J.E. Meyer, who provided invaluable guidance and advice. I particularly appreciate their availability, useful comments and challenging suggestions that helped me in my endeavors.

I want to thank all those who provided some assistance at some point in my work. In particular, my colleagues C.S. Handwerk and M.V. McMahon worked on related topics for their graduate degrees and were willing to share their knowledge on extended cycles. Assistance from professionals in the nuclear industry was essential. Special thanks to K. St.John, from Yankee Atomic Electric Company, now Duke Engineering & Services, who provided access to the code FROSSTEY-2 and was always ready to answer my questions on fuel performance.

I would like to thank La Caixa, whose financial support made possible my studies at MIT.

And last but not least, I am very grateful to my family, especially my parents, who supported me from afar.

Major Nomenclature

AVLIS: Atomic Vapor Laser Isotopic Separation

BC: Boron Coefficient

BOC: Beginning Of Cycle

CBC: Core Boron Concentration

CDF: Cumulative Distribution Function

EFPD: Effective Full Power Days

EFPM: Effective Full Power Months

EOC: End Of Cycle

FCT: Fuel Centerline Temperature

FGR: Fission Gas Release

$\mathbf{F_{\Delta H}}$: Maximum Enthalpy Rise Hot Channel Factor

FOR: Forced Outage Rate

$\mathbf{F_Q}$: Total Core Peaking Factor

FTC: Fuel Temperature Coefficient

HFP: Hot Full Power

IFBA: Integral Fuel Burnable Absorber

LOCA: Loss Of Coolant Accident

LWR: Light Water Reactor

MOX: Mixed Oxide

MTC: Moderator Temperature Coefficient

PC: Power Coefficient

PCI: Pellet-Clad Interaction

PWR: Pressurized Water Reactor

RBA: Radial Blanket Assembly

RCCA: Rod Cluster Control Assembly

RFO: Refueling Outage

Table of Contents

List of Tables

List of Figures

Chapter 1

Introduction and Background

1.1 Foreword

The increasing competition in the electricity generation market is forcing nuclear plants to analyze and implement options for reducing their operating costs. One way of cutting costs is to optimize the cycle length so that fuel and O&M costs are minimized.

With this goal in mind, cycle length extensions have been considered and effectively applied. Pressurized Water Reactors (PWRs) that used to operate on 12-month cycles have opted for cycle extensions up to 18-to-24 months. Within the US fleet, 11 PWRs are operating 18-month or longer cycles as of August 1997 [E-1]. The benefit of stretching the cycle length stems from the lower frequency of refueling outages that results in improved capacity factors. However, longer cycles require higher fuel enrichment, and, therefore are burdened with higher fuel costs. The tradeoff between these two opposite trends determines the optimum cycle length.

The decision to increase the cycle length involves more than economics considerations. First, longer cycles typically burn fuel at higher power late in life, therefore challenging the mechanical and structural properties of the fuel rods. Second, during refueling outages not only are the new fuel assemblies loaded into the core, but also maintenance tasks are performed. Cycle managers have to consider whether components and equipment can reliably operate if maintenance tasks are scheduled after longer intervals.

To date, cycle extensions in PWRs have been moderate, --from 12 to 18 months,-- and only a few plants have opted for cycles between 18 and 24 months. Extension of operating cycles far beyond 24 months may provide an additional economic benefit by significantly improving capacity factors. Research sponsored by the INEEL University Research Consortium has examined the technical feasibility of extended cycles up to 48 months, as well as the technical issues that could constrain plant operation and maintenance for such long cycles [G-1]. This research is focused on cycles that retrofit into currently operating plants and keep the current fuel burnup limits.

This radical increase in cycle length requires an integrated design effort that includes neutronics, fuel performance, economics, and maintenance analyses. From a neutronics point of view, the technical feasibility of extended cycles up to 44.6 months for PWRs was shown by McMahon et al.[M-1]. Fuel performance and economic issues of concern were identified and analyzed by Handwerk et al. in Refs. [H-1] and [H-2] respectively. Moore et al. [M-2] showed that maintenance strategies can support operating cycle lengths up to 48 calendar months. Research by Brodeur et al. [B-1] focused on identifying the sources of Forced Outage Rate (FOR) in nuclear plants and developing methods to improve operational reliability.

For a single-batch reload core --the strategy adopted in Ref. [M-1]-- the cycle length with the lowest operational costs is around 33 calendar months [H-2]. However, the cost curve is quite flat around the minimum with little cost differences in the region ranging from 28 to 38 calendar months.

The purpose of this thesis is to design an economically optimized 36-month reload core for a PWR. The analysis covers 3 main areas: neutronics, fuel performance and economics. The knowledge acquired from the previous work on extended cycles ([M-1], [M-2], [H-1], [H-2]) is applied here, but the goals and the approach are different. While Ref. [M-1] is focused on showing the technical feasibility of ultra-long cycles, the present work focuses on determining the most economical solution for a cycle shorter than in [M-1] but under the same design constraints. Although the core costs are a key criterion in the design, selection of a particular design approach is based on both technical and economic considerations.

1.2 Background on Extended Operating Cycles

1.2.1 Single-Batch Loading

The work of Ayoub and Driscoll [A-1] demonstrated that a single-batch reloading was the required strategy for achieving greater than 40-month cycles if the current fuel burnup limits were to be respected. Figure 1-1 shows the fundamental relationships between burnup, batch index number, fuel enrichment and cycle length for a typical PWR with a specific power of 38.7 kW/kgU operating with an overall capacity factor of 87%. Current

operation is constrained by the enrichment licensing limit of 5% U-235 and the discharge burnup limit. Cycles between 12 and 24 months can meet these requirements by using batch numbers between 2 and 3. Keeping the burnup limit imposes a severe constraint on extended cycles, and a 48-month cycle will meet this limit only if a single-batch strategy (n=1) is adopted. In that case, the required U-235 enrichment has to be over the current 5% licensing limit.

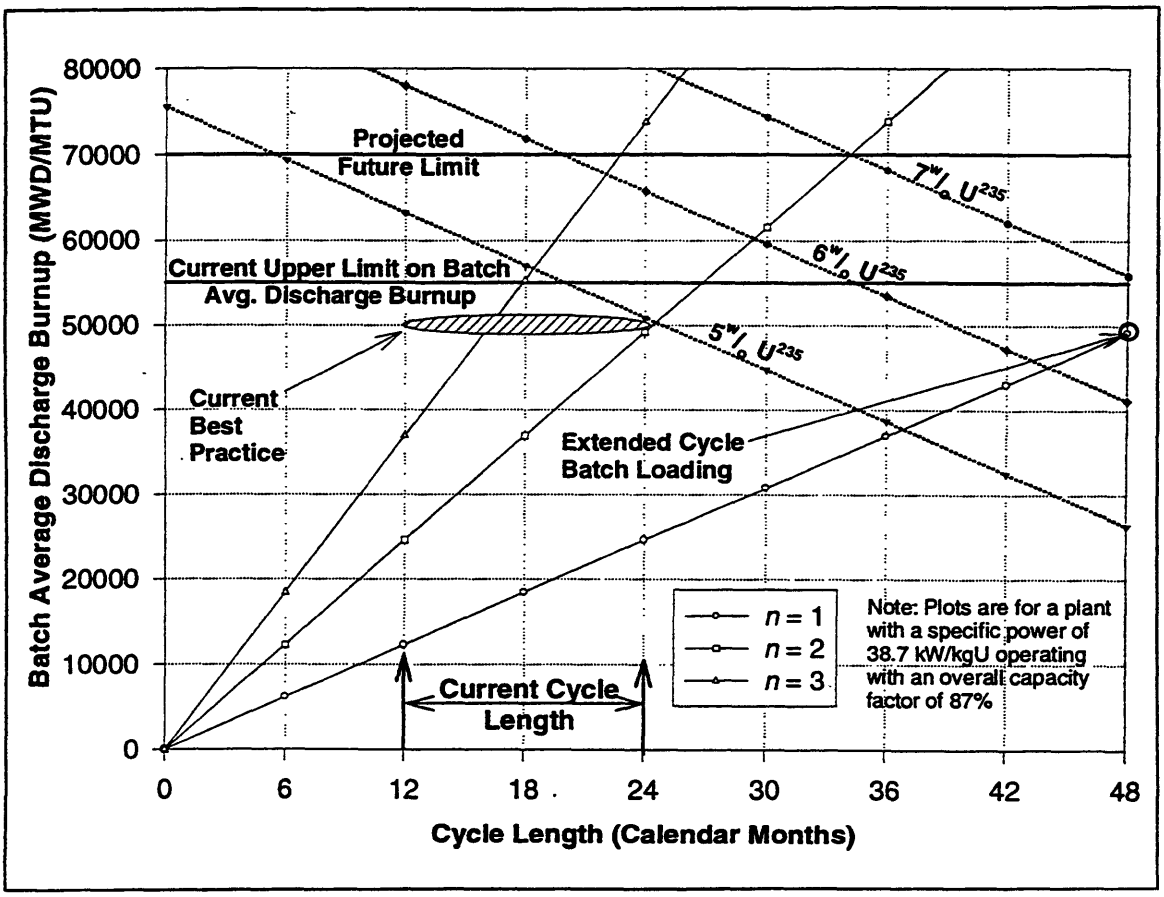

Figure 1-1: Burnup-cycle length map for a representative PWR [M-1]

A single-batch core lacks the flexibility of fuel management that multibatch cores have since the high reactivity of fresh fuel cannot be balanced with the lower reactivity of assemblies discharged from the previous cycle. An adequate burnable absorber distribution is key to compensate the high initial reactivity of a single-batch core. Moreover, the inability to mix high and low burnup (hence reactivity) assemblies causes some high bur-

nup assemblies to run at higher power over longer periods of time than in multibatch cores, therefore increasing concerns about fuel performance.

1.2.2 Extended Cycle Designs

McMahon et al. [M-1] have proposed core designs for both PWR and BWR extended cycles that show a satisfactory neutronics performance. The PWR reload core achieves a cycle length of 38.8 Effective Full Power Months (EFPM) or 44.6 calendar months when operating at a capacity factor of 87%. The BWR design achieves a cycle length of 45 EFPM or 48 calendar months at the target capacity factor of 93.8%.

The PWR core is a single-batch reload with fuel enriched to 7% U-235. The burnable absorbers are gadolinium oxide (Gd_2O_3) and zirconium diboride (ZrB_2) --the latter is commercialized as Integral Fuel Burnable Absorber, or IFBA. This core complies with the physics design limits, although control rods with higher worth are needed to meet the shutdown safety requirements. The fuel performance analysis for this core shows that issues such as fuel stress and strain, rod axial growth, corrosion or internal pressure are exacerbated in extended cycles when compared to current practice [H-1]. Although some of these factors are not easily quantifiable, solutions have been provided to mitigate the negative effect of cycle extension.

1.2.3 Economics Analysis

Handwerk et al. [H-2] presented a comprehensive analysis of the economic issues related to extended operating cycles and compared partial and total costs for an extended cycle --44.6 calendar months-- and the 18-month reference cycle that represents current industry practice. In this study, the operational parameters are 3% Forced Outage Rate (FOR) and 42 days Refueling Outage (RFO) length for the extended cycle, and 6% FOR and 49 days RFO for the reference cycle. These values yield capacity factors of 93.8% and 85.6% for the extended and reference cycles, respectively. Under these conditions, the extended cycle is about $1M/yr less expensive than the reference cycle. However, when the same operational parameters --3% FOR and 42 days RFO-- are assigned in both cases, this benefit disappears and the extended cycle is more costly by about $11M/yr.

In general, for a fixed batch number, total cycle costs change with cycle length, assuming constant FOR (%) and RFO (days). As cycle length increases, total costs decrease,

reach a minimum and finally go up. Total costs include fuel costs, refueling and maintenance outage costs and replacement power costs. Increasing cycle length has two effects on costs, considered on an annual basis:

- fuel costs increase because of the higher enrichment required;
- refueling outage and replacement power costs decrease because outages are spaced further apart.

There is an economic tradeoff between these effects which results in a cycle length with optimized, minimum total costs.

Handwerk et al. [H-2] developed a model to determine the optimum extended cycle length. For a single batch core, total costs were analyzed versus cycle length and the minimum was found to be a 33 calendar month cycle, considering 3% FOR and 30 days RFO. However, the cost curve is quite flat around the minimum, with little cost differences in the region ranging from 28 to 38 calendar months (Fig. 4-8 in [H-2]). The results were found to be fairly dependent on the operational parameters FOR and RFO length. As the operational performance improves, i.e. capacity factor increases, annual costs decrease for both the extended and reference cycles, but the decrease is more significant for the reference cycle. The achievement of increased cycle length requires a technical operating discipline that would concurrently yield shorter FOR and RFO length [G-1], and would provide a larger benefit to the reference cycle. On the other hand, extended operating cycles will be more competitive if fuel costs decrease or replacement power costs increase. In particular, the commercial development of AVLIS enrichment technology may significantly reduce fuel costs, making extended cycles more economically attractive.

1.3 Core Design Considerations

1.3.1 Design Constraints

Several constraints are imposed on this core design. First, since the core design effort aims to improve economics of currently operating PWRs, the core has to be retrofit into current PWR designs. In particular, the applicable reactor parameters are taken from a 4-loop 3411 MW_{th} Westinghouse PWR. Second, this project keeps the current fuel burnup limit for PWRs, which constrains the average burnup of any single pin within the core to

be below 60 GWD/MTU. This limit severely constrains the design options, and, as discussed in Section 1.2.1, requires implementation of the single-batch option. Third, the cycle length was set at 36 months based on the following considerations:

- from a practical point of view, plants have to be available for operation during periods of peak demand, that is, winter and summer, thus limiting the refueling outages to fall and spring;
- the economic optimum from Ref. [H-2] is 33 calendar months, although there is little difference in total costs for cycles between 28 and 38 months.

For this analysis, the FOR of the plant is taken as 3%, and the RFO is 30 days. Current average performance of PWRs is poorer than these parameters. However, these values are taken as best estimates of improved industry performance in the next 5- to 10- year period, when the extended cycles could be implemented. The FOR and RFO length along with the EFPM of the cycle allow determination of the capacity factor and the cycle calendar months, and have, therefore a key influence in the economics analysis.

1.3.2 Goals and Scope

The main goal of this thesis is to design an extended cycle ready for implementation in currently operating PWRs and capable of appealing to utility managers.

More specific goals are:

- determine the optimum fuel type and burnable absorber for this cycle;
- analyze different strategies for the peripheral assemblies of the core, which run at lower-than-average power and are a potential source of savings;
- identify the options to optimize fuel utilization and core economics;
- perform a detailed neutronics analysis for the subject core and show compliance with the design limits;
- maintain the core peaking factors and performance as close as possible to those of the 18-month reference cycle;
- identify possible strategies for further design improvements;
- design a transition cycle between a 24- and a 36- month cycle;
- analyze the core fuel performance, and show compliance with design limits;
- develop practical tools for analysis of cladding corrosion and fission gas release.

1.4 Structure of the Document

The plant used for the analysis, the computational tools and the models for the core and assemblies are described in Chapter 2. Chapter 3 covers the selection of fuel and poi-

son for the 36-month cycle. Chapter 4 analyzes and compares the options for the peripheral assemblies. Chapter 5 discusses the axial zoning of both fuel and burnable poison. In Chapter 6, the 36-month core and its neutronics performance are described, the improvement possibilities in the core design are identified, and a physics design for a transition cycle from a 24- to a 36-month core is presented. Chapter 7 analyzes the core fuel performance, with special attention to the cladding corrosion and the fission gas release. The economics aspects of the core are analyzed in Chapter 8. Finally, Chapter 9 summarizes the work, gathers the main conclusions, and identifies the areas where future work is desirable.

Chapter 2

Model Description

The plant used for this study is a Westinghouse 4-loop 1150 MW_e Pressurized Water Reactor. Within the US fleet of reactors, there are 72 operating PWRs, and 27 of them are Westinghouse 4-loop reactors [E-2]. In addition, this class of PWR reactors has the highest fuel specific power, 38.7 kW/kgU, and thus is the most demanding application. The 36-month cycle presented here is directly applicable to these plants and similar cycles could be considered for PWRs of different design.

In this chapter, the main characteristics of the plant are listed. The computer codes used in the design process are described. Then, general considerations for modeling a single assembly and a whole core are given. Finally, the design limits used as benchmark values are presented.

2.1 Plant Description

The operating parameters for this analysis are taken from the Seabrook Nuclear Station in Seabrook, New Hampshire. This plant is currently running on 18-month cycles. Although the cycle length was increased up to 22 months for one cycle, burnup and power distribution considerations have led to a return to the previous 18-month length [R-1]. The values --listed in Table 2.1-- were provided by Yankee Atomic Electric Company [M-1].

Throughout this study, an 18-month reference cycle with the same operating parameters is taken as the reference case in order to compare the performance of the 36-month cycle with a cycle representative of current industrial practice.

2.2 Computer Code Descriptions

Several computational tools were used in the design of the 36-month cycle. The neutronics analyses were performed with the suite of codes CASMO-3/TABLES-3/SIMULATE-3 from Studsvik of America. These powerful, licensing level codes perform high quality calculations and allow an accurate representation of the core physics. The fuel per-

formance analyses were done with the FROSSTEY-2 code from the Yankee Atomic Electric Company. Finally, the economics calculations were performed with an spreadsheet developed by Handwerk et al. [H-3].

Each of the codes is described in the next several Sections.

Table 2-1: Operating parameters for a Westinghouse 4-loop PWR

Operating Parameter	Value
Plant	
Number of primary loops	4
Total heat output of the core (MW_{th})	3411
Total plant thermal efficiency (%)	34
Electrical output of plant (MW_e)	1150
Energy deposited in the fuel (%)	97.4
Energy deposited in the moderator (%)	2.6
Core	
Core thermal inside diameter/outside diameter (m)	3.76/3.87
Mass of fuel UO_2 (MT)	101.0
Mass of fuel as U (MTU)	88.2
Mass of cladding material (MT)	23.1
Rated power density (kW/l)	104.5
Specific power (kW/kgU)	38.7
Average linear heat generation rate (kW/ft)	5.6
Core volume (m^3)	32.6
Design axial enthalpy rise ($F_{\Delta H}$)	1.65
Allowable core total peaking factor (F_Q)	2.5
Primary coolant	
System pressure (MPa)	15.51
Total core flow rate (Mg/sec)	18.63
Rated coolant mass flux (kg/m^2-sec)	2087.6
Core inlet temperature (^oC)	292.7

Table 2-1: Operating parameters for a Westinghouse 4-loop PWR

Operating Parameter	Value
Fuel rods	
Total number	50,952
Fuel density (% of theoretical)	94
Pellet diameter (mm)	8.19
Pellet height (mm)	13.4
Fuel-clad radial gap width (μm)	82
Cladding material	Zircaloy-4
Cladding thickness (mm)	0.57
Clad outer diameter (mm)	9.5
Total fuel height (m)	3.66
Fuel assemblies	
Number of assemblies	193
Number of fuel rods per assembly	264
Number of grids per assembly	7
Rod pitch (mm)	12.6
Overall dimensions (mmxmm)	214x214
Rod cluster control assemblies	
Neutron absorbing material	Ag-In-Cd
Cladding material	Type 304 SS
Cladding thickness (mm)	0.46
Number of clusters Full/Part length	53/8
Number of absorber rods per cluster	24
Assembly array	17x17
Array geometry	square

2.2.1 CASMO-3

CASMO-3 is a multigroup two-dimensional transport theory code for burnup calculations on BWR and PWR assemblies [E-2]. This code is completely written in Fortran 77. The code reads many parameters by default, therefore simplifying the input file preparation for usual cases.

The CASMO-3 calculation process is shown in Figure 2-1. In the first step, macroscopic group cross section data are calculated for the fuel assembly using the input data -- densities, geometries, composition, operation parameters,-- along with an integrated library of 70 or 40 energy groups.

Effective cross sections in the resonance energy region are calculated for important resonance absorbers (U-235, U-236, U-238, Pu-239) using an equivalence theorem. The resonance region is defined between 4 eV and 9118 eV. The Pu-240 and Pu-239 resonances below 4 eV lie in the thermal region where the concentration of thermal groups provides an accurate representation and, therefore, do not require special treatment. Dancoff factors account for the screening effect between different pins.

Then, a series of microgroup calculations are performed for each type of pin in the assembly using the previous macroscopic group cross sections. Detailed neutron energy spectra are obtained and used to homogenize pin cells and collapse the number of energy groups down to a maximum of 12. The auxiliary MICBURN code provides CASMO-3 with effective cross sections for the fuel pellets when gadolinium is used as burnable absorber in fuel rods.

The two-dimensional transmission probability routine COXY is then used to calculate the flux distribution in a PWR assembly, in a maximum of 12 energy groups. The effects of leakage are considered by using a fundamental buckling mode that modifies the previous results.

For each fuel pin and for each burnable absorber region, isotopic depletion is calculated. Burnup chains are linearized, and 24 fission products, 2 pseudo fission products and 17 heavy nuclides are considered. Depletion is calculated twice in each step, using both the spectra at the start and at the end of the step. This approach is particularly important

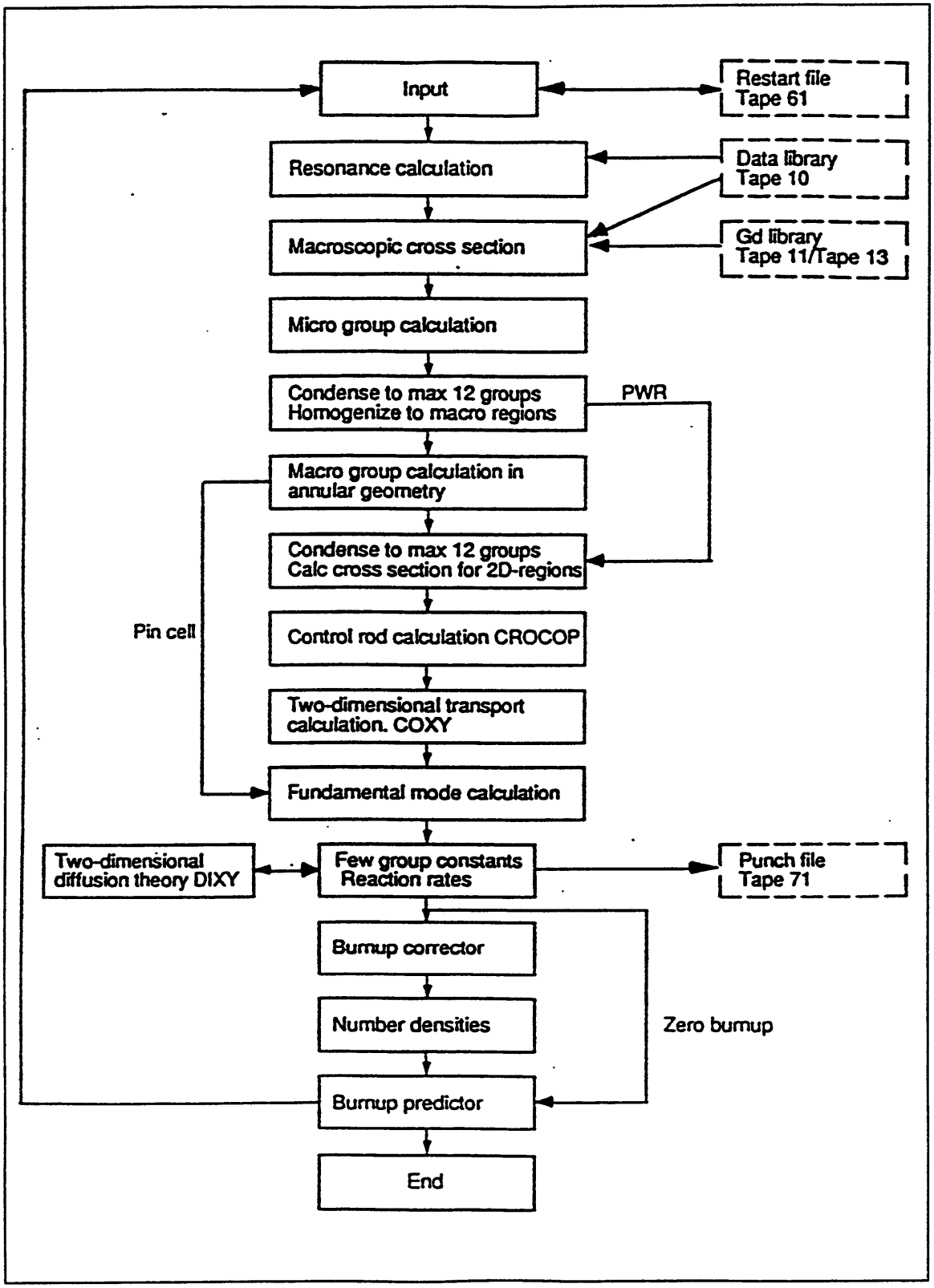

Figure 2-1: Flow of calculations in CASMO-3

when burnable absorber rods are involved. The next burnup step considers the average number densities from the previous two calculations.

CASMO-3 produces an output file and a card image file. The output is flexible and includes power distribution, reaction rates, few group cross sections for any region of the assembly, reactivity, discontinuity factors and nuclide concentrations. The card image file is the link with the following code of the suite, TABLES-3.

Assembly cross sections vary with core operational parameters and fuel depletion. In order to account for these changes and obtain an adequate library of cross sections, a set of CASMO-3 branch calculations are performed in the present work. For each of the assemblies modeled, five input files were prepared which included a base case and several branch cases. For each case, the fuel and moderator temperatures, boron concentration, and boron history were changed. The values for these parameters in the different runs are given in Table 2-2. The control rods were fully withdrawn unless otherwise stated. Calculations are performed at the specified depletion steps.

CASMO-3 performs the calculations for each depletion point using the Base Values indicated in the table. Then, branch calculations are performed using the values of the last column in the table. Assemblies were depleted up to 60 GWD/MTU. The fine mesh established for these variables insured a detailed library of cross sections.

2.2.2 TABLES-3

TABLES-3 is a data processing code that links CASMO-3 to SIMULATE-3 [S-1]. The code reads the CASMO-3 card image files and generates a library in the format required by SIMULATE-3. The following types of data are processed by TABLES-3:

- two-group cross sections;
- discontinuity factors;
- fission product data;
- detector data;
- pin power reconstruction data;
- kinetics data;
- isotopics data.

2.2.3 SIMULATE-3

SIMULATE-3 is an advanced two-group nodal code for the analysis of both PWRs and BWRs [S-2]. The code is based on the QPANDA neutronics model which employs fourth order polynomial representations of the intranodal flux distribution in both the fast and thermal groups. The code is entirely written in FORTRAN 77.

Table 2-2: Varied parameters in CASMO-3 runs

Parameter	Base Value	Branches
Base Case		
Core Boron Concentration (ppm)	450.0	0, 900, 2000
Moderator Temperature (°C)	310.0	292.7, 326.9
Fuel Temperature (°C)	626.9	292.7, 826.9
Control Rod Position	Fully Withdrawn	Fully Inserted
0 ppm Boron Case		
Core Boron Concentration (ppm)	0.0	450, 900, 2000
Moderator Temperature (°C)	310.0	-
Fuel Temperature (°C)	626.9	-
900 ppm Boron Case		
Core Boron Concentration (ppm)	900.0	0, 450, 2000
Moderator Temperature (°C)	310.0	-
Fuel Temperature (°C)	626.9	-
2000 ppm Boron case		
Core Boron Concentration (ppm)	2000.0	0, 450, 900
Moderator Temperature (°C)	310.0	-
Fuel Temperature (°C)	626.9	-
Low Moderator Temperature case		
Core Boron Concentration (ppm)	450.0	-
Moderator Temperature (°C)	292.7	310.0, 326.9
Fuel Temperature (°C)	626.9	-

In SIMULATE-3, the macroscopic and microscopic cross sections, discontinuity factors, fission product data, and detector data are generated by TABLES-3 after processing the multi-dimensional data from CASMO-3.

SIMULATE-3 performs depletion calculations in two or three dimensions, using 1/8, 1/4, 1/2 symmetry or the full core. The code can be used for fuel management and reload physics calculations. Depleted assemblies from one cycle can be reloaded and shuffled into the next cycle by creation of a restart file. Other code capabilities include reactivity coefficient calculations, criticality searches, and pin power reconstruction.

2.2.4 FROSSTEY-2

FROSSTEY-2 (**F**uel **RO**d **S**teady-**S**tate **T**hermal **E**ffects) is a state of the art code developed by Yankee Atomic Electric Company [S-3]. Pin specifications, such as materials, geometry, fuel composition and pin power history are taken as input values. The code calculates several parameters, including:

- fuel centerline temperature;
- gas fraction released;
- hot gap and gap conductance;
- clad temperatures;
- ZrO_2 thickness;
- fuel pin internal pressure;
- rod gas composition as a function of burnup.

2.2.5 Economics Code

The economics calculations were performed with the model prepared by Handwerk et al. and described in Ref. [H-2]. This model is implemented in a spreadsheet on a PC and it is easily applicable for different core configurations [H-3]. The total operating costs of the plant, appropriately discounted to cycle midpoint, (on an annualized basis) are calculated as the summation of the following terms:

- fuel costs, including mining, conversion, enrichment, and fabrication costs;
- cost of spent fuel, based on the government waste disposal fee;
- material and manpower costs during a refueling outage;
- material and manpower costs during a forced outage;
- replacement power costs.

Table 2-3 lists the main economics parameters (from Ref. [O-1]) embedded in the model that are common to all the cases analyzed in this thesis. Input values to this model

include plant parameters indicated in Table 2-1 as well as characteristics of each particular core, i.e, the cycle burnup, operational parameters (FOR, RFO) and core composition. The model accepts up to 6 types of fuel pins with 2 axial regions and up to 6 types of assemblies.

This model provides an acceptably accurate representation of the core costs and comparisons between different options can be quick and easily performed.

Table 2-3: Input to the economics model (from Ref. [O-1])

Fuel Cycle Economics Parameters	Value
Uranium purchase	$50/kgU
Conversion	$8/kgU
Enrichment	$110 /kg SWU
Fabrication	$ 275/kgU
Waste disposal fee	1 mill/kWhre
Replacement power	25 mills/kWhre
Carrying charge rate	10%/yr

2.3 Model

The design of the 36-month reload core was done in several steps involving analysis and selection of fuel and burnable poisons, peripheral assemblies and axial rod composition. For each of these steps, several options were studied and compared. The optimum solution was retained for each step and incorporated into the 36-month reload core. Comparison of the options was based on neutronics, economics and fuel performance. For the neutronics analysis, single assemblies and full cores were modeled following the general description given in the next two Sections.

2.3.1 Single-Assembly Modeling

For each type of assembly in the core, an input file was prepared for CASMO-3. The basic geometric parameters required to define the assembly are given in Table 2-1. Input values to CASMO-3 include dimensions and composition of pellets, rods, water holes,

assembly box and spacer grids, pin array structure and dimensions, and operating parameters such as fuel and moderator temperatures, boron concentration, and system pressure. Most assemblies were modeled with 1/8 symmetry as shown in Figure 2-2. However, due to the use of special burnable poison distributions and to the asymmetric radial blanket assembly design, some assemblies did not have 1/8 symmetry and were modeled in 1/4 or 1/2 symmetry.

Models of single assemblies were used to screen and select the type and distribution of fuel and burnable absorbers (see Chapter 3). For different assemblies, the two group k-infinities predicted by CASMO-3 were plotted versus the assembly average burnup, and then compared to each other. No branch calculations were performed in this case, since the

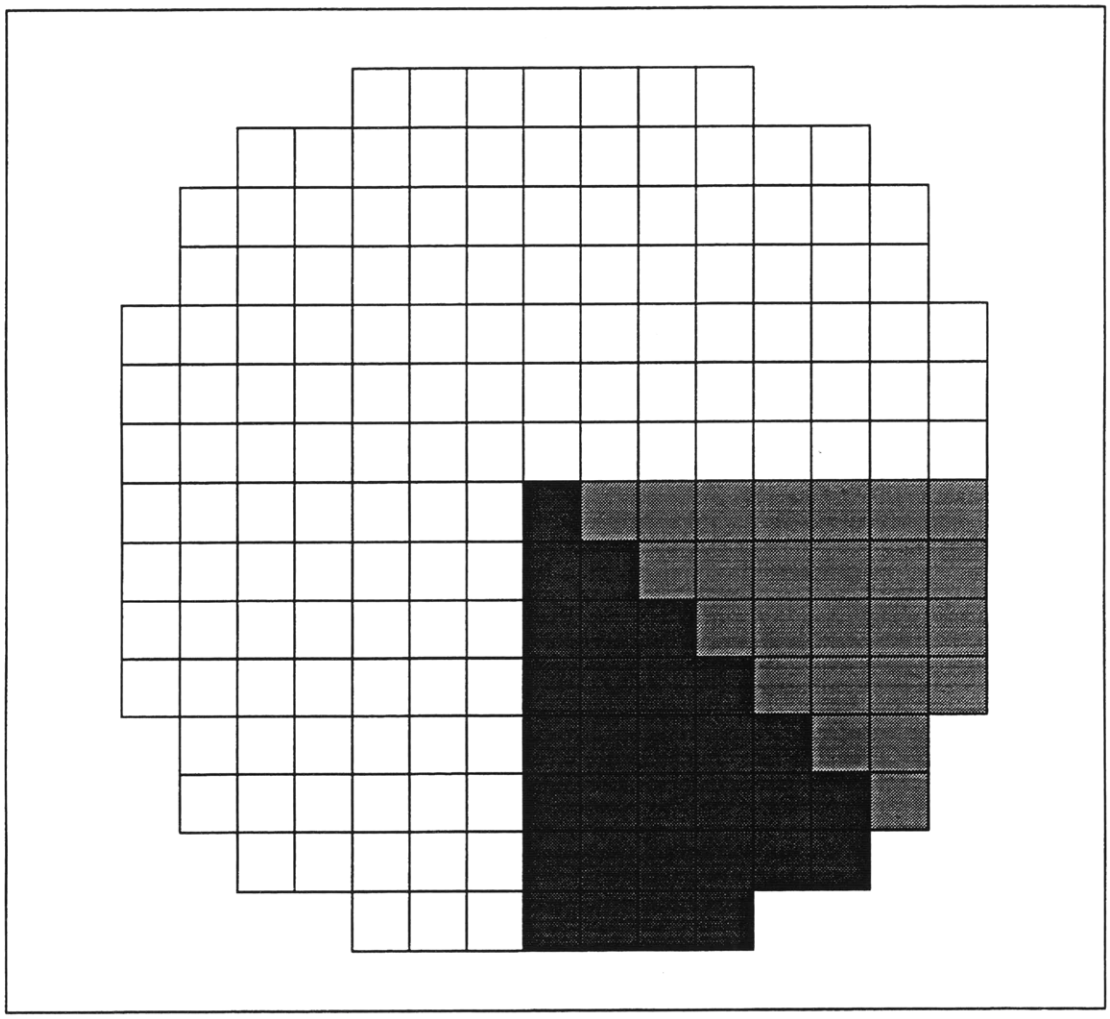

Figure 2-2: Core symmetry sections analyzed

purpose was not to create a library of cross sections. The operating parameters used for this application are indicated in Table 2-4. For these conditions, further work indicated that the amount of poison in the core is adequate when loaded with assemblies having k-infinity between 1.05 and 1.12 in the first half of the cycle.

Note in particular that the core boron concentration was set at 450 ppm, to represent an approximate cycle average value. Under these conditions, the assembly becomes subcritical when the k-infinity is below 1, and decreasing the boron concentration would therefore allow the assembly to be critical for a longer period. However, the value of the boron concentration is irrelevant for this analysis, since the k-infinities are not treated as absolute values, but are only interpreted in comparison to other assemblies that are operating under the same conditions.

Table 2-4: Operating parameters for reactivity comparisons

Parameter	Value
Core Boron Concentration (ppm)	450
Moderator Temperature (^{o}C)	310.1
Fuel Temperature (^{o}C)	627

2.3.2 Core Modeling

The model set up for analysis of the core with SIMULATE-3 is described here. The core was modeled in 3 dimensions with 24 axial nodes, and used 1/8 symmetry. Each assembly had 4 radial nodes, therefore providing a more accurate representation and allowing assembly rotation when shuffling. Preliminary analyses for option selection were performed with 2 dimensional models, which retained good accuracy and significantly reduced calculation time.

The core representation included radial and axial reflectors (top and bottom) that account for the coolant and structural materials. In the 2-D models, an input value for the axial buckling accounted for the axial leakage.

The core was analyzed at a condition of steady-state Hot Full Power (HFP) with all the control rods completely withdrawn, and was depleted to End Of Cycle (EOC). At each burnup step, a criticality search was established that adjusted the core boron concentration

(CBC) so that k_{eff}=1. The EOC was determined as the point where CBC=0 ppm. The core was initially free of fission product poisons.

2.4 Design Limits

The performance of the core was analyzed by comparison of neutronics and fuel performance parameters to a set of design limits. The technical feasibility of the design is demonstrated if the core complies with these limits. In addition, an effort was made to keep a good margin between the operational parameters and the design limits, so that the core performance is close to that of an 18-month cycle, and has sufficient margin to accommodate transient situations.

The design limits used for this project are described in the following sections. More details about the neutronics design limits and the impact of extended cycles on design parameters is provided in Ref. [M-1]. The fuel performance limits are also described in [H-1].

2.4.1 Neutronics Limits

Maximum enthalpy rise hot channel factor ($F_{\Delta H}$): defined as the ratio of 1) the axially integrated power along the rod with the highest integrated power to 2) the average rod power in the core. The $F_{\Delta H}$ limit for a Westinghouse 4-loop 1150 MW_e PWR is 1.65.

Total core peaking factor (F_Q): defined as the ratio of 1) the maximum local rod linear power density in any axial node to 2) the average fuel rod linear power density. The Westinghouse design limit for this core is 2.5.

Core critical boron concentration (CBC): soluble boron in the coolant has a great influence on the primary system chemistry. For the plant considered here, application of the EPRI recommendations [E-3] indicates that the CBC should be kept below 1780 ppm.

Pin burnup: the current licensing limit for burnup in PWRs establishes that the axially averaged burnup of any pin in the core has to be below 60 GWD/MTU.

Coefficients of reactivity: negative fuel temperature coefficient (FTC) and moderator temperature coefficient (MTC) are required to insure negative power feedback, and, therefore core stability.

2.4.2 Fuel Performance Limits

Fuel centerline temperature: this temperature has to be kept below the melting temperature for the UO_2 under transient conditions, which is a function of burnup and ranges from 2805 °C for unburned fuel to 2613 °C for an exposure of 60 GWD/MTU. Although no limit has been established for steady-state conditions, an adequate margin has to be provided to insure operation below the melting temperature.

Rod internal pressure: the pressure inside the rods increases as fission gases are released. Based on engineering judgment, an operational limit for steady-state conditions is to maintain this pressure below 2600 psia [H-1]. This value is slightly over the primary system pressure, which is 2250 psia.

Clad surface temperature: high clad temperatures may lead to increased reaction rates of water with zirconium, and the resulting production and pickup of hydrogen. This temperature has to be maintained below 400 °C.

Clad oxide thickness: the US Nuclear Regulatory Commission's Standard Review Plan defines a limit for oxide thickness at 17% of the cladding thickness during accident (LOCA) conditions [N-1]. For this study, an absolute limit will not be established, and the performance for the 36-month core will be evaluated by comparison to the 18-month reference core.

2.5 Summary

The plant parameters for the analysis are taken from a Westinghouse 4-loop 1150 MW_e PWR, more specifically those for the Seabrook Nuclear Station. The computational tools for the neutronics and fuel performance analysis are state-of-the-art codes that provide an accurate and reliable representation of the core performance. The economics model allows for quick comparisons between different cores. The main assumptions in the representation of a single assembly and the whole core were presented. Finally, the design limits for selected parameters were presented, which must be met to demonstrate the technical and licensing acceptability of the core.

Chapter 3

Fuel and Poison Selection

3.1 Fuel

In this Section, the enrichment required to operate a 36-month cycle is estimated. Furthermore, performance and characteristics of annular fuel are analyzed and its applicability to the 36-month cycle is assessed.

3.1.1 Enrichment

A preliminary analysis was performed to estimate the approximate fuel enrichment required to achieve a 36-month cycle. Several models were developed in 2-D with CASMO-3/SIMULATE-3 for cores loaded with different fuel enrichments. The cycle burnup and EFPM stemming from these calculations bound the maximum cycle length attainable with the given fuel. The final core design will have a shorter life for two reasons. First, no burnable absorbers were included in the analyses,[1] and second, the peripheral assemblies in the final 36-month core are shuffled from a previous cycle, and are hence less reactive than fresh fuel. Use of burnable absorbers in the core reduces the cycle length because of the residual penalty (see Section 3.2.1) and the displacement of fissile atoms.

The average core discharge burnups from SIMULATE-3 are given in Table 3-1 along with the EFPM and calendar months of the cycle for different core enrichments. The EFPM are calculated with the core and operational parameters of this study (see Chapter 8 for equations).

Of particular interest is the core with 5% U-235, since this is the current licensing limit for fuel enrichment. It can be seen that the maximum achievable cycle length for a 5% enriched core is 34.1 calendar months. If a capacity factor of 87% was instead considered, the 5% enriched core would yield 36.9 calendar months. Further analysis showed however, that when the poison residual penalty is taken into account, the resulting cycle length is too short for the purposes of this project.

1. One should note that the peaking factors and levels of soluble boron in an unpoisoned core are expected to be over the design limits.

Table 3-1: Cycle length for cores with different fuel enrichments (at 3% FOR and 30 days RFO)

Enrichment (%)	B_d (GWD/MTU)	EFPM	Calendar months
5.0	37.20	32.1	34.1
5.5	40.88	35.2	37.3
6.0	44.44	38.3	40.5
6.5	47.90	41.3	43.6

Subsequent calculations determined that only a 6.5% enriched core yields a 36 calendar month cycle with the operational parameters assigned (3% FOR and 30 days RFO), and the strategy adopted, i.e. gadolinium as burnable poison and a batch number of 1.29 (ratio of total assemblies in the core to new fuel assemblies in each reload).

3.1.2 Annular versus Solid Fuel Pellets

Mechanical and thermal benefits stem from the use of annular fuel pellets instead of solid pellets ([A-1],[S-4],[S-5]). These benefits include:

- increased space for accummulation of fission gas, and, hence reduced rod internal pressure;
- delayed and reduced pellet-clad-interaction (PCI);
- lower fuel temperatures;
- lower stored energy in the fuel pins, and therefore benefits for ECCS/LOCA limits.

Annular fuel affects the neutronics behavior since the fuel-to-moderator ratio changes. For a Westinghouse plant with 17x17 fuel, annular pellets will only offer an economic benefit if the H/U ratio is more optimum than in the reference core with solid pellets [M-3], [M-4]. An evaluation performed at B&W indicated that fuel cycle cost benefits are maximum for annular fuel with about 10% void volume [B-2]. Most reactors operate very near their optimum point, and the effect of annular fuel must be assessed in each particular case [S-5]. It is interesting to note that the Russian VVER-1000 PWR units employ 10% central void annular fuel pellets [P-1] and that this option is available from Western vendors such as Siemens [S-4].

The performance of annular fuel with 10% and 20% voids as well as solid fuel was analyzed. First, a single assembly was modeled with 6% U-235 and the results show that the average burnup is very close in the three cases. Then, full cores were modeled with 5% and 6% U-235. The core average discharge burnups and cycle lengths in calendar months are given in Table 3-2. The burnup differences are very small when annular fuel is used instead of solid fuel. For 10% void, the burnup increases about 0.65% and 0.88%, for 5% and 6% U-235, respectively. On the other hand, the content of fissile atoms is reduced by 10% and the cycle lengths are reduced by over 9%. The table also shows the fuel and total costs on a yearly basis. The fuel costs slightly decrease as the void percent increases. However, the total costs are essentially the same.

Table 3-2: Effect of annular fuel on cycle length and core costs

Fuel enrichment	Void percent	B_d (GWD/ MTU)	Calendar months*	Fuel costs ($M/yr)	Total costs ($M/yr)
5%	0-(solid)	37.20	34.1	79.5	103.0
5%	10 %	37.44	30.9	78.1	103.1
5%	20 %	37.47	27.6	77.0	103.9
6%	0 - (solid)	44.44	40.5	82.2	103.3
6%	10 %	44.83	36.8	80.5	102.9
6%	20 %	45.03	33.0	79.1	103.0

* at 3% FOR and 30 days RFO

It can be concluded from this analysis that the neutronic and economic benefits of annular fuel for this core are not significant, since the core burnup and the total fuel costs remain virtually unchanged. Moreover, for a given cycle length, a slightly higher enrichment will be required if annular fuel is used instead of solid fuel. The interest of annular fuel is, therefore, only linked to its thermal and mechanical benefits. For this core, annular fuel will be only used locally in axial blankets (see Section 5.1) to provide additional space for fission gas release.

3.2 Poison Selection

Selection of burnable absorbers is key to the feasibility of this extended cycle. The high U-235 enrichment in the fresh fuel along with the low batch number (close to 1) results in a considerable positive reactivity, greater than in a multibatch core at BOC and for a long part of the cycle. The excess reactivity is held down by both soluble boron and burnable absorbers. The amount of boron dissolved in the coolant is limited by chemistry considerations to 1780 ppm (see Section 2.5.2), and, therefore, burnable absorbers have to compensate the remaining positive reactivity.

3.2.1 Burnable Absorbers

Burnable absorbers are used to shape the power distribution in the core so that the physics design limits are met and hot spots are avoided. These limits are set to insure that the coolant has the capability of extracting all the energy locally generated in the fuel rods, and the fuel and clad temperatures do not exceed the design limits. Some fuel performance parameters such as fission gas release or internal pin pressure are closely related to the temperatures attained in the fuel. These parameters have a less favorable behavior as temperature increases. This thesis aims not only to keep peaking factors below limits, but also to maintain them as low as possible, an objective whose achievement relies on an appropriate burnable poison configuration.

The shortcoming of burnable absorbers is the reactivity residual penalty. The concentration of burnable absorber is reduced as it captures neutrons, in which process it competes with fissile atoms. Towards the last part of the cycle, burnable absorbers are less important or no longer needed, since the excess reactivity can be held down by an acceptable amount of diluted boron, and the less reactive core yields lower peaking factors. However, absorbing isotopes are generated in the neutron capture process (e.g. Gd-157 from Gd-156), producing a residual poisoning. The core reactivity is hence reduced and the core life shortened. Ideally, a burnable absorber for an extended cycle should:

- have a low residual penalty;
- yield low intra-assembly power peaking;
- create a fairly flat reactivity shape throughout core life, thus avoiding undesirable shifts in core power distribution.

McMahon et al. [M-1] used a combination of gadolinium oxide (Gd_2O_3) and Integral Fuel Burnable Absorber (IFBA) for the PWR 44-month core. This combination guarantees compliance with peaking factors and internal pressure limits, and should be suitable for a shorter (36-month) cycle.

In order to optimize the power distribution and minimize peaking factors other burnable absorbers were analyzed for the 36-month cycle. The performance of gadolinium oxide, erbium oxide and IFBA is analyzed in this thesis. It is found that a carefully tailored distribution of Gd_2O_3 in the core is the most suitable burnable poison for the 36-month cycle.

3.2.2 Gadolinium

3.2.2.1 Introduction

Gadolinium is a rare earth element with atomic number 64. It has several natural isotopes, with two main thermal absorbers: Gd-155 and Gd-157. The oxide form Gd_2O_3 (gadolinia) has been extensively used as burnable absorber in both PWRs and BWRs [H-4]. The thermal neutron absorption cross-sections of Gd-157 and natural gadolinium are 250,000 and 49,000 barns respectively [A-2]. Application of gadolinia to extended cycles requires relatively high concentrations within the UO_2 matrix so that the self-shielding effect slows down its depletion rate.

McMahon's core design [M-1] uses 12% Gd_2O_3 in selected pins within each assembly. By varying the number of burnable absorber pins, assemblies with different reactivities throughout core life are obtained. Less reactive assemblies are loaded in central parts of the core. This pattern provides control for the 7% U-235 enriched fuel and the core peaking factors are within limits. However, the reactivity of each assembly significantly changes with burnup, and the core power distribution considerably shifts from the periphery to the center and back to the periphery (see Figures 27 and 28 in [M-1]).

The reactivity control that gadolinia provides depends largely on the number of poisoned pins while the duration of effectiveness is proportional to the content of poison within the pins. Both factors are extensively analyzed here. The main goal is to optimize the poison distribution and to flatten the reactivity shape throughout core life.

3.2.2.2 Simple Loading

Calculations were performed for a single assembly with fuel enriched to 6% and 6.5% U-235. Since the trends observed are the same in both cases, only the results with 6.5% fuel are presented in this Section.

First, the analysis was focused on the effect of changing the number of poisoned pins with a fixed concentration of gadolinia. Figure 3-1 shows the two-group k-infinity versus assembly average burnup for an assembly loaded with 12% Gd_2O_3. The cases compared contain between 20 and 40 poisoned pins. The reactivity of the unpoisoned assembly is plotted as a reference. For a low number of poisoned pins, the k-infinity decreases from BOC to EOC. However, as more pins are loaded in the assembly, i.e. 40 pins, the k-infinity increases for about 3/4 of the cycle, reaches a maximum and finally decreases. For some intermediate poison loading, i.e. 32 pins, the assembly k-infinity is fairly flat for about 2/3 of the cycle. Then, with the burnable poison almost completely depleted, the reactivity decreases until EOC. It is aso observed that the reactivity residual penalty increases with

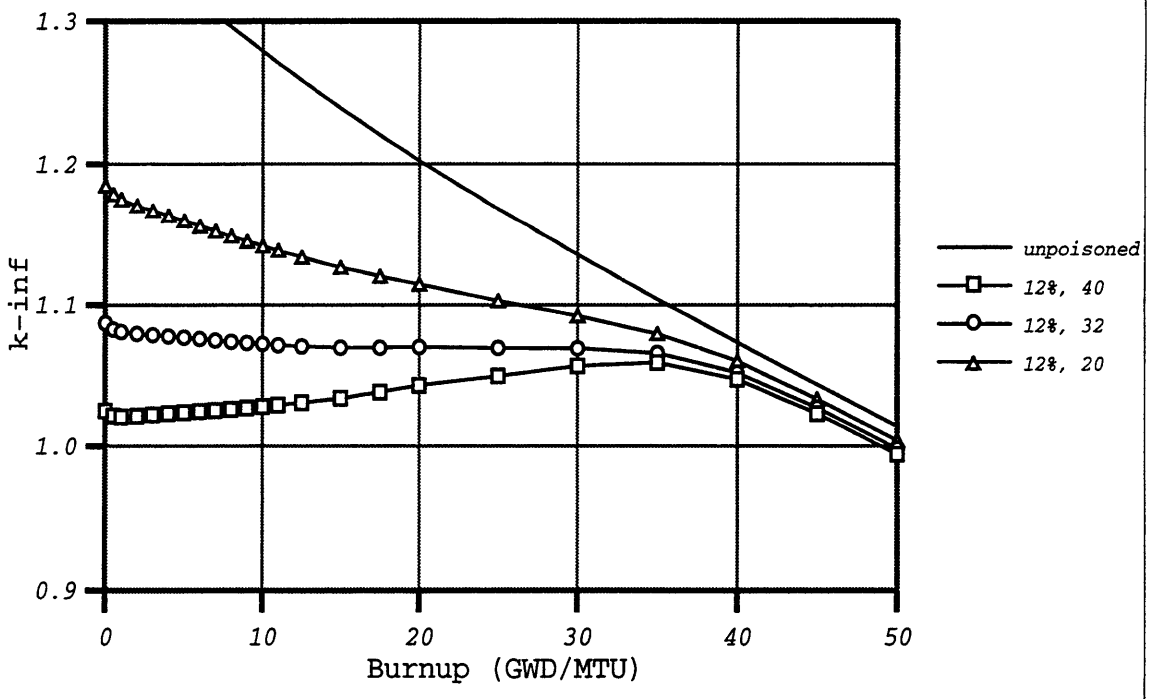

The legend "12%, 40" stands for 12% Gd_2O_3 in 40 pins

Figure 3-1: Assembly k-infinity for varying number of gadolinia-loaded pins

the number of poisoned pins.

Figure 3-2 shows the effect of increasing the content of gadolinia in a fixed number of poisoned pins. At BOC, the differences between the curves are small because of the self-shielding effect, and an increase of gadolinia content from 8% to 12% results only in a 1.4% decrease of k-infinity (0.017). As the burnable poison depletes, the differences in reactivity increase, reaching a maximum at about 25 GWD/MTU. Around 30 GWD/MTU, the 8% Gd_2O_3 is almost depleted, and its k-infinity runs parallel to that of the unpoisoned case. However, for the assembly with 12% Gd_2O_3, the poison is not completely depleted until about 40 GWD/MTU, so that the reactivity is controlled for a longer time. Finally, the residual penalty increases with the poison content.

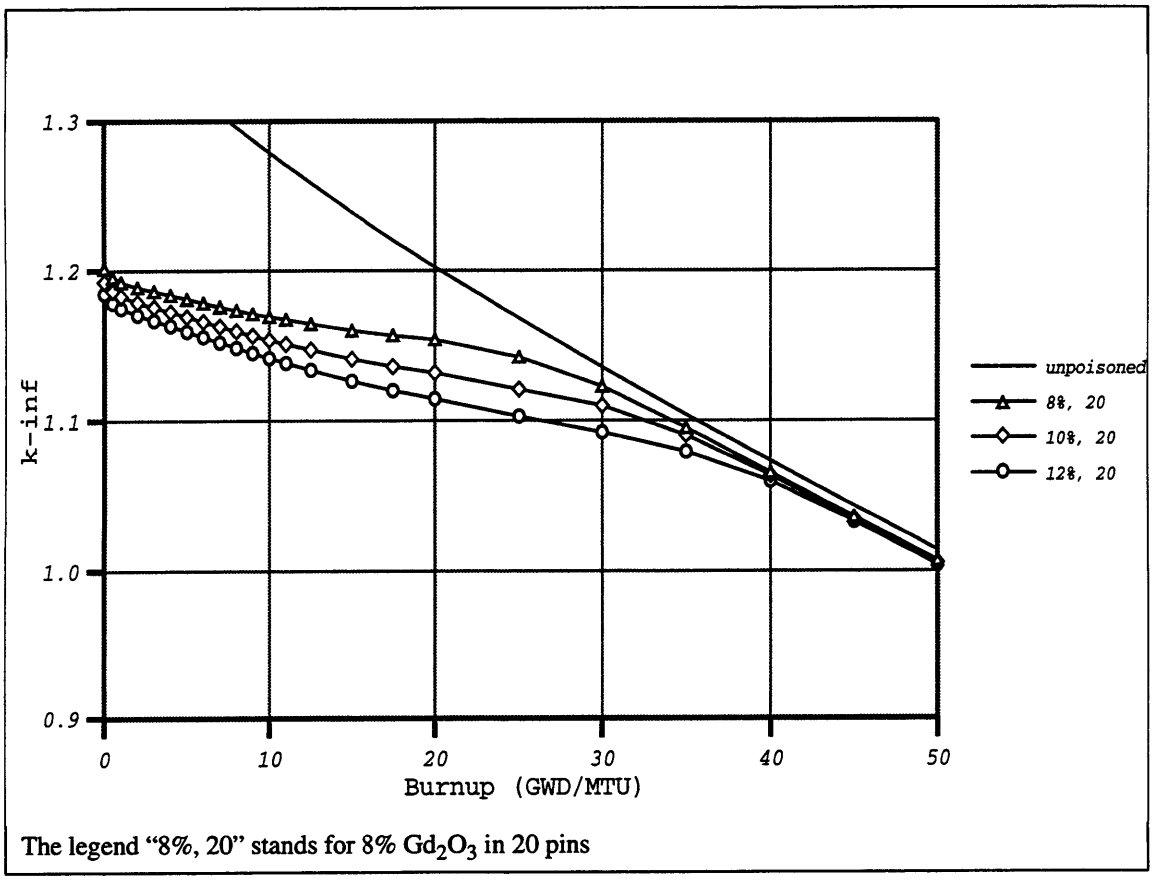

The legend "8%, 20" stands for 8% Gd_2O_3 in 20 pins

Figure 3-2: Assembly k-infinity for varying concentrations of gadolinia

3.2.2.3 Duplex Loading

Asou et Porta [A-2] obtained a very flat reactivity shape for an assembly with 4.5% U-235 by incorporating pins with two different gadolinia loadings, in a strategy they call

"duplex poisoning". A number of pins N_1 with a gadolinia content T_1 controls the poison burnup, and therefore, the duration of its effect, whereas a number of pins N_2 with lower gadolinia content, T_2, adjusts the initial reactivity.

This strategy is analyzed here for the 36-month core and the results are considered extremely satisfactory. Optimized assemblies present a fairly constant reactivity for about 2/3rds of the cycle. Moreover, by selecting the appropriate loading combination, assemblies with different levels of reactivity are obtained.

In Figure 3-3, the poisoned reference assembly contains 10% Gd_2O_3 (T_1) in 20 pins (N_1). The effect of adding 8 pins (N_2) with 4%, 6% and 8% Gd_2O_3 is shown. The figure also includes the cases in which T_2 is fixed (8%) and N_2 changes from 8 to 12 pins. In all the cases, the reactivity shape is flattened compared to the reference case. Moreover, the addition of the N_2 pins with burnable absorbers has a small effect on the residual penalty.

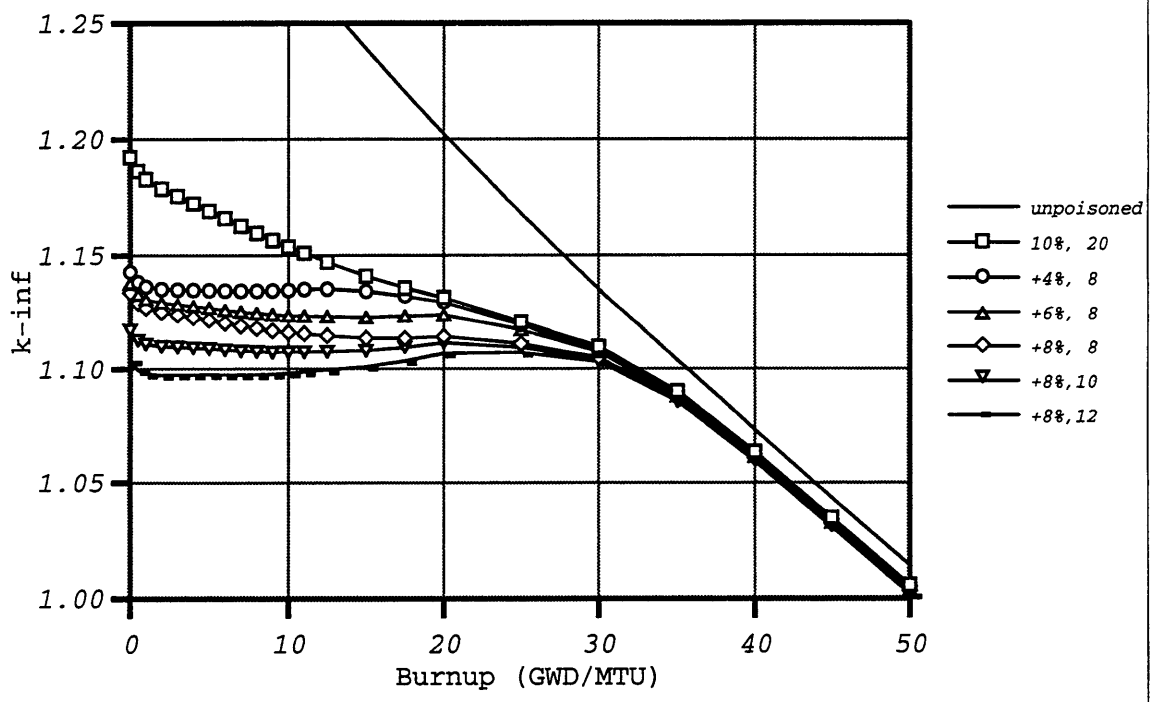

The legend "+4%, 8" indicates that 8 pins are loaded with 4% Gd_2O_3 in addition to the loading in the poisoned reference assembly (10% Gd_2O_3 in 20 pins)

Figure 3-3: Assembly k-infinity for the duplex loading of gadolinia

As discussed in Section 3.2.2.2, the effects of changing N_2 with a fixed T_2 is not the same as changing T_2 with a fixed N_2.

The possible combinations of N_1, T_1, N_2, and T_2 are multiple and provide the core designer with a great flexibility to optimize the core loading. Based upon the trends shown in Figure 3-3, several poison combinations were analyzed. Figure 3-4 represents the reactivity shapes for the assemblies that are part of the 36-month core described in Chapter 6. It can be seen that the reactivity of each assembly remains fairly constant for about 30 to 35 GWD/MTU.

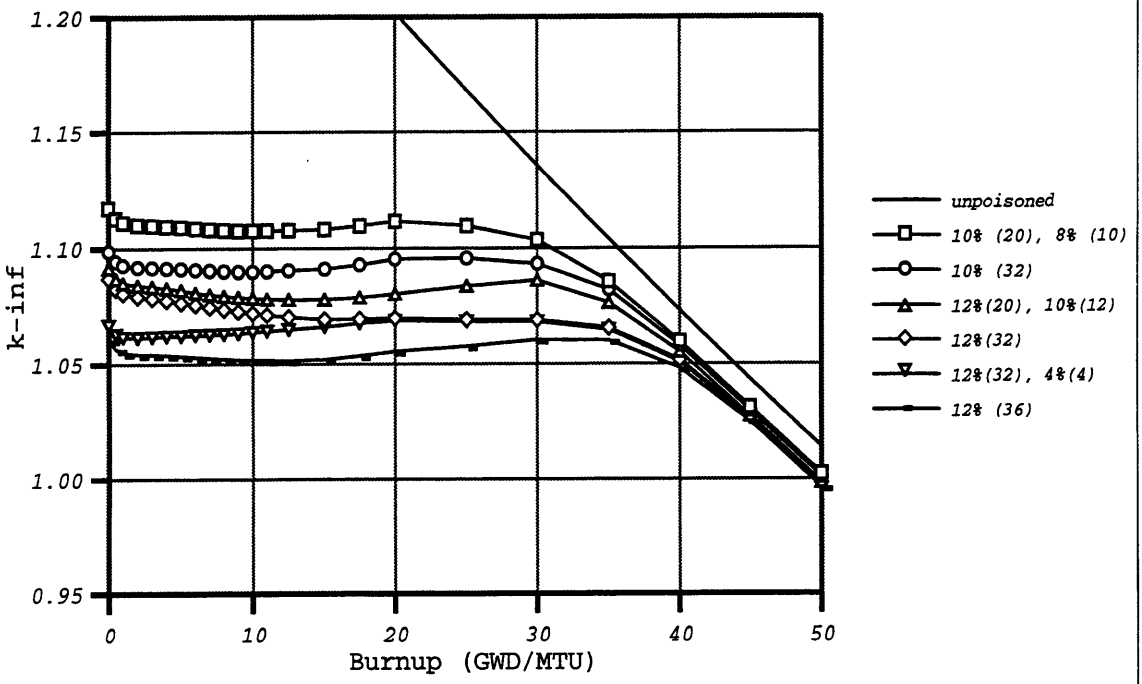

The legend "10% (20), 8%(10)" means that 20 pins contain 10% Gd_2O_3, and 10 pins contain 8% Gd_2O_3

Figure 3-4: K-infinity for the assemblies loaded with gadolinia in the 36-month core

3.2.3 Erbium

3.2.3.1 Characteristics

Erbium is a rare earth element with atomic number 68. It has several natural isotopes, the main one being Er-167. Its oxide form, Er_2O_3, known as erbia, can be mixed within the UO_2 matrix. The capture cross section of natural erbium takes moderate values --100

to 400 barns-- below 0.3 eV [J-1]. However, two resonances dominate the spectrum around 0.5 eV, reaching a peak value over 4000 barns.

The effective thermal cross section of Er-167 is significantly lower than that of gadolinium and similar in magnitude to that of boron. Unlike gadolinia, erbia is an effective poison when distributed relatively evenly at low concentrations throughout the core.

The main characteristics of erbia as burnable absorbers are [L-1]:

- its effectiveness at low concentrations reduces the impact on fuel, and changes in rod thermal conductivity and mechanical properties are minimized;
- the distribution of poison over many pins reduces local peaking within a fuel assembly;
- the large resonances in the upper part of the thermal spectrum provide a negative component to the moderator temperature coefficient. This behavior significantly differs from other burnable absorbers, where the cross section decreases with energy in this region;
- the low cross section and, therefore, slow depletion rate as compared to gadolinia, results in a larger reactivity penalty at EOC.

3.2.3.2 Reported Experience

Lindberg et al. [L-1] analyzed erbia --instead of gadolinia-- for an 18-month cycle in a 1300 MW_e EDF PWR, and found that $F_{\Delta H}$ was reduced by 4% at BOC and EOC, and by larger values during cycle life. An increase of $0.02^{w}/_{o}$ in U-235 enrichment was needed to compensate for the reactivity penalty.

Choi et al. [C-1] compared the performance of Gd_2O_3, Er_2O_3 and ZrB_2 in Korean PWRs and concluded that Er_2O_3 shows a higher residual penalty, and that both Er_2O_3 and ZrB_2 are more effective than Gd_2O_3 in controlling peaking factors.

Jonsson et al. [J-1] indicated that the Erbia residual penalty for 18- and 24- month cycles is comparable to that of gadolinia.

Fuel pins with erbia have been loaded in several US PWRs. Jonsson and Gunn [J-2] reported the experience from 5 PWRs that were operating on 18- and 24-month cycles using erbia as absorber. This report also indicates that erbia is economically competitive with other burnable absorbers.

Erbia is the proposed burnable absorber in the System 80+^{TM} Advanced Light Water Reactor (ALWR) from ABB Combustion Engineering as described in Refs. [R-2], [R-3] and [C-2]. One of the possible operational schemes in this reactor is a four year core, with

a new full core being inserted every four years and fuel being shuffled every year. The core is loaded with mixed oxide (MOX) fuel with erbia at an average concentration of $1.8^{w}/_{o}$.

The behavior of erbia in extended cycles described in the literature indicates that it may be a good candidate for the 36-month cycle. Accordingly, its performance was analyzed by studying the reactivity throughout cycle life of a single assembly and a full core.

3.2.3.3 Calculations for a Single Assembly

Calculations for a single assembly with erbia were performed with CASMO-3. The assembly was successively loaded with 5% and 6% U-235 fuel. Different loadings of Er_2O_3 were analyzed in which both the number of poisoned pins and the concentration of poison were changed. The two group k-infinity predicted by CASMO-3 was plotted versus the assembly average burnup. The results are presented and discussed in the following paragraphs.

Figure 3-5 corresponds to an assembly with 5% U-235 fuel and with different loadings

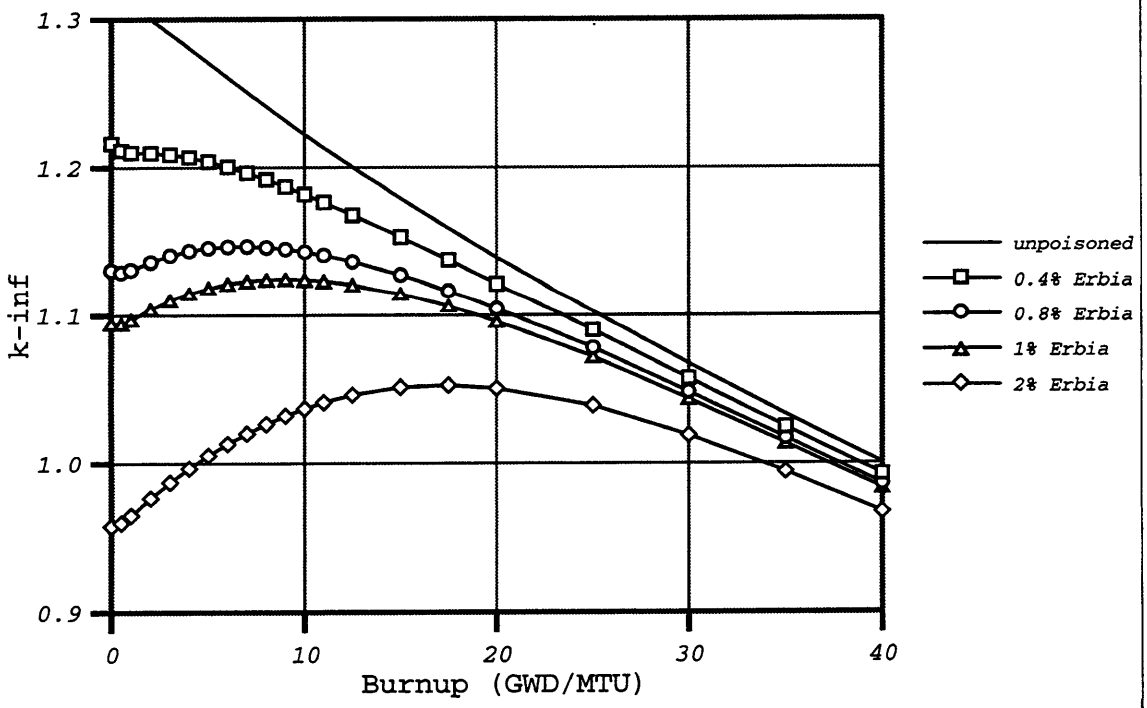

All fuel pins in the assembly are loaded with erbia

Figure 3-5: Assembly k-infinity for varying concentrations of erbia

of erbia in all the fuel pins (264 pins). In this Figure, the effect of increasing the erbia concentration is shown. The assembly reactivity decreases as the content of erbia increases. Considering the curves for two erbia enrichments, i.e. 1% and 2%, the differences in reactivity are larger at BOC, then gradually decrease, and at about 25 GWD/MTU, the curves become almost parallel. The reactivity residual penalty is increasingly larger for higher Er_2O_3 content, and it roughly doubles with twice the Er_2O_3 content. For 0.4% Er_2O_3, the assembly becomes subcritical about 0.8 GWD/MTU earlier than in the unpoisoned case. In the other limiting case, --2% Er_2O_3,-- the assembly life is about 6 GWD/MTU shorter than in the unpoisoned case.

Figure 3-6 corresponds to an assembly with 5% U-235 and different concentrations of erbia in 132 and 60 pins (out of a total of 264 fuel pins per assembly). Since less pins are loaded with the burnable absorber, a higher concentration is required to hold down the same initial reactivity. This figure suggests that, for the conditions of the assembly studied, a large fraction of the fuel pins must be poisoned to provide adequate reactivity control.

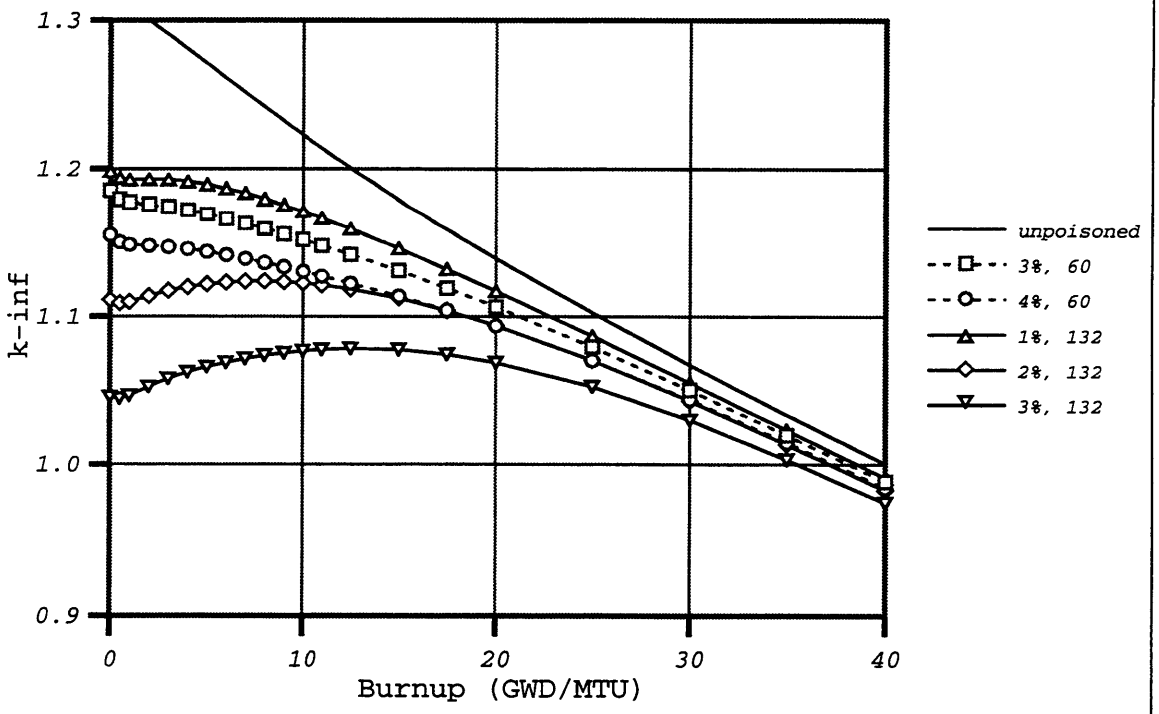

The legend "3%, 60" stands for 3% erbia in 60 pins.

Figure 3-6: Assembly k-infinity for various loadings of erbia

With erbia concentrations of 3% and 4% in 60 pins, the assembly is very reactive in the first half of the cycle. Further increasing the erbia content is not desirable, since fuel properties would degrade and the reactivity penalty would increase. When the poison is incorporated in 132 pins, the required erbia concentration would be between 2% and 3%. For the latter case, the residual penalty is about 5 GWD/MTU.

Figure 3-7 compares the performance of three cases extracted from Figures 3-5 and 3-6. The total amount of erbia in the assembly is the same in two of the cases: 1% Er_2O_3 in 264 pins and 2% Er_2O_3 in 132 pins. In the third case --4% in 60 pins-- the assembly has about 9% less erbia. The reactivity shapes are very close after 10 GWD/MTU with the same residual penalty in the three cases. The assembly with 1% Er_2O_3 in all the fuel pins has lower reactivity at BOC, confirming the interest in a relatively homogeneous distribution of the poison at low concentrations.

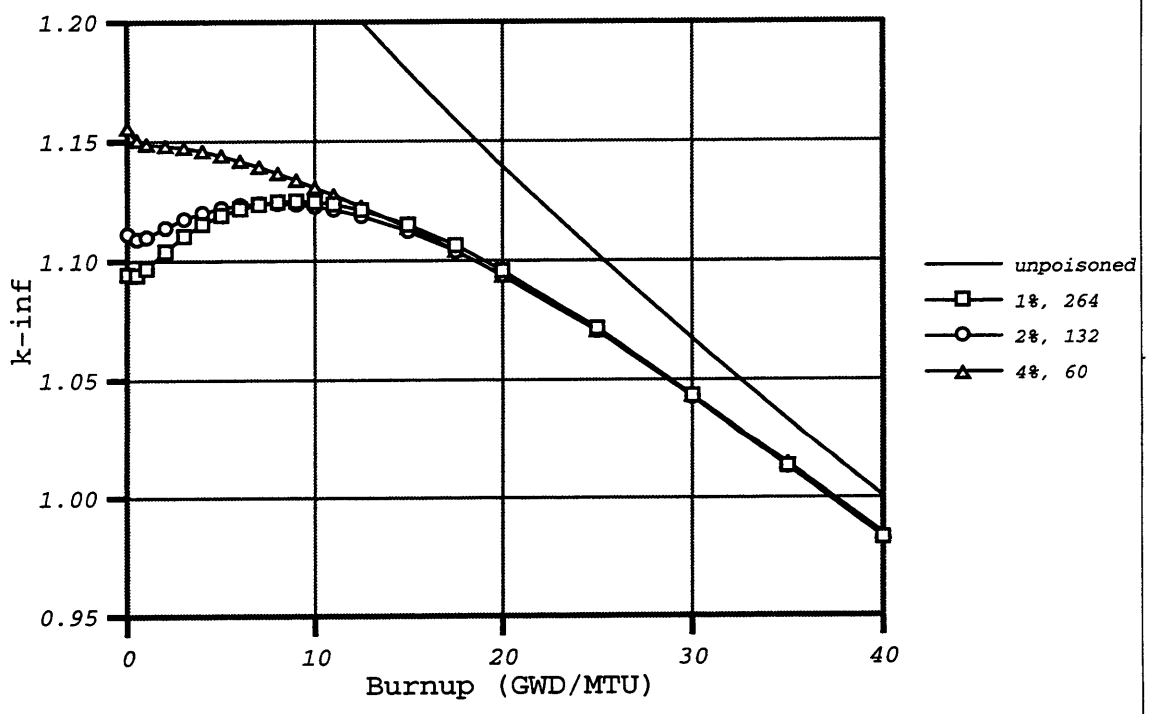

The legend "1%, 264" stands for 1% erbia in 264 pins.

Figure 3-7: Comparison of assembly k-infinities for different loadings of erbia

Similar calculations were performed for fuel with 6% U-235 and the same trends were observed. Figure 3-8 compares a 6% U-235 assembly loaded with gadolinia (10% in 44 pins) and 2 assemblies loaded with erbia (1% and 2% in all the fuel pins). It can be seen that:

- The gadolinia-loaded assembly has the same residual penalty as the assembly with 1% erbia. However, the reactivity of the former is significantly lower until about 35 GWD/MTU. In particular, at BOC, the k-infinity is about 0.16 lower.
- The gadolinia loaded assembly and the assembly with 2% Erbia show a reactivity peak of similar magnitude although at different burnups. However, the erbia loaded assembly has about twice the residual penalty of the assembly with gadolinia (~6 GWD/MTU for the Erbia case versus 3 GWD/MTU for the gadolinia case), and exhibits a higher reactivity in the first half of the cycle.

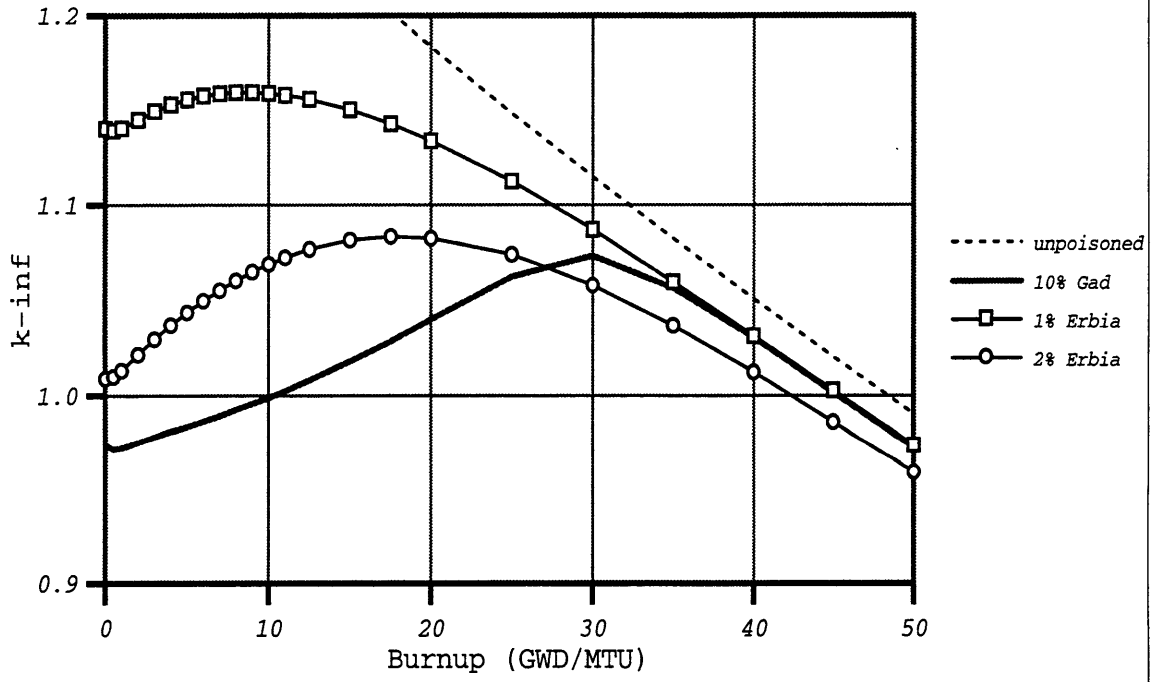

In the gadolinia case, 44 pins are poisoned. In the erbia cases, all the fuel pins are poisoned

Figure 3-8: Comparison of k-infinities for assemblies with erbia and gadolinia

3.2.3.4 Calculations for a Full Core

The previous CASMO-3 calculations for a single assembly provide useful information about the capability of a precise poison configuration to control the assembly reactivity,

and they are particularly useful to compare the performance of different burnable poison distributions.

Simulation of a whole core is a good complement to determine whether the amount of burnable poison in the core is adequate. As discussed earlier, soluble boron makes up for the excess reactivity not held down by the burnable absorbers, but its concentration is to be maintained below 1780 ppm. Modeling a full core allows one to determine whether the boron level is within this limit or, whether on the contrary, the boron concentration is too high and more burnable absorbers are required.

A core was modeled in 2 dimensions with SIMULATE-3 in which all the assemblies but those on the periphery had fuel with 6% U-235 and erbia in all pins. The concentration of erbia varied from 2% in the center assemblies to 1% in the assemblies closer to the periphery, with an average erbia loading in every pin of 1.4%. The peripheral assemblies were loaded with unpoisoned, 3% U-235 fuel. The peak boron concentration in the coolant was 2260 ppm, therefore confirming that the loading of burnable absorbers was not sufficient.

The residual penalty in an erbia poisoned core was quantified by comparing its cycle length with that of an unpoisoned core. All the assemblies in the core had 6% U-235. Every single pin in the core had between 1% and 2% erbia, with an average concentration of 1.31%. The average discharge burnup of the core was 40.26 GWD/MTU, 4.19 GWD/MTU shorter than an unpoisoned core with the same fuel enrichment (see Section 3.1.1). The core poisoned with erbia had a peak boron concentration of 2368 ppm, therefore indicating that the content of burnable absorber needed to be increased. This, of course, would lead to a higher residual penalty. A core with the same fuel enrichment was poisoned with gadolinia and its average discharge burnup was 42.61 GWD/MTU, 2.35 GWD/MTU more than the erbia poisoned core. The peak boron concentration was 2173 ppm, over the acceptable limit, but slightly lower than in the erbia core. These results indicate that the residual penalty for the erbia core is more than double that of the gadolinia core.

These simulations do not represent acceptable core designs since little concern was taken regarding design limits such as peaking factors. In fact, both poisoned cores showed unacceptable power peaking, indicating that more work is required in the distribution of

burnable poison. Therefore, residual penalty and boron levels results are to be taken as approximate values.

3.2.4 Erbium and IFBA

3.2.4.1 Characteristics of IFBA

The Integral Fuel Burnable Absorber (IFBA) is a burnable poison developed by Westinghouse Electric Corporation. It consists of a thin coating of zirconium diboride (ZrB_2), applied on the surface of the fuel pellets. The absorbing material B-10 depletes smoothly and almost completely by EOC. Neutron absorption does not generate residual absorbing daughter products [S-6]. Therefore, the residual penalty in extended cycles is negligible. IFBA has shown its ability to control power distribution and moderator temperature coefficients in 18- and 24-month cycles [S-7].

On the other hand, the boron releases helium after neutron absorption, and this gas accumulates in the rod plenum. As a result, internal pin pressure significantly increases throughout the cycle, raising concerns about clad integrity [H-1].

The smooth depletion rate suggests that IFBA alone does not provide sufficient reactivity control for a 36-month cycle. However, its properties as burnable absorber may be interesting if combined with another poison such as erbia or gadolinia. The simultaneous use of erbia and IFBA is studied in the next Section. A combination of gadolinia and IFBA was used for extended cycles in References [M-1] and [G-2]. McMahon's design [M-1] showed that high concentrations of IFBA yield unacceptable pin internal pressures. Therefore, the thickness of the IFBA coating has to be limited in order to keep this pressure within design limits. Other solutions such as using annular fuel or increasing the plenum length (see [G-2]) provide some extra space to accommodate the gas release, although some fuel is displaced and the cycle is shortened.

3.2.4.2 Calculations and Results

As described in Section 3.2.3, erbia provides good reactivity control at the expense of shortening the cycle length. Decreasing the amount of erbia in the core will reduce the residual penalty. However, this cannot be done unless an alternate burnable poison --such as IFBA-- is introduced. The simultaneous effect of the two poisons is studied here. An assembly was loaded with 6% U-235 and different concentrations of both poisons, and the

k-infinity was analyzed with CASMO-3. The results presented below show that this combination of poisons does not control the assembly reactivity as effectively as gadolinia, especially when the latter is used in a duplex combination (see Section 3.2.2.3).

The assembly with 1% erbia in 132 pins was taken as the reference case in this study. As shown in Figure 3-6, the residual penalty in this assembly is moderate, and the reactivity in the first part of the cycle relatively high. The assembly reactivity is affected by the thickness of the IFBA coating and the number of pins with IFBA.

Figure 3-9 shows the effect of increasing the IFBA loading in a fixed number of pins. Starting with the reference assembly --1% Erbia in 132 pins,-- IFBA coatings of 1.0X, 1.5X, and 2.0X were successively applied to the 132 pins. These loadings 1.0X, 1.5X, 2.0X correspond to the commercially available products from Westinghouse and refer to

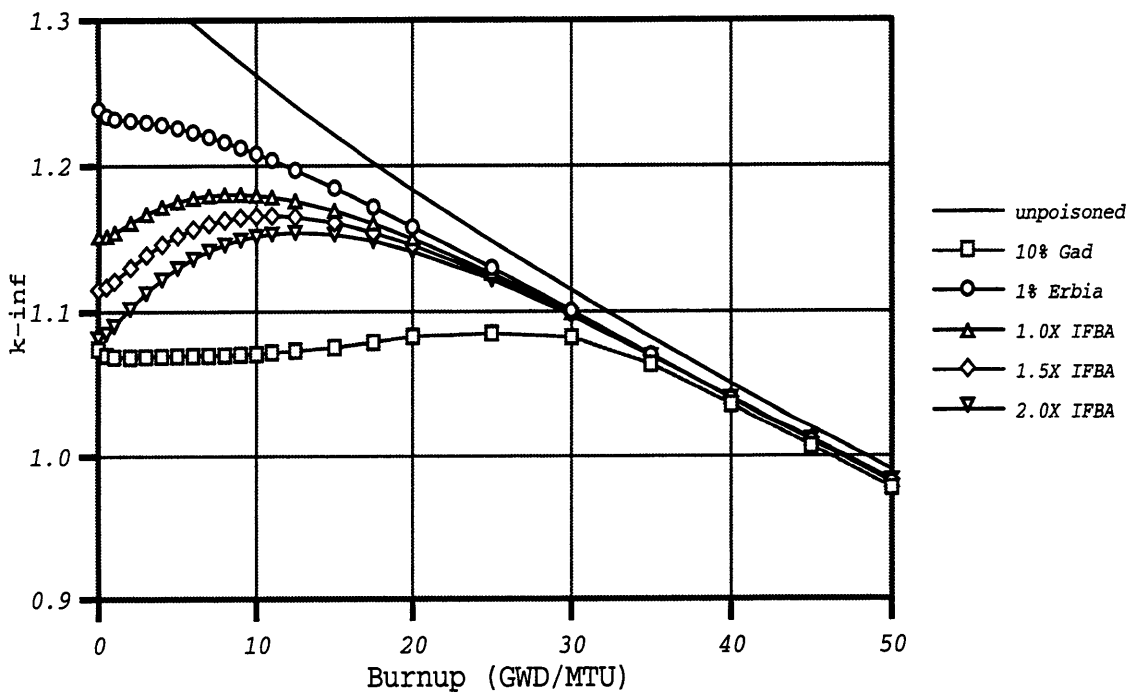

Pins with IFBA also have 1% erbia. All cases with erbia or IFBA have poison in 132 pins. The gadolinia case has 32 poisoned pins.

Figure 3-9: Effect of the combination of IFBA and erbia

the amount of absorber per inch.[2] For example, 1.0X IFBA is a coating with 1.545 mg B-10 /inch. It can be seen in Figure 3-9 that:

- the effect of IFBA is significant until 30 GWD/MTU. Afterwards, all the curves overlap and no residual penalty is added to that of the reference case;
- increasing the amount of IFBA significantly lowers the initial reactivity of the assembly. In particular, the initial k-infinity is reduced by 0.0875 for the case of 1.0X IFBA, and by 0.157 for 2.0X IFBA;
- the reactivity peak takes place later in cycle as the amount of IFBA increases;
- thicker IFBA coatings lead to steeper gradients in the k-infinity in the first part of the cycle, up to ~30 GWD/MTU in the figure for 2.0X.

Figure 3-10 shows the effect of changing the number of pins with IFBA. The reference assembly is loaded with only 1% Erbia in 132 pins. Three cases were analyzed which incorporated 1.0X IFBA in 40, 60, and 132 fuel pins. IFBA was applied only in all or part of the pins that contain erbia. The effect of IFBA is significant when it is loaded in

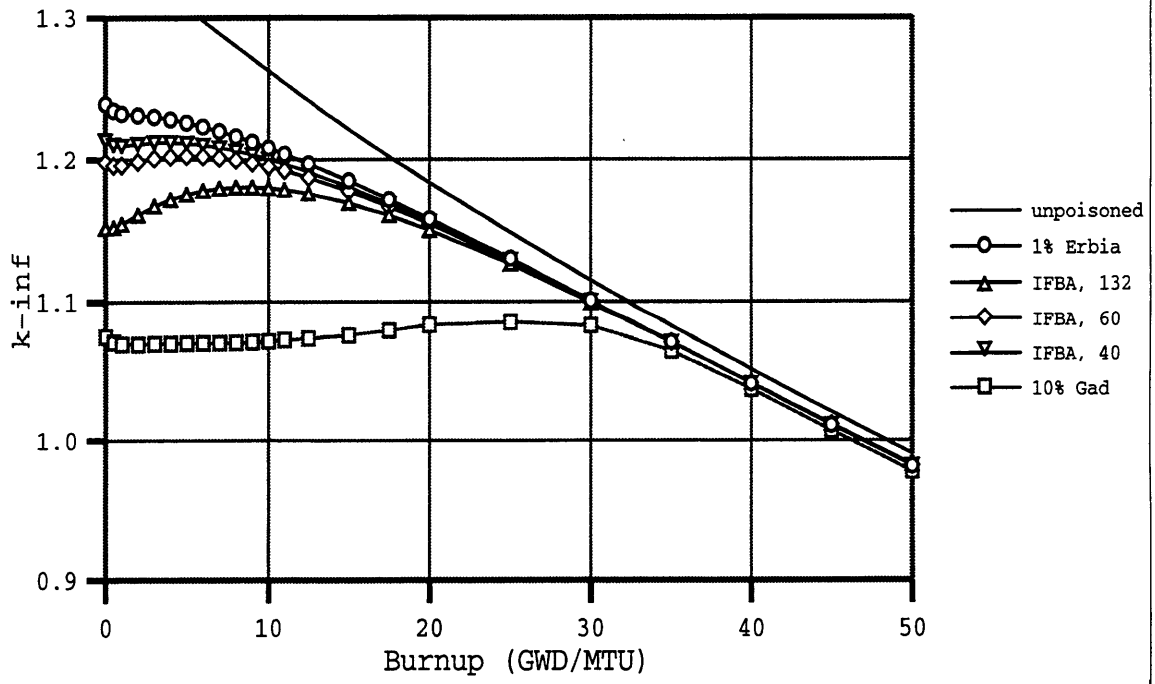

For the cases with IFBA, the assembly has 1% erbia in all pins plus IFBA in the number of pins indicated. For the case with gadolinia, the assembly has 32 poisoned pins.

Figure 3-10: K-infinity of an assembly with erbia and IFBA in varying number of pins

2. Recent indications are that 2.0X is no longer offered

a large fraction of the pins. The residual reactivity penalty caused by IFBA is negligible. In addition, both Figures 3-9 and 3-10 show the reactivity of an assembly poisoned with 10% Gd_2O_3 in 32 pins. This gadolinia loaded assembly keeps the reactivity at significantly lower levels than any of the erbia-IFBA combinations, with only a small increase in residual penalty.

An assembly with erbia in all pins and IFBA in some of them was not analyzed because of the limited capabilities of CASMO-3 to deal with a large number of burnable absorber regions. In particular, using erbia in all pins and collocating IFBA in more than 40 pins will cause an execution error in the code.

3.3 Conclusions

Reactivity analysis shows that an adequate and appropriately tailored distribution of gadolinia within the assembly may yield a fairly constant reactivity for a significant part of the cycle. The concentration of gadolinia controls the burnup kinetics, and the number of poisoned pins changes the level of reactivity. An optimal distribution is found by loading two sets of pins with two different concentrations of gadolinia in the same assembly.

In spite of the positive performance of erbia reported elsewhere (Refs. [L-1], [J-1], [J-2]), this analysis found that the high residual penalty outweighs the other benefits for the 36-month cycle. The high U-235 enrichment in the fuel would require a significant amount of poison that would lead to a very high residual penalty. The preliminary analysis of two cores loaded with erbia and gadolinia show that the discharge burnup is over 2.3 GWD/MTU lower for erbia. Moreover, the reactivity of the assemblies gradually increases for part of the cycle as erbia burns out. This would lead to undesirable shifts in the core power distribution.

IFBA is an effective burnable poison capable of holding down part of the excess reactivity in an assembly with 6% U-235. Its effect is considerable at the beginning of the cycle and gradually decreases as the B-10 burns out. For the case study, the effect of IFBA completely disappears after 30 GWD/MTU.

When a thick coating of IFBA is used, i.e. 2.0X IFBA, the reactivity hold down is more significant and its effect more lasting. However, the pin internal pressure consider-

ably increases due to helium production, degrading the fuel performance. Previous experience with extended cycles indicates that fuel pins have to be redesigned in order to meet the design limit for the pin internal pressure. If the IFBA content is kept at lower values (i.e. 1.0X IFBA), then the proposed erbia loading --1%Er_2O_3 in 132 pins-- is not sufficient to keep the assembly reactivity within acceptable limits. Therefore, a higher amount of erbia is required, which would result in a higher residual penalty.

To sum up, the combination of erbia and IFBA does not provide the desired reactivity control for extended cycles, and does not match the capabilities of gadolinia.

Chapter 4

Design of Peripheral Assemblies

The peripheral assemblies are a key element in the optimization of the neutronic and economic performance of the core. Multibatch cores load low reactivity assemblies --discharged from previous cycles-- in the periphery in order to reduce radial leakage, therefore reducing reactor vessel irradiation. This strategy also improves the neutron economy. However, the multibatch option is not available in the present core.

Applicable research, primarily focused on improving uranium utilization, has been conducted since the 1970's. Several ideas have been reported that include backfittable ([I-1], [F-1]) as well as nonbackfittable ([F-2],[M-5],[L-2],[U-1]) core concepts. The latter require structural modifications or changes in the reactor vessel.

In this chapter, four options are analyzed for the peripheral assemblies of the 36-month cycle and compared to each other.

4.1 Approach

The four strategies selected for analysis are:

- use several rows of natural uranium in the outer part of the assemblies;
- use peripheral assemblies for 2 cycles;
- use reflectors of beryllium;
- load the periphery with assemblies discharged from a previous cycle.

The neutronics and economics performance of these options are compared by using the same loading pattern in the common part of the core, that is, all the core but the peripheral assemblies. The main criterion to select the most desirable option is the core economics, provided that cycle length is acceptable and peaking factors are within limits.

The non-peripheral assemblies are enriched to 6% U-235, and poisoned with gadolinium oxide as indicated in Figure 4-1. This figure only includes the 149 assemblies that are common to the four options, that is, all the core but the peripheral assemblies.

The cores are modeled in 2 dimensions with SIMULATE-3. There are some differences in the results of a 2-D model and a 3-D model having the same axially uniform fuel

configuration. However, the 2-D models are accurate enough for the scoping studies performed here. Of particular attention is the analysis of peaking factors. The design limit for F_Q mentioned in Section 2.5.1 refers to the total core peaking, which includes both axial and radial effects. In a 2-D model, only the radial effect is accounted for. A conservative radial peaking design limit for this case can be obtained if the F_Q limit is divided by the $F_{\Delta H}$ limit:

$$\frac{2.5}{1.65} = 1.52$$

This assumes that both peaks --radial and axial-- take place simultaneously in core life, which is not generally the case. For the type of core design in this study, experience with 2-D and 3-D models showed that radial peaks of up to 1.60 in 2-D models will yield $F_{\Delta H}$ values around 1.55 (below the 1.65 design limit) in the 3 dimensional representation.

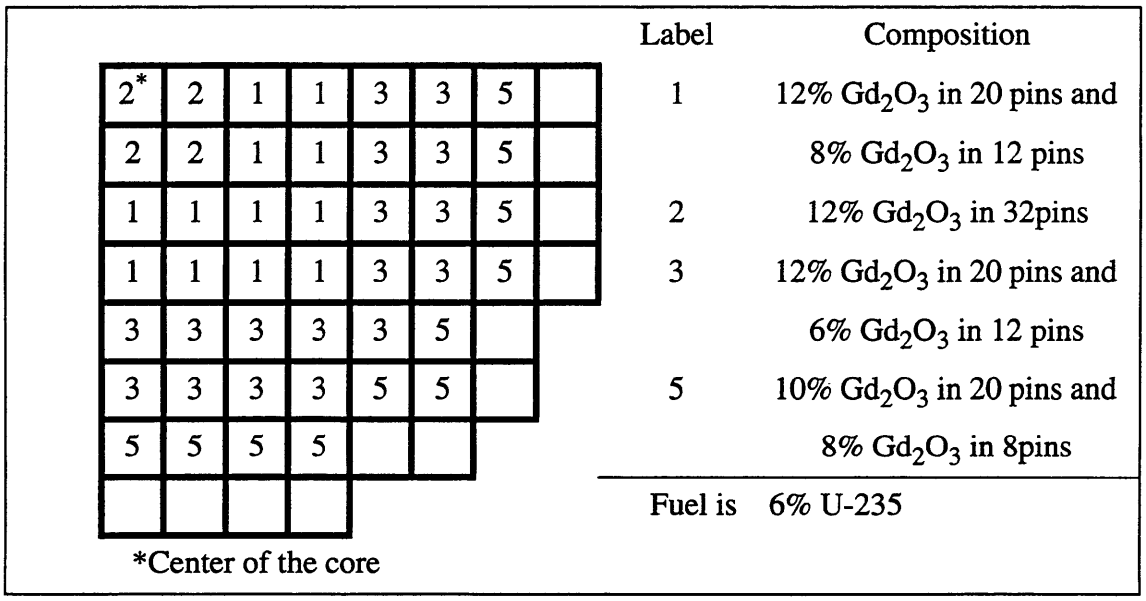

Figure 4-1: Loading of assemblies in the core interior for analysis of the periphery

4.2 Natural Uranium as Radial Blanket

Radial leakage may be reduced by using natural uranium in the outer rows of pins in assemblies on the periphery. This concept is included in the 44.6-month core designed in [M-1], which also indicates that the core performed best when using 4 rows of natural ura-

nium. Adding more rows of natural uranium pushes power towards the center of the core and increases power peaking. In McMahon's design [M-1], the peripheral assemblies have 2 regions: the inner region is made of annular unpoisoned fuel with the same enrichment as the rest of the core, whereas the outer region is made of natural uranium.

The performance of a 6% U-235 core with radial blankets of this design yields a core average discharge burnup of 40.96 GWD/MTU, or equivalently, 34.8 EFPM. The total core costs are $105.9 M/yr. The average burnup of the peripheral assemblies is 25.07 GWD/MTU, about 61% of the core average. Since the periphery generates a good fraction of the power, radial peaking is well controlled and the maximum radial peaking factor is 1.44. The maximum CBC is 1819 ppm, slightly over the limit, although a small increase in the amount of burnable poison in the core will be enough to bring this parameter within limits.

4.3 Use of Periphery for Two Cycles

4.3.1 Model

Since the periphery runs at lower power than the rest of the core, the assemblies in this area have a lower discharge burnup. One strategy to improve the uranium utilization is to use the peripheral assemblies for two cycles. Two possibilities are considered:

1. use enrichment lower than core average, i.e. 3% U-235;
2. use natural uranium in the outer rows of pins, as described in Section 4.2.

In both cases, the peripheral assemblies discharged from one cycle are shuffled to another location in the periphery since not all positions lead to the same assembly burnup. Shuffling maximizes the uranium utilization by locating less-burned assembies in more reactive positions. The shuffling scheme is provided in Figure 4-2. The notation indicates that assembly B1 is shuffled to B2 in the next cycle. In the SIMULATE-3 model, the assemblies are divided into 4 quadrants. The two quadrants facing the core interior have a higher burnup than the two quadrants facing the core shroud. When shuffling is performed in option 1), the peripheral assemblies are rotated 180^{o} to present the less burnt half to the interior of the core. However, this is not done for option 2) because the enrichment of the outer rows is already reduced.

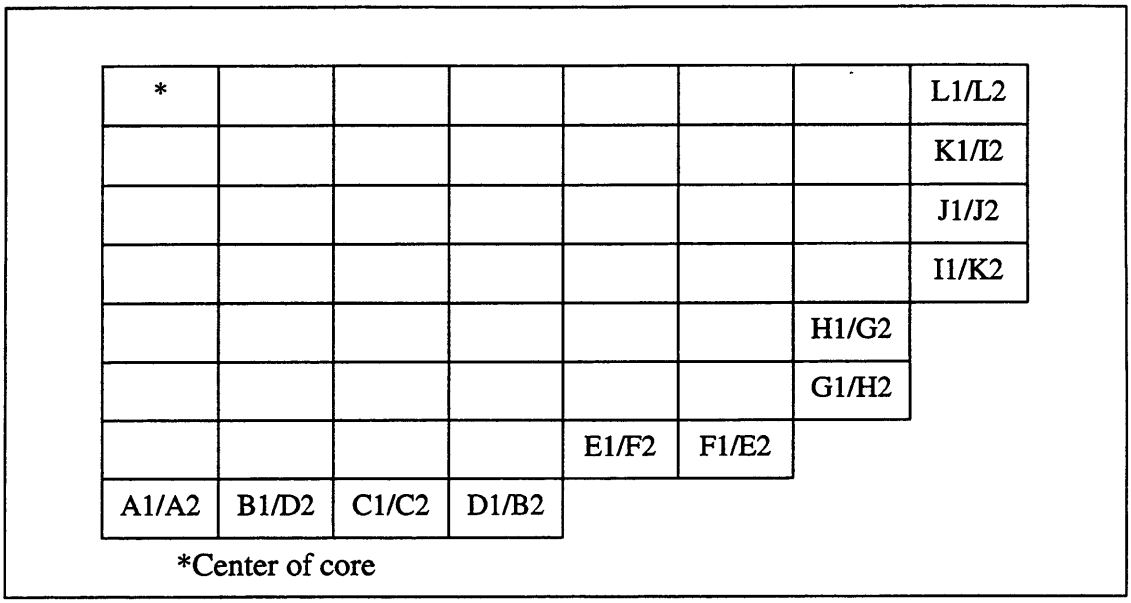

Figure 4-2: Shuffling scheme for peripheral assemblies

4.3.2 Results and Discussion

4.3.2.1 Periphery at 3% U-235

The average relative power fractions of the periphery at various points in core life are given in Table 4-1. The energy extracted from the periphery is far below the core average, especially during the second cycle, when the periphery is partially depleted and the core interior has the same reactivity as in the first cycle. For cycle 1, the power drawn from the periphery is between 0.41 and 0.60 of core average, whereas for cycle 2, it is between 0.27 and 0.49. In both cases, the periphery produces more power at the EOC, when the rest of the core is depleted.

Table 4-1: Average relative power fraction of the peripheral assemblies

	BOC	At step having max F_Q	EOC
Cycle 1	0.53	0.41 (at 12 GWD/MTU)	0.60
Cycle 2	0.33	0.27 (at 15 GWD/MTU)	0.49

The main core parameters are included in Table 4-2. The average discharge burnups of the core are 38.24 and 36.11 GWD/MTU for the first and second cycle, respectively. The average burnup of the periphery during the first cycle is 17.18 GWD/MTU, about 45% of

core average, whereas for the second cycle, the periphery is burned for 11.81 GWD/MTU or 33% of core average.

The lower reactivity of the periphery in the second cycle has two main consequences. First, the second cycle is about 2 GWD/MTU shorter. Second, the radial peaking increases as more power is produced in the inner assemblies. Peaking is within acceptable limits for the first cycle, but it is over the design limit for about 3/5 of the second cycle. The core costs are about $7.5M/yr more expensive for the first cycle since it includes the cost of 193 assemblies versus 144 in the second cycle. The average cost of the two cycles is $ 101.8 M/yr.

Table 4-2: Core performance with 3% U-235 in peripheral assemblies

	B_d (GWD/ MTU)	Peak pin exposure	Max CBC (ppm)	Max F_Q	Total core costs ($M/yr)
Cycle 1	38.24	52.23	1622	1.50	105.5
Cycle 2	36.11	52.49	1548	1.66	98.1

4.3.2.2 Natural Uranium in the Outer Rows of Pins

In this case, the peripheral assemblies have the configuration described in Section 4.2, that is, 4 rows of natural uranium in the outer part, and 6% U-235 annular unpoisoned fuel in the inner part. These assemblies are now kept for 2 cycles in the core.

The main parameters for both cycles are given in Table 4-3. The core discharge burnup is almost 4 GWD/MTU lower during the second cycle, due to the depletion of the periphery. The average burnup of the peripheral assemblies is 25.07 GWD/MTU and 14.3 GWD/ MTU for the first and second cycles respectively.

Table 4-3: Core performance with RBAs for two cycles

	B_d (GWD/ MTU)	Peak pin exposure	Max CBC (ppm)	Max F_Q	Total core costs ($M/yr)
Cycle 1	40.96	51.79	1819	1.44	105.6
Cycle 2	37.04	63.09	1621	1.55	95.9

Radial peaking is controlled during the first cycle, but high for the second cycle. If the burnup of the periphery could be controlled, this region would be more reactive during the second cycle. Adding some poison to the peripheral assemblies decreases their reactivity for part of the first cycle, therefore reducing their burnup. However, as the poison depletes, the power shifts towards the periphery resulting in high peaking factors. The discharge burnup after one cycle is slightly lower than for the case of an unpoisoned periphery. However, the effect on the second cycle is not significant, and the power is concentrated in the center of the core.

The Table shows two additional concerns:

- the most exposed pin is in a peripheral assembly and hits the design limit for peak pin exposure by the end of the second cycle;
- the maximum CBC is slightly over the limit. As discussed earlier, this parameter can be controlled with a small increase in the amount of burnable poison in the core.

Total core costs are almost $10M/yr more expensive for the first cycle. The average for both cycles is $100.8 M/yr, about $1M/yr less expensive than in the previous case.

4.4 Reflectors of Beryllium

4.4.1 Introduction

Neutrons leaking radially from the core travel through the borated water, and the structural materials --core shroud and core barrel-- and many of them are absorbed in these elements. Some neutrons are reflected and go back into the fuel assemblies. Changing the thicknesses of the water gap and core shroud may improve uranium utilization [M-5]. However, this is a nonbackfittable concept and hence beyond the scope of this study. Nevertheless, neutron economy may be improved if an adequate material reflects the leaking neutrons back to the core. A good reflector such as beryllium oxide (BeO) can yield an improvement in uranium utilization of 5% [M-5]. This material has been used in test reactors, but not commercial LWRs. Other reactivity analyses with the code PDQ-7 indicate that the maximum savings in ore when using a BeO reflector is 5.0% [F-2]. The reflector capabilities of BeO increase with thickness, significantly up to 12 inches and moderately thereafter, as shown in Figure 3-10 of [M-5].

Use of reflectors will increase the neutron flux in the peripheral assemblies, and, therefore, the power drawn from this region. The combination of an optimized poisoning scheme and a reflector would ideally lead to perfect flattening of the power distribution. Assuming a realistic value for the intra-assembly peaking factor of 1.1, the maximum core average discharge burnup that could be obtained from the core is approximately and optimistically on the order of

$$\frac{60}{1.1} = 54.54\frac{GWD}{MTU}$$

4.4.2 Model

The existing gap between the core baffle and the core shroud is small in the PWR considered in this study. Therefore, there is not much space available to insert a BeO reflector. In order to retrofit this design, BeO reflectors have to replace the outer ring of assemblies.

The analysis is carried out in two steps. First, BeO reflectors of different thicknesses are added to a full core, in order to measure its effectiveness. Second, the reflector is applied to a smaller core, in which the BeO substitutes for the outer ring of assemblies.

For the first step, the reference case is a core with the configuration of Figure 4-1 and the periphery at 3% U-235. The core is analyzed using reflectors 10 cm and 21 cm thick, cases labelled C-I and C-II respectively. The reflector is modeled as a water gap, a slab of BeO and a 2-cm thick steel plate.[3] Further analyses showed that moderate changes in the dimensions of the water gap do not have any influence on the results.

4.4.3 Results

The main results for these two cases and the reference case are shown in Table 4-4. When compared to the reference case, the 10- and 21-cm reflectors increase the core discharge burnup by 6.1% and 7.4% respectively. Furthermore, the maximum and average peaking factors are significantly reduced. For the 10-cm reflector, the maximum F_Q is reduced by almost 5% and takes place near the center of the core. For the thicker reflector, the periphery is more reactive, and the peak takes place in one of the assemblies close to it, and it is slightly higher than for the previous case. For case C-II, the discharge burnup of

3. Modeling the reflector with CASMO-3 as a single slab of BeO yields negative values in some cross sections, causing an error in the execution of the code.

Table 4-4: Core performance with reflectors of beryllium oxide

Label	Case	B_d (GWD/ MTU)	ΔB_d	F_Q	Core costs ($M/yr)	Cycle length (EFPM)
	Reference	38.24	-	1.50	105.5	32.5
C-I	Reflector 10 cm	40.57	6.1%	1.43	101.1	34.5
C-II	Reflector 21 cm	41.06	7.4%	1.46	100.3	34.9
C-III	144 assemblies	44.16	15.5%	1.29	104.6	29.0
C-IV	idem opti-mized	45.29	18.5	1.33	102.5	29.8

the peripheral assemblies increases by 6.76 GWD/MTU or 39.3% with respect to the reference case.

The increase in cycle length yields a significant economic benefit since the total fuel costs are the same. Savings of more than $5M/yr can be made by using a reflector 21 cm thick. The additional costs of the BeO reflector are not included in the analysis.

In the second step, the outer ring of assemblies is substituted by a reflector of BeO, modeled as a plate 21.4 cm thick, which is the size of the assembly box. This results in a smaller core, with only 144 assemblies. In order to produce the same thermal output, the average power density has to be increased. This has several important consequences:

- a higher coolant flow is required to insure compliance with thermal hydraulics criteria;
- more energy is stored in each rod, creating concerns for transient and LOCA analysis;
- peaking has to be radically restrained to avoid spots with very high heat generation rate.

Two cores are modeled with this scheme. In the first one (case C-III), the pattern of Figure 4-1 is used. This model is kept for comparison with previous cases but can be optimized if more reactive assemblies are loaded in the outer ring to take advantage of the improved reflective properties (case C-IV). The main parameters for both cases are

included in Table 4-4. The discharge burnup is higher than in the case with 193 assemblies, up to 18.5% improvement in the optimized case. This burnup is still far below the maximum theoretical of 54.54 GWD/MTU. The average burnup of the periphery is 38.0 GWD/MTU, or 83.9% of the core average. Figure 4-3 shows a 3 dimensional representation of the discharge burnup of the optimized case in an assembly basis.

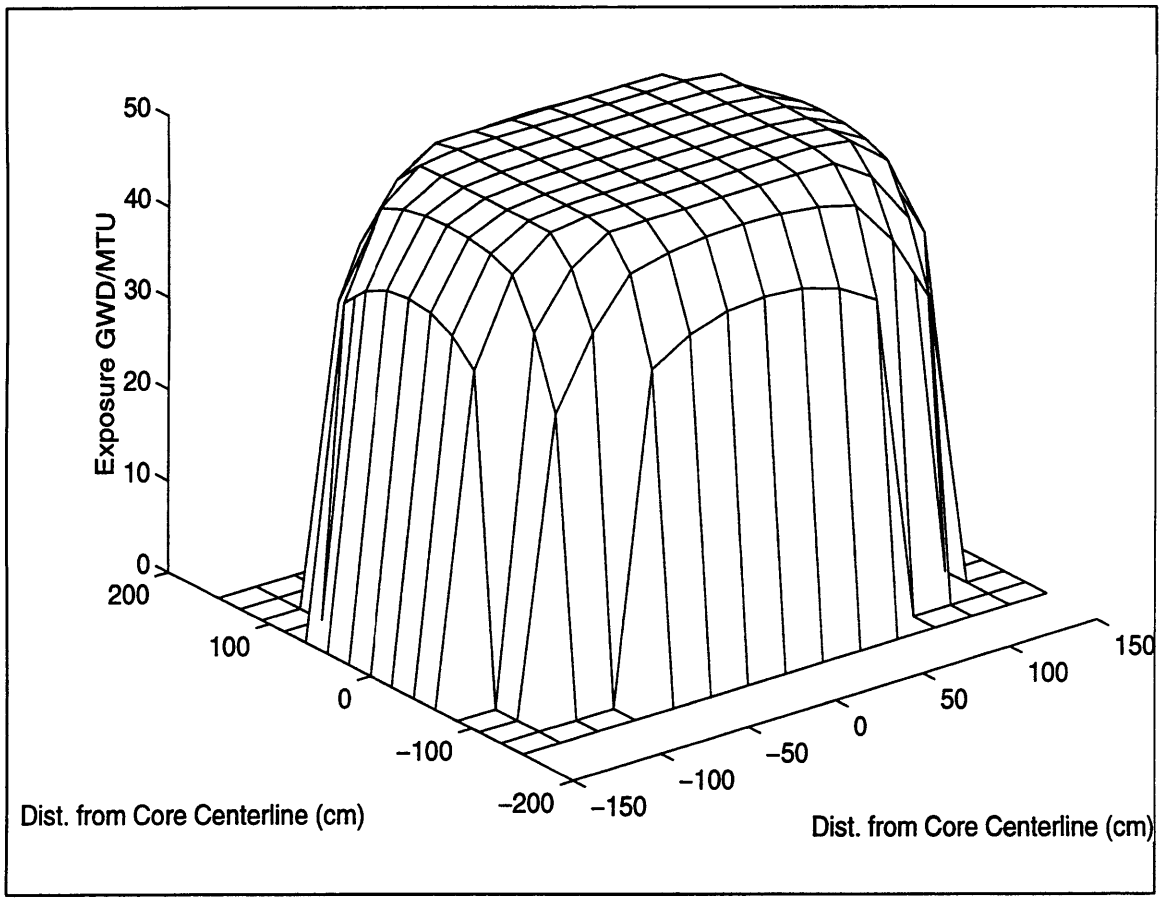

Figure 4-3: Discharge burnup on an assembly basis for an optimized core with 144 assemblies and a reflector of BeO

The maximum peaking factors are reduced by 14% and 11%, respectively, with respect to the reference case. In the optimized case, the change in power distribution results in a slightly higher peaking factor. However, the reduction in fuel material yields a significantly shorter cycle length, which is the product of heavy metal mass times burnup. Comparison of costs for C-III and the reference case shows that the 15.5% increase in discharge burnup only yields a $1M/yr benefit in the core costs. The smaller core also yields a shorter cycle than the optimum cycle length.

4.5 Shuffling Interior Assemblies into the Periphery

4.5.1 Model

The assemblies discharged after one cycle are depleted to a high extent but still contain fissile material. Thus, the core periphery may be loaded with assemblies discharged from internal positions of the previous cycle. This strategy may provide an economic benefit since each reload contains only 144 fresh fuel assemblies and fuel costs are lower. On the other hand, two drawbacks may be anticipated:

- the low reactivity of the reused assemblies requires a good distribution of power over the rest of the core in order to control radial peaking;
- assemblies staying for two cycles in the core are likely to hit the peak pin exposure limit.

The core is modeled with the fresh fuel loading of Figure 4-1. For the first cycle, discharged assemblies are not available and the periphery is loaded with 3% U-235 unpoisoned fuel. After depletion to EOC, the periphery of the second cycle is loaded with discharged assemblies according to the scheme of Figure 4-4. In this Figure, the assembly labelled A1 is shuffled into the location A2 in the next cycle. The results of this cycle are slightly dependent on the initial configuration of the periphery. A third and fourth cycle are modeled with the same shuffling scheme in order to get an equilibrium cycle in which the effects of the initial periphery completely fade out. When shuffled, assemblies are rotated 180° to present the less burned face to the core interior.

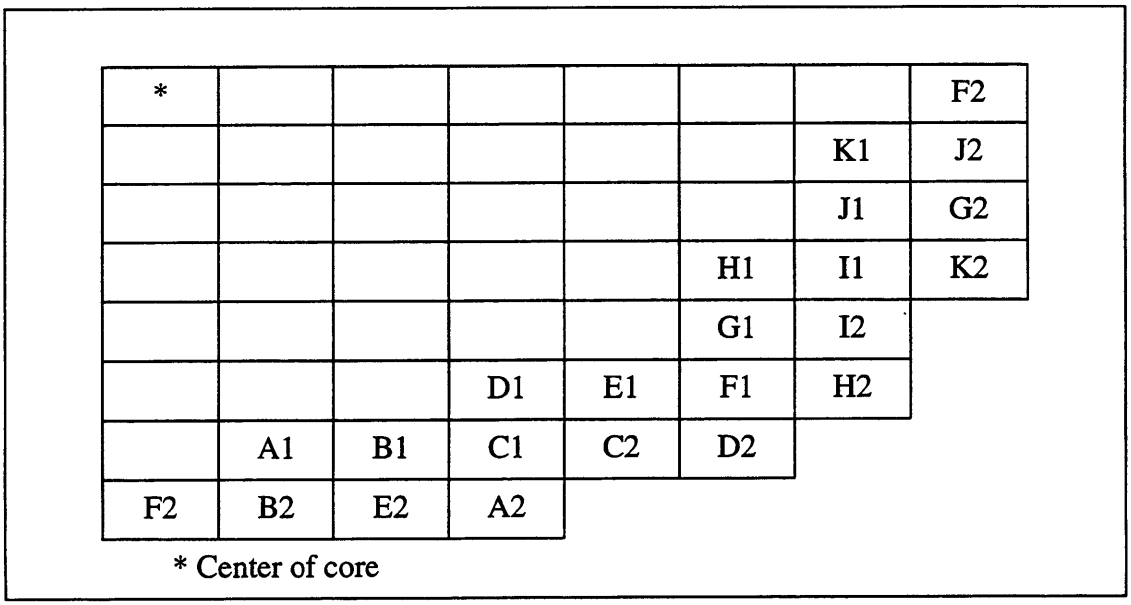

Figure 4-4: Scheme to shuffle 44 interior assemblies into the periphery

4.5.2 Results

The main results for cycles 1 to 4 obtained with this strategy are given in Table 4-5. The first cycle is longer than the following cycles since the initial periphery (3% U-235) is more reactive than the discharged assemblies. The discharge burnups of cycles 3 and 4 are very close. In fact, the difference is only 0.18 GWD/MTU, less than 0.5%. Cycle 3 is hence considered the equilibrium cycle. Radial peaking is lower in the first cycle because more power is drawn towards the periphery. Core costs for the equilibrium cycle are \$6 to \$10M/yr lower than in the options presented in Sections 4.2, 4.3 and 4.4.

Table 4-5: Shuffling assemblies into peripheral positions: core performance

Cycle #	B_d (GWD/ MTU)	Peak pin exposure	CBC	F_Q	Core costs (\$M/ yr)
1	38.24	52.28	1622	1.50	93.7
2	36.52	58.64	1551	1.61	96.9
3	37.19	56.27	1579	1.56	95.5
4	37.01	56.93	1573	1.57	96.0

Figure 4-5 shows the discharge burnup for cycle 3 for the assemblies in a quarter core. The assemblies discharged after one cycle in the core have an average burnup of 47.23 GWD/MTU. The average discharge burnup of the shuffled assemblies after two cycles is 49.29 GWD/MTU. These assemblies have an average depletion of 35.1 GWD/MTU and 14.2 GWD/MTU for their first and second cycle in the core respectively. In summary, the burnup of one cycle is 37.19 GWD/MTU, and the burnup of all the discharged assemblies is 47.75 GWD/MTU.

An additional benefit might be obtained if more assemblies are reused in the core. There are 2 main constraints on an increase in the number of shuffled assemblies:

- the burnup of the additional assemblies that would be reused is relatively high after 1 cycle;
- there are few locations aside from the periphery where assemblies can run at relatively low power in the second cycle.

The possibility of reusing 48 assemblies, i.e. 4 more than previously, is analyzed here. In the new shuffling scheme, assemblies from locations B-8, H-14, D-12 (see Figure 4-5)

	H	G	F	E	D	C	B	A
8	47.24*	47.63	48.90	49.28	48.84	45.99	37.99	44.51
9	47.63	47.93	48.99	49.22	48.67	45.63	37.32	51.28
10	48.90	48.99	49.16	48.99	48.04	44.33	35.08	50.76
11	49.28	49.22	48.98	48.29	46.56	41.44	30.00	47.54
12	48.84	48.67	48.03	46.56	46.39	36.19	48.13	
13	45.99	45.61	44.31	41.44	36.19	26.27	51.31	
14	37.99	37.23	35.04	29.99	48.11	51.30		
15	44.51	51.06	50.72	47.44				

*Center of core

Figure 4-5: Assembly discharge burnup for the equilibrium shuffled-to-periphery cycle

and symmetric positions in the rest of the core are reused for a second cycle. Location C-13 and its symmetric counterparts in the core are the additional positions where the reused assemblies are loaded for a second cycle. The simulation performed for a 2-D model indicates that the average discharge burnup is 36.26 GWD/MTU, almost 0.8 GWD/MTU shorter than before. Fuel costs are reduced, but the economic advantage of reusing 4 more assemblies is almost completely eliminated by the loss in cycle length. The total core costs are only about $0.2 M/yr less costly in this case. Furthermore, the power is slightly pushed towards the center of the core, and the peaking factors increase. The economic benefit is very small and does not justify the worsening of the neutronics performance. So, given the constraints of this analysis, reusing 44 assemblies is a better option than reusing 48 assemblies.

4.6 Discussion and Conclusions

Four main options have been analyzed for the peripheral assemblies. Within each option, one or more cases have been explored, as listed in Table 4-6.

Table 4-6: Summary of cases analyzed for the peripheral assemblies

Label	Description
A-I	4 rows of natural uranium in the peripheral assemblies. No reuse
B-I	Use periphery for two cycles. Assemblies with 3% U-235
B-II	Use periphery for two cycles. Assemblies with 4 rows of U-nat.
C-I	Reflector of Be, 10 cm thick, outside core
C-II	Reflector of Be, 21 cm thick, outside core
C-III	Smaller core (144 assemblies), & reflector assemblies of BeO
C-IV	Smaller core (144 assemblies), improved distribution & reflector of BeO
D-I	Reuse 44 assemblies in the periphery
D-II	Reuse 48 assemblies in or near the periphery

Table 4-7 summarizes the neutronics and economics performance of the most favourable case for each option. Option D-I is the most economic of the four. It is over $10M/yr less expensive than option A-I (similar to the design in Ref. [M-1]) and over $6 M/yr less expensive than options B-I and C-IV. This economic advantage stems from the lower annualized fuel costs, due to the lower number of fresh assemblies in each reload.

Radial peaking for option D-I is slightly over the desired limit (1.52) and higher than in options B-I and C-IV. However, this value can be reduced by improvements in the radial distribution of assemblies and axial zoning (see Chapter 5). Option D-I yields a 33.7 calendar month cycle, shorter than the targeted 36 months. This limitation can be surmounted by increasing the fuel enrichment to 6.5% U-235.

In summary, the best economic performance is obtained when 44 assemblies from the first inward ring are reused in the periphery of the next cycle. The preliminary analysis suggests that the neutronics parameters will meet the design limits, and indicates that the fuel enrichment is to be increased.

Table 4-7: Comparative performance of the different options for the periphery

	A-I	B-I	C-IV	D-I
Burnup (GWD/MTU)	40.96	37.17 (38.2/36.1)*	45.29	37.19
Calendar months	37.0	33.7 (34.7/32.7)*	31.7	33.7
Maximum peaking	1.44	1.66	1.33	1.56
Max CBC (ppm)	1819	1622	1708	1579
Fuel costs ($M/yr)	83.7	78.3	78.3	72.4
Total costs ($M/yr)	105.9	101.7	102.5	95.6

* The bottom values refer to the first and second cycles respectively. The top value is the average of both cycles.

Chapter 5

Axial Zoning

5.1 Introduction

Power generation is not uniform in the axial direction. Neutrons leak through the top and bottom of the core, reducing the energy extracted from the rod ends. The coolant temperature in the bottom half of the core is lower than in the top half, leading to increased moderation and higher thermal flux in this region. As a result, the typical power shape for axially uniform fuel rods is a cosine type, skewed towards the bottom. This power shape changes throughout core life as fuel depletes, and peaking shifts to other axial locations.

In this Chapter, the axial blankets are analyzed for the 36-month cycle in order to obtain the optimum composition. Then, the benefits of axially zoning the burnable poison concentration are shown.

5.2 Axial Blankets

Neutrons leak axially through the top and bottom of the core. Optimization of neutron economy calls for implementation of strategies that minimize axial leakage. Current PWR cores use axial blankets of lower enrichment than core average, thus improving uranium utilization in these regions. The optimum length for axial blankets determined in a published Westinghouse analysis is 15.24 cm [M-1].

5.2.1 Model

For the 36-month core, axial blankets are analyzed with enrichments ranging from 6.5% to 3%. The axial blankets incorporated in this core are composed of unpoisoned annular fuel pellets with 10% void. In addition to reducing fuel mass (hence cost), annular fuel provides some extra space to accommodate fission gases, therefore reducing the pin internal pressure. Unpoisoned fuel also provides more reactivity in the axial blankets by increasing the H/U ratio, drawing more power to these regions, and reducing the peaking

factors in the center of the core. This effect is graphically shown and explained in the next Section.

The analysis is performed with 3-dimensional models in SIMULATE-3. The core is enriched to 6.5% U-235 with the assembly composition of Figure 5-1. The peripheral assemblies are shuffled from a previous cycle, following the strategy described in Figure 4-4 (Section 4.5). The performance of the core is assessed by comparison of the values from the equilibrium cycle.

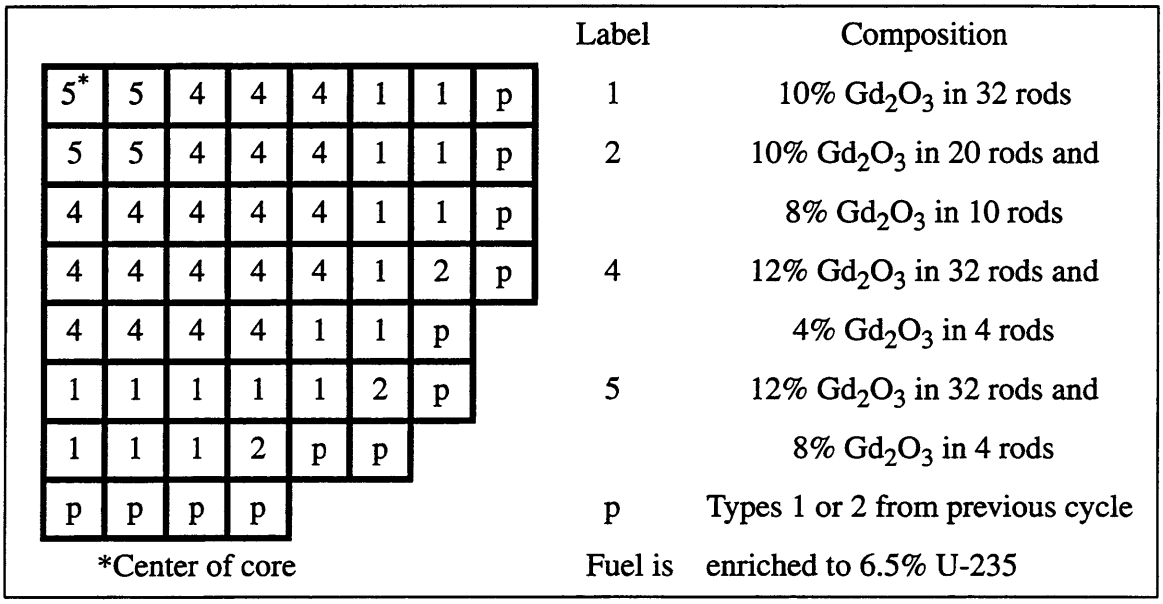

Figure 5-1: Loading of assemblies in the core used to evaluate axial fuel options

5.2.2 Performance

5.2.2.1 Comparison of Parameters

Table 5-1 compares the performance of the core for the cases analyzed. The first case corresponds to an axially uniform core, without axial blankets, which is taken as reference. Then, six cases are listed in which the axial blanket enrichment ranges from 6.5% to 3%.

It can be observed in the table that:

- The core without axial blankets --axially uniform rods-- has an average discharge burnup 0.86 GWD/MTU lower than the core with axial blankets at 6.5%. The only difference between these two cores is that the fuel is annular and unpoisoned in the

axial blankets of the latter case. Total costs are essentially the same for both cores, but they are spread over a longer cycle in the second case, yielding an economic benefit of $1.4M/yr.

- Reducing the enrichment of the axial blankets yields lower core average burnups since the content of fissile material decreases. However, the fuel costs (not indicated in the table) also decrease due to the lower enrichment in the blankets.The effects are balanced, and the total annual costs are very similar for blanket enrichments between 6.5% and 3% U-235. The minimum costs occur for blankets at 4%-5% U-235 but the differences among all the cases analyzed are below $0.2 M/yr.
- The reference case (no blankets) has the same burnup as a core with about 4.5% U-235 in the axial blankets. This behavior indicates the benefit in uranium utilization derived from the axial blankets.
- The maximum $F_{\Delta H}$ is essentially the same in all cases. Since the changes in the axial blankets affect the whole core, the power is not significantly shifted towards any particular rod or assembly.
- Changes in the total peaking factor are more important. Of all cases in the table, the case without blanket presents the highest peaking factor F_Q. For this core, the peak takes place at medium elevations. In the blanketed cases, the power generated in the rod ends decreases with decreasing enrichment of the axial blankets. As a result, power is shifted towards the center of the rods, yielding higher peaking.

Although not included in this table, the maximum peak pin exposure follows the same trend as the core discharge burnup. Lowering the enrichment of the blankets results in a lower peak pin exposure, since this is an axially integrated parameter. The core boron concentration decreases with the content of fissile material, and it meets the design limits in all cases.

Table 5-1: Comparative performance of axial blankets

Axial blanket	B_d (GWD/MTU)	Calendar months	$F_{\Delta H}$	F_Q	Total annual costs ($M/yr)
NO	40.22	36.0	1.528	2.110	95.8
6.5%	41.08	36.7	1.530	1.948	94.4
6%	40.90	36.6	1.530	1.967	94.3
5.5%	40.69	36.4	1.529	1.987	94.3
5%	40.47	36.2	1.529	2.006	94.2
4%	40.03	35.8	1.529	2.050	94.2
3%	39.53	35.4	1.528	2.099	94.3

5.2.2.2 Analysis of Axial Shapes

The core averaged relative power fractions generated in each axial node of the model throughout core life are shown in Figure 5-2 for the cases with axial blankets at 6.5% and 3% enrichment, which bound the range of axial blankets analyzed. In this figure, nodes #1 and #24 represent the top and bottom of the core, respectively.

For the 6.5% axial blanket, the axial power is relatively well distributed in the axial direction at BOC. The bottom half of the core produces more power due to the coolant temperature effect. As the core depletes, the reactivity rapidly decreases in the unpoisoned blankets, and remains fairly constant for the rest of the core. As a result, the power fraction decreases towards the edges and increases towards the center. Between 10 and 20 GWD/MTU, the power shape is a cosine type skewed towards the bottom of the core. The maximum peak for the core takes place in axial node 9 at 19 GWD/MTU. Thereafter, the power shift is significant. The power fraction rapidly decreases in the central nodes and two humps arise around nodes 4 and 20, in the areas that had been less reactive to this point. The upper hump is bigger since the top half of the core has produced less power in previous stages of the cycle. Axial peaking is higher at 30 GWD/MTU than at 20 GWD/MTU. However, the radial flattening late in life (not represented here) leads to lower total peaking factors. At EOC, the two-hump-shape remains, and the top and bottom regions of the core produce significantly more power than the center. In summary, this core shows a significant shift in the axial power shape. During the first part of the cycle, the power is a cosine shape with more power being drawn from the bottom half of the core, whereas later in core life, the less depleted top and bottom of the rods draw the power towards the ends.

For the axial blanket at 3%, the rod ends are less reactive throughout core life. At BOC, the axial shape is a cosine type slightly displaced towards the bottom half of the core. This shape remains fairly constant up to 20 GWD/MTU, and then changes significantly. After 30 GWD/MTU, the central region is more depleted, and the power is pushed towards the edges, producing a 2-hump-shape as in the previous case. Again, the top half of the core produces more power than the bottom half.

Comparison of both cases, --6.5% and 3%-- shows that peaking is higher for the latter case. With 6.5% U-235 in the blankets, the rod ends generate more energy, and the peaks are lower.

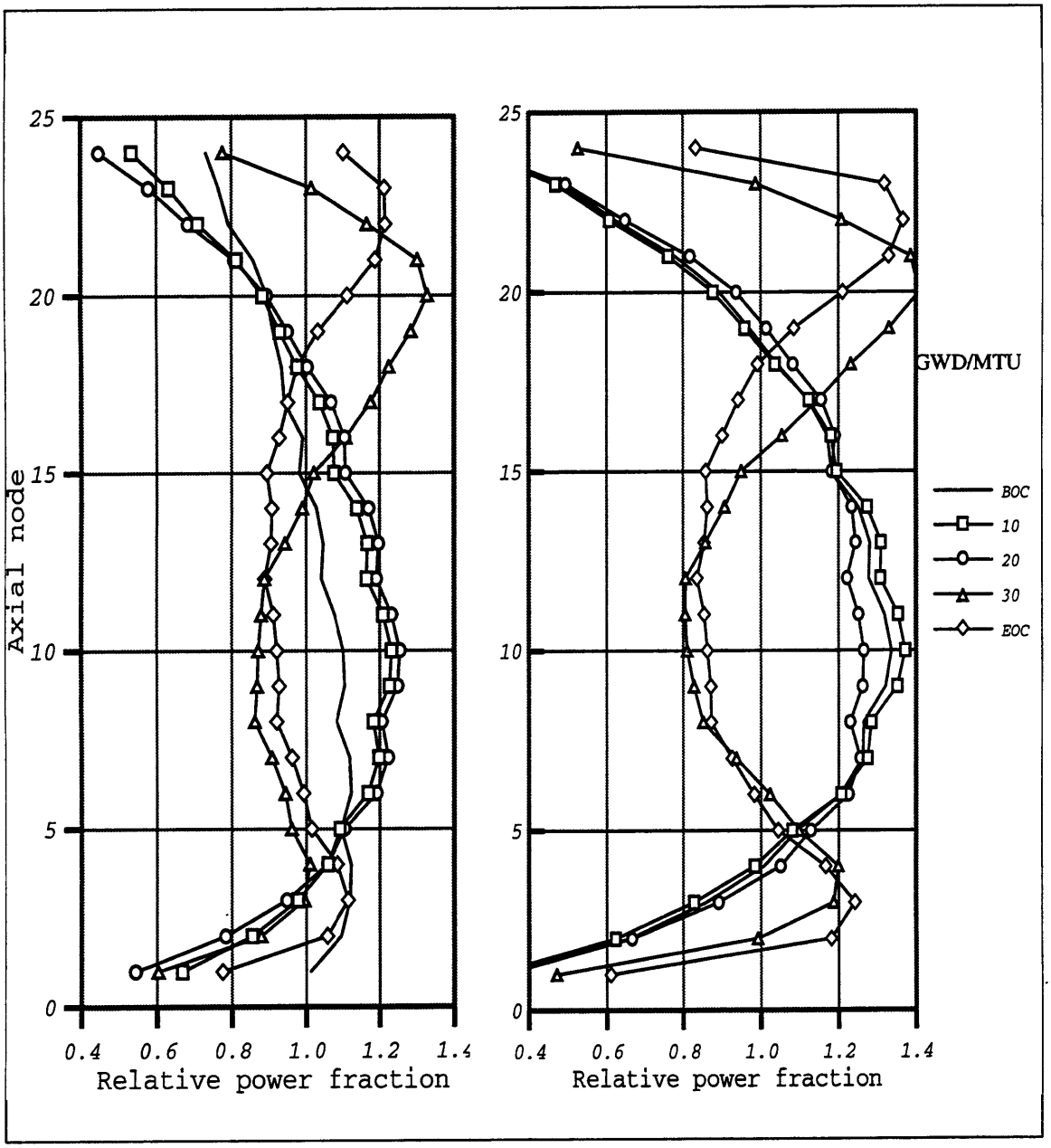

Figure 5-2: Axial power shapes for axial blankets enriched to 6.5%(left) and 3% (right)

The previous discussion refers to the core average parameters. However, the relative power fractions differ from one assembly to another. In general, the peaks are more significant in central assemblies, whereas assemblies on the periphery and close to the periphery show flatter axial shapes.

Figure 5-3 shows the axial distribution of the discharge burnup for the central assembly of the core in the cases without axial blankets, and with blankets enriched to 6.5%, 5% and 3% U-235. It can be seen that the burnup is quite uniform in a broad region in the center of the rods, but rapidly decreases towards the ends. Moreover, burnup in these regions decreases with decreasing enrichment of the axial blankets.

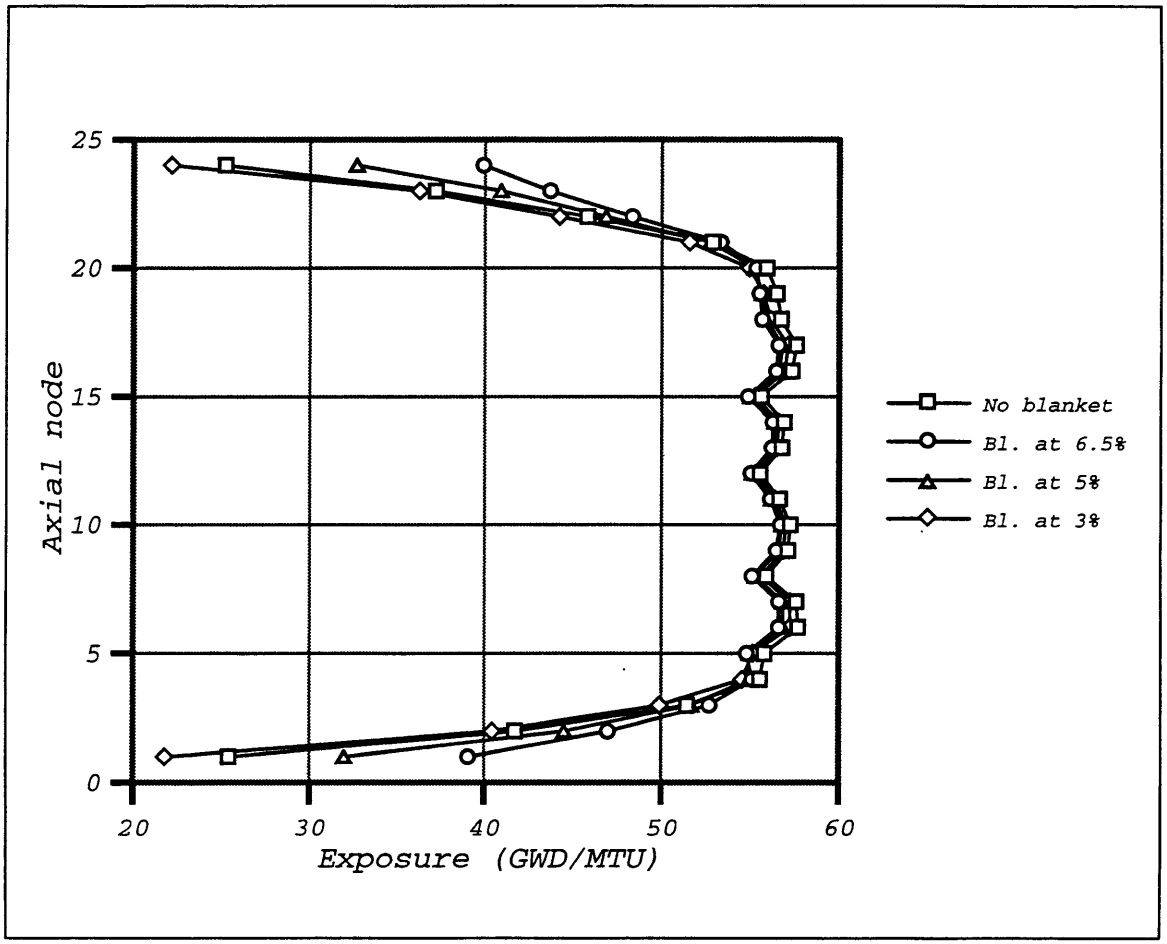

Figure 5-3: Axial representation of the discharge burnup for the central assembly of the core as a function of blanket enrichment

Figure 5-4 shows the maximum peaking factors versus core life for the previous cases. The total peaking factor includes the effects of both axial and radial peaking. Since radial peaking decreases with depletion, F_Q is only a relative measure of the axial peaking. The maximum and average values for F_Q are about 8% lower for the case with axial blankets at 6.5% U-235. The other peaking factor, $F_{\Delta H}$, is very similar for both cases. Although not shown in the figure, the location of the maximum peak migrates throughout the core, both radially and axially.

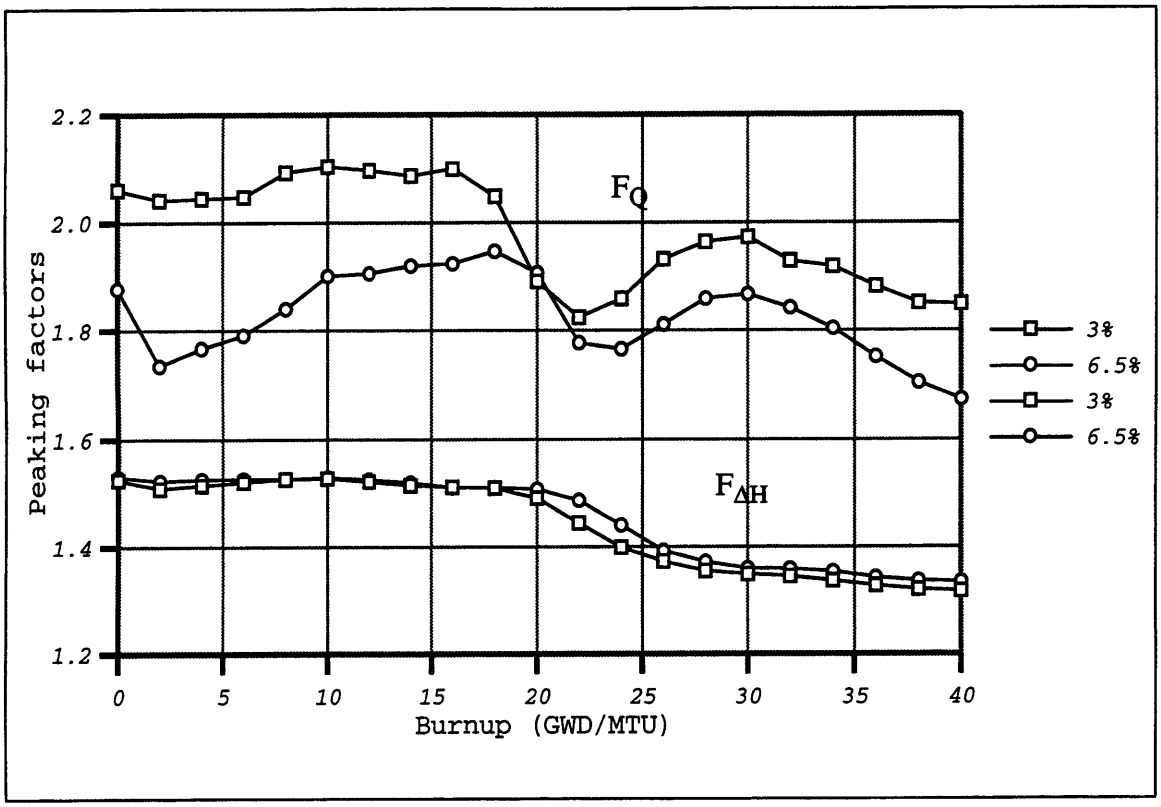

Figure 5-4: Peaking factors versus burnup for cores with axial blankets with 6.5% and 3% U-235

5.3 Poison Zoning

Axial zoning of both fuel enrichment and burnable poison can provide a benefit in peaking reduction. Ideally, a perfectly tailored distribution of fuel and burnable poison would yield a very flat axial power shape throughout core life. In practice, some degree of axial poison zoning is likely to provide a significant reduction in power peaking. Fuel enrichment zoning is another option, but not considered in this project since any reduction in core fissile loading will reduce cycle length and we also want to keep maximum enrichment as low as possible to mitigate fuel fabrication and handling problems.

Chapter 4 showed that grading the concentration of burnable poison is a good strategy to control radial power peaking. The higher burnable poison loading in the center of the core balances the higher reactivity of this region in a core of uniformly enriched fuel. A

similar strategy could be considered in order to control the axial power peaking and obtain a more uniform burnup of the axial regions throughout core life. In this Section, the benefits stemming from implementation of some degree of axial poison zoning are shown.

5.3.1 Model

The analysis is performed with 3 dimensional models in SIMULATE-3. The reference case is a core with the assembly composition of Figure 5-1, and the axial blankets enriched to 4%, an intermediate value within the range analyzed in Section 5.2. This reference core is compared to a "zoned" core with 3 axial regions, aside from the axial blankets. The design philosophy for this case is based on the following considerations:

- The assembly radial distribution of Figure 5-1 provides good control of radial peaking. Therefore, the assembly average reactivity should not be significantly modified by changes in the axial loading.
- Axial peaking is more significant towards the center of the core. For this analysis, axial poison zoning is applied only to the inner ring of assemblies that includes assemblies of types 4 and 5 in Figure 5-1.

The content of poison for the non uniform assemblies is given in Table 5-2. The central part of the rods (nodes 6 to 16) have the higher poison loading for both types of assemblies.

Table 5-2: Axial composition of the axially zoned rods

Nodes	Assembly type 4	Assembly type 5
1	Ax. blanket. 4% U-235	Ax. blanket. 4% U-235
2-5	12% Gd_2O_3 in 32 rods	12% Gd_2O_3 in 32 rods + 8% Gd_2O_3 in 4 rods
6-16	12% Gd_2O_3 in 36 rods	12% Gd_2O_3 in 36 rods
17-23	12% Gd_2O_3 in 32 rods	12% Gd_2O_3 in 32 rods + 8% Gd_2O_3 in 4 rods
24	Ax. blanket. 4% U-235	Ax. blanket. 4% U-235

5.3.2 Results

The performance of the core for both the reference case and the "zoned" case are summarized in Table 5-3. The average discharge burnup is the same for both cores. Since the fuel costs have little variation, there is no effect on the core economics.

Table 5-3: Core performance for cases with and without axial poison zoning

	B_d (GWD/MTU)	Max. $F_{\Delta H}$	Av. $F_{\Delta H}$	Max. F_Q	Av. F_Q
Reference	40.03	1.529	1.443	2.050	1.934
Zoning	40.03	1.559	1.438	1.927	1.768

Maximum and average values for F_Q and $F_{\Delta H}$ are shown in Table 5-3, and their evolution throughout core life in Figure 5-5. The maximum $F_{\Delta H}$ increases by about 2% for the zoned case, although the average decreases by 0.3%. The new poison configuration causes a small radial redistribution of the power generation that yields this slight change in $F_{\Delta H}$. A finer tuning of the burnable poison concentration should allow elimination of this change. Maximum and average values for the total peaking factors indicate that zoning the poison leads to lower peaking. The maximum peaking factor decreases by 6% and the

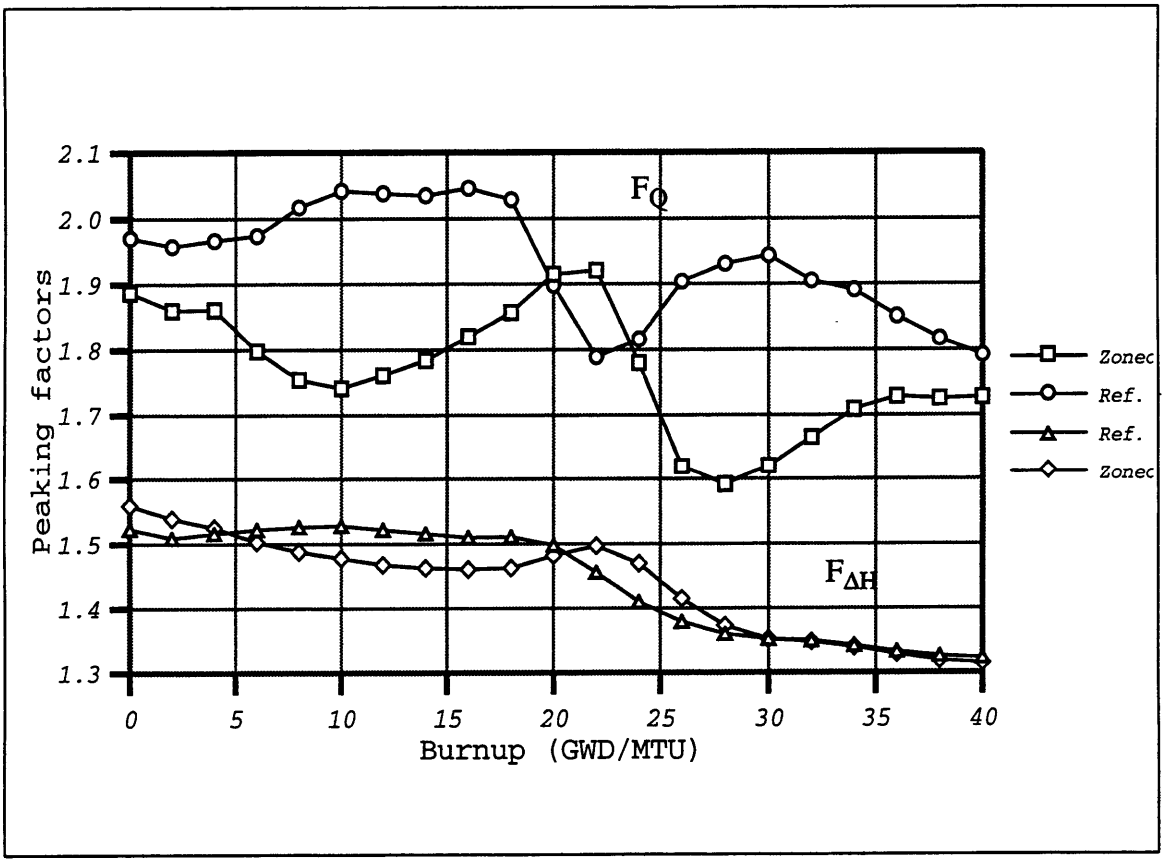

Figure 5-5: Effect of axial poison zoning on power peaks for cases with and without axial poison zoning

average value in core life by 8.6%. The reduction in peaking is particularly advantageous late in life. For the zoned case, the average F_Q after 26 GWD/MTU decreases by 11.0%.

Figure 5-6 shows the core averaged relative power fractions in each axial node at various steps in core life. The zoned case shows a flatter shape at BOC, with a fairly uniform distribution between nodes 3 and 21. At about 20 GWD/MTU, the axial shape is very similar for both cases. Afterwards, peaks are lower for the zoned case, since the central region is less depleted than in the reference case.

5.4 Conclusions

The effects of including several axial regions in fuel rods with different composition has been analyzed. The axial blanket concept is currently being used in commercial reactors and improves the uranium utilization in the rod end regions. The enrichment of the blankets affects other parameters of importance to the 36 month cycle. Increasing the blanket enrichment results in longer cycles, higher average pin burnups and lower core peaking factors. The maximum pin burnup was found to be the more constraining parameter for this core design, and, therefore, the axial blankets were selected with the lowest enrichment that would yield a 36-month cycle, i.e. blankets at 4% yield 35.8 calendar months.

Adequate axial zoning of the poison concentration provides a significant benefit to extended cycles by reducing axial peaking. In particular, the core analyzed here with three axial regions in some assemblies yields total peaking factors that are 8.6% lower on average throughout core life.

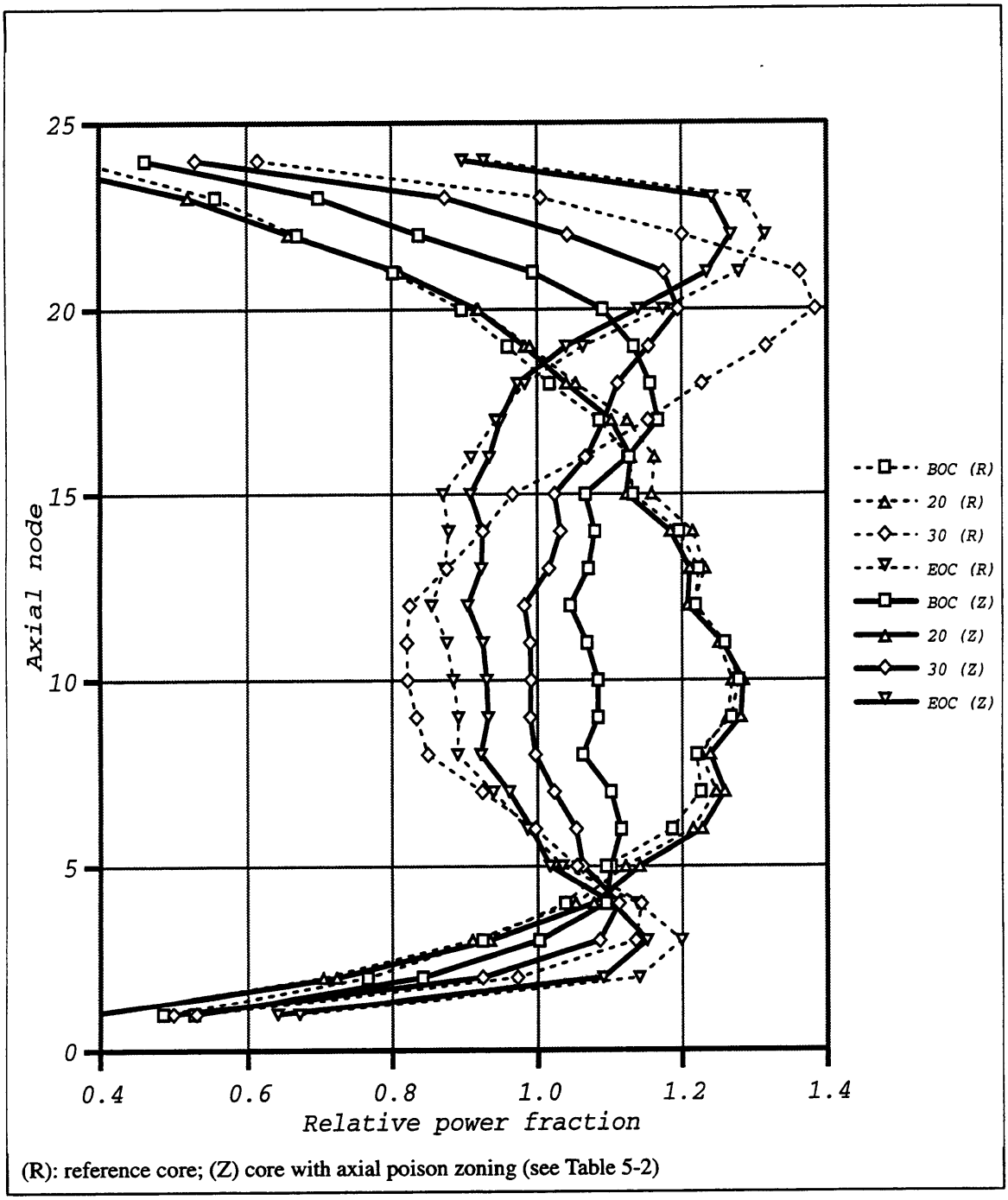

(R): reference core; (Z) core with axial poison zoning (see Table 5-2)

Figure 5-6: Effect of axial poison zoning on the axial power shape

Chapter 6

Description of the Thirty-Six Month Core

The loading pattern for the 36-month reload core is described in this Chapter. The core neutronics performance is analyzed and compared to the design limits. This includes the analysis of the assemblies' burnup and power distribution, peaking factors, core boron concentration, reactivity coefficients, and control rod worth.

6.1 Loading Pattern

The 36-month core incorporates the results presented in previous Chapters. Chapter 3 indicated that an adequate combination of duplex gadolinia provides an optimum control of reactivity and power distribution. In Chapter 4, it was shown that loading the periphery with the assemblies discharged from a previous cycle provides the best economics performance while preserving acceptable neutronics parameters. The enrichment in the axial blankets was analyzed in Chapter 5. These elements were combined into the design of the 36-month core. The final reload was obtained after an optimization of the assembly distribution. This was done by iteratively running SIMULATE-3 and adjusting the type and distribution of assemblies to tune the core performance and insure compliance with the neutronics design criteria.

The reload core contains 149 fresh fuel assemblies, and 44 assemblies shuffled from a previous cycle. Therefore, 149 assemblies are discharged as spent fuel after each cycle, or equivalently, 75 assemblies per year. This number is higher than in the 18-month reference core, for which 72 assemblies are discharged after each cycle, or 48 assemblies per year.

The fuel is enriched to 6.5% U-235 except in the axial blankets, --the top and bottom 6 inches of the fuel rods. There are 6 types of assemblies, with different concentrations of gadolinia that are distributed as indicated in Figure 6-1. The amount of burnable poison is higher in the center of the core and decreases towards the periphery. The axial blankets have annular unpoisoned fuel pellets and are enriched to 4% U-235 except in the type 4 assemblies, where they are enriched to 2.5% U-235. This lower enrichment helps to maintain the peak pin exposure within limits. For the quarter core shown in the figure, eleven

assemblies are in the core for the first cycle and will be shuffled into peripheral locations for the second cycle. When shuffled, the assemblies are rotated 180° in order to present the least burned face to the core interior.

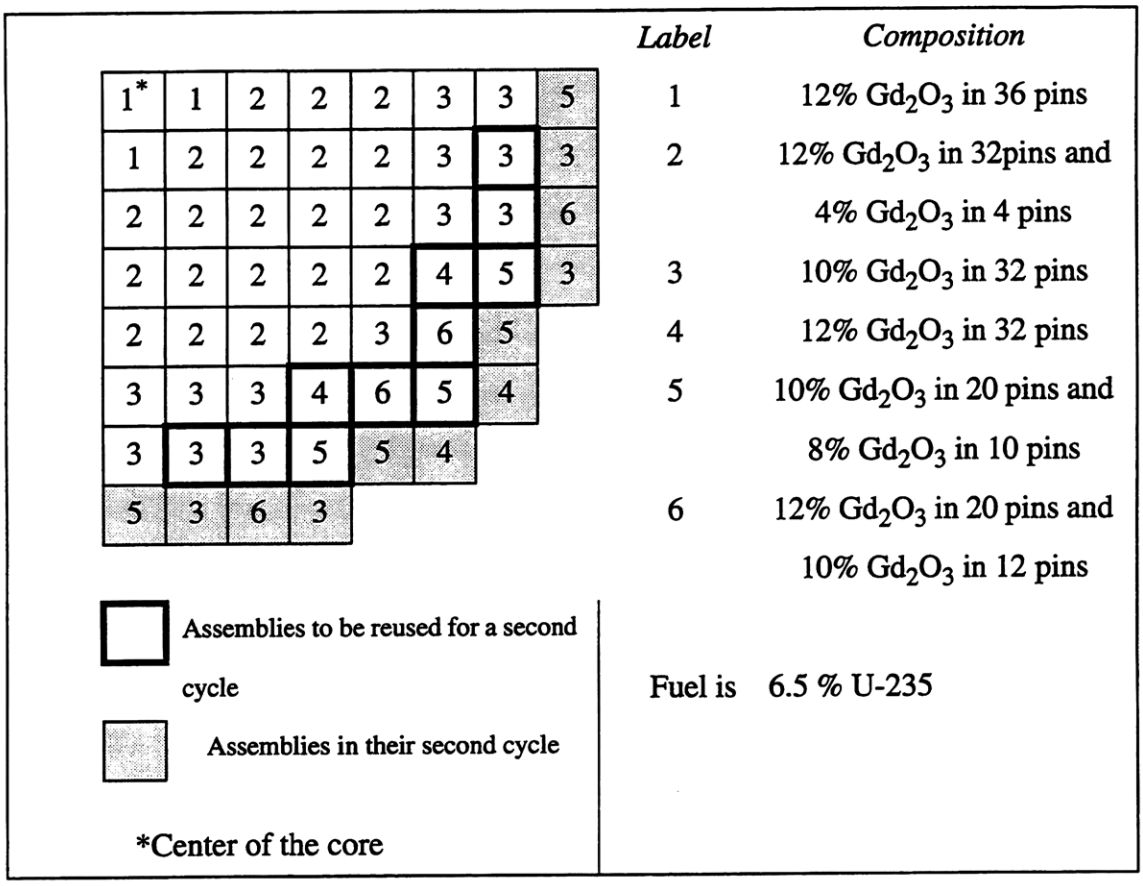

Figure 6-1: Loading pattern for the 36-month core

6.2 Core Performance

6.2.1 General Characteristics

The equilibrium cycle for this reload core achieves an average discharge burnup of 39.90 GWD/MTU, or 33.7 EFPM. For the reference operational parameters --3% FOR and 30 days RFO,-- a capacity factor of 94.3% is obtained, yielding a cycle length of 35.7 calendar months, which is very close (i.e. 9 days, well within a potential coastdown duration) to the targeted 36 months. The main neutronics parameters are shown and compared to the design limits in Table 6-1. It can be seen that the four parameters analyzed are within the design limits.

Table 6-1: Comparison of 36-month core neutronics performance to design limits

	Max F_Q	Max $F_{\Delta H}$	Max CBC (ppm)	Max pin exposure (GWD/MTU)
36-month core	2.094	1.568	1,666	59.87
Design limit	2.500	1.650	1,780	60.00

6.2.2 Cycle Exposure

The average discharge burnup for each of the assemblies in one eighth of the core is shown in Figure 6-2. This parameter is a measure of the total power extracted from each assembly during its life in core.

The assemblies in the core can be grouped into the following three sets, which are differentiated in Figure 6-2:

A. Assemblies that are discharged after one cycle,

B. Assemblies in their first cycle that will be reused in the next cycle,

C. Assemblies in their second cycle in the core.

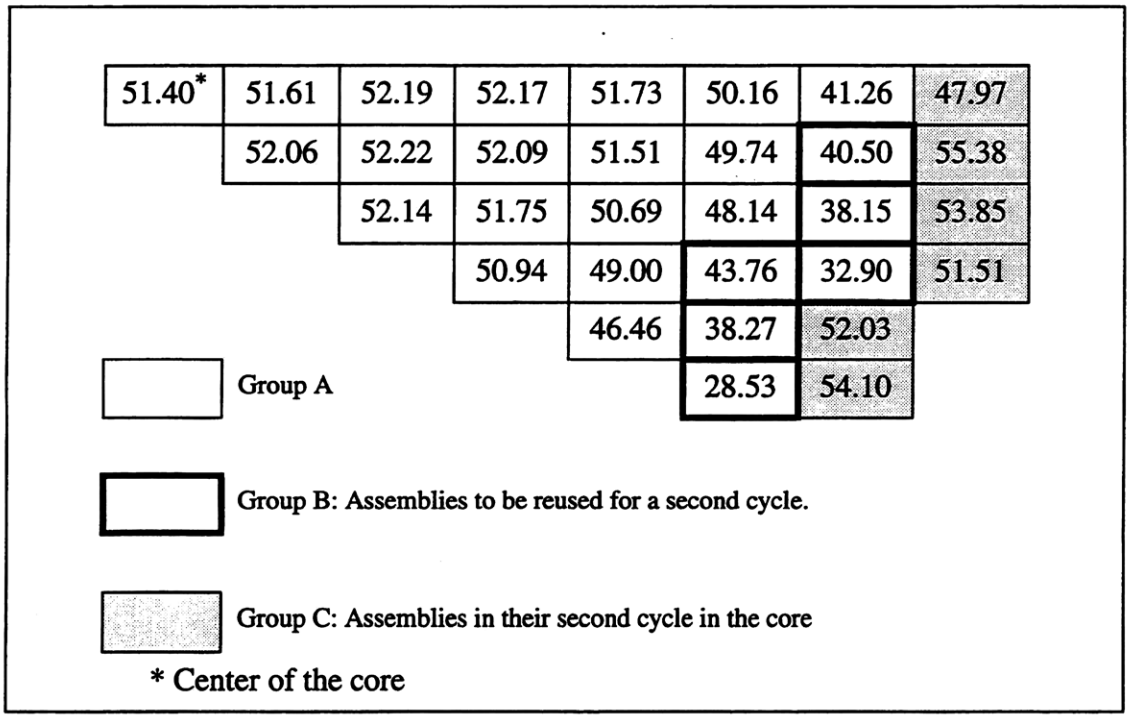

Figure 6-2: Assembly average discharge burnup for one eighth core for the 36-month core

It can be seen that:

- the burnup is high and fairly uniform (49-52 GWD/MTU) for the assemblies in group A;
- the assemblies that are shuffled (group B) have lower burnups (28-44 GWD/MTU) than assemblies in group A; and
- the burnup is high in group C (48-55 GWD/MTU), since these assemblies have been retained in the core for two cycles.

The average discharge burnup for each group and the percentage of the core average burnup are given in Table 6-2. The average discharge burnup of the 149 assemblies discharged as spent fuel (groups A and C) is 51.13 GWD/MTU. The shuffled assemblies have average incremental burnups of 37.78 GWD/MTU and 15.07 GWD/MTU in the first and second cycles in the core, respectively, yielding a total discharge burnup of 52.85 GWD/MTU. The peripheral assemblies run on average at 37.8% of the core average assembly power and the assemblies in the ring immediately inwards run below core average, but close to it. Finally, the assemblies in group A run on average at 126.4% of the core average assembly power.

For the periphery, the initial burnup of the outer and inner halves of the assemblies is 39.75 and 32.73 GWD/MTU, and the average increase in burnup during the second cycle is 11.89 and 18.27 GWD/MTU, or 29.8% and 45.8% of core average, respectively. The low exposure in the region close to the core shroud insures low neutron leakage and protects the vessel from receiving excessive neutron irradiation.

Table 6-2: EOC burnup for the three groups of assemblies of the 36-month core

	A. Discharged after one cycle	B. Reused: first cycle	C. Reused: second cycle
# of assemblies	105	44	44
Discharge burnup	50.41 GWD/MTU	37.78 GWD/MTU	52.85 GWD/MTU
% of core average	126.4%	94.7%	37.8%

6.2.3 Core Power Distribution

While the assembly average discharge burnups indicate the cumulative power generated in its life in core, the relative power fractions and the peaking factors give an idea of the power distribution throughout core life.

One of the big challenges for the 36-month core was to distribute the power evenly over a great region of the core so that the radial peaking was maintained within limits, and the peak pin exposure limit was not exceeded in the less reactive twice-burned peripheral assemblies. The loading pattern was obtained after manually trying several configurations in which assemblies with different reactivities were placed in different locations. Throughout this process, a balance had to be found between two oppositing effects. On the one hand, the central assemblies in the core run at higher power than the periphery, as indicated in Section 6.2.2 for core life average power. In order to reduce $F_{\Delta H}$, the power fraction of the assemblies on the periphery and in the region immediately inwards has to be increased. On the other hand, the peripheral assemblies attain high burnups after two cycles in the core, leading to peak pin exposures close to the design limit. In order to reduce the peak pin exposure, the power fraction in the periphery has to be reduced. Since the core thermal power remains constant, a reduction in the power generated in one region will result in an increase in power in other regions, and a compromise solution had to be found.

The complexity in the search for the balance increases when the temporal variable is taken into account. Assemblies with lower reactivity will have a lower depletion rate. However, the differences in reactivity among assemblies change throughout core life, and, therefore, the core power distribution changes. Pushing the power towards a region early in life may deplete this region faster, resulting in a power depression later in life.

6.2.3.1 Radial Distribution

The core incorporates assemblies having different reactivity in order to minimize radial leakage and flatten the power shape. The k-infinity was plotted versus core burnup for all the assemblies in the core in Figure 3-4 in Section 3.2.2.3.

Due to the high gadolinia loading, the intra-assembly peaking factor for the assemblies of this core has a maximum value of 1.16, as calculated by CASMO-3. For a perfectly uniform distribution of the power in the assemblies of group A, the maximum $F_{\Delta H}$ could be estimated as the product of the average power generated in this group (see Table 6-2) and the intra-assembly peaking, or $1.264 \cdot 1.16 = 1.466$. Since the maximum allowable value for $F_{\Delta H}$ is 1.65, there is only a small margin for deviation from the perfect power distribution,

and the variability of the assemblies' relative power fraction has to be minimized. Maintaining an almost uniform power distribution for 36 months is the great challenge for design of this core.

Figure 6-3 shows the core radial power distribution. The 2D averaged relative power fraction is plotted for all the assemblies in the core at various points in core life. The discussion of the radial power distribution is complemented by the analysis of $F_{\Delta H}$ over cycle duration, which is shown in Figure 6-4. At BOC, a broad region in the center of the core shows a fairly uniform power distribution. The relative power fraction rapidly decreases in the two outer rings of assemblies. This shape is maintained with slight modifications until 20 GWD/MTU. During this period, the value of $F_{\Delta H}$ oscillates between 1.520 and 1.568.

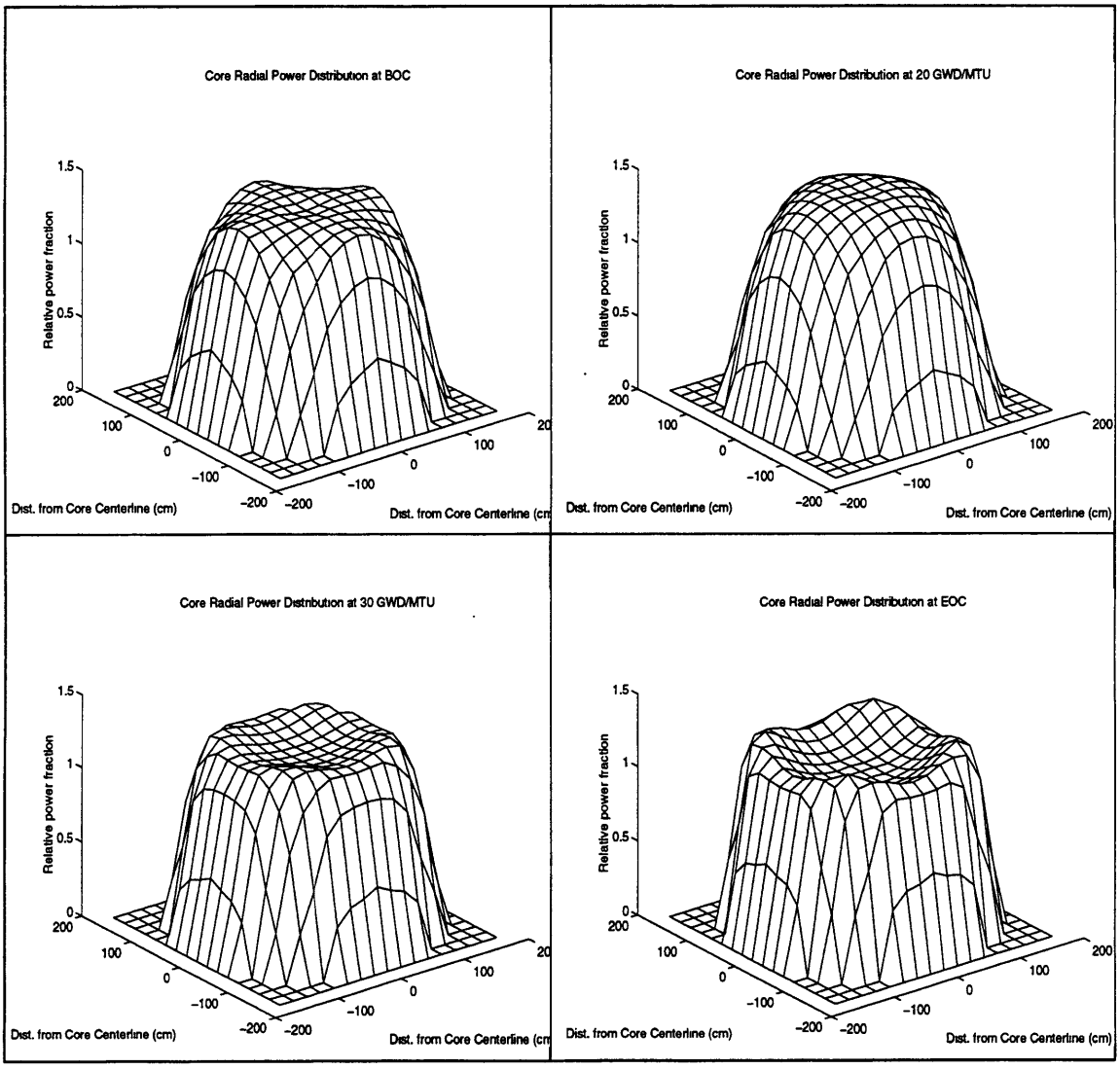

Figure 6-3: Core radial power distribution throughout core life

Afterwards, the relative power fraction decreases in the central assemblies of the core, and the importance of the assemblies located farther from the center increases. This shift in the power shape happens between 20 and 25 GWD/MTU and leads to a rapid decrease in $F_{\Delta H}$. In the last part of the cycle (after 26 GWD/MTU), the changes in the power shape are small, and $F_{\Delta H}$ has values below 1.390.

Figure 6-4 also shows that the $F_{\Delta H}$ values for the 18-month reference cycle are of similar magnitude to the $F_{\Delta H}$ values in the last part of the 36-month cycle.

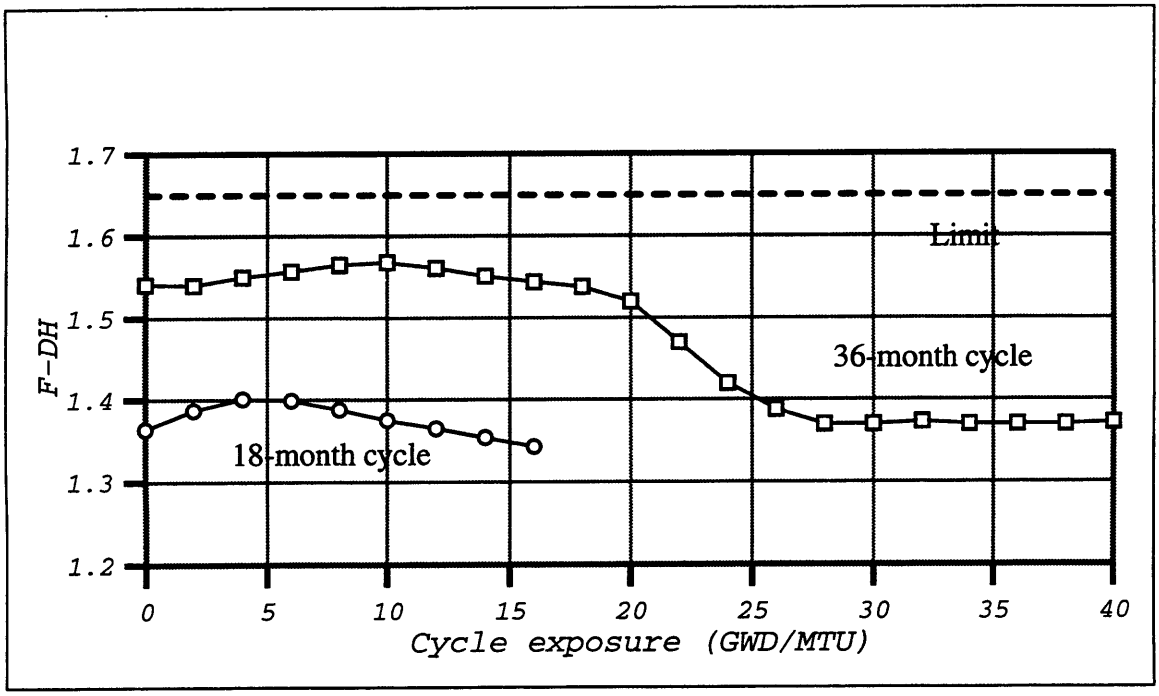

Figure 6-4: Evolution of $F_{\Delta H}$ for the 36-month and the reference 18-month cycles

6.2.3.2 Total Peaking Factor

The maximum core peaking factor is 2.094 and occurs at 10 GWD/MTU. Figure 6-5 shows the behavior of F_Q throughout core life for the 36-month core and for the 18-month reference cycle. For the 36-month cycle, the total peaking factor is well below the design criteria of 2.5 and significantly lower than for the 44.6 month core presented in Ref. [M-1]. It is especially desirable to avoid high peaking factors late in core life since this leads to high temperatures that increase the fraction of fission gas released. For the 36-month cycle, F_Q is lower during the second part of the cycle (after 20 GWD/MTU) than early in core life.

The location of the maximum peaking factor changes throughout core life both radially and axially. The hot spot is near the center of the core from BOC to about 30 GWD/MTU, and then moves towards assemblies closer to the periphery. This is consistent with the radial power distribution presented in Figure 6-3. As for the axial behavior, the hot spot is close to the axial center of the rods --heights between 122 and 152 cm-- from BOC to about 20 GWD/MTU. Then, the peak jumps to a height of 244 cm and steadily climbs up in the rods to 335 cm. This axial shift is consistent with the evolution of the axial shape described in Chapter 5.

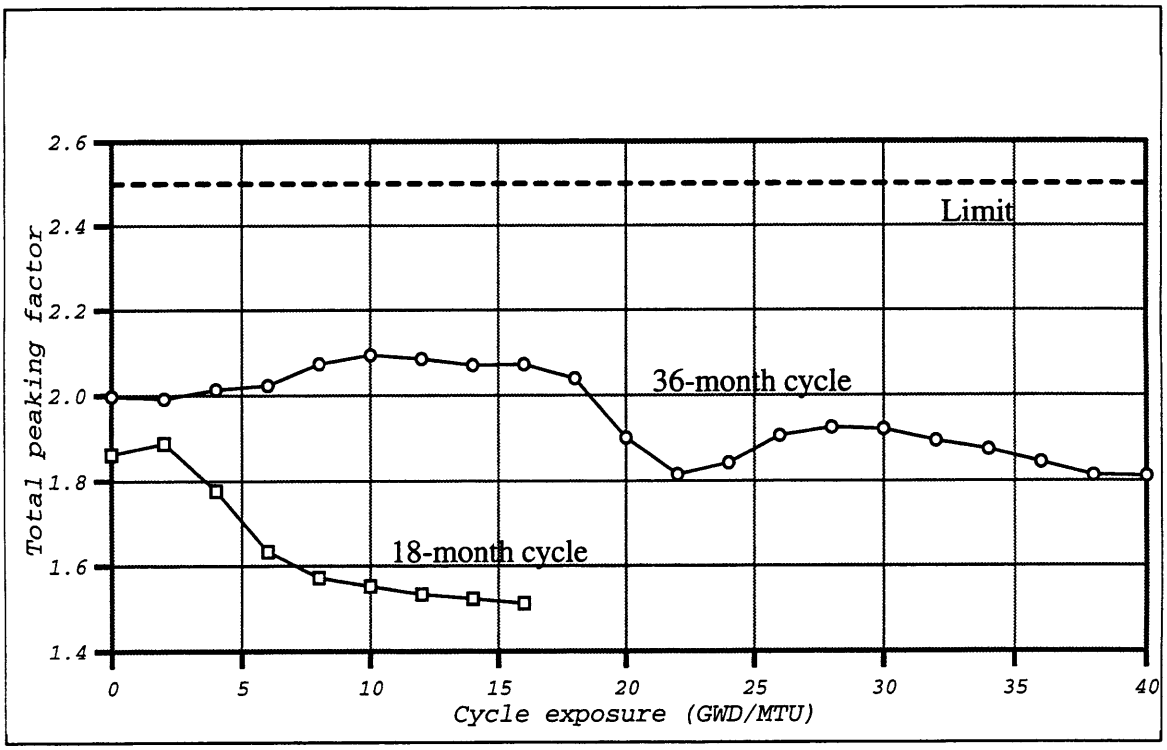

Figure 6-5: Evolution of F_Q for the 36-month and the 18-month cycles

The peaking factor for the 18-month core decreases steadily after 2 GWD/MTU. Since the cycle is shorter, the power shape and, therefore, the location of the peak changes less than in the 36-month cycle.

6.2.4 Core Boron Concentration

The soluble boron concentration in the core is plotted as a function of core life in Figure 6-6 for both the 36-month and the 18-month cores. In the 36-month core, the boron concentration is kept at all times below the design criterion of 1,780 ppm, and shows rela-

tively high values --between 1,550 and 1,665 ppm-- for about 20 GWD/MTU. This corresponds to the period where the reactivity of the assemblies is maintained at a fairly constant level thanks to the burnable poison distribution (see Fig. 7 in Section 3.2.2.3). Afterwards, the reactivity decreases steadily and so does the boron concentration. The lifetime average CBC is higher for the 36-month core than for the 18-month core. As a result, the core water chemistry is affected and the cladding corrosion rate may be enhanced. This issue is discussed in Chapter 7.

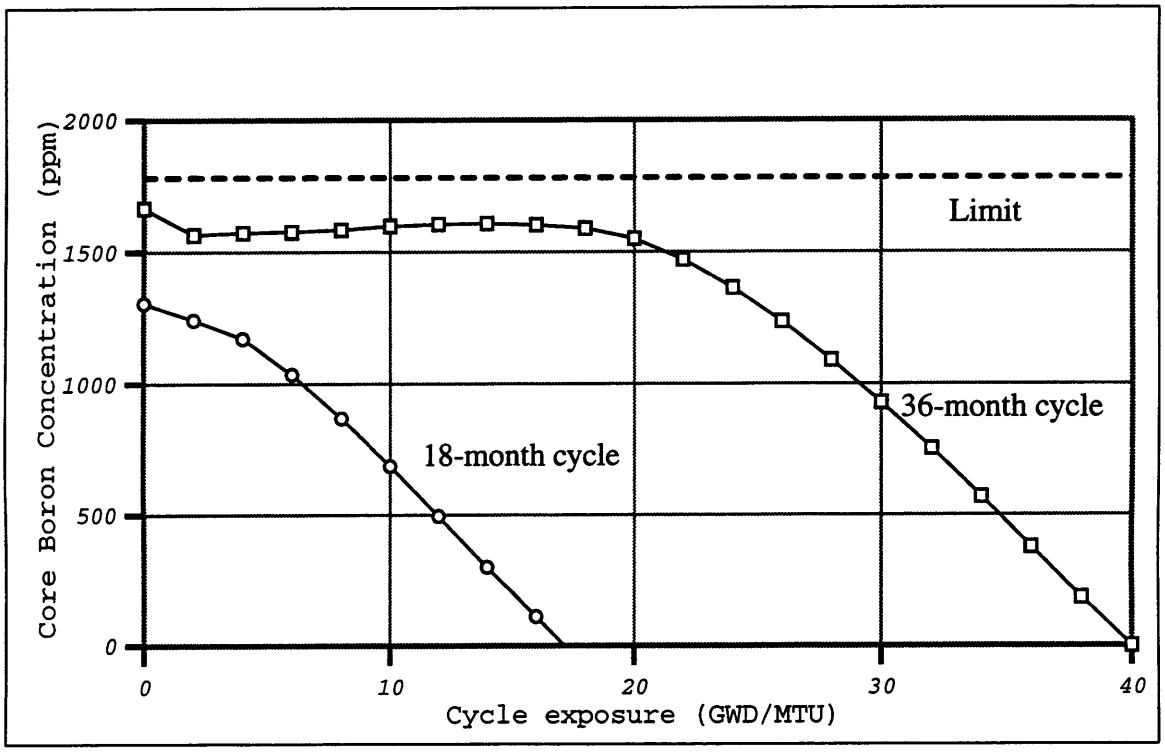

Figure 6-6: Core boron concentration versus cycle duration for the 36-month and 18-month cycles

6.2.5 Reactivity Related Issues

Enriching the fuel in the 36-month cycle to 6.5% U-235 increases the macroscopic cross sections for absorption and fission in the thermal energy range, shifting the neutron spectrum to higher energies and reducing the thermal neutron flux. This leads to changes in the core reactivity coefficients and control rod worth, and, therefore, these parameters have to be analyzed.

6.2.5.1 Coefficients of Reactivity

The reactivity coefficients measure the reactivity changes when core parameters are perturbed and indicate the stability of the reactor under perturbations. The following parameters were calculated for the 36-month core using SIMULATE-3:

- Moderator Temperature Coefficient (MTC): defined as the reactivity change associated with a change in the moderator inlet temperature divided by the change in the core-averaged moderator temperature.
- Fuel Temperature Coefficient (FTC): defined as the reactivity change associated with uniform change in the fuel temperature divided by the change in the core-averaged fuel temperature.
- Boron Coefficient (BC): defined as the reactivity change associated with a uniform perturbation of the boron concentration divided by the boron change.
- Power Coefficient (PC): defined as the reactivity change associated with a uniform change in the power level divided by the percent change in power.

Table 6-3 shows the MTC, FTC, BC, and PC for the 36-month core as well as for the 18-month reference core for 3 conditions:

- BOC, with no Xenon;
- BOC, with Xenon in equilibriun concentration;
- EOC, with Xenon in equilibrium conccentration.

The MTC has similar values for both cycles at BOC, and more negative values for the 36-month core at EOC. The values do not exceed the safety analysis limit, which is -42 pcm/^{o}F [M-1], and, therefore, the 36-month core maintains adequate values for the MTC.

The FTC shows little variation with respect to the reference cycle. The BC are lower than for the reference core due to the neutron energy spectral shift. Finally, the power feedback coefficients are close to those of the reference cycle.

6.2.5.2 Control Rod Worth

The control rod worth was quantified for the 36-month core. The analysis was done by running a type 2 assembly with CASMO-3 and studying the rod worth, defined as $\Delta\rho = ln(k_1/k_2)$, where k_1 and k_2 represent the k_∞ values for the assembly with the control rods fully withdrawn and fully inserted, respectively. The assembly of type 2 is the most common type of assembly in the core and, hence, the most likely to be under a control rod position (see Figure A.2 in Appendix A). The analysis was done with standard Westinghouse 24 finger silver/indium/cadmium ($80^{w}/_{o}$ Ag/ $15^{w}/_{o}$ In/ $5^{w}/_{o}$ Cd) Rod Control Cluster Assemblies (RCCA).

Table 6-3: Comparison of coefficients of reactivity for the 36-month and 18-month cores

Coefficient	Conditions	36-month core	18-month core
MTC (pcm/°F)	HFP, BOC, No Xe	-6.03	-5.67
	HFP, BOC, Eq. Xe	-8.12	-9.03
	HFP, EOC, Eq. Xe	-39.70	-34.32
FTC (pcm/°F)	HFP, BOC, No Xe	-1.39	-1.37
	HFP, BOC, Eq. Xe	-1.50	-1.38
	HFP, EOC, Eq. Xe	-1.60	-1.53
BC (pcm/ppm)	HFP, BOC, No Xe	-4.06	-6.85
	HFP, BOC, Eq. Xe	-4.10	-6.83
	HFP, EOC, Eq. Xe	-6.21	-8.52
PC (pcm/%)	HFP, BOC, No Xe	-12.36	-11.59
	HFP, BOC, Eq. Xe	-13.30	-12.35
	HFP, EOC, Eq. Xe	-20.32	-19.12

The control rod worth for the 36-month cycle is between 14% and 25% lower than for the reference cycle and, therefore, new control rods are needed to insure an adequate shut-down margin. Since the 36-month core control rod worth is between 2% and 8% higher than for the previously designed 44.6-month core, the new control rods proposed in Ref. [M-1], --i.e., B_4C or hybrid RCCAs-- would also be a valid solution for the 36-month core. These new control rods are based on the more highly poison loaded control rods of this type specified for the PWR cores proposed for weapons grade plutonium burning.

6.3 Improvement Margin in the 36-Month Core

The performance of the 36-month core is satisfactory since the targeted design limits are met. However, further efforts to reduce peaking factors and improve the core econom-

ics are desirable and will contribute to make the core more attractive to utility managers. This section reviews three concepts that will benefit the 36-month core. First, the benefits of isotopic separation technology on the performance of gadolinia is analyzed. Second, computer codes are described that automatically perform loading pattern optimization. Finally, the benefits of axially zoning the burnable poison are reviewed.

6.3.1 Elimination of Reactivity Residual Penalty

The importance of the reactivity residual penalty when selecting a burnable absorber was indicated in Chapter 3. It was shown there that the residual penalty in the 36-month core is larger for erbia than for gadolinia, and negligible for IFBA. If an ideal gadolinium absorber were available, the residual penalty could be reduced or completely eliminated, yielding a longer cycle, and, therefore, providing an economic benefit. This is possible by selective use of the isotope Gd-157 and elimination of the other isotopes from natural gadolinium, which could be feasible with AVLIS technology. In this Section, the isotopic composition of gadolinium is analyzed and the benefits of selective use of the isotope Gd-157 are assessed.

6.3.1.1 Isotopic Composition of Gadolinium

The isotopic composition of natural gadolinium and the 2200 m/s capture cross section for each isotope are shown in Table 6-4 [G-3]. Of the seven isotopes listed, two can be considered as poisons (Gd-155 and Gd-157), with Gd-157 being the most interesting because of its larger cross section.

Table 6-4: Isotopic composition of gadolinium and capture cross sections

	Gd-152	Gd-154	Gd-155	Gd-156	Gd-157	Gd-158	Gd-160
$y(^{w}/_{o})$	0.20	2.18	14.80	20.47	15.65	24.84	21.86
σ_o (barns)	700	60	61,000	2	255,000	2	1

The residual penalty of gadolinia is caused by the isotopes remaining in the last part of the cycle. Due to their relatively low capture cross sections, all the isotopes but Gd-155 and Gd-157 deplete relatively slowly and their presence is significant at EOC. The isotopes Gd-154 and Gd-156 can capture neutrons and create more of the poison species. As the poison isotopes Gd-155 and Gd-157 are created, they quickly capture neutrons and

yield transmutation products, Gd-156 and Gd-158, which can also capture more neutrons. The isotopes Gd-152 and Gd-160 can also absorb neutrons.

Figure 6-7 (reproduced from [H-5]) shows the fractions of neutrons in a PWR lattice cell absorbed in each of the gadolinium isotopes for fuel with 8.0% gadolinium. From 0 to 15,000 MWD/MTU, it can be observed that:

- neutron absorption in Gd-155 and Gd-157 is dominant;
- the fraction of Gd-156 increases with time since this isotope is formed by capture of Gd-155;
- the combined fraction of Gd-152, Gd-158 and Gd-160 slightly increases. Although the concentration of Gd-152 and Gd-160 decreases by neutron capture, the concentration of Gd-158 increases by transmutation of Gd-157.

After 15,000 MWD/MTU, the fractions absorbed in each isotope remain fairly constant. This behavior is explained as follows:

- the original Gd-155 and Gd-157 are depleted, and these isotopes are now formed by neutron capture in Gd-154 and Gd-156. In this quasi-steady-state, the fractions absorbed in Gd-155 and Gd-157 are approximately equal to to those of Gd-154 and Gd-156 respectively;
- the isotopes Gd-152, Gd-154, and Gd-160 capture neutrons and disappear at a slow rate;

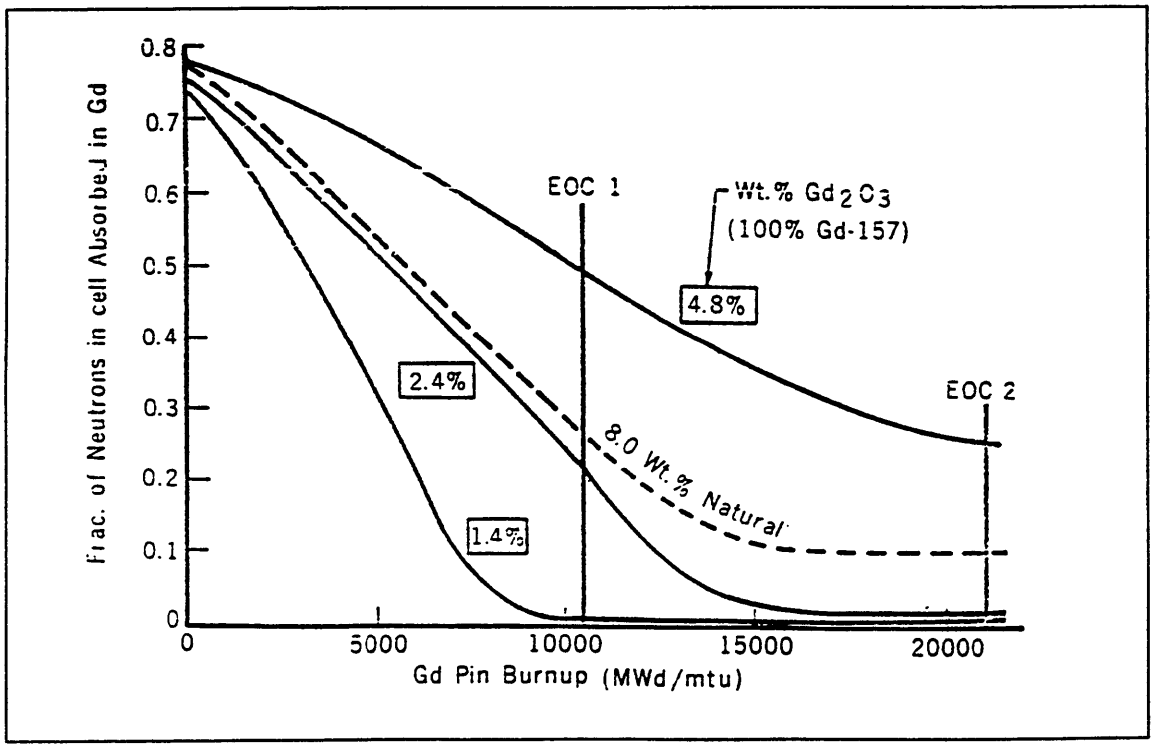

Figure 6-7: Natural gadolinium absorption by isotope (from [H-5])

- the concentration of the isotope Gd-158 increases by capture in Gd-157, and so does the fraction absorbed in it.

A burnable absorber made exclusively of Gd-157 would result in a very low residual penalty. Once the Gd-157 depleted, only the transmutation product Gd-158 would be present, and the undesired neutron captures would be greatly reduced.

The effective capture cross sections of an initial loading of natural gadolinium and pure Gd-157 at the EOC in the 36-month core are 6.3 and 2 barns, respectively (see Appendix B.) For a given concentration of natural gadolinium, N, the macroscopic residual cross section is 6.3N. Using separated Gd-157 requires only a concentration of 0.19N (Appendix B), and yields a macroscopic residual cross section of 0.38N, or about 6% of the residual found for natural gadolinium. Note that these calculations do not account for the self-shielding effect of the gadolinium.

6.3.1.2 Estimate of Residual Penalty

Hove [H-5] compared the neutron absorption of fuel with 8.0% natural gadolinium and with lower concentrations of pure Gd-157. He showed that by loading 2.4% Gd-157 instead of 8.0% natural gadolinium, the residual absorption is cut by about a factor of 4 while keeping a similar absorption rate early in life.

It is of interest to estimate the increase in cycle length and the economic benefit that a perfect poison --with no residual penalty-- would yield in the 36-month cycle. The code used in this study (CASMO-3) does not include the capability of changing the isotopic composition of gadolinium. An alternate analysis was done by comparing the reactivities at EOC for otherwise identical poisoned and unpoisoned assemblies with the same fuel enrichment (6.5%U-235.) The poisoned assembly was of type 4 (see Figure 6-1), with 12% Gd_2O_3 in 32 rods and 4% Gd_2O_3 in 4 rods, which is the most typical assembly in the 36-month core design. As shown in Figure 3-4 (Section 3.2.2.3), the curve for this poisoned assembly intersects the horizontal line k=1 at a burnup of 49.6 GWD/MTU. The intersection point for the unpoisoned assembly is 52.4 GWD/MTU, about 2.8 GWD/MTU more than for the poisoned assembly. Hence, if the residual penalty could be completely eliminated, the batch-loaded core burnup would be increased by this amount. Therefore, the core average burnup would increase from 39.90 GWD/MTU (see Section 6.2) to 42.70

GWD/MTU, yielding a cycle of 36.0 EFPM, or 38.1 calendar months. The total costs would be reduced by $4.5M/yr down to $89.8M/yr, which are about the same costs as for the 18-month reference cycle. However, this analysis does not include the additional costs for isotopic separation of gadolinium. The 36-month core uses 935 kg of Gd (see Appendix C), and, therefore, 178 kg of separated Gd-157 (=935kgx0.19) would be required to hold down the same reactivity. If the price of separated Gd-157 were below $25281/kg (=$4.5M/178kg) an economic benefit would be obtained. One should note, however, that the 18-month reference cycle could also benefit from the use of separated Gd-157 --albeit by a lesser amount since it uses less poison, and pays less for enrichment.

6.3.2 Radial Optimization of the Loading Pattern

The core physics analyses were carried out by iteratively loading an assembly pattern, analyzing the results and modifying the initial configuration based on engineering judgement. This "trial-and-error" technique provided valuable insights about the core behavior. However, the limitations of a "trial-and-error" method are obvious since the number of cases that can be run is constrained by the time required to analyze the results and manually prepare new input files.

Several state-of-the-art computational codes automatically perform loading pattern optimization, and they are in widespread use for fuel and poison management. These codes, however, were not available for this project. Using linear correlations between state and control variables, maximization of cycle length can be reduced to a linear programming problem subject to a set of constraints [O-2]. As an example, the capabilities of three optimization computer codes are briefly described as follows:

- SIMAN is an algorithm for stochastic optimization that searches for optimal patterns within a large sample of candidates [S-8]. This algorithm has been added to the X-IMAGE code in which SIMULATE-3 is incorporated. With this tool, thousands of patterns can be accurately evaluated in an overnight run [S-9].
- FORMOSA-P is a code developed at North Carolina State University that utilizes the nonlinear stochastic optimization approach of simulated annealing to determine the family of near-optimum loading patterns for PWRs [K-2].
- AUTOLOAD is a code developed at Penn State University that completes optimal reload designs for PWRs. It maximizes cycle length by searching for the optimum placement of the fuel, and establishes the burnable poison loading in the fresh fuel assemblies [Z-1].

Application of any of the optimization tools to the 36-month core design will very likely provide some improvement by yielding longer cycles and reduced peaking factors. It is difficult, however, to quantify the possible improvements without running the codes. A preliminary estimate of the improvement margin may be made by analyzing the distribution of the most limiting parameters in this design, namely, the peak pin exposure and $F_{\Delta H}$.

The peak pin exposure remains below 55.50 GWD/MTU for the assemblies that are discharged after one cycle, and is close to the design limit (60 GWD/MTU) in the peripheral assemblies, where it attains a maximum value of 59.87 GWD/MTU (see Appendix D). At EOC, the peak pin exposure is between 59.50 and 59.87 GWD/MTU in 24 peripheral assemblies, and between 56 and 57 GWD/MTU in the remaining 20 assemblies. With more than half of the periphery within 0.5 GWD/MTU of the design limit, it is difficult to draw more power towards this region without exceeding this limit. The margin for optimization seems, therefore, small.

As for $F_{\Delta H}$, Figure 6-4 in Section 6.2.3.1 shows that the maximum value for this parameter is 1.568 at 10 GWD/MTU and over 1.520 between 0 and 20 GWD/MTU. The cumulative distribution functions (CDFs) for the maximum $F_{\Delta H}$ values in each assembly are plotted in Figure 6-8 for the assemblies in group A (see Appendix A) and for two steps in core life: BOC and the step of maximum $F_{\Delta H}$. For a given value of $F_{\Delta H}$ in the plot, the CDF indicates the fraction of assemblies in which $F_{\Delta H}$ takes on that value or lower. The CDF is a function continuously growing from 0 to 1. At BOC, the maximum $F_{\Delta H}$ value is 1.541, and about half of the assemblies have values between 1.525 and 1.541. At 10 GWD/MTU, about 34% of the assemblies have values between 1.450 and 1.525, about 5% between 1.525 and 1.550, and about 30% above 1.550. The graph shows that the maximum $F_{\Delta H}$ at 10 GWD/MTU could be reduced if a CDF closer to that of BOC is obtained.

This analysis suggests that computational tools for fuel management optimization may yield some improvement in core performance, although quantifying it without running the codes is very difficult.

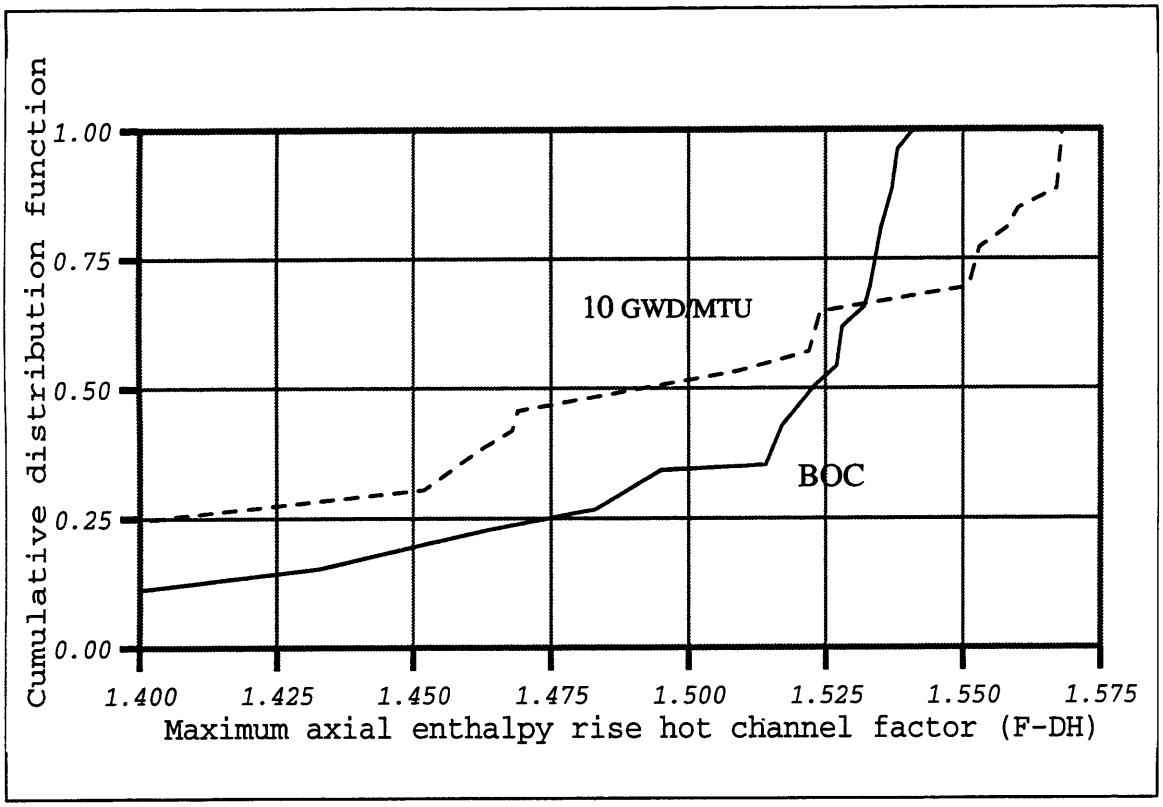

Figure 6-8: Cumulative distribution function for the maximum $F_{\Delta H}$ in each assembly

6.3.3 Axial Poison Zoning

Section 5.3 showed that axial poison zoning is an effective way to reduce peaking factors in the core. It may seem contradictory that, after explaining this benefit and showing the numerical results, the core design presented in Section 6.1 did not include this concept and was made of axially uniform rods except for the axial blankets.

Some degree of axial poison zoning was applied to the 36-month core and the effect on the peaking factors was similar to that displayed in Figure 5-5, i.e. reduction of the life-averaged core peaking factor by more than 8%. However, the changes in the axial composition also led to small variations in the core power distribution. As a result the values of $F_{\Delta H}$ and peak pin burnup were slightly increased and went over the targeted design limits. These initial efforts indicated that finding a good axial zoning pattern without exceeding the design limits for the two constraining parameters ($F_{\Delta H}$ and peak pin burnup) would

require loading and analyzing several patterns in subsequent trials. As explained in Section 6.3.2, the effort and time required to manually prepare the loading patterns is significant. Given the time constraints and goals of this thesis, no further work was pursued in this area. Future design efforts are desirable that will result in lower peaking factors, hence, better fuel performance. The availability of optimization tools such as those presented in Section 6.3.2 will definitely help in successfully applying this strategy.

6.4 Transition Cycle

6.4.1 Introduction

The technical feasibility of the 36-month core has been shown for an equilibrium cycle in the previous chapters. This core is to be retrofitable, and a first reload has to be designed to establish the transition from currently operating cycles. In this Section, a strategy for shifting from a 24- to a 36-month cycle is presented that has the objective of minimizing the economic penalty. The 24-month cycle represents the longest cycle for a PWR currently operating in the US, and the transition is carried out in one single step.

To date, cycle extensions in PWRs have been moderate, --e.g. in 6-month increments: for example from 12 to 18 months,-- and only a few plants have opted for cycles between 18 and 24 months. If a decision is taken to further increase the cycle length, it is very likely that utility managers will do so in incremental steps of 6 months or less. This decision would likely not be based on core technical constraints of the longer cycles, but rather on the ability to reliably operate the plant for such a long period without unacceptably increasing the forced outage rate due to equipment wearout. In other words, a plant running an 18-month cycle would go first to a 24 month cycle, then to a 30-month and finally to a 36-month cycle, rather than straight from an 18- to a 36-month cycle. However, it is beyond the scope of this work to design a reload core for an intermediate cycle for 30-months, which would involve physics simulations of a core enriched to some level below 6.5% U-235, and would not add any significant results to this work.

6.4.2 Twenty Four Month Cycle

A two dimensional model was established for a 24-month cycle with the codes CASMO-3/SIMULATE-3 based on information provided by Yankee Atomic Electric Company [W-1]. The fuel in the core is enriched up to 4.6% U-235, the burnable absorber is IFBA, and half the core is loaded with fresh fuel during each refueling. The calculations show that the cycle average burnup is 22.51 GWD/MTU, or equivalently, 19.1 EFPM. For a capacity factor of 79.8% --well within current industrial achievements,-- a cycle of 24 calendar months is obtained. This core design meets both the peak pin exposure and the peaking factor limits. The CBC is over the design limit early in core life, but a refinement in the poison loading will bring this value within the limits. Due to the negligible residual penalty of the IFBA, these changes will have a very small influence in the core and assembly average discharge burnups, which are the parameters of interest for this study. Moreover, experience in core design throughout this work shows that a full 3-D design yields lower CBC values once the less reactive axial blankets are introduced. Therefore, the design was considered acceptable for the goals of this Chapter.

After one cycle in the core, the assemblies reloaded during the preceding refueling have burnups between 18.5 and 30 GWD/MTU, and, therefore, have enough reactivity to be reused in the following cycle. The assemblies can be grouped in 4 sets according to their locations in the core. In this analysis, core periphery refers to the 44 outer assemblies in the core, and core interior refers to the remaining 149 assemblies. The description of the sets and the discharge burnups are given in Table 6-5. For an equilibrium sequence, the assemblies in set X will be reused in the periphery of the core in the next cycle, whereas the assemblies in set W will be reused in different locations of the core interior. The

Table 6-5: Sets of assemblies for the 24-month cycle

Label	Description of assemblies	Number of assemblies	Burnup (GWD/MTU)
Z	Twice burned, second cycle in periphery	44	38.32
Y	Twice burned, second cycle in core interior	53	48.40
X	Once burned, to be reused in the periphery	44	26.56
W	Once burned, to be reused in the core interior	52	26.56

assemblies in sets Y and Z will be discharged as spent fuel.

6.4.3 Strategies for the Transition Cycle

6.4.3.1 Description of Options

The goal in the design of this transition cycle is to get the most economical option that meets the technical design limits. In order to shift to the desired cycle length in one single step, two options are considered, which are schematically represented in Figure 6-9. The assemblies in the 24-month cycle are grouped and labeled as described in Table 6-5. The assemblies in the 36-month cycle are grouped in 3 rings, as described in Appendix A. The basic characteristics in both options are as follows:

Option 1. The once-burned assemblies from the 24-month cycle --sets X and W-- are reused for the first and second 36-month cycles, respectively. These assemblies are loaded in the periphery of the core. The other assembly sets in the 36-month cycles (V, U, T, and S) are loaded with fresh fuel. After the first 36-month cycle, all the assemblies are discharged, and after the second 36-month cycle, the set T is kept for reuse in the periphery of the third 36-month cycle, which corresponds to the equilibrium cycle described in Chapter 6.

Option 2. Half of the once-burned assemblies in the 24-month cycle (set W) are discharged as spent fuel, whereas the other half are used in the periphery of the first 36-month cycle. The assemblies in set V (in the first 36-month cycle) are reused in the periphery of the second 36-month cycle, which corresponds to the equilibrium cycle.

The main difference between these two options is that in option 1 the sets X and W are reused, and the set V is discharged after one cycle, whereas in option 2 the sets X and V are reused, and the set W is discharged after one cycle in the core.

6.4.3.2 Transition Penalty

In the transition process, the initial and end points are the 24-month and equilibrium 36-month cycles, respectively. The cost penalty was evaluated for both options by estimating the residual worth of the underburned assemblies when discharged. The calculations are described in Appendix E, and indicate that the penalties are about $18.5M and $18.1M

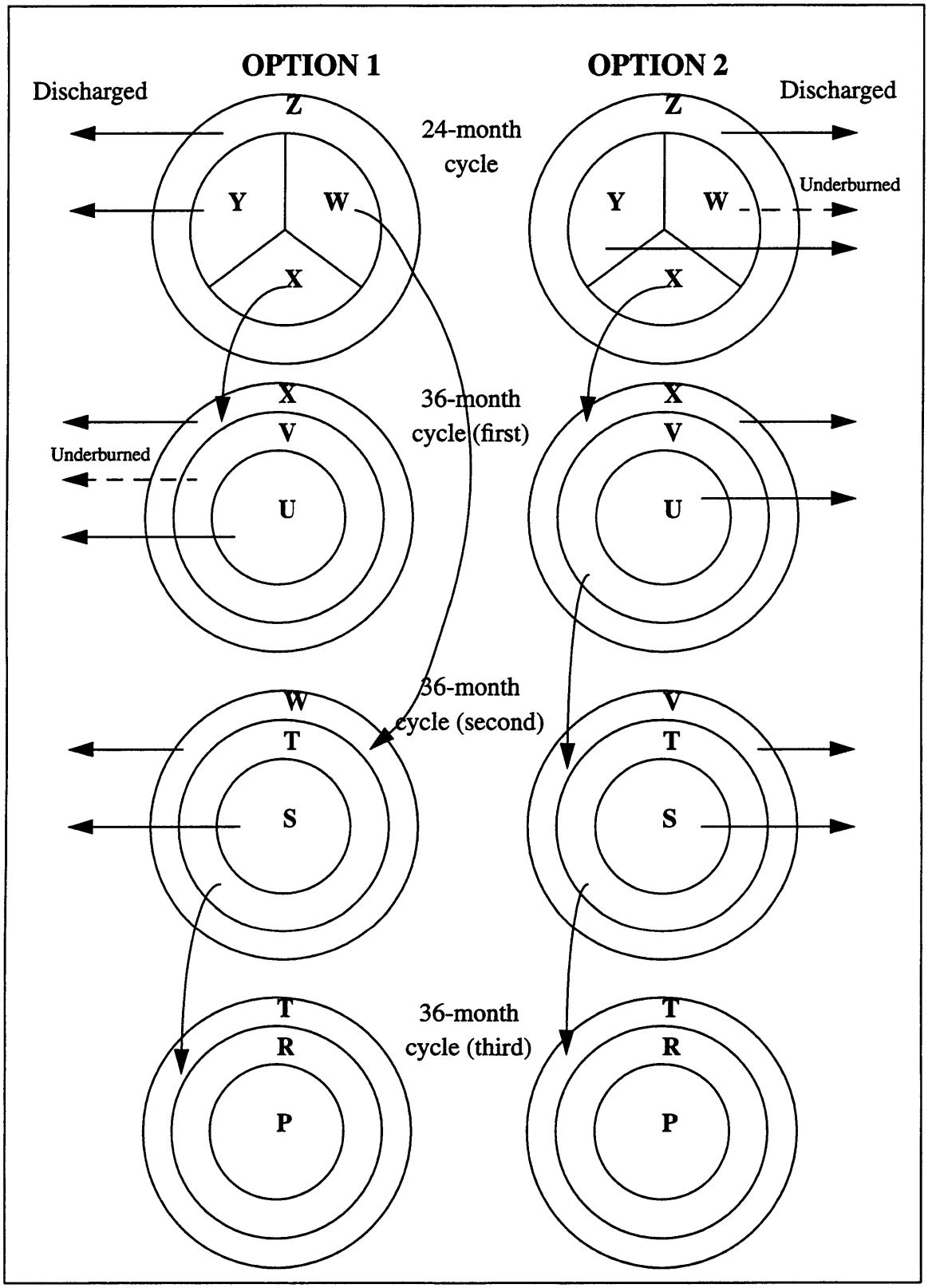

Figure 6-9: Schematic representation of options for transition strategy

for options 1 and 2, respectively. Therefore, option 2 was retained to pursue furtheranalysis of the transition cycle. The total penalty, when spread over the remaining life of the plant --estimated to be 20 years,-- and considering a carrying charge rate of 10%/yr., yields an annualized penalty of $2.10M/yr.

The transition penalty depends on the strategy selected for the 36-month cycle, and one could argue that the penalty could be reduced in a core that applies the RBA strategy described in Chapter 4; however, the extra costs for this strategy are over $10M/yr (see Table 4-7), and this amount would not be offset by the possible reduction in transition costs.

6.4.4 Physics Analysis for the Transition Cycle

Using SIMULATE-3, a core was modeled in 2 dimensions with the assembly distribution of the 36-month core given in Figure 6-1 (Section 6.1) except for the periphery, which was loaded with discharged assemblies from the 24-month cycle, with an average burnup of 24.66 GWD/MTU. The main results for this core are summarized in Table 6-6 and compared to those from a 2D model for the 36-month equilibrium cycle. It can be seen that the cycle burnup and maximum CBC are very similar for both cycles, and the peaking factor is higher but within acceptable limits for the transition cycle. The exposure of the peak pin is higher for the equilibrium cycle, where the assemblies have been in-core for 2 cycles of 36 months, versus 1 cycle of 24 months and 1 cycle of 36 months in the transition cycle. Figure 6-10 shows the average discharge burnup on an assembly basis for both the transition and the equilibrium cycles. The assembly burnups are very close in both cases except for the peripheral assemblies, which in the equilibrium cycle have been in-core for a longer time. Looking at the assemblies that will be reused in the next cycle, the average burnups are 37.99 and 37.73 GWD/MTU for the transition and equilibrium cycles, respectively, the difference being 0.26 GWD/MTU, or 0.7%. These results show that the peripheries for both cycles have similar reactivities. The total core costs for the first 36-month cycle are about the same as for the equilibrium cycle since the fuel costs are the same and the difference in cycle lengths is negligible.

Table 6-6: Core performance for the transition and equilibrium cycles

	Cycle burnup (GWD/MTU)	Peak exposure (GWD/MTU)	Max CBC (ppm)	Max F_Q
Transition cycle	39.72	56.15	1,589	1.580
Equilibrium cycle	39.82	60.41	1,581	1.542

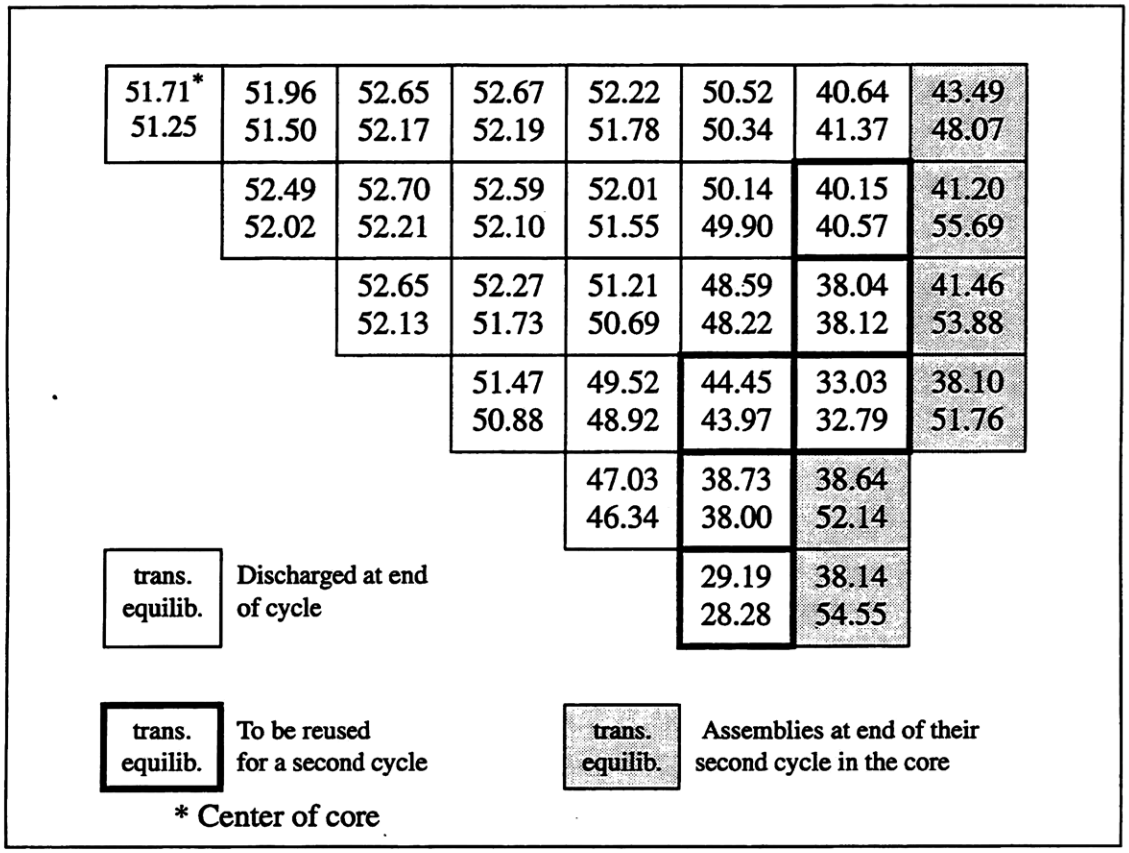

Figure 6-10: Assembly average discharge burnup in GWD/MTU for one eighth core for the equilibrium 36-month cycle and the transition cycle (first cycle after last 24-month cycle)

6.5 Conclusions

The loading pattern described in this Chapter yields a 36-month reload core that complies with the neutronics and thermal-hydraulics design limits. The parameters analyzed

include the peak pin exposure, total peaking factor, maximum enthalpy rise hot channel factor, core boron concentration, coefficients of reactivity and control rod worth. The shift in the neutron spectrum reduces the control rod worth, and new control rods are required in order to insure an adequate shutdown margin.

Peaking factors in the 36-month core may be reduced by axially zoning the burnable poison and by using computer codes that automatically perform loading pattern optimization. Moreover, selective use of the isotope Gd-157, which could be feasible with AVLIS technology, would reduce the reactivity residual penalty and provide an economic benefit.

The physics design for a transition cycle has been proposed that minimizes the economic penalty when shifting from a 24- to a 36-month cycle, leading to an annualized additional cost penalty of approximately $2.1M/yr.

Chapter 7

Fuel Performance

7.1 General Considerations

7.1.1 Comparison Between 18- and 36-Month Cores

A comprehensive study to assess the technical feasibility of the 36-month core requires that the fuel performance be analyzed. Extension of the cycle length exacerbates some fuel performance issues because of the differences existing between current cores (reference core) and the 36-month core:

- Power distribution: in the 36-month core, assemblies in a broad region of the center of the core run at high power (approx. 126% of core average) throughout core life. In multibatch 18-month cores, different loading strategies are possible that lead to variable power histories for the assemblies, that, in general, are less demanding than for the 36-month core. For example, in a Low Leakage Loading Pattern (L^3P), assemblies that run at higher power during the first cycle are shuffled to locations where they run at lower power in subsequent cycles.
- Fuel burnup: the average discharge burnups for the assemblies in the 36-month and the reference cores are 51.13 GWD/MTU and 39.50 GWD/MTU, respectively.
- In-core residence time: in the 36-month core, the not-reused and reused assemblies stay in-pile for 36 and 72 months, respectively. In 18-month cores, the assemblies stay in-pile for 2 or 3 cycles, that is, 36 or 54 months.
- Water chemistry: the concentration of soluble boron in the coolant is higher (both peak and cycle-averaged values) for the 36-month core than for the 18-month core. CBC is maintained wihtin the design limit, but its higher value leads to a higher concentration of lithium that affects the water chemistry.

As will be seen in the sections which follow, these differences have a strong influence on the thermal and mechanical performance of the pellets.

7.1.2 Fuel Performance in Extended Cycles

The fuel performance issues that could limit the implementation of extended cycles were identified by Handwerk et al. [H-1], and their main findings are summarized here. Table G.1 in Appendix G lists the ten issues analyzed for steady-state conditions, as well as the prescribed limits as indicated by the U.S. Nuclear Regulatory Commission's Standard Review Plan, the predicted performance for the extended cycle as compared to the

reference cycle and the the proposed solutions. Some of the issues are difficult to quantify and only a qualitative prediction of the expected trends is provided. The extended cycle considered in the analysis of Ref. [H-1] runs for 38.8 EFPM or 41.4 calendar months.

Of the ten issues analyzed, extended cycles will pose unique challenges with respect to:

- design stress and strain,
- fatigue cycling,
- fretting,
- waterside corrosion,
- rod bowing / axial growth,
- rod internal pressure,

and will degrade the margin for transients for

- clad overheating,
- fuel centerline melt.

7.1.3 Goals and Scope of this Analysis

FROSSTEY-2, the fuel performance code available for this study, models the rod behavior with burnup and calculates many thermal and mechanical parameters of interest. The performance of the 36-month core can be analyzed for an envelope pin (see Section 7.2 for description) using this code, and the fuel centerline temperature, rod internal pressure and oxide layer thickness can be compared to the targeted design limits. Although the code is easy to use and provides useful information, some limitations exist:

- FROSSTEY-2 is a proprietary code. Although execution of the code and information about it has been provided by YAEC, explicit discussion of the equations used in the code is limited.
- Codes are built with some degree of conservatism that cannot be quantified unless the equations are explicitly analyzed and the sources of conservatism identified.
- The corrosion model in FROSSTEY-2 is under reevaluation.

The preliminary analysis for the 10 fuel performance issues in [H-1] showed that further research is desirable in many areas. In particular, the cladding corrosion and the fission gas release are predicted to be worse in extended cycles since they will be affected by the more demanding power distribution. Although not specifically included in Table G.1, it should be noted that the fission gas release drives the rod internal pressure. Given the above limitations, it was considered that developing models for these two phenomena

would provide valuable insights about the processes. Both phenomena are analyzed by FROSSTEY-2. However, establishing simplified models and performing the calculations in addition has some advantages:

- The models can be based on information published in the open literature that may be discussed without restrictions.
- Parametric analyses can be performed to identify the factors that affect the processes.
- The sources of conservatism can be best identified by explicit analysis of the equations, and the code's conservative estimate can be replaced by a best estimate reflecting an average behavior of the rods.

The cladding corrosion and fission gas release are driven by the cladding and fuel temperatures, respectively. An accurate representation of these phenomena would require a full thermal analysis in the rod, which is linked to other processes such as fuel swelling or mechanical behavior (stress and strain) in fuel and clad. Fuel performance codes such as FROSSTEY-2 perform an integral analysis and model the interdependencies among all these processes. The simplified models in this study do not represent the fuel behavior with the same accuracy as the codes. However, by establishing appropriate boundary conditions and fixing selected parameters, practical tools may be developed that predict the cladding oxide layer thickness and the fractional gas release in the rod.

The goals of the fuel performance analysis for the 36-month core are:

- to show compliance with the design limits for fuel centerline temperature and rod internal pressure by using FROSSTEY-2. This is done in Section 7.2.
- to develop simplified models for cladding corrosion and fission gas release to compare the behavior of representative pins for the 36-month core with those for the reference 18-month core. This is done in Sections 7.3 and 7.4.

7.2 Fuel Performance Analysis with an Envelope Pin

7.2.1 Description of the Envelope Pin

In order to assess the performance of the fuel, pins subject to the most demanding conditions must be analyzed. The power shifts throughout core life and assemblies running at higher power early in life are more depleted towards the end of the cycle and, hence, run at lower power. Moreover, heavily poisoned assemblies are initially less reactive and run at low power early in life, but draw more power once the poison is depleted. Within each assembly an analogous phenomenon is observed for the pins. For these reasons, it is

extremely difficult to determine which pin in the core has the most demanding operation from thermal and mechanical points of view. Therefore, an envelope pin is created that is subject to more severe conditions than any pin in the core. At each burnup step, the envelope pin is assigned the average power distribution of the pin with the maximum axially integrated power. The input values to FROSSTEY-2 include the axially averaged power of the pin and the average pin exposure in each step, as well as the axial power shape every 4 or 5 steps.

It was found that the hottest pin at the end of core life is not the pin with the highest burnup. In order to account for the full range of pin exposures, a tail was added to the envelope pin so that the burnup range was extended to the maximum pin average burnup.

This analysis must account for the different types of pins in the core and for the assembly in-core residence times. First, the pins that contain burnable absorbers generate considerably less power than the unpoisoned pins, especially early in life. However, the presence of gadolinia within the fuel matrix reduces the pellet conductivity. The overall effect on the rod temperatures is difficult to predict and a separate analysis has to be performed for the poisoned and unpoisoned pins. Second, although the assemblies that are not reused run at higher power than the reused assemblies, those reused are kept for two cycles in the core, and run at very low power during the second cycle. The parameters that depend largely on the instantaneous values of the heat generated, such as the fuel centerline temperature, are expected to be worse for the assemblies that are not reused. However, it is difficult to predict the behavior of parameters that depend on cumulative effects throughout the cycle, such as corrosion or fission gas release.

Hence, a complete analysis that accounts for these differences requires creation of four envelope pins: one for each type of pin (poisoned and unpoisoned) within each type of assembly (reused and not reused). For practical considerations in input data preparation, it was reasonably assumed that the hottest poisoned pin is in the same assembly as the hottest unpoisoned pin.

Figure 7-1 shows the location of the peak pin throughout core life for the envelope pins. The figure displays an order number indicating the sequential motion of the peak pin, the core average burnup range for which the assembly houses the hot pin and the range of

peak pin power --both unpoisoned and poisoned-- during that burnup range. For the assemblies that are not reused, the peak pin is located in assembly 8-F for more than half of the cycle (from BOC to 23 GWD/MTU). Then it moves away from the center, to assemblies 10-F, 10-E, 11-E, 11-D and finally, 12-D. The tail for this envelope pin is taken from assembly 9-G, in which the maximum pin burnup is 54.9 GWD/MTU. Although not represented in the graph, it should be noted that the peak pin also migrates within each assembly. For example, the hot spot moves to six different pins in assembly 8-F from BOC to 23 GWD/MTU.

For the assemblies that are reused, the peak pin moves from assembly B-9 to C-11 and C-12 during the first cycle. During the second cycle, the peak pin stays in the same assembly (B-12). The tail in this case is taken from assembly A-9, where the pin with the maximum average burnup is located.

As for the 18-month core, the envelope pin was taken from work by Handwerk et al. [H-1]. This envelope is made of contributions from each of the three batches that form the

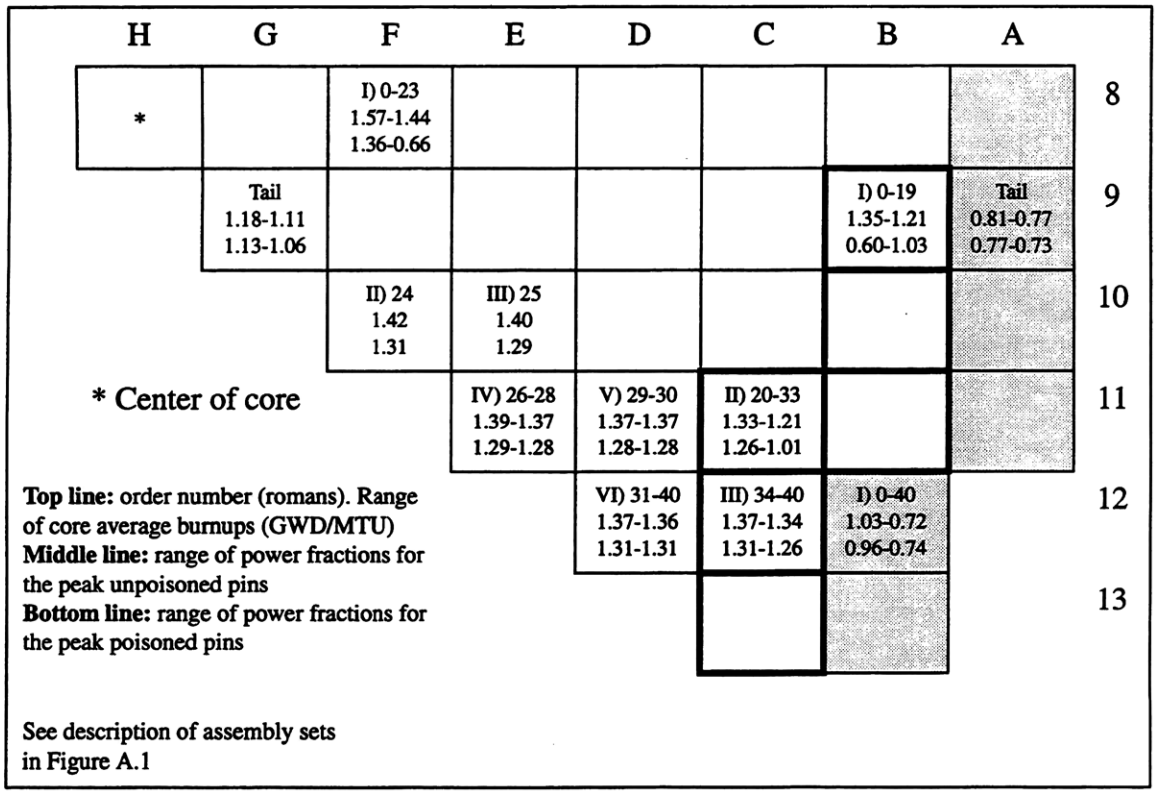

Figure 7-1: Location and values of the peak pin throughout core life for the three sets of assemblies in the 36-month core

core. The poisoned envelope pin in the 18-month core is not included because of limited information availability.

7.2.2 Envelope Pin Power History

It is essential to describe the pin power history since it drives the rod fuel performance. Of the parameters analyzed here, the fuel centerline temperature strongly depends on the local power at each burnup step, whereas the internal rod pressure depends on the integrated power both axially and in time. In this section, the average and peak pin powers are analyzed, and the conservatism of the envelope pin procedure is illustrated.

The analysis is performed with FROSSTEY-2 for the 4 envelope pins in the 36-month core and for the unpoisoned envelope pin in the 18-month core.

7.2.2.1 Average Pin Power

The average linear heat generation rate for the unpoisoned envelope pin is shown in Figure 7-2. It can be seen that:

- the envelope for the not-reused assemblies keeps a value between 25 and 28.6 kW/m for over 45 GWD/MTU. In the final stage of the cycle, the reduced values correspond to the more depleted exposure tail.
- the envelope for the reused assemblies is significantly lower than the previous envelope for a great part of the pin life and matches it around 40 GWD/MTU, when the core power is shifted towards the outer assemblies. The envelope for assemblies in the second cycle in the core is represented by only a short stage around 50 GWD/MTU since the rest of the envelope is hidden by the envelope of the first cycle. The final stage, with values below 15 kW/m, corresponds to the exposure tail.
- the envelope for the 18-month reference core is about 3 to 4 kW/m lower than the envelope for the not-reused assemblies. The reference envelope is slightly higher than the reused assemblies envelope during the first part of the cycle, then stays below it. Moreover, the reference envelope has a shorter life than both envelopes for the 36-month core.

Similar values are plotted for the poisoned pins in Figure 7-3. These envelopes show significantly lower power than the unpoisoned pins' envelopes early in life. It can be seen that:

- for the not-reused assemblies, the pin power steadily increases until about 20 GWD/MTU. At this point, the poison is depleted. The residual poisoning and the initially lower content of uranium oxide in the pellet (due to the presence of the gadolinium oxide) keep the envelope poisoned pin below the envelope unpoisoned pin. After 20GWD/MTU, the pin power is fairly constant and close to the value in the unpoisoned case. Finally, the power is reduced in the exposure tail.

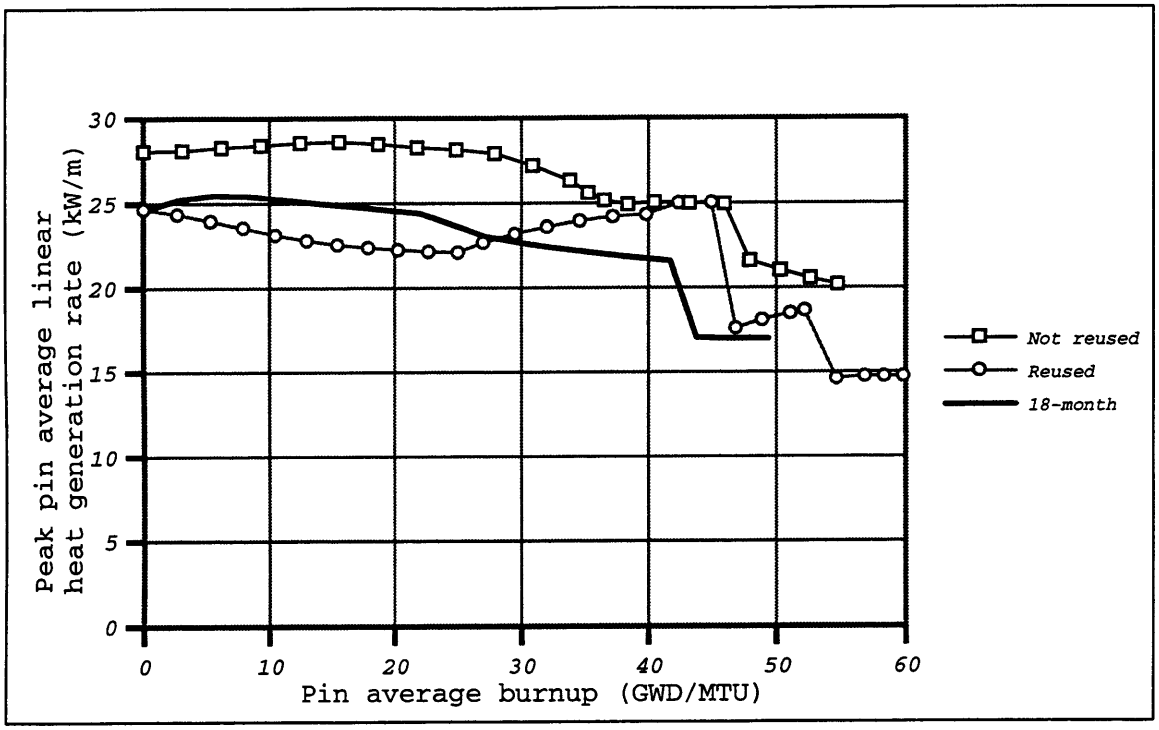

Figure 7-2: Average linear heat generation rate for the envelope unpoisoned pin

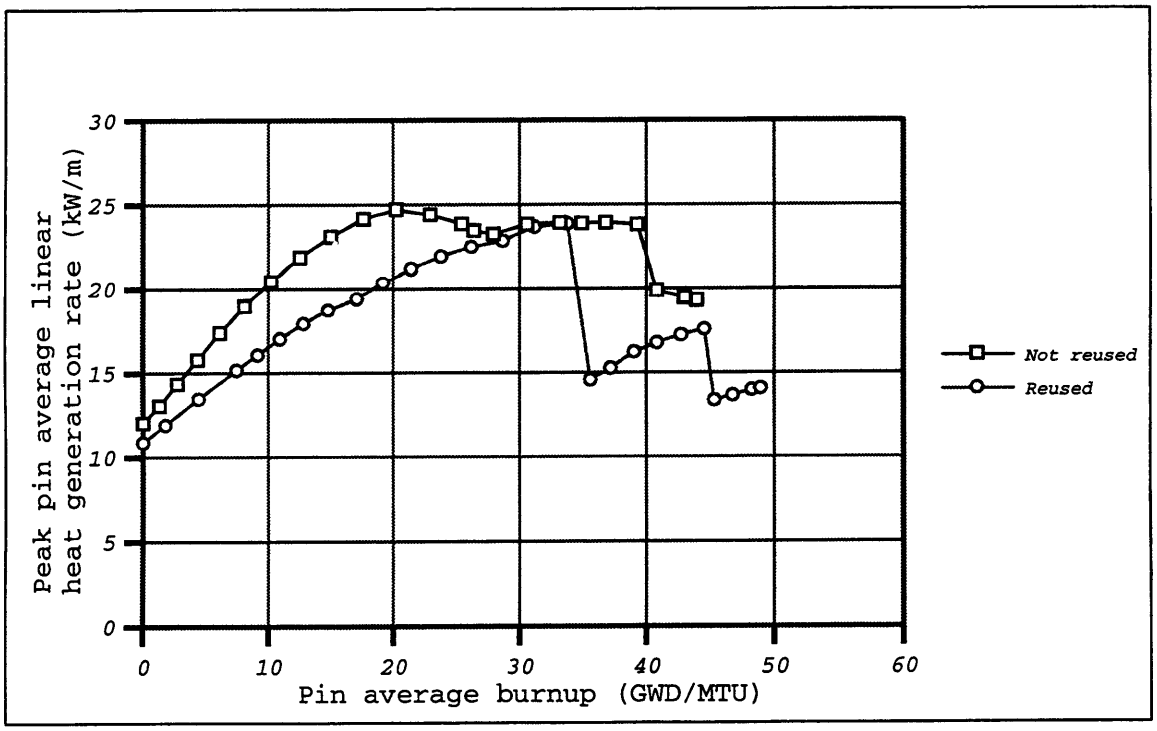

Figure 7-3: Average linear heat generation rate for the envelope poisoned pin

- for the reused assemblies, the envelope pin lies below the not-reused envelope and burns longer. The pin power also increases steadily, although for a longer time than in the previous case. The reason is that the poison depletion coincides with the power shift towards the periphery, and the power increases until 33 GWD/MTU. The next stages represent the second cycle, (partially hidden by the first cycle,) and the exposure tail.

7.2.2.2 Conservatism of the Analysis

The envelope pin provides a conservative estimate of the demands on the fuel and any pin in the core will have a more favorable behavior. It is interesting to estimate the existing margin between the actual pins in the core and the fictitious envelope pin. This is done in the following by comparing the average power of the envelope pin and two actual pins which contribute to create it. Of the two pins selected, one is part of the envelope early in life, whereas the other is part of it late in life. The analysis is performed both for the not-reused and the reused assemblies.

Figure 7-4 illustrates this margin for the assemblies that are not reused. Pin A is located in assembly F-8 (see Figure 7-1 for description), and forms the envelope pin between 3 and 13 GWD/MTU. During the rest of the cycle, this pin is very close to the envelope, except for a period between 39 and 47 GWD/MTU where the difference increases. As for pin B, it is located in assembly D-12 --relatively close to the core periphery,-- runs at lower power early in life and contributes to the envelope pin between 39 and 47 GWD/MTU. The average power in this pin is significantly lower than the power of the envelope pin for most of the cycle. It should be noted that the final burnup of pin B is lower than that of the envelope. It can be concluded that the envelope pin represents fairly well the power shape for some of the actual pins in the core. However, the margin of conservatism is significant for many other pins.

A similar analysis is provided in Figure 7-5 for the assemblies that are reused. Pin C is located in assembly B-9 and contributes to the envelope pin for about 25 GWD/MTU. For the rest of the first cycle, the pin power lies below but close to the envelope pin. During the second cycle, pin C is located in the core periphery and runs at very low power, at all times below 5 kW/m. The pin power in this region is far below and burns to a lesser extent than the envelope. Pin D is located in assemblies B-11 and B-12 for the first and second cycles,

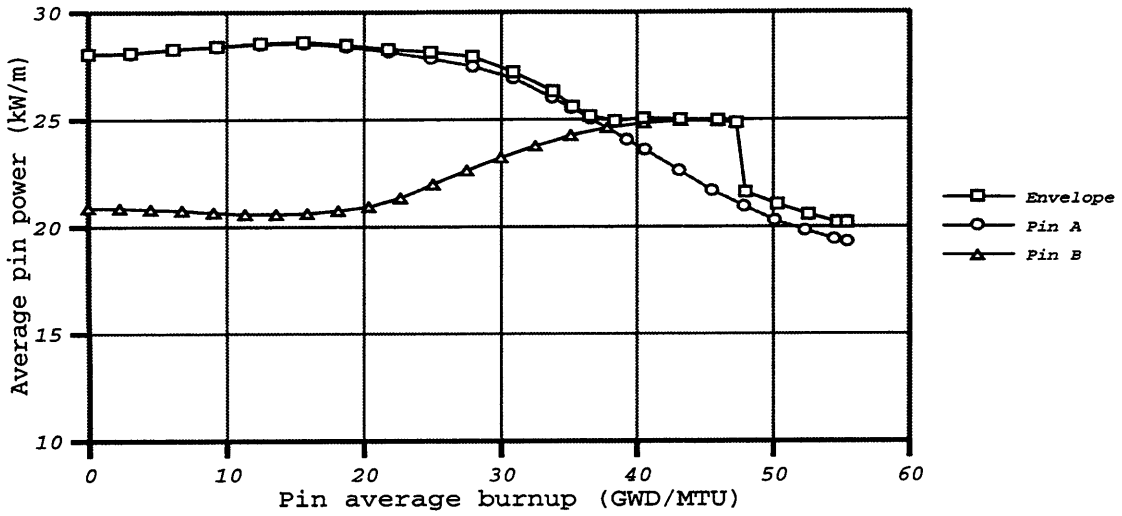

Pin A is in location (11,15) within assembly F-8 (see Figure 7-1 for assembly designation).
Pin B is in location (12,12) within assembly D-12

Figure 7-4: Conservatism in the envelope pin analysis for the assemblies that are not reused in the 36-month core

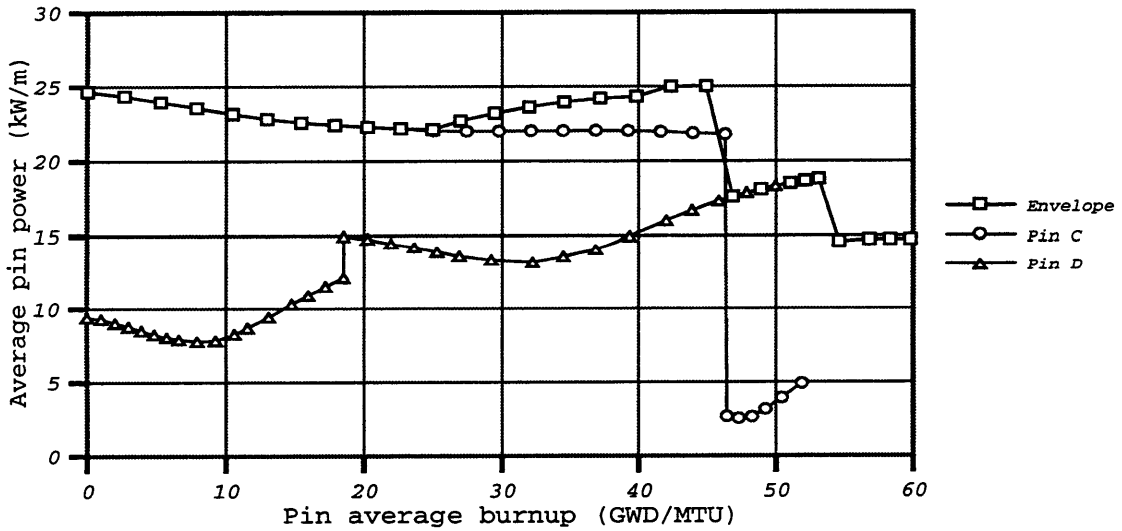

Pin C is in location (6,2), in assemblies B-9 and A-10 during the first and second cycles, respectively
Pin D is in location (17,17) in assemblies B-11 and B-12 during the first and second cycles, respectively

Figure 7-5: Conservatism in the envelope pin analysis for the assemblies that are reused in the 36-month core

respectively. This pin runs at low power early in life, and during its second cycle represents an envelope for the assemblies that are reused. Although pin D contributes to the envelope between 45 and 53 GWD/MTU, its power is far below the envelope for all burnups below 45 GWD/MTU. The analysis for the reused assemblies show that the conservative margin is significant.

7.2.2.3 Peak Pellet Power

The power for the peak nodes in the envelope pin are shown in Figures 7-6 and 7-7 for the unpoisoned and poisoned cases, respectively. The values in these plots are the product of the average pin power and the maximum normalized axial peaking factor for the pin.[4] The trends for the peak pellet power for the 36-month core are relatively similar to the trends of the peak pin power shown in figures 7-2 and 7-3. This is because the axial shape shifts but the maximum axial peak does not change much throughout core life. As for the reference core, the peak pellet power shows more variability than the pin average power

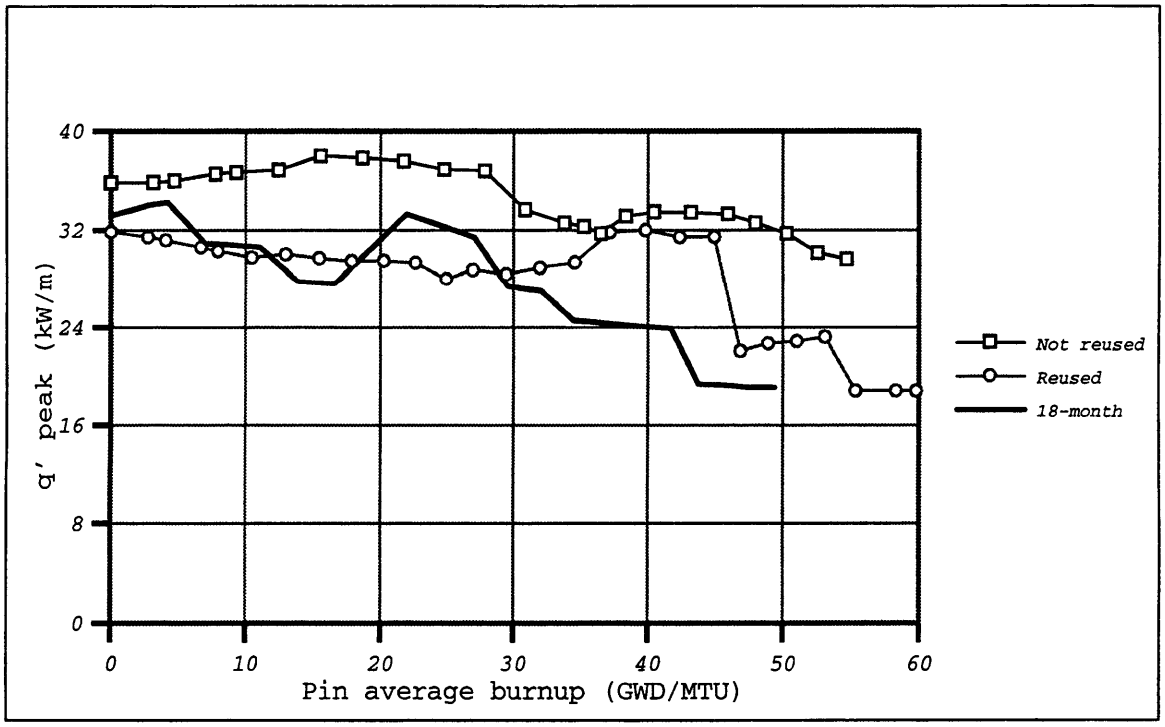

Figure 7-6: Peak linear heat generation rate for the envelope unpoisoned pin

4. These factors change throughout core life and are not shown here. However, the axial shape factors for the peak pin are similar to the core average axial factors that were plotted in Figure 5-6 for an axially uniform core.

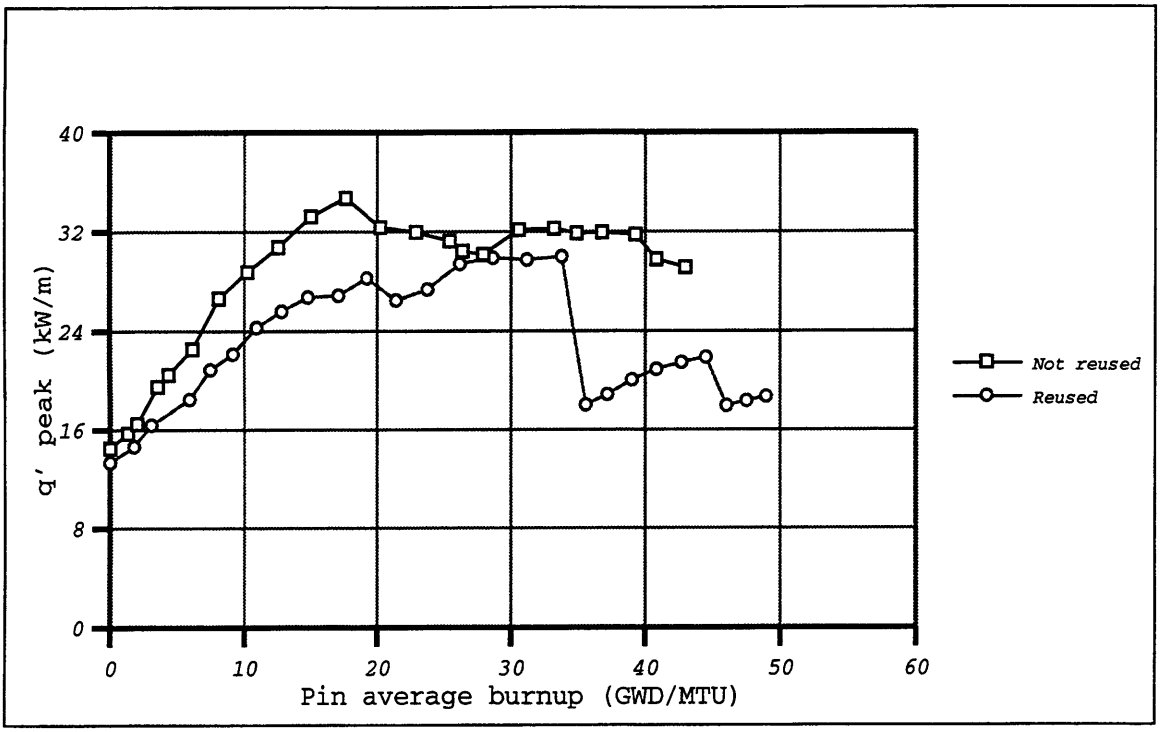

Figure 7-7: Peak linear heat generation rate for the envelope poisoned pin

because the maximum axial factors change more. This can be deduced from figures 6-4 and 6-5, since the radial peaking remains fairly constant and the total peaking shows a fast decline. Moreover, this happens for each 18-month cycle, and, therefore, up to three times in the pin life.

7.2.3 Fuel Centerline Temperature

The peak fuel centerline temperature (FCT) as calculated by FROSSTEY-2 is shown versus core average burnup in figures 7-8 and 7-9 for the unpoisoned and poisoned envelopes, respectively. By comparison to figures 7-6 and 7-7, it can be seen that FCT closely follows the peak linear heat generation rate in the rod. There are, however, several phenomena that affect the fuel-to-clad gap conductance, which lead to changes in the fuel surface temperature, and ultimately in the fuel centerline temperature. These phenomena are fuel swelling, relocation and densification, clad creepdown, and relative clad-fuel thermal expansion, and they will not be analyzed here. Furthermore, the effective fuel conductivity changes both with temperature, burnup, and cracking, affecting the heat transfer within the rod. The FCT is kept far below the melting temperature at all times.

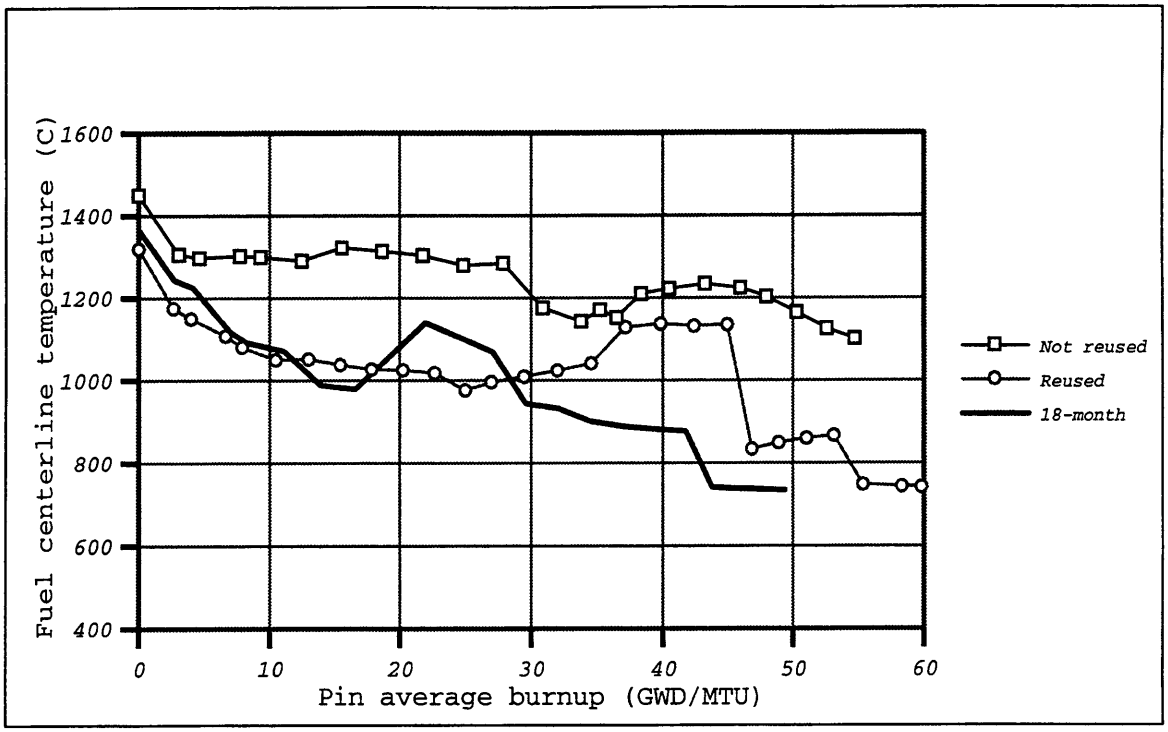

Figure 7-8: Peak fuel centerline temperature for the envelope unpoisoned pin

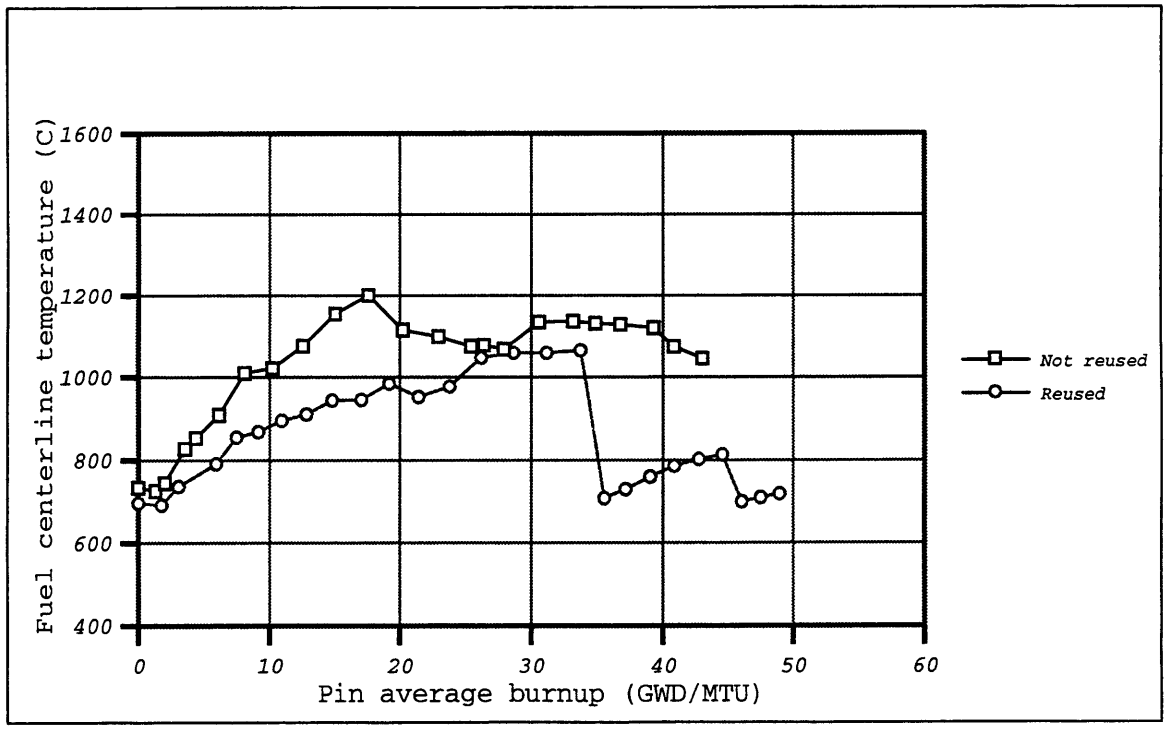

Figure 7-9: Peak fuel centerline temperature for the envelope poisoned pin

Inspection of Figure 7-8 shows that:

- although the peak power does not change much early in the cycle (between BOC and 5 GWD/MTU, as indicated in figure 7-5), the FCT decreases by more than 100 °C. This is due to the initial rapid reduction in gap size caused by relocation, that significantly increases the fuel-to-clad gap conductance.
- for the not-reused assemblies, the maximum FCT is 1450 °C at BOC, and oscillates between 1320 °C and 1100 °C for the entire cycle.
- for the reused assemblies, the FCT oscillates between 980 °C and 1200 °C up to 45 GWD/MTU, then stays below 900 °C until the end of pin life.
- for the reference core, the initial value for FCT is 1384 °C. Throughout the cycle the FCT is significantly lower than for the reused assemblies, especially after 30 GWD/MTU.

Figure 7-9 shows the FCT in the envelope poisoned pin. Comparison with figure 7-9 indicates that the degradation of the fuel conductivity due to the burnable absorber does not offset the lower heat generation. The maximum FCT in core life are 1066 °C and 1220 °C for the reused and not-reused assemblies, respectively.

7.2.4 Rod Internal Pressure

It is desirable to keep the pressure inside the fuel rods below the primary system pressure (2250 psia). Rods are initially prepressurized with a fill gas (He) in order to provide a good fuel-to-clad gap conductance. As fission occurs, part of the produced fission gases are released from the fuel matrix. This phenomenon will be described in more detail in Section 7.4. The free volume between clad and gap changes because of relocation, densification, swelling, creep and thermal expansion.

Figure 7-10 displays the rod internal pressure for the envelope unpoisoned pin. This pressure is higher for the 36-month core than for the reference core, but it is kept at all times below the design limit (2600 psia). The pressure is higher for the not-reused assemblies as expected from the previously discussed FCT.

The rod internal pressure for the envelope poisoned pin is shown in Figure 7-11. The lower heat generation and temperatures lead to moderate rod internal pressures that do not exceed 1200 psia.

These values indicate that the rod internal pressure is not a concern for the 36-month-core.

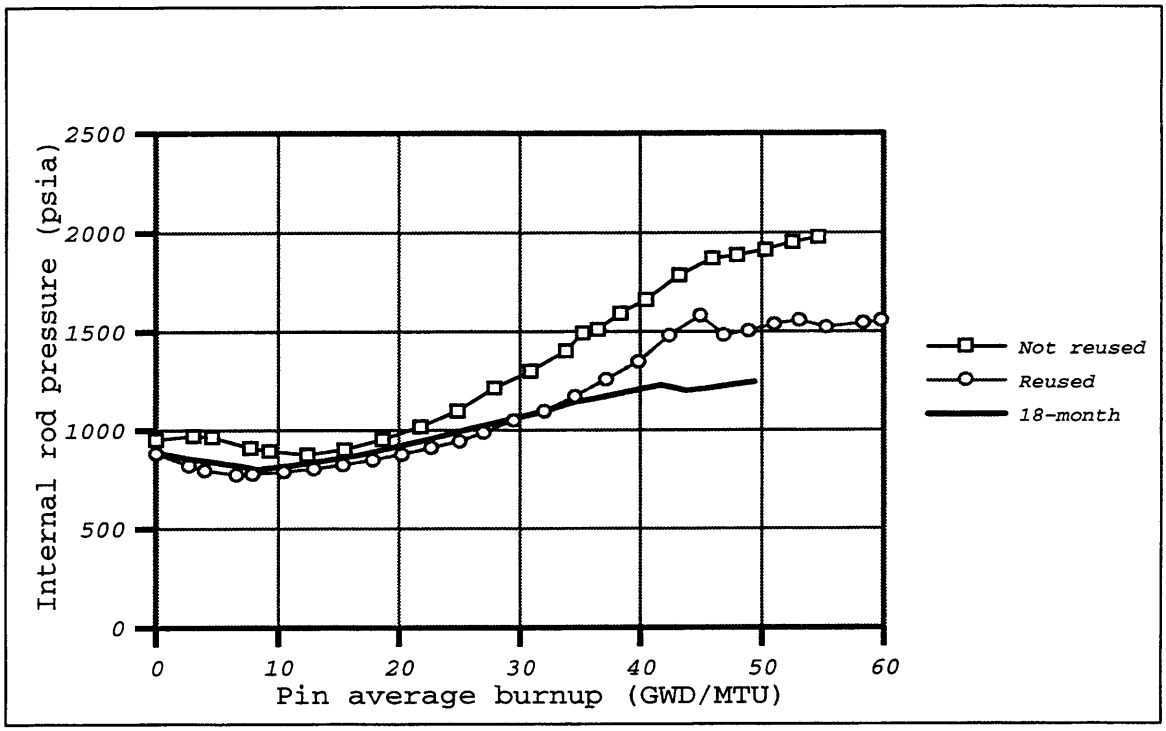

Figure 7-10: Rod internal pressure for the envelope unpoisoned pin

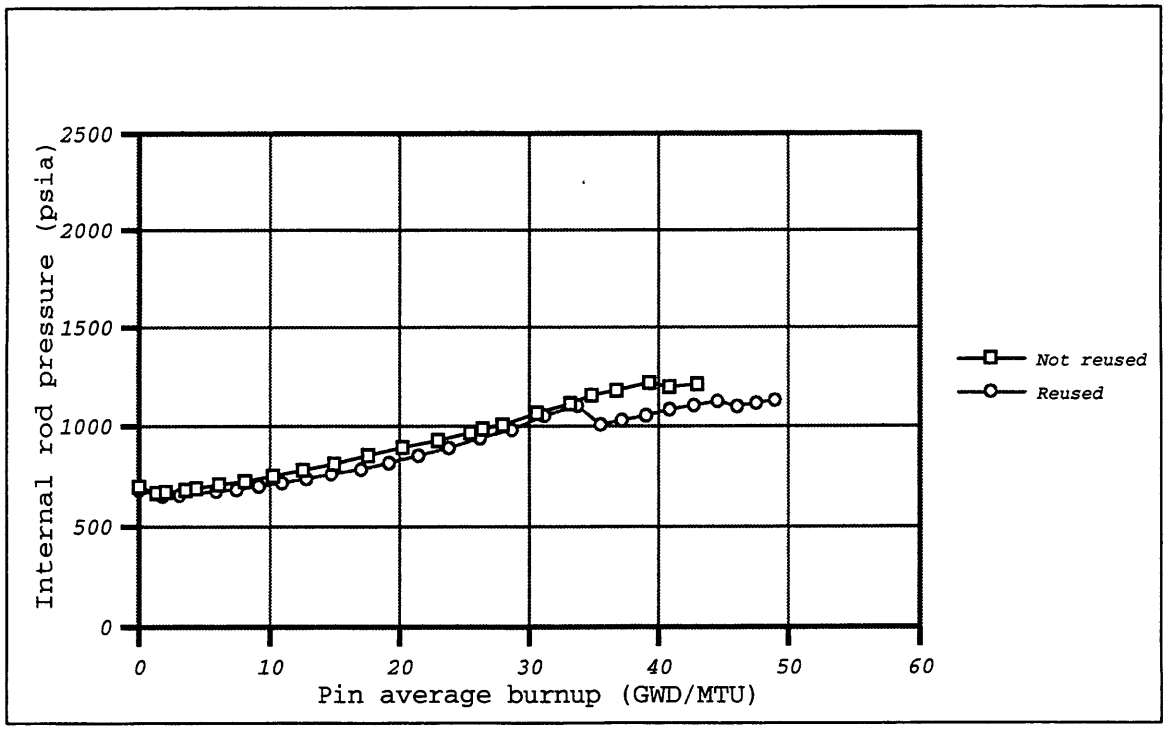

Figure 7-11: Rod internal pressure for the envelope poisoned pin

7.3 Cladding Corrosion

7.3.1 General Considerations

Zircaloy cladding oxidizes under normal operating conditions in PWRs, and an oxide layer covers the cladding. Thin oxide films do not constrain reactor operation. However, film growth over a certain thickness may have deleterious effects. First, heat transfer is degraded as the oxide layer thickens, leading to higher temperatures in the cladding metal-oxide interface, and, hence, in the fuel itself. Moreover, the oxidation reaction is accelerated as the temperature rises, creating a positive feedback mechanism. Second, parts of the oxide film may detach from the clad and be transported by the coolant throughout the primary system. These products may be deposited or get stuck in assembly flow paths, altering the regular coolant flow and degrading the heat removal from the rods. Finally, the structural integrity of the cladding is weakened as the oxide is substituted for metal.

Predictions of oxide layer thickness in Zircaloy rods is difficult. There is a large variability from one reactor to another, and even within the same reactor for rods manufactured by the same process and experiencing similar irradiation histories [F-3]. The thermalhydraulic conditions of the plant, the power history, the water chemistry, the fuel rod surface heat flux, and the fabrication variations in the rods play very important roles [G-4].

7.3.2 Model

The model by Forsberg et al. [F-3] is used to calculate the oxide layer thickness in the 36-month core and to compare it to the reference 18-month core. The corrosion mechanisms and basis for the calculations in the model are described in the following paragraphs. The main equations are included in Appendix H, and the FORTRAN code used for the calculations is listed in Appendix I.

Two stages are observed in the oxidation of Zircaloy. In the first stage, also called the pre-transition oxidation, the oxide layer is very compact and protective, and grows according to a cubic rate equation. The breakaway or first transition leads to the second oxidation stage, also called post-transition oxidation, in which the corrosion rate significantly increases due to the formation of cracks in the oxide that gives oxygen easier access to the metal-oxide interface.

The oxidation process in the pre-transition oxidation is governed by an equation of the form

$$\frac{ds}{dt} = \frac{F_{c1}(T)}{s^2}, \tag{7.1}$$

where s is the oxide thickness, t is the exposure time and $F_{c1}(T)$ defines the behavior of the corrosion rate as a function of the metal-oxide interface temperature. For oxidation at constant temperature, Eq. (7.1) may be solved to yield the oxide thickness at the end of a time step Δt, as a function of the oxide thickness at the beginning of the step, s_o,

$$s^3 = s_o^3 + F(T) \cdot \Delta t \tag{7.2}$$

Hence, the corrosion in the pre-transition oxidation shows a cubic behavior. For a constant metal-oxide interface temperature, the corrosion rate undergoes a transition to linear behavior at time t_a (also called time to breakaway) given by

$$t_a = F_{c2}(T) \tag{7.3}$$

The time to breakaway varies significantly from sample to sample, and is shorter as the temperature increases. At low temperatures, i.e. 500 K, for a 1000 day oxidation time, the transition does not take place [A-3]. This point is very important since the oxide growth rate changes from cubic to linear after the transition so that it is desirable to maintain the pre-transition conditions for as long as possible.

For the post-transition oxidation, the governing equation has the form

$$\frac{ds}{dt} = F_{c3}(T, \phi, s) \tag{7.4}$$

For modest increases in oxide thickness, F_{c3} is only a function of the metal-oxide interface temperature and thus gives a linear solution in this range. However, for thicker films, F_{c3} is enhanced by both fast neutron flux (ϕ) and oxide thickness (s). The fast neutrons modify the structure of the oxide and cause radiolysis of the coolant. Equation (7.4) can be solved as

$$s = s_o + F_{c4}(T_o, \phi, \Delta t, s_o) \tag{7.5}$$

This expression is simplified to a linear relationship for moderate film thicknesses, and adopts a non-linear form when the enhancements are considered.

A thermal hydraulic model is used to calculate the bulk coolant temperature at a given axial position, and the clad-to-coolant heat transfer. This is calculated for either forced convection or nucleate boiling. The axial distribution of the rod power as a function of burnup, the subchannel geometry, the coolant inlet temperature and mass flow are inputs to the model. The main assumptions and simplifications in this model are:

- A single, closed subchannel is considered, in which cross flows are neglected. This simplification is conservative, since heat transfer is more efficient in a multichannel model with cross flows.
- The coolant properties are taken at an estimated average temperature.
- No crud deposition is considered.

The oxidation correlations depend on the rod materials. This analysis is based on Zircaloy-4 with reduced tin content (1.3 $^{w}/_{o}$ Sn). The fast flux enhancement requires that the flux over 1MeV be considered. Average values in the fuel were taken from the FROSSTEY-2 output.

7.3.3 Power Histories

Instead of using the envelope pin approach, simplified power histories representative of both the 18- and 36-month cycles were selected for the cladding corrosion analysis. The simplified histories reduce the amount of work necessary to input the power shapes in the code and yet represent fairly well the envelope pin. Furthermore, power histories appropriately selected are closer to actual pins than the envelope pin thereby eliminating some of the conservatism inherent to the envelope. Section 7.2 indicated that the rod power and FCT are higher for the unpoisoned envelope pin than for the poisoned envelope pin. Since cladding corrosion depends mainly on the cladding temperature, and, hence, on the rod power and temperature, only the power histories for unpoisoned pins are considered here.

In this simplified model, the power history in each 36-month cycle is represented by two steps, whereas each 18-month cycle is represented by a single step. The rod average power and the axial power shape are described in the following.

Figure 7-12 displays the rod average power versus core life for both the 36- and the 18-month cores. Two steps are considered in each 36 month cycle, lasting for 568 and 465 Effective Full Power Days (EFPD), respectively. The cut point corresponds to a core average burnup of 22 GWD/MTU. The power in each step is approximately the average power

of the envelope pin for the same period. This can be seen by comparison with Figure 7-2, although it should be noticed that different variables are plotted on the X-axes: pin average burnup in Figure 7-2, and effective full power days --which is a measure of core average burnup-- in Figure 7-12. Similar comments are valid for the first cycle in the core for the reused assemblies. As for the second cycle, the values are less conservative than in the envelope pin. Based on the analysis in Section 7.2.2.2, rod average powers are taken as 9.9 and 11.5 kW/m, which are lower than in the envelope pin, but still relatively higher than those for the actual pin of Figure 7-5. For the 18-month core, one power step is considered for each cycle. The values are approximate averages of the envelope pin values for that period, i.e. 26.5, 23.4 and 18.0 kW/m.

It should be noted that the 36-month cycle is longer than two 18-month cycles. This is so because the capacity factor assumed for the reference core is lower than that of the extended cycle. As a result, each 18-month cycle lasts for only 439 EFPD per cycle (or 1317 EFPD for 3 cycles), versus the 1033 EFPD for the 36-month cycle.

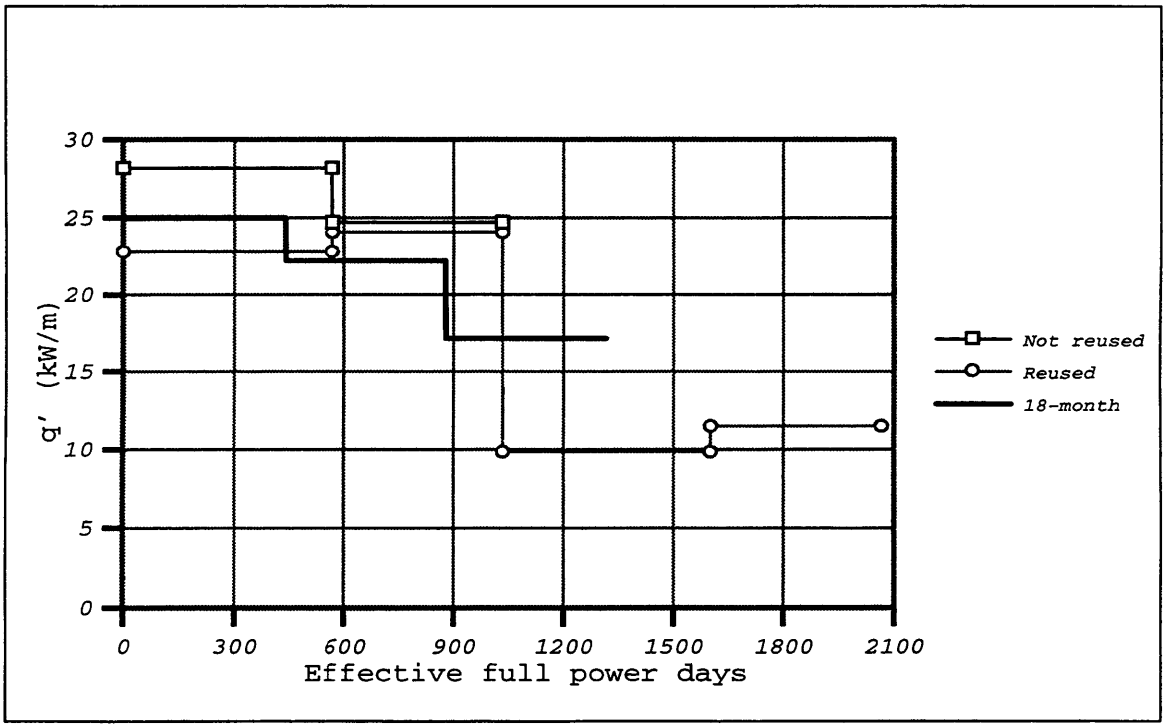

Figure 7-12: Simplified power history: rod average power for the 36-month and 18-month reference cores

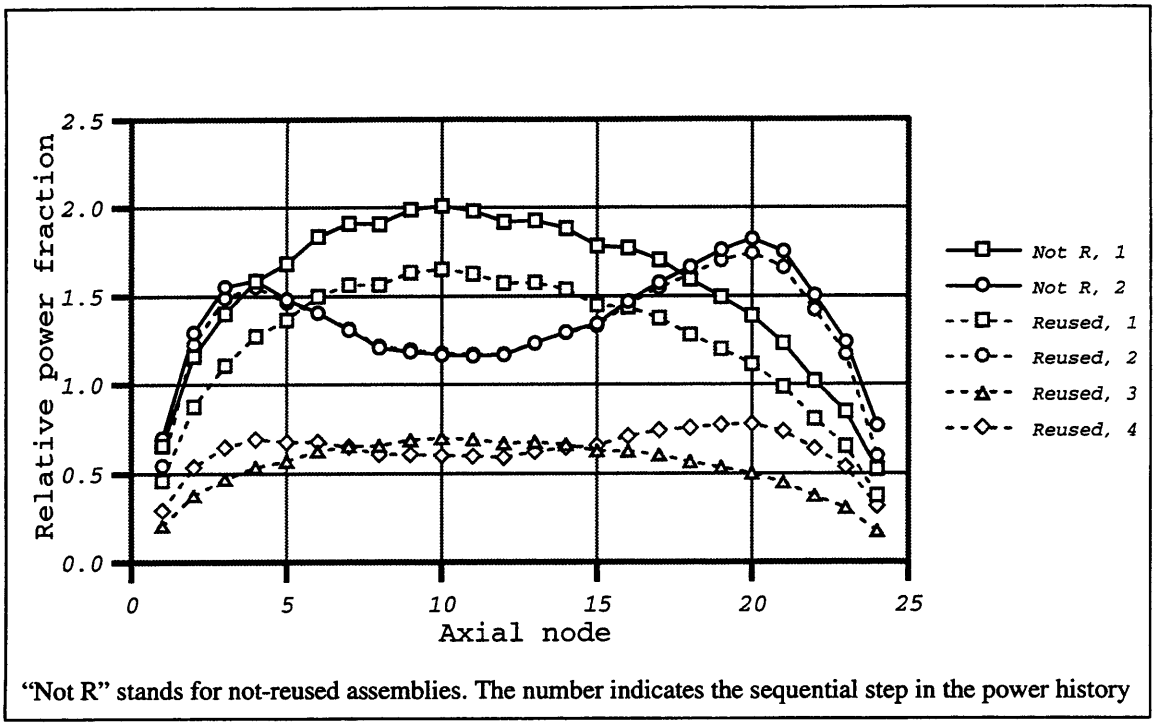

"Not R" stands for not-reused assemblies. The number indicates the sequential step in the power history

Figure 7-13: Axial shapes (local linear heat rate/core average linear heat rate) for the simplified power history in the 36-month core

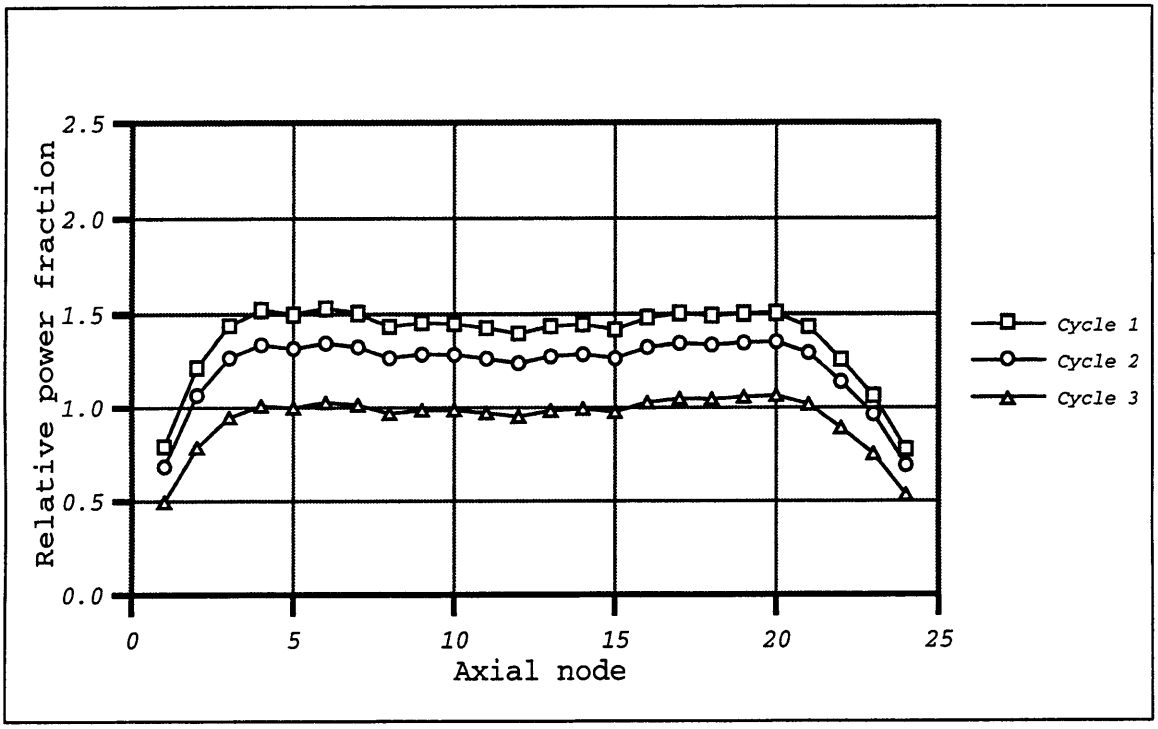

Figure 7-14: Axial shapes (local linear heat rate/core average linear heat rate) for the simplified power history in the 18-month core

Figures 7-13 and 7-14 show the axial power shapes (core averaged peaking factors) assigned to each of the steps in the simplified histories. These are the axial shapes for the envelope pin at intermediate points within each step, and are fairly constant for the step.[5]

The assemblies that are not reused show a first peak in node 10, slightly below the core center, and a second peak in node 20, close to the top of the reactor. For the reused assemblies, the behavior in the first cycle is similar, although the peaks are lower, and the second cycle shows very smooth curves. The axial shape for the 18-month cycle is very smooth for the three cycles.

7.3.4 Results

The corrosion mechanism was analyzed using the model presented in Section 7.3.2 and the power histories of 7.3.3. For simplicity, only one axial location was studied, which corresponds to the point where the thickest oxide layer is expected at the end of pin life. This location is at an elevation of about 300 cm (axial node 20), as indicated in experimental and calculated results in Ref. [F-3]. Above this elevation, the local power decreases and so does the oxidation rate. Below this elevation power peaks have similar values, the coolant temperature is lower and there is less oxidation.

The calculated oxide thickness is plotted versus operating days in Figure 7-15 for both the 36-month and the reference core, and the important values are listed in Table 7-1. In the first stage of oxidation, a cubic growth rate is observed in the 3 curves. The time to the breakaway point is temperature-dependent, and, as indicated in Table 7-1, occurs earlier for the not-reused assemblies, which have higher power. Once the post-transition regime is established, the oxide growth is linear but the fast flux and thickness enhancements soon accelerate the corrosion rate. The oxide growth is faster for the not-reused assemblies since the power conditions are more demanding. After one cycle in the core, the oxide layer thicknesses are 40.7 μm and 59.1 μm for the reused and not-reused assemblies, respectively. The latter are discharged, and the former are shifted to peripheral locations, where the lower power slows down the oxide growth. As a result, the oxide layer increases only by 16.4 μm in the second cycle, for a total thickness of 57.0 μm. Both cases in the 36-

5. This can be seen in Figure 5-2, which shows the axial shapes versus core life for a loading pattern similar to the 36-month core

Table 7-1: Comparison of corrosion performance for the 36-month core and the reference core

	Not reused	Reused	18-month
Time to transition (days)	133.5	176.3	148.9
Thickness at transition (μm)	3.0	3.0	3.0
Final thickness (μm)	59.1	57.0	42.3

month core lead to thicker oxide layers than in the reference core for two reasons: the more demanding power history in the not-reused assemblies --which lead to an accelerated growth rate,-- and the longer in-core residence time (about 752 EFPD more than in the reference core) in the reused assemblies.

The corrosion mechanism is driven by the temperature at the metal-oxide interface. This temperature depends on the bulk coolant temperature --which depends on the power generated in lower elevations of the rod-- on the local power, and on the oxide thickness,

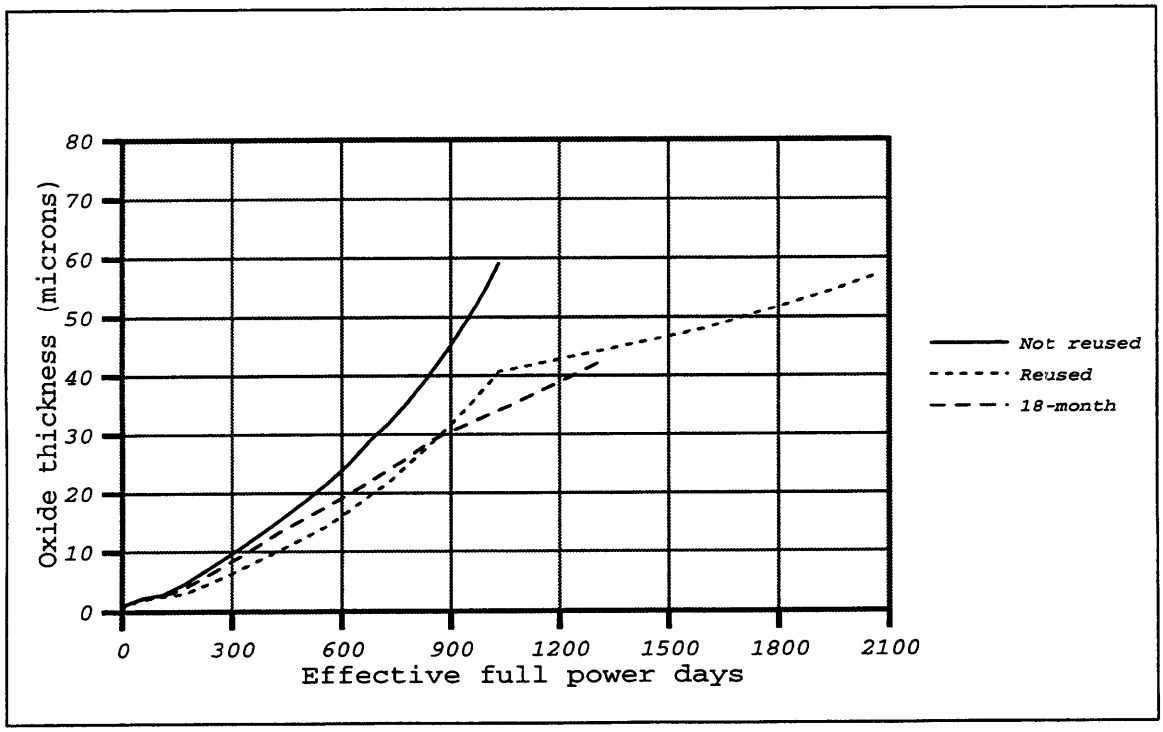

Figure 7-15: Oxide thickness versus time at an axial elevation of 300 cm for the 36-month and the reference core

which degrades the heat removal from the rod. Figure 7-16 depicts the evolution of the temperature in the metal-oxide interface. For the not-reused assemblies, the maximum temperature is 379 °C, well below the design limit (400 °C). For the reused assemblies the maximum value after one cycle is 366 °C, and the temperatures significantly decrease in the second cycle. As for the reference core, the temperatures are more moderate, reaching a maximum value of 352 °C. The discontinuities in the curves correspond to the step changes in the power history.

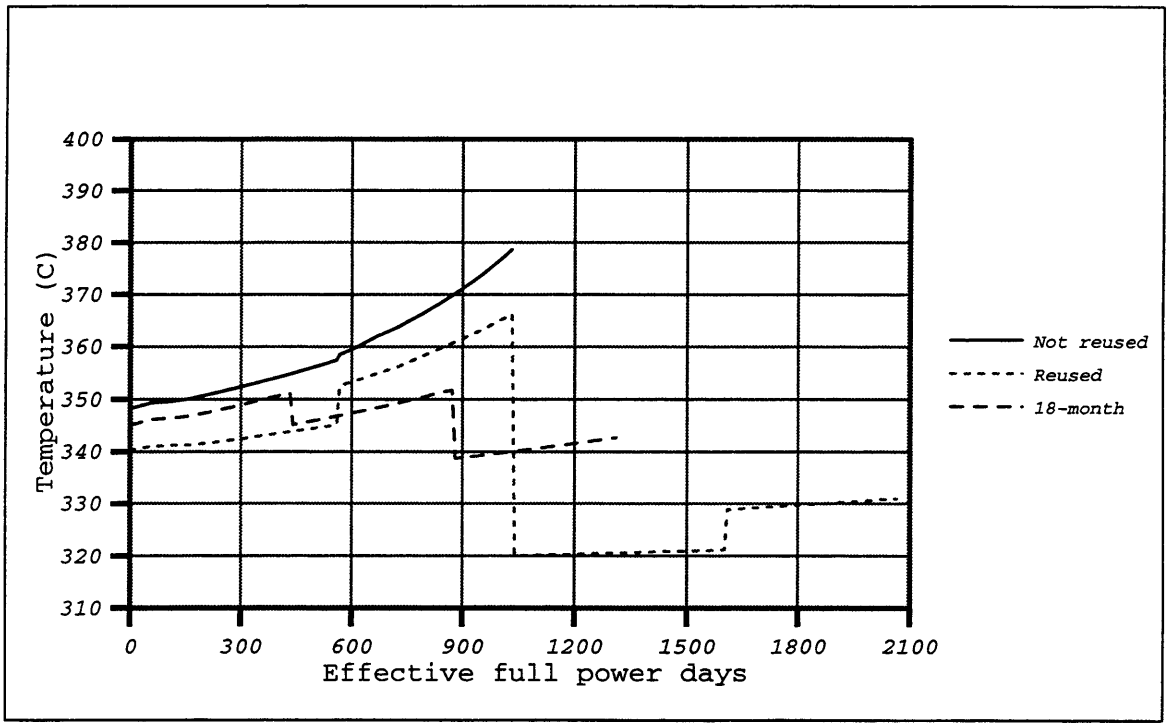

Figure 7-16: Temperature in the metal-oxide interface versus time at an axial elevation of 300 cm for the 36-month and the reference core

7.3.5 Discussion

The previous results show that cladding corrosion is enhanced in the 36-month core when compared to the 18-month core. Maximum oxide layer thicknesses are predicted to rise from 42 to 59 μm for improved low-tin Zircaloy-4 rods. This moderate increase in oxide thickness does not appear to be an operating constraint for 36-month cycles. Data from eight actual PWRs are represented in Figure 23 of Ref. [G-4], and most of these reactors develop oxide thicknesses between 20 and 60 μm, with two of them exceeding 100

μm. The predictions for the 36-month cycle are, hence, well within the range of operational experience.

Some uncertainties are expected in the calculations, which stem from simplifications in the analysis or from the model itself. These are reviewed here:

- The model presented in Section 7.3.2 uses some parameters experimentally adjusted by in-reactor ABB corrosion data. However, the model may be applied to reactors operating under different conditions. A variability of 20 to 30% can be expected from the combination of particular reactor fabrication variations, thermal-hydraulic conditions and water chemistry [M-6].
- Different sources in the literature quote different constants for the oxidation correlations and for the time-to-transition calculation [G-4].
- The more demanding water chemistry in the 36-month core may enhance the corrosion rate. The core boron concentrations are higher than in the reference core for long intervals, leading to increased concentrations of lithium in the coolant. Ref. [A-4] indicates that the oxidation rate constant for Zircaloy in the presence of Li^+ is $K_r = K_r^o \cdot [1 + 13.125 \cdot [Li^+]_{H2O}]$, where K_r^o is the rate constant for pure ZrO_2 and $[Li^+]_{H2O}$ is the concentration of Li^+ in water (mol/L). This enhancement has not been analyzed in the present work.
- CRUD deposits have not been considered in this analysis. CRUD layers degrade the clad-to-coolant heat transfer, increasing the metal-oxide interface temperature, and, hence, the corrosion rate.

Finally, the rod material plays a very important role. For example, calculations for the 36-month cycle indicate that use of Zircaloy-4 with 1.5 $^{w}/_{o}$ Sn (instead of 1.3$^{w}/_{o}$) results in maximum thicknesses of 82 and 99 μm for the reused and not-reused assemblies, respectively. Therefore, low-tin Zircaloy-4 leads to oxide layers which are 25 and 44 μm thinner. More corrosion-resistant materials such as ZIRLO™ have been developed that further reduce corrosion rates. This material is currently available from Westinghouse. Demonstration test results in PWRs indicate that corrosion rates in ZIRLO are 58% lower than in improved low-tin Zircaloy-4 for irradiations up to 37,800 MWD/MTU [W-2]. Furthermore, ZIRLO shows a very high resistance in lithiated water.

In spite of the uncertainties in the model, cladding corrosion will not limit operation of 36-month cycles provided that improved materials, such as low-tin Zircaloy-4 or ZIRLO, are used as cladding material.

7.4 Fission Gas Release

7.4.1 General Considerations

Release of fission gas from the fuel matrix is a mechanism which is quite complex and fairly dependent on fuel temperatures and its distribution in time. Higher temperatures lead to higher releases, and, therefore, the fission gas release in the 36-month core is expected to be higher than in the 18-month core. Several analytical models have been proposed and the results compared to experimental values. The variability in both predicted and measured values is large, and some controversy has arisen about the effects of burnup. In this Section, the release mechanisms are described, and models developed in the literature are reviewed. Then, a particular model is described and applied to calculate the fission gas release in the 36-month core.

7.4.2 Description of Release Mechanisms

Gases (predominantly xenon and krypton) are produced by fission, and, ultimately, are either trapped in the fuel matrix or released. Fission gases are released from the fuel matrix when they reach the pores and cracks directly connected to the fuel-cladding gap, the fuel outer surface, or a central void. Within the fuel rod, the gas atoms are subject to the following processes [O-3]:

- solution within the oxide material,
- diffusion to the grain boundaries,
- nucleation of bubbles,
- bubble growth by atomic migration,
- resolution of gas atoms within the bubble,
- migration of bubbles due to temperature, stress gradients, dislocation or grain boundary effects,
- coalescence of bubbles,
- interaction of bubbles with crystal defects.

The above processes are affected by many variables, such as temperature, temperature gradient, stress, stress gradient, fission rate, irradiation, time, fuel properties, fission gas properties and fuel microstructure. The fission gas release regimes as a function of fuel temperatures and temperature gradients are discussed in Ref. [O-3]:

- At low temperatures, below 1300 K, the mobility of the gas atoms is very low, and only the gases formed very close to an external surface can escape. The release mechanisms are recoil --direct flight from the fuel,-- and knockout --interaction of a fission

fragment or collision cascade with a stationary atom near the surface.

- At temperatures between 1300 and 1900 K, the mobility of the gas atoms becomes important, and release by diffusion to escape surfaces can occur. Bubble migration is, however, limited.
- At temperatures above 1900 K, thermal gradients drive gas bubbles over distances comparable to grain sizes, therefore facilitating the transfer of fission gas to cracks or surfaces in the free volume.

7.4.3 Literature Review

Many authors have proposed analytical or numerical methods to predict the fission gas release. Modeling all the processes affecting the fission gas release and taking into account all the variables is a complex problem.

Some models consider the microstructural mechanisms to predict bubble growth and gas diffusion:

- Bernard and Bonnaud developed a model that includes gas diffusion, resolution and gas saturation, and calculates the release using a finite volume method [B-3].
- Denis and Piotrkowski proposed a model that considers diffusion of gas atoms, precipitation of gas in bubbles, resolution, interconnection and sweeping of gas by grain boundary movement [D-1].
- Kogai established a model that simulates gas diffusion, and treats the grain boundary and bubble interlinkage. The model was verified with four kinds of data, and the release is consistently predicted [K-4].

Other models follow a temperature-zone approach, in which the fuel pellet is divided into rings according to the temperature ranges, and a given gas fraction is released from each ring. The effect of burnup in this type of model has been a source of disagreement. This is an important issue for the 36-month core since discharge burnups are higher than for the reference core (although within the 60 GWD/MTU limit). Prior to 1978, most codes had little or no burnup dependence in their predictions of fission gas release. The US Nuclear Regulatory Commission (NRC) recognized the experimental evidence that the fission gas release was enhanced above 30,000 MWD/MTU. In 1978, the NRC required all vendors to include the burnup effect in their models and derived a correction factor to be used until the vendors developed their own expressions [M-7]. Thus, fission gas release predicted with a given function F(T) should be corrected to become

$$F'(Bu,T) = F(T) + [1 - F(T)] \cdot \frac{1 - \exp[A \cdot (Bu - 20,000)]}{1 + [B/F(T)] \cdot \exp[C \cdot (Bu - 20,000)]} \tag{7.6}$$

where A, B, C are constants empirically derived, and Bu is the local burnup in MWD/MTU. The correction factor is to be applied for burnups above 20,000 MWD/MTU. Comparison with experimental data shows that the predictions rapidly increase with burnup and are fairly conservative. It should be noted that the correlation was derived from LMFBR data.

Beyer and Hann [B-4] developed a temperature-zone correlation and adjusted the parameters with experimental data up to 18,300 MWD/MTU. Three temperature regions are considered (1200-1400 ^{o}C, 1400-1700 ^{o}C, >1700 ^{o}C) and different fractions are released in each of them. A modification factor is applied to the correlation so that it represents the upper 95% confidence limit of the experimental data.

Carlsen [C-4] compared results from two test rods to predictions from the fuel performance code WAFER-2. This code includes a temperature-ring correlation similar to Beyer and Hann's. The test rods had burnups of about 38,000 MWD/MTU and the releases were predicted with errors of 13% and 16%.

The High Burnup Effects Program (HBEP), coordinated at Batelle Pacific Northwest Laboratories aimed to identify the effects of high burnup on fission gas release [B-5]. This effort was intended to solve the previous controversy about increased release at extended burnup levels. The program examined 82 LWR fuel rods with rod-average burnups ranging from 22 to 69 GWD/MTU. The conclusion was that local burnup up to 83 GWD/MTU does not enhance the gas release mechanisms. The only high-burnup effect encountered was the development of a low-temperature rim region that can potentially enhance athermal release for local burnups above 65 MWD/MTU.

A probabilistic approach is described in Ref. [T-1] in an original model developed by Weisman et al. [W-3]. This approach was incorporated into the computer code FREDOM by Loftus et al. [L-3]. The rate of gas release is given as the sum of two terms:

- immediate release, that considers atoms escaping without being trapped,
- deferred release, that considers atoms temporarily retained in the fuel before being released.

7.4.4 Model for the 36-Month Core

For this study, the model by Weisman et al. [W-3] was selected, and coded in FORTRAN. A general description of the model is given in the following paragraphs, the equa-

tions are included in Appendix J, and a listing of the FORTRAN code is included in Appendix K.

For any portion of the fuel that may be considered to be operating at an approximately uniform temperature, the moles of gas currently trapped in the fuel (C) are given by the following equation:

$$\frac{dC}{dt} = (1 - K_1) \cdot P - \frac{C}{\tau} \tag{7.7}$$

where P is the current rate of gas production (mol per unit time), $K_1 = F_{g1}(T)$ is the fraction of gas being produced that escapes immediately without being trapped, $\tau = F_{g2}(T)$ is a time constant that describes the rate at which trapped gas is released, and t is the time after start of irradiation. The first term in Eq. (7.7) expresses the rate of new gas being trapped, and the second term represents the delayed release of trapped gas.

For a time interval Δt_i in which P, K_1, and τ may be considered to be constant, Eq. (7.7) can be solved as

$$C_i = (1 - K_1) \cdot P \cdot \tau \cdot \left(1 - \exp\left(-\frac{\Delta t_i}{\tau}\right)\right) + C_{i-1} \cdot \exp\left(-\frac{\Delta t_i}{\tau}\right) \tag{7.8}$$

where C_{i-1} and C_i represent the gas trapped in the fuel at the beginning and end of the time step, respectively.

The fractional gas release at the time t_i is

$$FGR_i = 1 - C_i / \left(\int_0^{t_i} P dt\right) \tag{7.9}$$

Application of this model requires that the temperature distribution in the fuel be known as well as its evolution with time. Therefore, a relationship between rod power -- which is known-- and temperatures has to be established. For a given q', the temperature difference across the fuel rod is independent of radius and given in [T-2] as

$$\int_{T_{fo}}^{T_{max}} k(T) dT = \frac{q'}{4\pi} \tag{7.10}$$

where T_{fo} and T_{max} are the fuel surface and fuel centerline temperatures, and k(T) is the temperature-dependent fuel thermal conductivity. Other complication exist when cracking and other effects are incorporated but Eq. (7.10) remains as a plausible guide.

Two relationships for the desired parameters (q' and T) were extracted from the literature:

- Maki [M-8] developed a model to analyze the effects of cracking and relocation in the fuel pellet. In his work, the fuel centerline temperature and the fuel surface temperatures are given as a function of rod power and burnup in plots which are reproduced in Figures L.1 and L.2 of Appendix L. For a fixed rod power, it can be seen that the fuel centerline temperature decreases from 0 to 20 GWD/MTU, then increases until 40 GWD/MTU (except for the case of q'=10 kW/m, where it remains fairly constant.) This change in thermal behavior occurs because there is no hard contact in the left region of the plot and the cracks add resistance to heat flow in the pellet, whereas in the right region there is hard contact leading to better heat transfer in the cracked pellet.
- Garner et al. [G-5] performed a series of tests at Idaho National Engineering Laboratory to analyze gap conductance in the rods. The FCTs are given as a function of rod power for rods with different initial gap sizes in Figure 1 of Ref [G-5]. This figure is reproduced as Figure L.3 in Appendix L. The initial gap size[6] in the 36-month core pellets is about 1% (using values from Table 2-1), which is very close to the case of 0.94% represented in Figure L.3.

Furthermore, simulations with the code FROSSTEY-2 (see Section 7.2) provided the FCT for the 36-month core. These values are used only as a check, and not as a direct input for the desired relationships. The reasons for developing a fission gas release model independent of FROSSTEY-2 were outlined in Section 7.1.

Comparison of data in Figures L.1 and L.3 indicates that the FCT predicted in Ref. [M-8] for q'=30kW/m and 0 burnup overpredicts the value from Ref. [G-5] by over 400 ^{o}C and the value from FROSSTEY-2 by over 200 ^{o}C. In view of these results, the following procedure is adopted to obtain the temperature distribution in the fuel:

- The FCT values from Figure L.1 are retained after 20 GWD/MTU, and the initial FCT is taken from Figure L.3. For the intermediate region between 0 and 20 GWD/MTU, a straight line is traced linking the values at 0 and 20 GWD/MTU. The FCT obtained in this way is shown in Figure L.4 in Appendix L. Since the x-axis in this graphs goes only up to 40 GWD/MTU, the temperatures are extrapolated linearly beyond this point.
- The fuel surface temperatures as a function of rod power are taken from Figure 4.3 in Ref. [M-8].
- For each rod power and burnup step, the FCT and fuel surface temperature are obtained by linear interpolation in the previous graphs. Then, the temperature distribution is obtained by fitting a parabola with these two temperatures.

---

6. The gap size is calculated in percent of the nominal design pellet diameter.

The power histories used for this analysis are the simplified histories described in Section 7.3.3 for the cladding corrosion model. The general procedure for gas release calculations is as follows:

- for a given time step, 24 axial nodes and 20 radial nodes are considered in the fuel;
- in each axial node, q' is obtained from the power history, and the temperature distribution is obtained as indicated above, using local linear heat rate and local burnup;
- for each radial node, the equations in Appendix J are used to calculate the amount of gas produced, the immediate released fraction, the deferred release fraction, and the amount stored in the pellet at the end of the step;
- these calculations are repeated for each radial node at a given elevation, then for each axial node, and finally for each time step.

7.4.5 Results and Discussion

The fractional gas release is an integral quantity that indicates how much of the gas produced up to a certain time has been released. The predicted fractional gas release is plotted versus time in Figure 7-17 for both the 36-month and the 18-month cores. It can be seen that the release is enhanced in the 36-month core and the final values before discharge are 0.098 and 0.043 for the not-reused and reused assemblies, respectively.

The evolution with time is linked to the power histories displayed in Figure 7-12. For the not-reused assemblies, the first step in the power history leads to a rapid increase in the released fraction, reaching a value of 0.083 after 600 days of operation. The reduction in rod average power of about 3 kW/m leads to a lower release rate, and the slope of the release function decreases. The final value after 1033 days of operation is 0.098. For the reused assemblies, the release fraction increases steadily during the first cycle up to a value of 0.058. The low rod average power during the second cycle (10-12 kW/m) results in a reduction of the gas release rate down to values below the FGR up to this point. As a result, FGR decreases and before discharge only 0.043 of the total gas produced has been released. As for the 18-month core, the release increases in the first cycle up to 0.023, in the second up to 0.033 and remains about constant in the third cycle.

The fractional releases at end of life for the envelope pin predicted by FROSSTEY-2 are 0.135, and 0.085 for the not-reused and reused assemblies, respectively. Differences are expected between the two models since the FCTs predicted by FROSSTEY-2 are higher than those taken as input for the model derived in this Section.

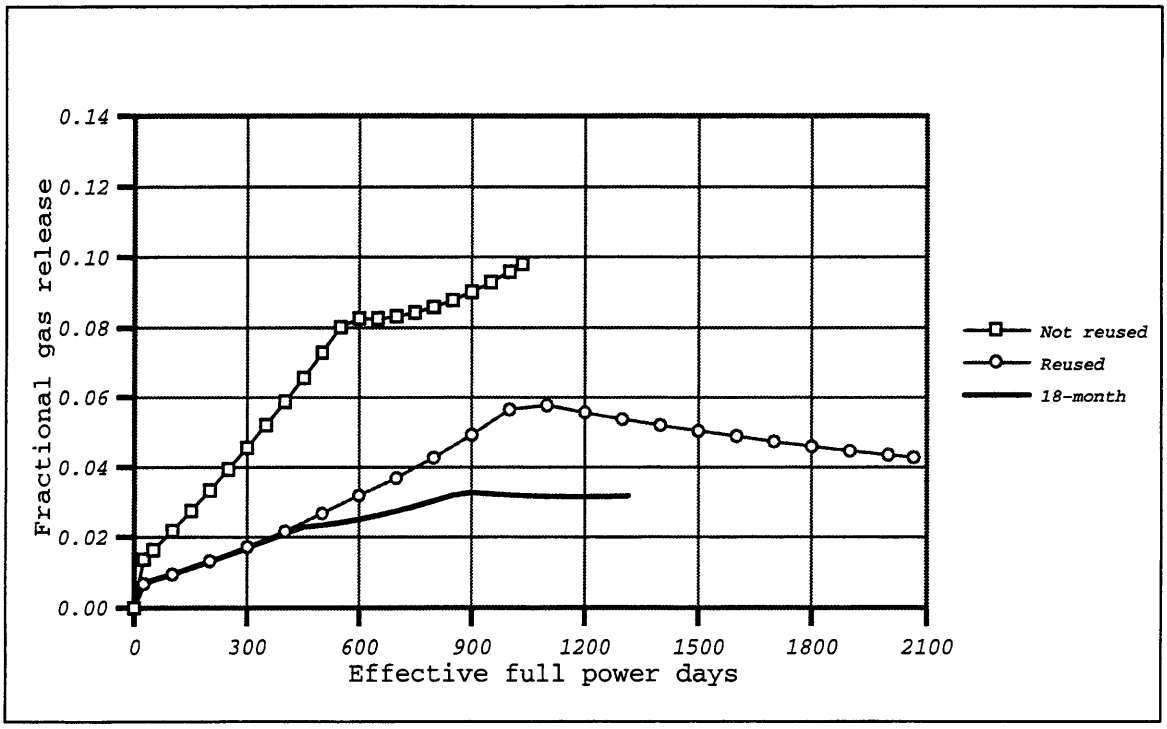

Figure 7-17: Comparison of predicted fractional gas release for the 36-month and the 18-month core

The final effect of the gas release is to increase the rod internal pressure. The calculations with FROSSTEY-2 and the envelope pin in Section 7.2 indicate that the rod internal pressure is within acceptable limits. Since the releases predicted with the new model are lower than those predicted by FROSSTEY-2, the rod internal pressure is expected to be within limits for the 36-month core.

To summarize, the fission gas release in the 36-month core is predicted to be higher than in current cores due to the more demanding power histories. Although the rod internal pressure will be higher than in the reference core, this parameter will not limit the operation of the 36-month cycle.

7.5 Conclusions

The more demanding power history of the 36-month cycle as compared to the 18-month cycle will degrade the thermal and mechanical performance of the fuel pellets. Five variables were quantitatively analyzed in this Chapter: fuel centerline temperature, rod

internal pressure, cladding oxide thickness, cladding surface temperature, and fission gas release. Although these variables are higher for the 36-month cycle than for the 18-month cycle, they are well within the established design limits and do not appear to be a constraint on operation for a 36-month cycle. Material with improved corrosion resistance such as Zircaloy-4 with low tin content or ZIRLO are required to prevent excessive cladding corrosion.

Chapter 8

Core Economics

The core fuel plus outage costs for the 36-month cycle have been calculated as $94.34 M/yr. However, this value is fairly dependent on the operational and economics parameters selected in the analysis. In this Chapter, the economic characteristics of extended cycles are reviewed. Then, the total and fractional costs of the 36-month core are discussed. Finally parametric analyses are performed to evaluate the effect of changes in key assumptions for the operational and economics variables.

8.1 Economics of Extended Cycles

Reduction of operating costs is the main driving force behind research on extended operating cycles. The benefit of stretching the cycle length stems from the lower frequency of refueling outages that results in improved capacity factors. However, longer cycles require higher fuel enrichment, and, therefore are burdened with higher fuel costs. The tradeoff between these two opposite trends determines the optimum cycle length.

Handwerk et al. [H-2] examined the generic economic aspects of extending operating cycles in LWRs and compared fractional and total costs for a PWR extended cycle --44.6 calendar months-- and the 18-month reference cycle. Their main findings are summarized here. In their study, the operational parameters are 3% FOR and 42 days RFO for the extended cycle, and 6% FOR and 49 days RFO for the reference cycle. These values yield capacity factors of 93.8% and 85.6% for the extended and reference cycles, respectively. Under these conditions, the extended cycle is about $1M/yr less expensive than the reference cycle. However, when the same operational parameters --3% FOR and 42 days RFO-- are assigned in both cases, this benefit disappears and the extended cycle is more costly by about $11M/yr.

Keeping the current fuel burnup limit for PWRs (60 GWD/MTU) constrains the design options and requires implementation of the single-batch core. As indicated in Section 1.2.3, Handwerk et al. [H-2] determined that the economic optimum extended cycle length for a single-batch core was about 33 calendar months, although the cost differences

are small in the region ranging from 28 to 38 calendar months. The results are fairly dependent on the operational and economics parameters. As the operational performance improves, i.e. capacity factor increases, annual costs decrease for both the extended and reference cycles, but the decrease is more significant for the reference cycle. On the other hand, extended operating cycles will be more competitive if fuel costs decrease or replacement power costs increase. In particular, the commercial development of AVLIS enrichment technology may significantly reduce fuel costs, making extended cycles more economically attractive.

8.2 Costs for the 36-Month Cycle

For the 36-month core to be attractive to utility managers, the competitiveness with currently operating 18-month cycles has to be shown. Core economics has been an important criterion for selection of options throughout the design process. The final configuration for the radial blanket assemblies was selected because it minimized costs. Similarly, the radial distribution of assemblies aimed to maximize cycle length, therefore, spreading costs over a longer period and reducing their annualized value. Enrichment in the axial blankets was also selected at the economical optimum.

The operating costs of the plant are calculated as the sum of the following terms:

- fuel costs, including mining, conversion, enrichment, and fabrication costs;
- cost of spent fuel, based on the government waste disposal fee;
- material and manpower costs during a refueling outage;
- material and manpower costs during a forced outage;
- replacement power costs.

A detailed description of how to calculate these costs is given in Ref. [H-2]. The main economics parameters embedded in the model are listed in Table 8-1.

Table 8-2 displays the fractional and total costs on an annualized basis appropriately discounted to cycle midpoint for both the 18-month and the 36-month cores. It can be seen that the total costs for the 36-month cycle are about $4.9M/yr higher than for an 18-month reference cycle. The analysis of fractional costs indicates that:

- fuel is about $17.5M/yr more expensive for the 36-month core. As indicated before, this difference stems from the higher enrichment required in the longer cycle.

- disposal of spent fuel is slightly more expensive for the 36-month core since more assemblies per year are discharged. The difference, however, is very small, and less than 1% of the total cost difference.
- replacement power is an important source of savings for the 36-month core, yielding a benefit of $6.6M/yr.
- refueling outage costs are the second source of savings for the 36-month core, since the outage period, and, hence outage costs are spread over a longer cycle. The 36-month core enjoys a benefit of almost $6.0 M/yr over the 18-month cycle.
- forced outage rate costs are the same, since both cores operate with a 3% FOR.

Table 8-1: Input to the economics model (from Ref. [O-1])

Fuel cycle economics and operational parameters	Value
Uranium purchase	$50/kgU
Conversion	$8/kgU
Enrichment	$110 /kg SWU
Fabrication	$ 275/kgU
Waste disposal fee	1 mill/kWhre
Replacement power	25 mills/kWhre
Carrying charge rate	10%/yr
Forced outage rate	3%
Refueling outage length	30 days

Table 8-2: Comparison of annual component and total costs in $M/yr using parameters from Table 8-1

	36-month cycle	18-month cycle
Fuel	71.87	54.40
Spent fuel	1.02	0.98
Replacement power	14.31	20.95
Refueling outage	6.05	12.00
Forced outage	1.10	1.10
Total	94.34	89.42

This analysis suggests where the sources of savings for the 36-month core are. If the operational parameters and the unit costs are different from the values in Table 8-1 and

remain the same for both cores, two of the fractional costs are the same or very close for both cores: spent fuel and forced outage rate costs. However, the values of the operational and economics parameters affect the remaining three items: the fuel costs depend on the SWU costs; the replacement power costs depend on both the unit cost of power and the the refueling outage length; and the refueling outage costs depend on the outage length.

8.3 Parametric Analysis

Variations in any of the values in Table 8-1 affect both the 36-month and the 18-month reference cycle, although the effects are different. Changes in the operational parameters, SWU costs, and replacement power costs are analyzed in the present section.

8.3.1 Operational Parameters

The base operational parameters in this study --30 days RFO and 3% FOR-- were selected as to characterize expected optmistic performance of US plants in a near future when extended cycles could be implemented. Current performance in US plants is, however, worse than these values. In spite of extraordinary short outages in some plants --17 days for South Texas-2 and 19 days for Browns Ferry-3 in spring 1997,-- the median outage length for 24 plants in the spring of 1997 was 57 days [R-4]. For the units completing refueling in the fall of 1996, the outage median was 42 days. Therefore, it may not be unreasonable to assume that the US median outage length may remain at about 40 days for a significant period.

Figure 8-1 compares the annual costs for the 36-month and 18-month cores for different values of RFO and FOR. The figure displays two sets of almost parallel lines, corresponding to the 18-month and 36-month cycles. For a given RFO, core costs increase with FOR since the plant downtime is greater, and the increase is similar for both cores. For the base conditions of the analysis (30 days, 3%FOR), the plot gives (via interpolation) the values of Table 8-1, that is, $94.3 M/yr and $89.4 M/yr. For a given FOR, an increase in the RFO length leads to a larger increase in the total costs of the 18-month core than in the 36-month core since the additional outage days are spread over a shorter time, and, therefore, the additional replacement power costs and refueling outage costs on an annual basis are higher for the 18-month core. This is reflected in Figure 8-1 by steeper lines for the 18-

month core. For the case of 3% FOR, the costs for both cores are similar when the RFO is 42 days. For longer outages, the 36-month core is less expensive than the 18-month core. For the highest value represented in the plot, i.e. 60 days RFO, the 36-month core is about $6.7 M/yr less expensive than the reference core. Conversely, RFO shorter than 30 days will benefit the reference core more.

Changes in FOR hardly affect the above statements if the FOR are the same for both the reference and 36-month cores. For the range of FOR in the plot --between 2% and 6%,-- the break even RFO length oscillates only between 42 and 44 days. If, however, either option has a 1% FOR advantage over the other, this translates into approximately $2.1M/yr.

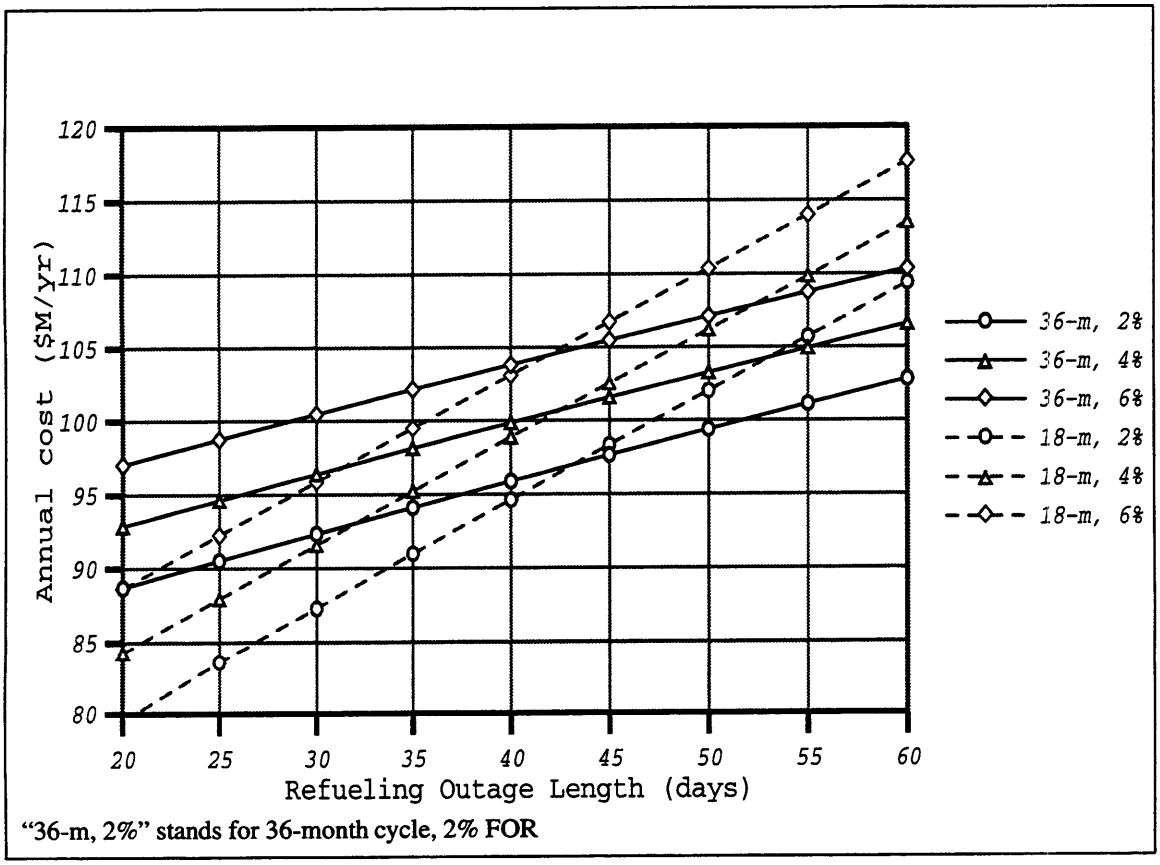

"36-m, 2%" stands for 36-month cycle, 2% FOR

Figure 8-1: Influence of the operational parameters on core costs

8.3.2 SWU Costs

The higher fuel enrichment in the 36-month core leads to higher fuel costs. The cost of enrichment is indicated by the Separative Work Units (SWU). The required base value of the unit cost in this analysis is 110 $/kg SWU. Gaseous diffusion or centrifuge technology

are the current means used in enrichment plants. New enrichment technologies, especially atomic vapor laser isotopic separation (AVLIS) are predicted to significantly cut enrichment costs. Recent experiments with AVLIS conducted at Lawrence Livermore National Laboratory approached levels needed for commercial operation. According to the United States Enrichment Company (USEC), construction and startup for a commercial AVLIS plant are scheduled for 2001-2005 [N-2]. Other enrichment processes such as Molecular Obliteration LIS (MOLIS) and Chemical Reaction by Isotope Selective Laser Activation (CRISLA) predict unit enrichment costs on the order of $10/kg SWU [E-4].

The influence of the SWU costs on the total core costs is shown in Figure 8-2. In this plot, two pairs of operational parameters are considered:

A: 3% FOR, 30 days RFO,

B: 3% FOR, 42 days RFO.

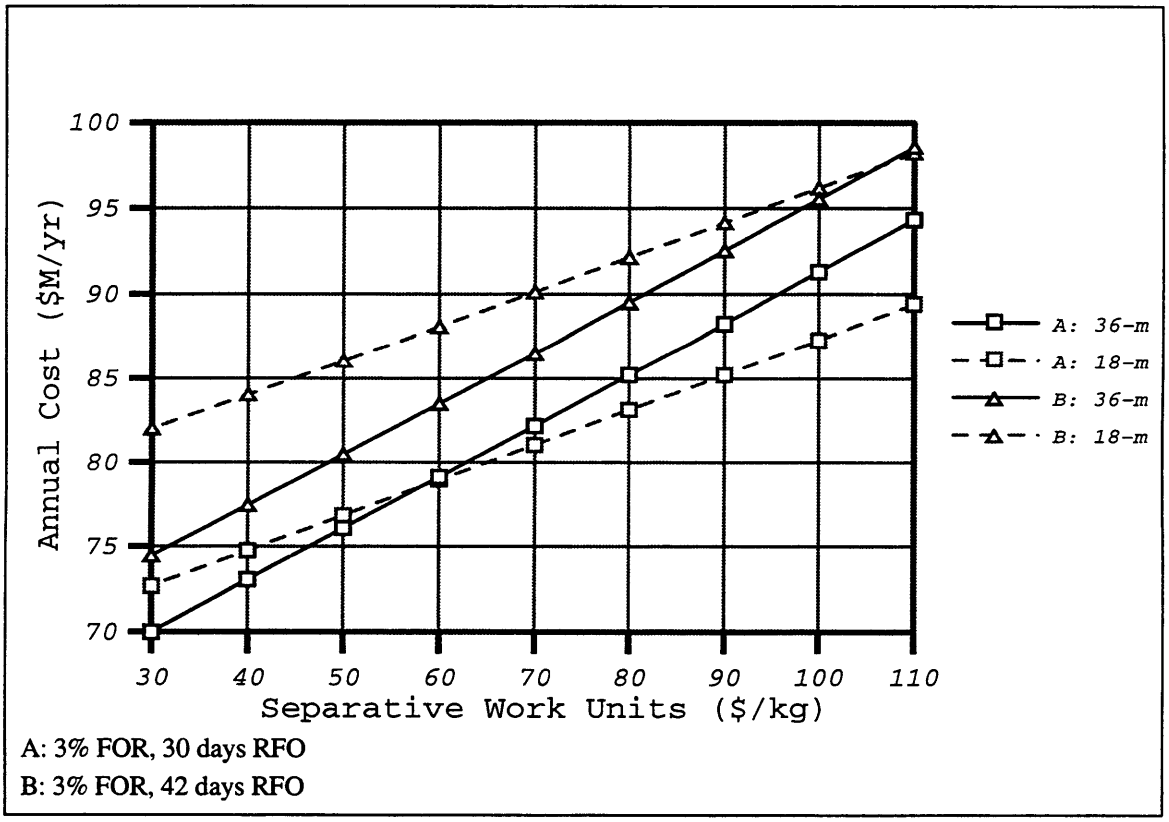

Figure 8-2: Influence of SWU costs on total cycle costs

The rightmost value on the X-axis ($110/kg) corresponds to the base condition of the analysis. Under conditions A, the 36-month core is about $5M/yr more expensive for SWU=110$/kg, and the difference between the 36-month and the 18-month core reduces as the SWU costs decrease. The breakeven point is at $58/kg. For conditions B, the breakeven point for the SWU is about $110/kg. Therefore, any reduction in SWU costs results in an economic benefit for the 36-month core. For example, for SWU=58 $/kg, the 36-month core is $4.8M/yr less expensive than the reference core under scenario B.

8.3.3 Replacement Power Costs

The last variable considered in this parametric analysis is the cost of replacement power. Figure 8-3 shows the influence of replacement power costs on total cycle costs. The analysis considers the two sets of operational parameters indicated in Section 8.3.2. The base value for the replacement power cost is 25 mills/kwhre. It can be seen in the figure that the lines for the 18-month cycle are steeper than those for the 36-month cycle because the number of RFO days per year for the 18-month cycle is higher than for the 36-month

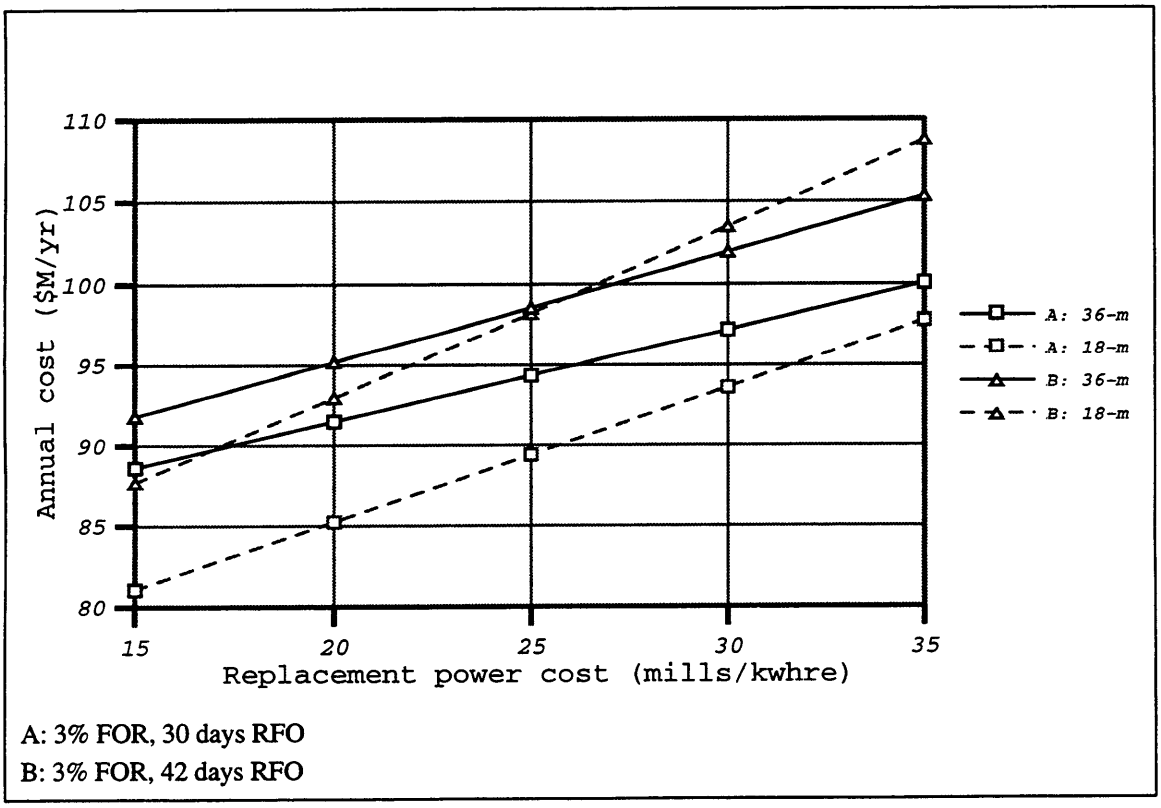

A: 3% FOR, 30 days RFO
B: 3% FOR, 42 days RFO

Figure 8-3: Influence of replacement power costs on total cycle costs

cycle, and, hence, more replacement power is required per year. Therefore, the 18-month core costs change more for a given change in replacement power costs, and an increase in replacement power costs will benefit the 36-month core. For example, for the conditions A --3%, 30 days,-- if replacement power costs increase by 5 mills/kwhre, the 18-month core-costs increase $1.3M/yr more than the 36-month core costs. For the conditions B --3%, 42 days,-- the trends are similar and the 5mills/kwhre increase leads to a $1.9 M/yr differential increase in core costs.

The opposite trend is also true, and lower replacement power costs benefit the 18-month core.

8.4 Conclusions

Core costs are a key criterion in the design process in this work, and economics considerations are integrated into the physics design. If the 36-month core is to appeal to utility managers, the 36-month core has to be competitive with the 18-month cycle representative of current industrial practice. For the base conditions of this study, the 36-month core is about $4.9M/yr more expensive than the 18-month core. However, the costs are sensitive to the operational and economics parameters. In particular, if the RFO length is increased by 12 days, from 30 days up to 42 days, the above cost difference disappears and the 36-month core breaks even with the reference cycle.

The development of AVLIS technology will cut enrichment costs and benefit the 36-month cycle. A reduction of SWU costs from 110$/kg down to 58$/kg will wipe out the $4.9M/yr difference. Finally, an increase in replacement power costs will benefit the 36-month cycle by about $1.3M/yr per 5 mills/kwhre increase.

Chapter 9

Summary, Conclusions and Future Work

9.1 Summary

A PWR core for a 36-calendar month cycle has been designed that meets current physics and fuel performance design limits. The core was modeled in 3 dimensions and steady-state using the codes CASMO-3 and SIMULATE-3. The design is for 4-loop Westinghouse reactors, with 193 assemblies. Although the initial work was done on a single-batch core, an economic benefit was found when loading the core periphery with assemblies discharged from the previous cycle. The main design challenge is to distribute the bulk of the power evenly over a broad region so that the axial enthalpy rise is maintained within limits in the center of the core and the burnup design criterion is met in the periphery. This is achieved with an optimized distribution of the burnable poison.

The fuel is enriched to 6.5% U-235 and selected pins use Gadolinia (Gd_2O_3) as burnable poison mixed with UO_2. The core has 6 types of assemblies which differ from each other in either the number of poisoned pins or the concentration of Gadolinia. Assemblies have between 20 and 36 poisoned pins with Gadolinia content ranging from 4% to 12%. A very flat reactivity shape throughout core life is obtained in each assembly by including pins with two different concentrations of Gd_2O_3. The axial blankets --top and bottom 6 inches of the rods-- have unpoisoned fuel with 4% U-235. Fuel in these regions is 10% annular, providing extra space to accommodate fission gases.

After one cycle in the core, 149 assemblies are discharged, whereas the other 44 assemblies are shuffled to new positions but remain in the core for two cycles. The reused assemblies are loaded in the periphery since they are far less reactive than the fresh fuel. In this way, the periphery runs at low power and the vessel fluence is reduced. When shuffled, assemblies are rotated 180° to present the least-burned face to the core interior. The EOC core average burnup is 39.89 GWD/MTU, which corresponds to a cycle length of 33.9 EFPM, or 36 calendar months when operating at a capacity factor of 94.1%. The average burnup of the assemblies discharged as spent fuel is 51.13 GWD/MTU. This com-

pares to a reference 18-month cycle where the incremental core average burnup in one cycle is 17.00 GWD/MTU and the assemblies discharged as spent fuel have an average exposure of 39.50 GWD/MTU.

The core meets the design criteria for peak pin exposure (<60 GWD/MTU), axial enthalpy rise hot channel factor (<1.65), total peaking factor (<2.5), and core boron concentration (<1,780 ppm). The hardening of the neutron spectrum reduces the control rod worth by 14% to 25% as compared to the reference core, and new control rods are required in order to insure an adequate shutdown margin.

In the future it is expected that peaking factors in the 36-month core may be further reduced by axially zoning the burnable poison and by using computer codes that automatically perform loading pattern optimization. Moreover, selective use of the isotope Gd-157, which could be feasible with AVLIS technology, would reduce the residual penalty and provide an economic benefit.

The physics design for a transition cycle has been proposed that minimizes the economic penalty when shifting from a 24- to a 36-month cycle. An annualized penalty of approximately $2.1M/yr is predicted.

The more demanding power history (longer intervals at higher power, hence temperature) of the 36-month cycle as compared to the 18-month cycle will degrade the thermal and mechanical performance of the fuel pellets. Fuel centerline temperature, rod internal pressure, cladding oxide thickness, cladding surface temperature, and fission gas release were analyzed. Although these parameters are higher for the 36-month cycle than for the 18-month cycle, they are well within current design limits and do not seem a constraint for operation of the 36-month cycle. Material with improved corrosion resistance such as Zircaloy-4 with low tin content or ZIRLO are required to prevent excessive cladding corrosion.

Economics considerations were integrated throughout the physics design process. The 36-month core is economically competitive with 18-month reference cycles under certain operational conditions. Considering a refueling outage of 30 days and 3% forced outage rate, the 36-month core is about $4.9M/yr more expensive than an 18-month reference core. However, if the outage length increases to 42 days, costs are similar for both cores.

The development of AVLIS technology should cut enrichment costs and benefit the 36-month cycle. A reduction of SWU costs from 110$/kg down to 58$/kg will wipe out the $4.9M/yr difference, therefore making the 36-month cycle more economically attractive.

9.2 Conclusions

For the 36-month core to be attractive to utility managers, not only the technical feasibility but also the economic benefits as compared to current cores have to be shown. The technical problems related to the cycle length extension have been solved. However, the economic benefits depend on operational and economic conditions.

Keeping the core burnup under current limits constrains the design options and leads to a batch loaded core -except for the peripheral assemblies. Such a core lacks the flexibility of fuel management that multibatch cores enjoy, since fresh fuel assemblies cannot be mixed with depleted --less reactive-- assemblies. The most distinctive characteristics of the physics design are the optimized distribution of the burnable poison and the loading pattern, in which the peripheral assemblies are reused. The tailored poison loading leads to an even distribution of the power over a broad region of the core and for a long period of time. The design of the core periphery reduces fuel costs and provides the best economics within the options analyzed.

Assemblies are subject to a demanding power history and many of them run at high power for a long period of time. As a result, the fuel performance is somewhat degraded as compared to 18-month cycles. However, none of the variables analyzed was found to constrain the operation of a 36-month core.

Once technical feasibility is accepted, the only constraints to implementation of the 36-month core are the costs. For the reference operational conditions of 30 days RFO length and 3% FOR, the core is not competitive with current 18-month cores. However, actual operational and economics conditions may differ from the values assumed in the analysis. The commercial development of AVLIS technology is predicted by the US Enrichment Company for the year 2005, and prospects are encouraging. Within seven years, enrichment costs could be significantly reduced, making the 36-month core a viable alternative to current 18-month cycles.

9.3 Future Work

The present analysis only considers steady-state conditions. To complete the design, the core should be analyzed under transient conditions. In addition, some specific physics and fuel performance studies are desirable as described in the following paragraphs.

9.3.1 Physics Design

This Section describes several strategies that were not analyzed within this project, but may lead to improvements in core performance.

Fuel enrichment zoning

Fuel in the 36-month core is uniformly enriched to 6.5% U-235 except for the axial blankets. The reactivity distribution in this core is controlled by the burnable poison loading. Using assemblies with different fuel enrichments may also be used to shape the core reactivity. In order to keep the desired cycle length, the core average enrichment --excluding the peripheral assemblies-- should remain around 6.5% U-235. Performing some degree of fuel zoning enrichment in the 36-month core is left as future work. It should be noticed that this strategy would require enriching some assemblies beyond the core average value, which is already over the current licensing limit of 5% U-235.

Mixed gadolinia loading

A new burnable poison scheme can be envisaged in which gadolinium oxide is inserted in the hole of an annular pellet [Y-1]. In this way, the fuel properties, in particular the thermal conductivity, are not degraded by the presence of a burnable absorber. Appendix G shows that application of this concept does not seem advantageous for the 36-month cycle. However, a mixed gadolinia loading scheme can be considered in which Gd_2O_3 is both mixed within the UO_2 matrix of an annular pellet and inserted in the central annulus.[7] This scheme is illustrated in Figure 9-1. The reactivity hold-down and duration of the burnable poison effect with this mixed loading are expected to be larger than in the case of

7. Although Ref. [Y-1] calls this strategy duplex loading, it will be referred to here as "mixed loading" to avoid confusion with the duplex loading concept introduced in Section 3.2.2.3, which indicated that pins with two different concentrations of gadolinia are loaded in the same assembly.

a single loading of gadolinia. Further work is required to evaluate the effects and benefits stemming from this poisoning scheme.

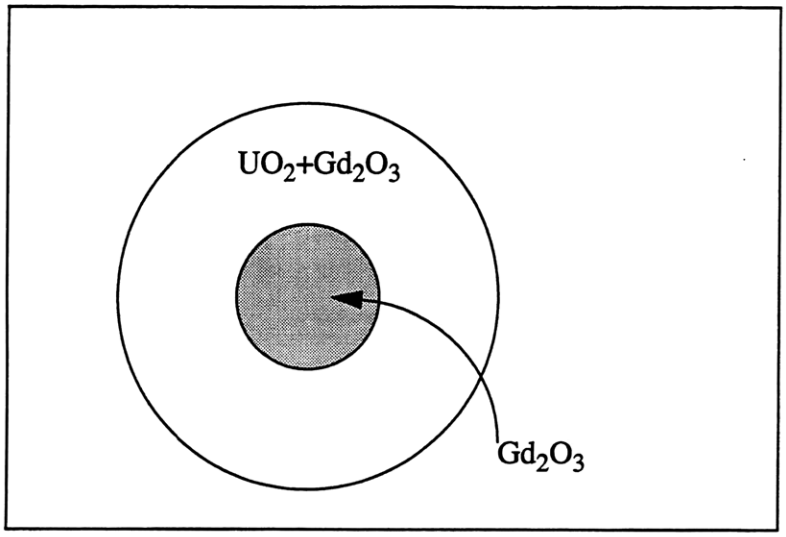

Figure 9-1: Poisoning scheme for a mixed loading of gadolinia

Fuel pins in water holes

The 17x17 assemblies in the 36-month core have 264 fuel rods, 24 guide tubes and 1 instrumentation thimble (see figure A.4). The guide tubes house the control rods in the assemblies located below the control rod clusters (see figure A.2), and are filled by flowing coolant in the remaining assemblies.

The amount of fuel and the reactivity of the assemblies that are not located below the control rod clusters may be increased by inserting fuel rods in the guide tubes. Application of this strategy to assemblies in groups B and C will draw more power towards peripheral assemblies, therefore reducing $F_{\Delta H}$. In particular, 28 assemblies in group B and 32 assemblies in group C (see figure A.1) are not located under control rod banks. The peak pin burnup will be reduced, since the energy generated in the outer assemblies (where the maximum peak pin burnup is attained) is distributed over a larger number of rods. The increase in fuel mass, and hence reactivity will require that more burnable poison be added to keep the soluble boron concentration within limits. Moreover, the cycle length and fuel costs will increase, although the annual costs are not expected to change significantly.

Two main strategies may be considered:

- Insert fuel rods with 6.5% U-235 or lower enrichment in selected assemblies in group B. For the equilibrium cycle, the shuffled assemblies (group C) will also be filled with the extra fuel rods, and more power will be drawn towards both rings of assemblies. Inserting 24 extra fuel rods in 28 assemblies of group B, and hence of group C in the equilibrium cycle, will yield an increase in fuel mass of

$$\frac{24}{265} \cdot 100 = 9.5\ \%\ \text{in each assembly ,and}$$

$$\frac{24}{265} \cdot \frac{28+28}{193} \cdot 100 = 2.6\ \%\ \text{in the core}$$

- Insert fuel rods with low enrichment (i.e. 3% U-235) in the guide tubes in assemblies in group C when these assemblies are shuffled during the refueling outage. In this case, the power will be drawn only towards the peripheral ring of assemblies.

This strategy is conceptually interesting and may improve the core radial power distribution. Quantifying the effects on $F_{\Delta H}$ and peak pin burnup requires that detailed neutronics analyses be performed. Fuel performance issues are also to be considered, since drawing more power towards the periphery will reduce thermal loading in the central assemblies of the core, but will degrade the performance of the outer rings, formed by assemblies that stay for two cycles (72 months) in the core.

Analysis of 19x19 lattices

Throughout the years, fuel designers have increased the number of pins per assembly to improve the fuel-to-moderator ratio and the thermal performance of the fuel pellets. Current designs run at or very close to the optimum H/U ratio. Using a 19x19 instead of a 17x17 pin array will probably yield a negligible neutronics improvement, if any. However, as in the case of annular fuel (see Section 3.1.2.) the mechanical and thermal benefits may be significant.

For the same assembly size, core power and fuel mass, Ayoub and Driscoll [A-1] showed that shifting from a 17x17 to a 19x19 lattice reduces the linear power and the pin stored energy to 80% and 64% of the original values, respectively, and increases the margin to DNB up to 112% of the original value. Pellet temperatures will be lower and so will be the oxide layer thickness, fission gas release and rod internal pressure.

Although the assembly dimensions are kept the same, the spiders holding the control rods and the upper core internals must be redesigned and replaced to accommodate the new lattice. The economic penalty associated with these changes has to be quantified.

Other rare earths as burnable absorbers

In addition to gadolinium and erbium, other rare earth nuclides, like dysprosium, samarium or europium, have interesting properties for control of core reactivity. The thermal cross sections for these elements are 930 barns (Dy), 5800 barns (Sm) and 4600 barns (Eu). Their depletion chains generate several absorbing isotopes by capture, and the reactivity residual penalty can be a constraint to their utilization [A-2]. Dysprosium is used as burnable absorbers in CANDU reactors and is placed in the inner elements of the bundle [C-3].

It may be worthwhile in future work to analyze the efficacy of these rare earths as alternative burnable poisons.

9.3.2 Fuel Performance

The fuel performance analysis in this document was reduced to the evaluation of important parameters that could be easily quantified. Some of the issues that could be exacerbated by cycle length extension were not studied here. Future work is, hence, desirable in these areas, which include:

- stress and strain,
- axial growth and rod bowing,
- fretting,
- CRUD deposition.

The higher concentration of soluble boron in the coolant of the 36-month cycle leads to a more demanding water chemistry that might enhance the cladding corrosion process. This effect was not included in the corrosion model and is left as future work.

9.3.3 Additional Remarks

As discussed in some detail in earlier work at MIT on extended cycle cores, a considerable amount of administrative work is a prerequisite to adopt this strategy. All aspects of fuel manufacture and subsequent handling will have to be relicensed to handle fuel of greater than $5^{w}/_{o}$ U-235 [H-2]. On the plant side, surveillance and repair intervals will have to be revised (see Ref. [M-2], [B-1]).

Finally, it would be beneficial if advanced fuels capable of higher burnup were to be developed, since then the advantages of multibatching and long cycles could both be exploited.

References

[A-1] A.F.A Ayoub and M.J. Driscoll, "A Strategy for Extending Cycle Length to Improve Pressurized Water Reactor Capacity Factor," MIT-ANP-TR-032, MIT, Nuclear Eng. Dept., Cambridge, MA, (June 1995).

[A-2] M. Asou and J. Porta, "Prospects for Poisoning Reactor Cores of the Future," *Nuclear Engineering and Design*, **168**, pp 261-270 (May 1997).

[A-3] A.I.A. Almarshad, "A Model for Waterside Oxidation of Zircaloy Fuel Cladding in Pressurized Water Reactors," *Journal of Nuclear Materials*, **183**, pp 186-194, (1991).

[B-1] D.L. Brodeur, V.T. Angus, and N.E. Todreas, " Optimization of Nuclear Power Utility Operating Performance," MIT, Nuclear Eng. Dept., Cambridge, MA, (May 1998).

[B-2] A. Badruzzaman, "Economic Implications of Annular Fuel in PWRs," *Trans. Am. Nucl. Soc.*, **34**, pp. 384-385 (1980).

[B-3] L.C. Bernard, E. Bonnaud, "Finite Volume Method for Fission Gas Release modeling," *Journal of Nuclear Materials*, **244**, pp 75-84, (1997).

[B-4] C.E. Beyer, C.R. Hann, " Prediction of Fission Gas Release from UO_2 Fuel," Batelle Pacific Northwest Laboratories, BNWL-1875, Richland, WA, (Nov. 1974).

[B-5] J.O. Barner, M.E. Cunningham, M.D. Freshley, D.D. Lanning, "Evaluation of Fission Gas Release in High-Burnup Light Water Reactor Fuel Rods," *Nuclear Technology*, **102**, pp 210, (May 1993).

[C-1] K.Y. Choi, S.K. Chung, K.J. Lee, S.W. Park and D.I. Chang, "Comparative Integral Burnable Absorber Study For Pressurized Water Reactors in Korea," ANS Proc. Topical Mtg on Advances in Fuel Management, Myrtle Beach, SC, March 23-26, 1997.

[C-2] M.W. Crump, E.P. Flynn, "System 80+ Plutonium Disposition Capability," ABB Combustion Engineering Nuclear Power, Technical Paper TIS 93-101, (1993).

[C-3] P. Chan, H. Feinroth, J. Luxat, D. Pendergast, " Safety of CANDU Reactors Utilizing Plutonium-Enriched Mixed-Oxide Fuel," *Trans. Am. Nucl. Soc.*, **71**, pp. 299-300 (1994).

[C-4] H. Carlsen, "Fission Gas Release in LWR Fuel Rods Exhibiting Very High Burnup," *Nuclear Engineering and Design*, **56**, pp 183-187, (1980).

[D-1] A. Denis, R. Piotrkowski, "Simulation of Isothermal Fission Gas Release,"*Journal of Nuclear Materials*, **229**, pp 149-154, (1996).

[E-1] F. Emerson, NEI, personal communication with C. Handwerk, 5 August 1997.

[E-2] M. Edenius and B.H. Forssen, "CASMO-3 a Fuel Assembly Burnup Program, User's Manual," STUDSVIK/NFA-89/3 Rev. 3, STUDSVIK AB (June 1993).

[E-3] Electric Power Research Institute, "PWR Primary Water Chemistry Guidelines: Revision 3," EPRI TR-105714 (November 1995).

[E-4] J. Eerkens, "Laser Separation of Isotopes for Medial Applications," presentation at the Annual Idaho National Engineering and Environmental Laboratory (INEEL) University Research Consortium, July 1997.

[F-1] E.K. Fujita, M.J. Driscoll, D.D. Lanning, "Design and Fuel Management of PWR Cores to Optimize the Once-Through Fuel Cycle," MIT-EL 78-017, MIT, Nuclear Eng. Dept., Cambridge, MA, (August 1978).

[F-2] R.M. Fleischman, S. Goldsmith, D.F. Newman, T.J. Trapp, B.I. Spinrad, "Advanced Reactor Design Study: Assessing Nonbackfittable Concepts for Improving Uranium Utilization in Light Water Reactors," PNL-3654, Pacific Northwest Laboratory, Richland, Washington, (September 1981).

[F-3] K. Forsberg, M. Limback, A.R. Massih, "A Model for Uniform Zircaloy Corrosion in Pressurized Water Reactors," *Nuclear Engineering and Design*, **154**, pp 157-168 (1995).

[G-1] L. Garcia-Delgado, N.E. Todreas, "Improvement in Nuclear Plant Capacity Factors Through Longer Cycle Length Operation, Final Report," MIT-NFC-TR-011, MIT, Nuclear Eng. Dept., Cambridge, MA, (May 1998).

[G-2] L. Garcia-Delgado, A. Marques, F.M. Nielsen, J. Rangel, "Steady-State Analysis and 3-Dimensional Design of an Advanced PWR Core for an Extended Fuel Cycle," Internal Report, MIT, Nuclear Eng. Dept., Cambridge, MA, (June 1997).

[G-3] GE Nuclear Energy, "Nuclides and Isotopes, Chart of Nuclides," 15th Edition, 1996.

[G-4] F. Garzarolli, R. Holzer, "Waterside Corrosion Performance of Light Water Power Reactor Fuel," *Nucl. Energy*, **31**, pp 65-86, (Feb. 1992).

[G-5] R.W. Garner, R.H. Smith, D.H. Schwieder, D.T. Sparks, P.H. Klink, P.E. MacDonald, "Gap Conductance Test Series-2. Test Results Report for Tests GC 2-1, GC 2-2 and GC 2-3," NUREG/CR-0300, TREE-1268, Idaho National Engineering Laboratory, Idaho Falls, Idaho, (Nov. 1978).

[H-1] C.S. Handwerk, J.E. Meyer, N.E. Todreas, "Fuel Performance Analysis of Extended Operating Cycles in Existing LWRs," MIT-NFC-TR-008, MIT, Nuclear Eng. Dept., Cambridge, MA, (January 1998).

[H-2] C.S. Handwerk, M.J. Driscoll, N.E. Todreas, M.V. McMahon, "Economics Analysis of Extended Operating Cycles in Existing LWRs," MIT-ANP-TR-049, Rev. 1, MIT, Nuclear Eng. Dept., Cambridge, MA. (January 1998).

[H-3] C.S. Handwerk, M.J. Driscoll, N.E. Todreas, M.V. McMahon, " MUSCLE, -MIT-Utility Study on Cycle Length Economics,"MIT-NFC-TR-012, Nuclear Eng. Dept., Cambridge, MA (April 1998).

[H-4] L.C. Hill, D. Hartley, "Siemens Power Corporation -Nuclear Divison: Gadolinia Fuel Experience," Proc. of the 1994 Intl. Top. Mtg. on LWR Fuel Performance, West Palm Beach, Florida, April 17-21, 1994.

[H-5] C.M. Hove, S.W.Spetz, "Improved PWR Gadolinia Fuel Assembly Design Using Isotopic Enrichment of Gd-157," Proceedings of Topical Meeting in Advances in Fuel Management, Pinehurst, N.C., March 2-5, 1986.

[I-1] H.P. Iskenderian, "Use of Depleted Uranium in Thermal Reactors with Slightly Enriched Fuel to Achieve High Neutron Economy and High Burnup," Argonne National Laboratory, ANL-6843, Argonne, Illinois, (February 1964).

[J-1] A. Jonsson, J.R. Parrette, N.L. Shapiro, "Application of Erbium in Modern Fuel Cycles," The 6th KAIF/KNS Annual Conference, Seoul, Korea, Combustion Engineering, Inc. (1991).

[J-2] A. Jonsson, J.E. Gunn, "The Erbium Burnable Absorber in the Design and Operation of 18- and 24-Month Fuel Cycles," *Trans. Am. Nucl. Soc.*, **73**, pp. 376-377 (1995).

[K-1] A. Kamal, M.J. Driscoll, D.D. Lanning, "The Selective Use of Thorium and Heterogeneities in Uranium-Efficient Pressurized Water Reactors," MIT-EL-82-033, MIT, Nuclear Eng. Dept., Cambridge, MA, (August 1982).

[K-2] P. M. Keller, P. J. Turinsky, "FORMOSA-P Multiple Adaptive Penalty Function Methodology," *Trans. Am. Nucl. Soc.*, **75**, pp. 341-342 (1996).

[K-3] J.H. Keenan, F.G. Keyes, P.G. Hill, J.G. Moore, "Steam Tables. Thermodynamical Properties of Water Including Vapor, Liquid and Solid Phases," John Wiley&Sons, (1978).

[K-4] T. Kogai, "Modelling of Fission Gas Release and Gaseous Swelling of Light Water Reactor Fuels," *Journal of Nuclear Materials*, **244**, pp 131-140, (1997).

[L-1] M. Lindberg, C. Piantato, J.F. Gy, "PWR Fuel Design with Erbium as Burnable Absorber," ANS Proc. Topical Mtg on Advances in Fuel Management, Myrtle Beach, SC, March 23-26, 1997.

[L-2] D.W. LaBelle, M.F. Sankovich, S.W. Spetz, V.O. Uotinen, "Assessment of Non-backfittable Concepts to Improve PWR Uranium Utilization," Babcock&Wilcox, BAW-1644, Lynchburg, VA, (December 1980).

[L-3] P.A. Loftus, L.E. Hochreiter, "Fuel Rod Design Evaluation Model for Use as a Teaching Tool," Internal Report, MIT, Cambridge, MA, (1979).

[M-1] M.V. McMahon, C.S. Handwerk, H.J.MacLean, M.J.Driscoll, and N.E. Todreas, "Modeling and Design of Reload LWR Cores for an Ultra-Long Operating Cycle,"MIT-NFC-TR-004, Rev.1, MIT, Nuclear Eng. Dept., Cambridge, MA, (September 1997).

[M-2] T.J. Moore, J.H. Maurer, R.S. McHenry, and N.E. Todreas, "Surveillance Strategy for a Four-Year Operating Cycle in Commercial Nuclear Reactors," MIT, Nuclear Eng. Dept., Cambridge, MA, MIT-ANP-TR-036, (June 1996).

[M-3] C.M. Mildrum, W.B. Henderson, "Evaluation of Annular Fuel Economic Benefits for PWRs," *Trans. Am. Nucl. Soc.*, **33**, pp. 806-807 (1979).

[M-4] C.M. Mildrum, "Evaluation of Annular Fuel for PWRs," *Trans. Am. Nucl. Soc.*, **35**, pp. 78-79 (1980).

[M-5] R.A. Matzie, R.S. Daleas, D.D. Miller, "Industrial Assessment of Nonbackfittable PWR Design Modifications," Combustion Engineering, Inc (CEND-385), Windsor, CT, (November 1980).

[M-6] A. Massih, personal communication with L. Garcia-Delgado, (April 1998).

[M-7] R.O. Meyer, C.E. Beyer, J.C. Voglewede, " Fission-Gas Release from Fuel at High Burnup," *Nuclear Safety*, Vol. **19**, No. 6, (Nov.-Dec. 1978).

[M-8] J.T. Maki, "Thermal Effects of Fuel Pellet Cracking and Relocation," MS Thesis, MIT, Nuclear Eng. Dept., Cambridge, MA, (1979).

[N-1] United States Nuclear Regulatory Commission, Standard Review Plan, NUREG-0800, Rev. 1 and 2, 1981.

[N-2] Nuclear News "AVLIS U Enrichment Test a Success, Says USEC," Nuclear News, p 65, (March 1998).

[O-1] Organization for Economic Co-operation and Development (OECD), "The Economics of the Nuclear Fuel Cycle," (1994).

[O-2] K.C. Okafor, T. Aldemir, "Cycle Length Maximization in PWRs Using Empirical Core Models," *Trans. Am. Nucl. Soc.*, **54**, pp. 55-56 (1987).

[O-3] D.R. Olander, "Fundamental Aspects of Nuclear Reactor Fuel Elements," Oak Ridge, TN, TID-26711-P1, (1976).

[P-1] V.I. Pavlov, "Analysis of the Neutron-Physical Characteristics of the Fuel Lattice of the VVER-1000 Reactor," Atomic Energy, Consultants Bureau, NY, (July 1993).

[R-1] J. Robertson, personal communication with L. Garcia-Delgado at Seabrook Nuclear Station, January 27th, 1998.

[R-2] P.C. Rohr, U.N. Singh, "Physics and Safety Characteristics of the System 80+^{TM} Plutonium Burner," ABB Combustion Engineering Nuclear Power, Technical Paper TIS 94-101, (1994).

[R-3] P.C. Rohr, G.A. Davis, R.A. Matzie, "Safety Aspects of the System 80+TM Plant with Mixed Oxide Cores," ANS Proc. Intl. Topical Mtg on Safety of Operating Reactors, Seattle, WA, Sept. 17-20, 1995.

[R-4] M.L. Ryan, "Length of U.S. Refueling Outages Appears To Be Leveling Off," Nucleonics Week, pp 5-6, August 7, (1997).

[R-5] J.T.A. Roberts, "Structural Materials in Nuclear Power Systems," Plenum Press, New York, (1981).

[S-1] STUDSVIK of America, "TABLES-3 User's Manual," STUDSVIK/SOA-92-03-Rev.0 (April 1992)

[S-2] STUDSVIK of America, "SIMULATE-3 User's Manual," STUDSVIK/SOA-92-01-Rev.0 (April 1992)

[S-3] K.E. St.John, S.P. Schultz, and R.P. Smith, "Methods for the Analysis of Oxide Fuel Rod Steady-State Thermal Effects (FROSSTEY-2)," Yankee Atomic Electric Company, Bolton, MA, YAEC-1912P, (January 1995).

[S-4] Siemens Power Generation, "Fuel Assemblies -References '94," Erlangen, Germany, July 1994.

[S-5] J.A.Sefick, M.J.Driscoll, D.D. Lanning, "Analysis of Strategies for Improving Uranium Utilization in Pressurized Water Reactors," MIT-EL-80-032, MIT, nuclear Eng. Dept., Cambridge, MA, (January 1981).

[S-6] J.R. Secker, J.E. Pitchett, D.Y.Chung, and H.W. Keller, "Design and Operational Experience with Westinghouse ZrB_2 Integral Fuel Burnable Absorbers in

Advanced PWR Fuel," Proc. Intl Reactor Physics Conf., p.I-135, Jackson Hole, WY, Sept 18-22, 1988.

[S-7] J.R. Secker, R.D. Erwin, "ZrB2: The Optimum Integral Fuel Burnable Absorber for PWRs," *Trans. Am. Nucl. Soc.*, **62**, pp. CHECK (1990).

[S-8] J.G. Stevens, K.S. Smith, K.R. Rempe, T.J. Downar, "Simplified Automated Loading Pattern Generation for Multicycle Analysis," *Trans. Am. Nucl. Soc.*, **69**, pp. 420-422 (1993).

[S-9] J.G. Stevens, K.S. Smith, K.R. Rempe, T.J. Downar, "The PWR Loading Pattern Optimization in X-IMAGE," *Trans. Am. Nucl. Soc.*, **69**, pp. 453-455 (1993).

[T-1] L.S. Tong, J.Weisman, "Thermal Analysis of Pressurized Water Reactors," ANS, La Grange Park, Illinois, (1979).

[T-2] N.E. Todreas, M.S. Kazimi, "Nuclear Systems I: Thermal Hydraulic Fundamentals," (1990).

[U-1] V.O. Uotinen et al. "Preliminary Feasibility Study of an Advanced PWR Employing a Radial Blanket and Zircaloy Core Baffles and Formers," Babcock&Wilcox, BAW-1668, Lynchburg, VA, (May 1981).

[W-1] R. Weader, Yankee Atomic Electric Company, personal communication with L. Garcia-Delgado, January 28, 1998.

[W-2] Westinghouse, Commercial Nuclear Fuel Division, " ZIRLO™ Cladding: Meeting the Demanding Nuclear Fuel Performance Challenges of the 90's," Pittsburgh, PA, (1991).

[W-3] J. Weisman, P.E. MacDonald, A.I. Miller, H. Ferrari, "Fission Gas Release from UO_2 Fuel Rods with Time Varying Power Histories," *Trans. Am. Nucl. Soc.*, **12**, pp. 900 (1969).

[Y-1] T. Yamaguchi, Y. Syuji, S. Uematsu, "Neutronics Analysis of a Duplex-Type MOX-Gd Fuel in ATR," ANS Proc. Topical Mtg on Advances in Fuel Management, Myrtle Beach, SC, March 23-26, 1997.

[Z-1] L. Zhian, S.H. Levine, "AUTOLOAD, An Expert System Code that Automatically and Optimally Reloads a PWR," *Trans. Am. Nucl. Soc.*, **69**, pp. 456-458 (1993).

Appendices

Appendix A. Core and Assembly Detailed Representation

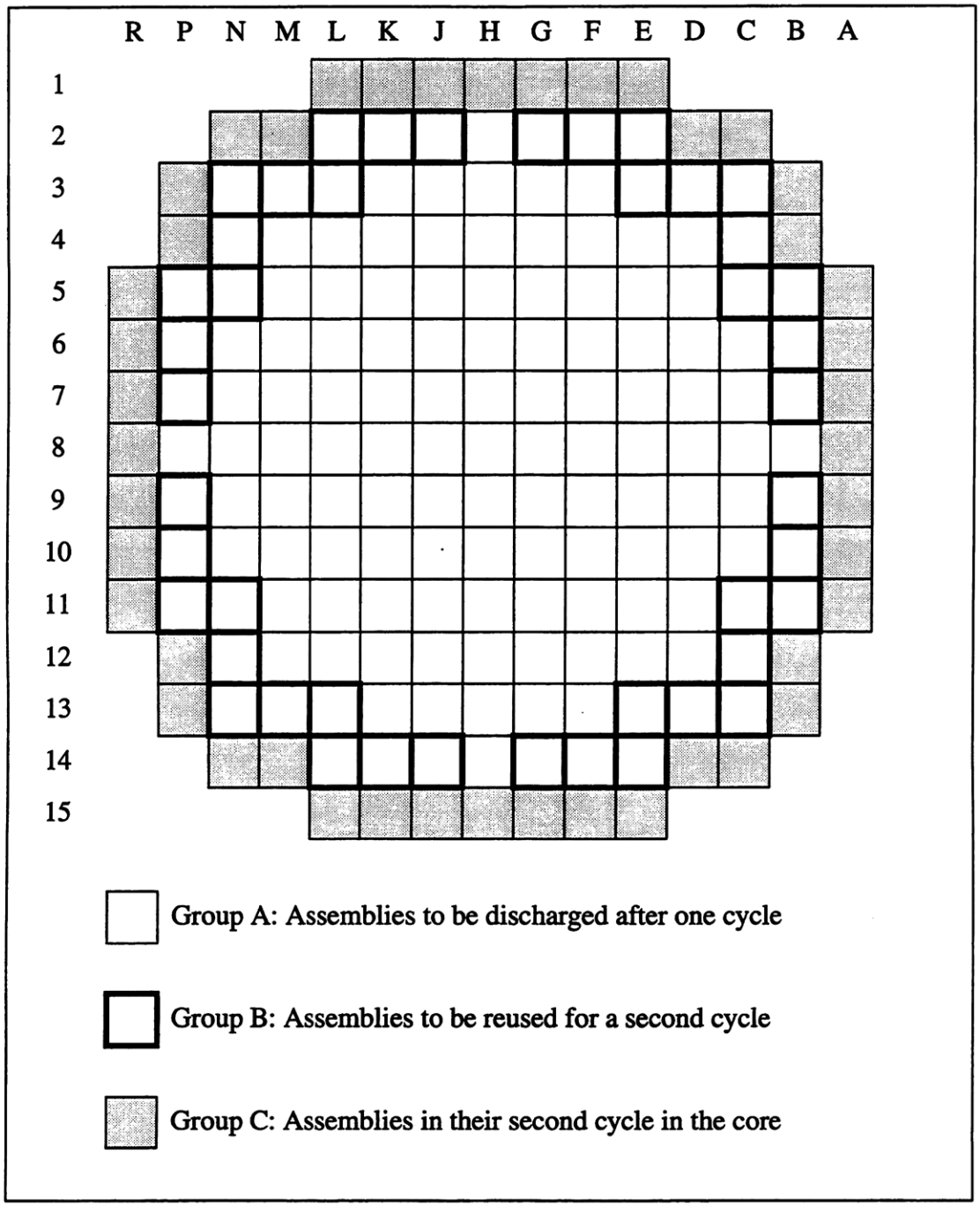

Figure A.1: Groups of assemblies according to reload strategy

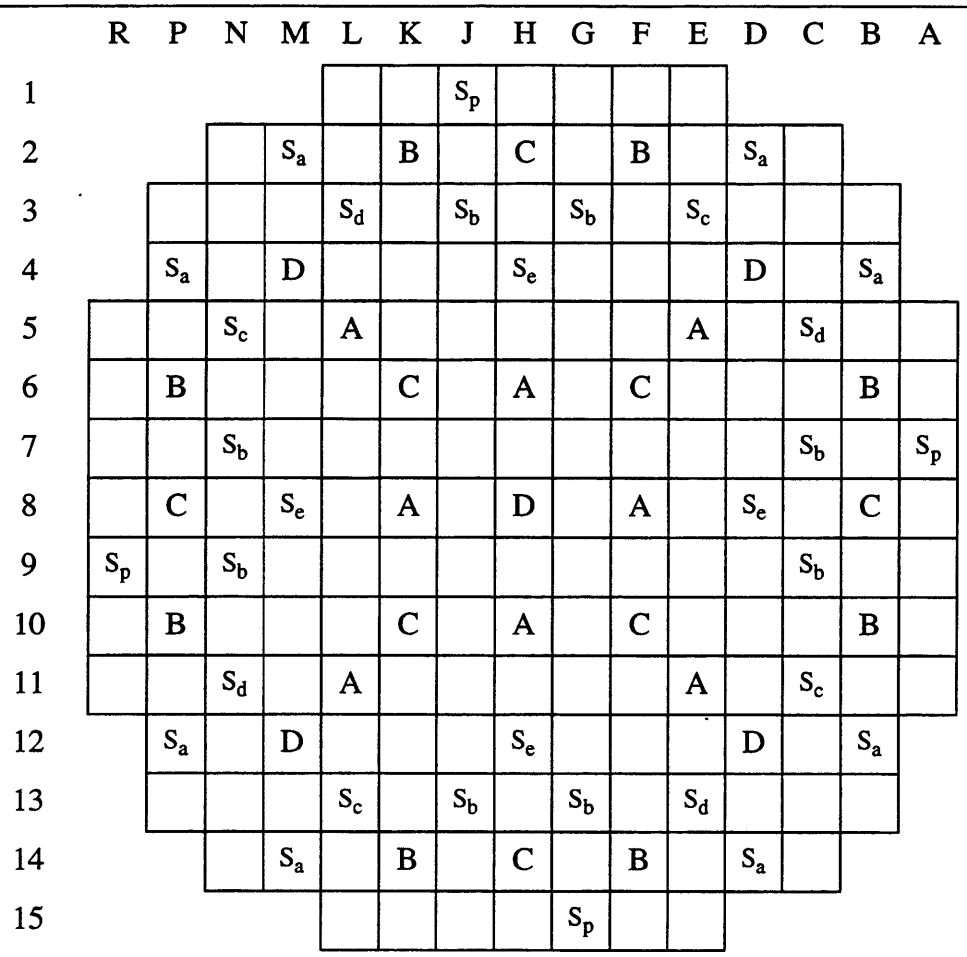

Control Bank	Number of Rods
A	8
B	8
C	8
D	5
Total	29

Shutdown Bank	Number of Rods
S_a	8
S_b	8
S_c	4
S_d	4
S_e	4
Total	28

S_p-Spare Locations

Figure A.2: Rod cluster control assembly pattern

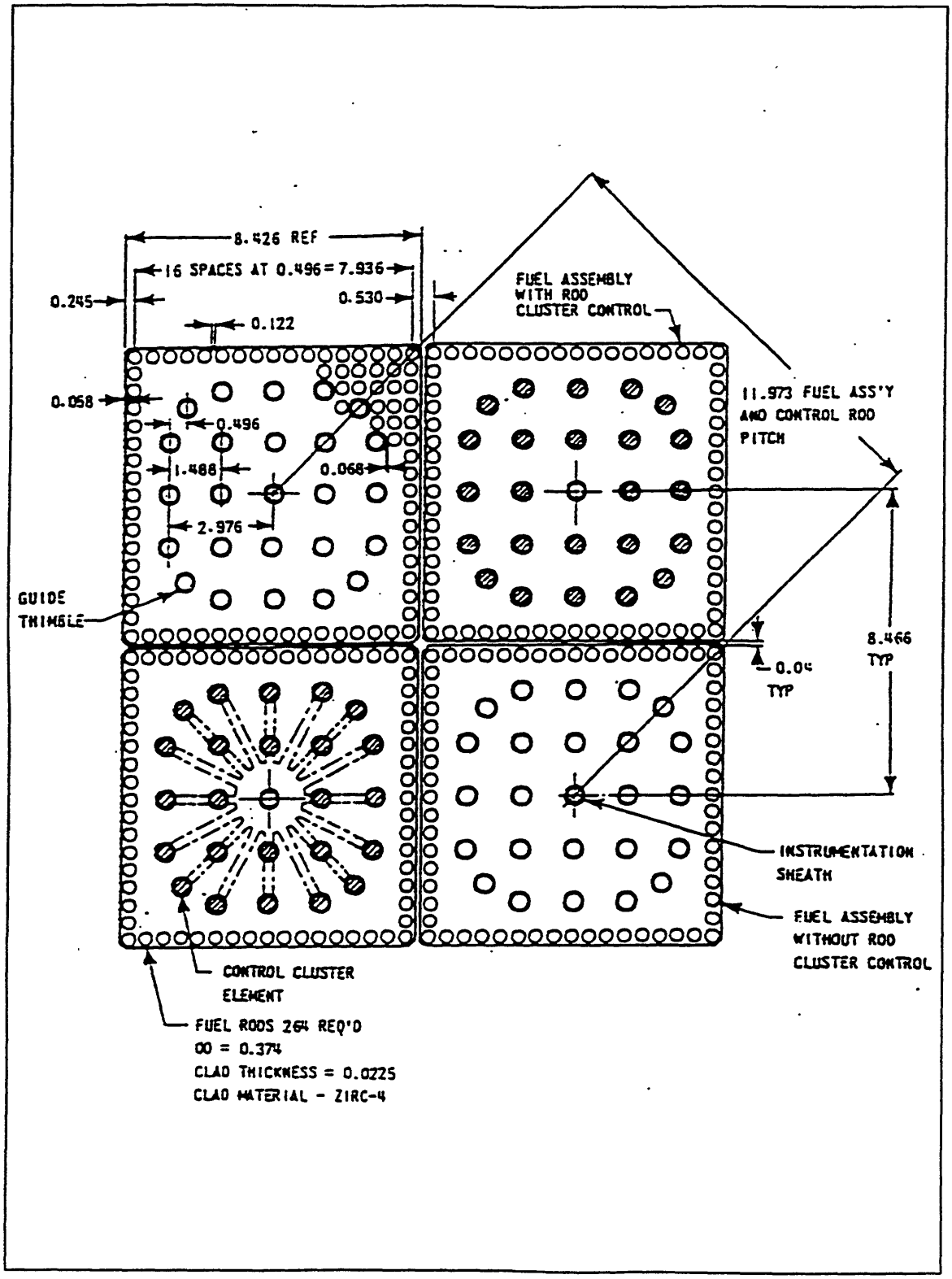

Figure A.3: Fuel assembly cross section - 17x17 array

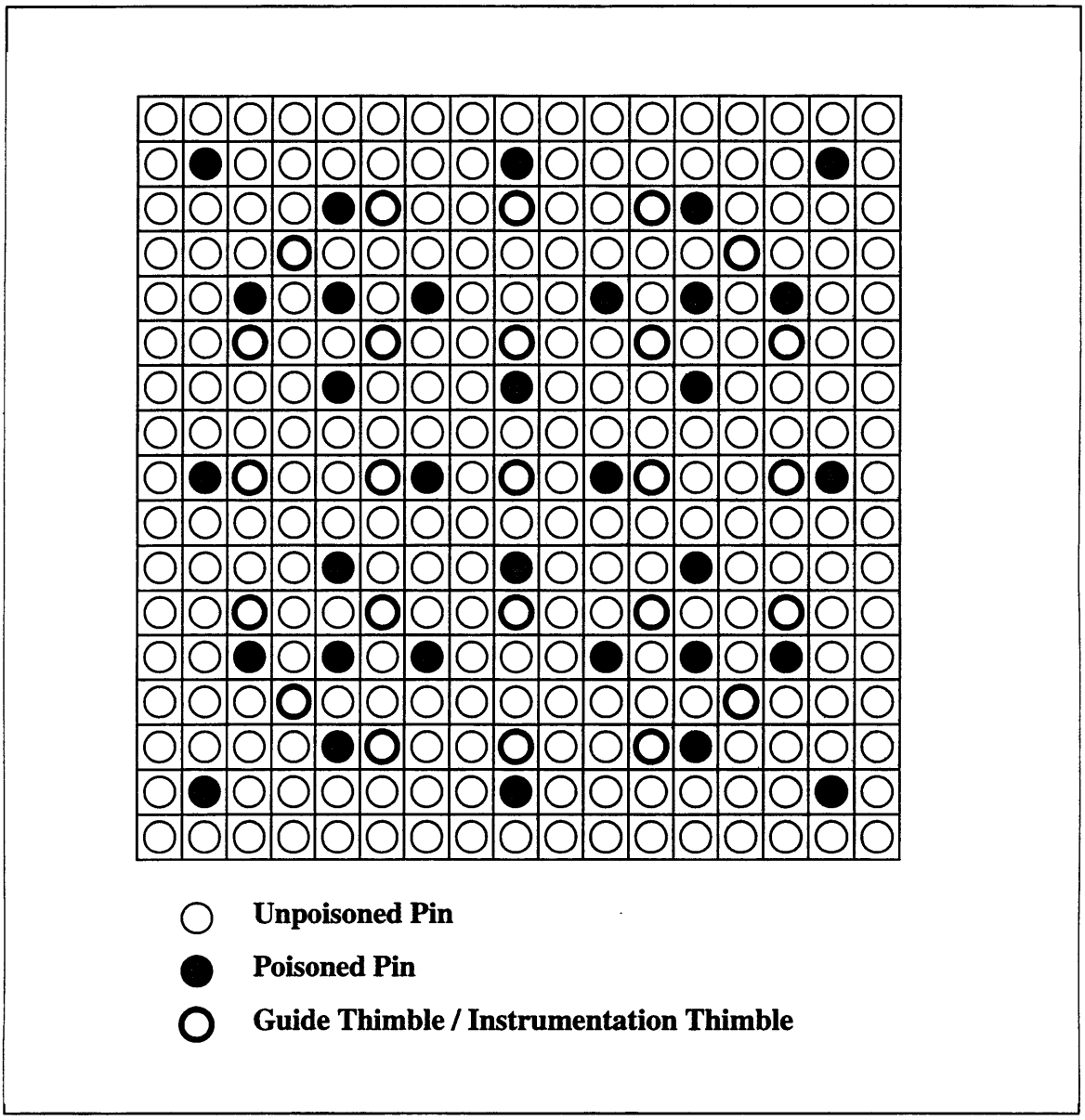

Figure A.4: Interior design for an assembly with 32 poisoned pins

Appendix B. Effective Capture Cross Section of Natural Gadolinium at EOC

The abundance-weighted capture cross section can be estimated by summation of the products of cross sections and isotope percentages,

$$\sigma_{ab} = \sum_i \sigma_i \cdot y_i$$

where σ_i and y_i are the capture cross section and percentage of the isotope i, respectively, and the index i extends the summation to all the isotopes of gadolinium.

At the EOC in the 36-month core, it can be reasonably assumed that

- the initial concentrations of Gd-155 and Gd-157 have been completely depleted, and their absorption rates equal those of Gd-154 and Gd-156;
- the initial concentrations of Gd-156 and Gd-158 have been increased by transmutation of all the Gd-155 and Gd-157 respectively.

Table B.1 shows the isotopic composition at EOC, and the capture cross sections, which remain unchanged from Table 6-4.

Application of the above equation yields

$$\sigma_{ab} = [0.2x700 + (2.1x60)x2 + (34.81x2)x2 + 40.62x2 + 21.86x1]x0.01 = 6.3 barns,$$

an approximate relative value since we have considered only 1/v thermal neutron captures.

A similar value can be determined at BOC --considering that only the capture in isotopes Gd-155 and Gd-157 is significant,-- using the values from Table 6-4 (Section 6.3.1.1):

$$\sigma_{ab} = [14.80x61\times10^3 + 15.65x2.55\times10^5]x0.01 = 48935 barns,$$

Table B.1: Isotopic composition of gadolinium and capture cross sections at EOC

	Gd-152	Gd-154	Gd-155	Gd-156	Gd-157	Gd-158	Gd-160
$y(^w/_o)$	0.20	2.18	~0	34.81	~0	40.62	21.86
σ_o (barns)	700	60	61,000	2	255,000	2	1

Starting with pure Gd-157 allows use of only 48935/255000=0.19 of the natural gadolinium. At EOC, it can be assumed that the Gd-157 has been completely depleted and only the transmutation product Gd-158 remains. The microscopic absorption cross section at EOC is, hence, $\sigma_{ab} = 1.0x2 = 2barns$.

Appendix C. Mass of Gadolinium in the 36-Month Core

The total mass of Gd_2O_3 for the 36-month core can be calculated as

$$Mass = \left(\sum_i NA_i \cdot NP_i \cdot Gd_i\right) \cdot M_p ,$$

where

NA_i=Number of assemblies of type i in the core

NP_i=Number of poisoned pins per assembly

Gd_i=Mass fraction of Gd_2O_3 in the pins,

M_p=Total mass of heavy metal oxide (UO_2) per unpoisoned pin (kg),

and the summation is extended to all the fresh assemblies in each reload.

M_p is calculated using the fuel dimensions in Table 2-1:

$$M_p = V \cdot \rho = \left(\pi \cdot (0.4095cm)^2 \cdot 365.76cm \cdot 10.3\frac{gr}{cm^3}\right) = 1.984kg ,$$

The values for NA_i, NP_i, and Gd_i are taken from the 36-month core loading pattern given in Figure 6-1. The total mass can be calculated as

$$Mass = [5 \cdot 36 \cdot 0.12 + 72 \cdot (32 \cdot 0.12 + 4 \cdot 0.04) + 44 \cdot 32 \cdot 0.12 + 12 \cdot (20 \cdot 0.1 + 10 \cdot 0.08)] \cdot 1.984 +$$

$$+8 \cdot (20 \cdot 0.12 + 12 \cdot 0.1) \cdot 1.984 = 1078.4 \text{ kg Gd2O3}$$

and considering the atomic mass of the gadolinium and oxygen atoms, the mass of gadolinium in the core (M_{Gd}) is found:

$$M_{Gd} = \left(\frac{2 \cdot 157}{2 \cdot 157 + 3 \cdot 16} \cdot 1078.4\right) = 935.4 \text{ kg Gd}$$

Appendix D. Numerical Values for Radial Optimization Analysis

The following Figures include the values used to analyze the margin for radial improvement in the 36-month core. Figure D.1 shows the maximum peak pin exposure for each assembly. Figure D.2 shows the $F_{\Delta H}$ for each assembly at two steps in core life: BOC and 10 GWD/MTU, which is the burnup step of maximum $F_{\Delta H}$ in core life.

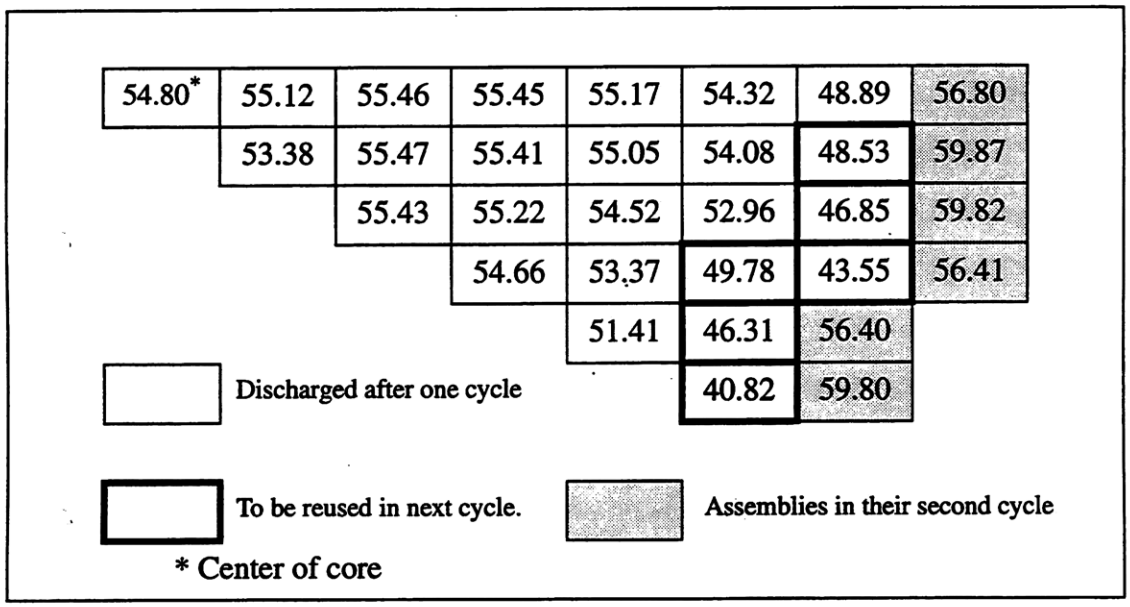

Figure D.1: Peak pin exposure (GWD/MTU) for each assembly in one eighth of the 36-month core

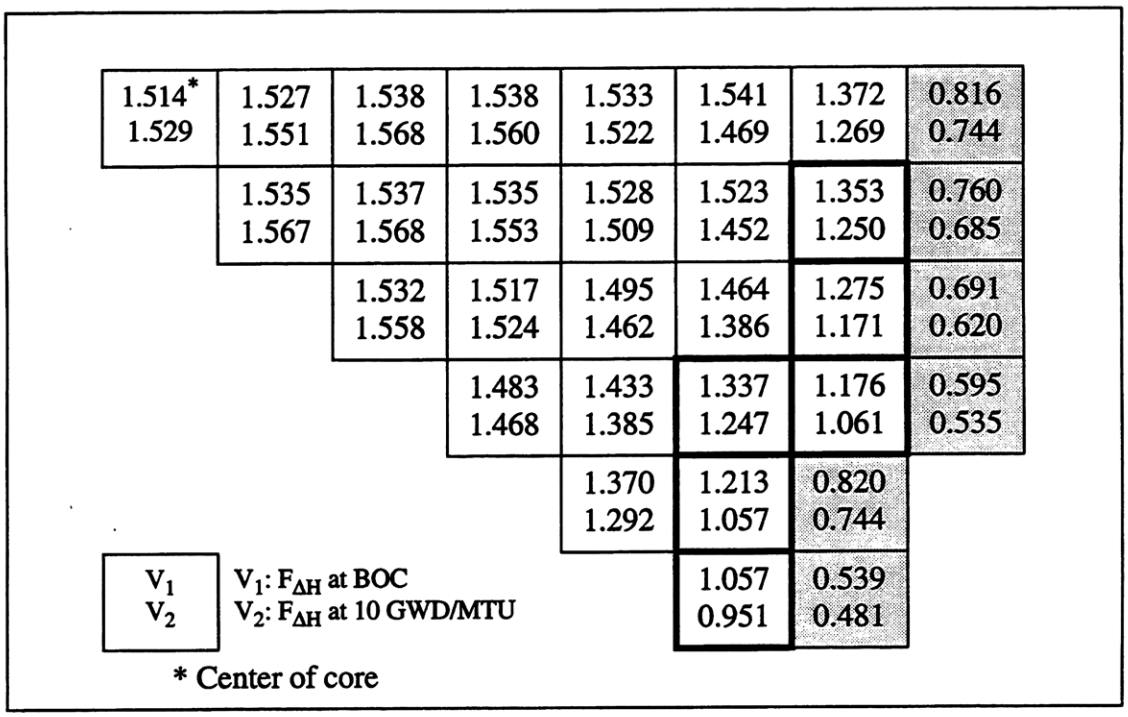

Figure D.2: $F_{\Delta H}$ for the assemblies in one eighth of the 36-month core at two steps in core life

Appendix E. Estimate of Transition Penalty

The transition penalty is estimated as the residual worth of the underburned assemblies in the transition process when compared to the assemblies of the 24-month cycle and the equilibrium 36-month cycle. For this calculation, the values in Tables E.1 and E.2 are used. The discharge burnups for the different groups of assemblies in the 24-month, 36-month and transition cycles are given in Table E.1. These values are taken from the physics analyses described in the main body of this document. Table E.2 indicates the worth ($/kg) of the fresh fuel as calculated with the economics model MUSCLE [H-3].

Table E.1: Discharge burnup for groups of assemblies in the 24-, 36-month and transition cycles

Set of assemblies	Burnup (GWD/MTU)
24-month cycle	
Assemblies discharged from the periphery (set Z)	38.32
Assemblies discharged from the core interior (set Y)	48.40
Assemblies after one cycle (sets X and W)	26.56
36-month cycle (equilibrium)	
Assemblies capable of reuse (group B in Figure A.1)	37.78
Peripheral assemblies	52.85
Transition cycle number 1	
Peripheral assemblies	43.80

Table E.2: Original fuel worth

Initial U-235 enrichment	Worth ($/kg)
4.6%	2300
6.5%	3250

Consider the transition scheme of Figure 10-1 and the numerical values of Table D.1. If the 24-month cycle were to be maintained, the assemblies in groups X and W would burn up to 38.32 and 48.40 GWD/MTU, respectively. In the equilibrium 36-month cycle, the intermediate ring of assemblies is reused and burns up to 52.85 GWD/MTU. These values are considered as reference to evaluate the transition penalty in both options.

Penalty for option 1

The assemblies in set X burn up to a higher extent than in the reference case, providing an economic benefit (computed as negative here). The sets of assemblies W and V are underburned when compared to the reference values. The fractional losses for the three groups of assemblies are:

$$Loss_X = \frac{38.32 - 43.80}{38.32} = -0.144$$

$$Loss_W = \frac{48.40 - 43.80}{48.40} = 0.095$$

$$Loss_V = \frac{52.85 - 37.78}{52.85} = 0.285$$

and the penalty for this option can be calculated as

$$Penalty_1 = \sum_i Loss_i \cdot Worth_i \cdot \text{Number of assemblies} \cdot \text{Fuel mass/assem},$$

where the summation is extended to the 3 groups of assemblies X, W, V.

The fuel mass per assembly can be calculated considering that:

- the fuel mass for an unpoisoned pin is 1.97 kg/pin (see Appendix C),
- there are 264 fuel pins per assembly.

$$\text{Fuel mass/assem} = 1.98 \text{ kg/pin} \cdot 264 \text{pin/assem} = 523 \text{ kg}$$

Therefore, the penalty is

$$Penalty_1 = (-0.144 \cdot 48 \cdot 2300 + 0.095 \cdot 49 \cdot 2300 + 0.285 \cdot 3250 \cdot 44)523 = \$18.6M\ \$$$

Penalty for option 2

As in the previous case, the assemblies in set X burn to a higher extent than in the reference case. However, the assemblies in set W are discharged after only one cycle, and, therefore, underburned by a larger amount. The fractional losses for these two groups of assemblies are:

$$Loss_X = \frac{38.32 - 43.80}{38.32} = -0.144$$

$$Loss_W = \frac{48.40 - 26.56}{48.40} = 0.451$$

and the penalty is

$$Penalty_2 = (-0.144 \cdot 2300 \cdot 48 + 0.451 \cdot 2300 \cdot 49)523 = \$18.3\ \text{M}$$

It can be seen that the values are very similar in both cases.

These up-front costs may be levelized over the remaining life of the plant, using the model described in [H-2]. The costs are multiplied by the capital recovery factor for continuous compounding of a continuous cashflow, ϕ:

$$\phi = \frac{i}{1 - e^{-it}}$$

For t=20 years, and assuming a carrying charge rate of i=10%/yr, ϕ=0.116. Therefore, the levelized costs for options 1 and 2 are \$2.15M/yr and \$2.10M/yr, respectively.

Appendix F. Gadolinia in the Fuel Pellet Annulus

The reactivity hold-down and poison duration are compared for the following cases:

a) solid fuel pellet with 10% Gd_2O_3,

b) annular pellet with Gd_2O_3 in the central annulus, and no poison within the fuel matrix.

Case a) represents the standard gadolinia loading scheme in fuel pellets, and case b) illustrates the strategy presented in [Y-1]. For a black cylinder, the initial reactivity hold-down is proportional to the surface area, hence circumference:

$$\frac{\Delta\rho_b}{\Delta\rho_a} = \frac{d_b}{d_a} = \sqrt{\frac{V_b}{V_a}}$$

where ρ is the reactivity, d and V are, respectively, the diameter and volume of the region in which the burnable poison is distributed. Note that V_a is the voume of the pellet since the burnable poison in case a) is mixed with the fuel, and V_b is the volume of the annulus since the burnable poison in case b) is only in this region.

Hence for a 10% annular hole (in volume),

$$\frac{\Delta\rho_b}{\Delta\rho_a} = \sqrt{0.1} = 0.32$$

So, the initial reactivity hold-down for case b) is greatly reduced when compared to case a). In Ref. [Y-1] this effect is compensated for by increasing the number of poisoned pins by a factor of 4.

The poison duration is proportional to the poison mass

$$\frac{T_b}{T_a} = \left(\frac{\delta_b}{\delta_a} \cdot \frac{V_b}{V_a} \cdot \frac{X_b}{X_a}\right),$$

where,

T_b, T_a=time to burnout for both cases

δ_b= density in central poison = density of Gd_2O_3 = 7.4 g/cm^3

δ_a= density of normal poisoned fuel pellet $\approx$ density of UO_2 = 10.2 g/cm^3

X_b= weight fraction of Gd in Gd_2O_3 = 0.87

X_a=weight fraction of Gd in normal burnable poison fuel=0.10

Thus for $V_b/V_a=1/10$, as considered above, the time to burnout is $T_b/T_a=0.63$, which indicates that the poison in the central annulus is depleted faster.

Therefore, this new concept cannot help much in the 36-month core, since the duration of the poison effect is of the greatest importance.

Appendix G. Fuel Performance Effects on Extended Cycles

Table G.1: Summary of unique fuel performance effects on extended cycle operation as indicated by Handwerk et al. [H-1]

Issue	Prescribed Limit	Extended Cycle Result	Potential Solutions (if required)
Stress and strain	"limits... should be provided"	Predicted worse	Increase number of pins per assembly
Fatigue cycling	"should be significantly less than design fatigue lifetime"	May have an inherent advantage	None necessary
Fretting	"should be limited"		
debris		Uncertain, competing effects	Improved awareness during outages
grid-to-rod		Not a concern	Improved grid design
Waterside corrosion	"should be limited"		Water chemistry control Improved cladding alloys Annular fuel pellets Increase number of pins per assembly
oxide layer		Uncertain, competing effects	
secondary hydriding		Uncertain, competing effects	
CRUD deposition		Predicted worse	
Rod bowing / axial growth	"should be limited"	Predicted worse	Unidentified
Rod internal pressure	"nominal system pressure unless otherwise justified"	Higher pressures	Change in burnable absorber loading Annular fuel, larger plena Increase number of pins per assembly
Primary hydriding		Not affected by cycle extension	None necessary
Cladding collapse		Not affected by cycle extension	None necessary
Cladding overheating	"should be prevented"	Steady State CHF within design envelope Degraded thermal margin for transient	None necessary
Fuel centerline melt	"is not permitted"	Within envelope	None necessary

Appendix H. Equations for the Cladding Corrosion Model

Pre-transition oxidation

For the pre-transition oxidation, the corrosion rate ds/dt is given by the Dyce correlation:

$$\frac{ds}{dt} = \frac{A}{s^2} \cdot \exp\left(-\frac{Q_1}{RT}\right) \tag{H.1}$$

where s is the oxide layer thickness in μm, T is the absolute temperature (°K) at the metal oxide interface, R is the universal gas constant and A and Q_1 are constants presented in Table H.1.

For a time step between t_o and t (days), the temperature change throughout the oxide film formed in the step is given by

$$T = T_o + f \cdot (s - s_o) \cdot 10^{-6} \tag{H.2}$$

where T_o (K) and s_o (μm) are the temperature in the metal-oxide interface and the oxide thickness at time t_o; T and s are the same parameters at time t; $f = q/\lambda_{ox}$, q is the heat flux (W m^{-2}) and λ_{ox} is the oxide thermal conductivity, taken as 2.0 W m^{-1} K^{-1}

For the problem under consideration,

$$s = \left(\frac{\Sigma^3 - s_o^3 c \cdot (\Sigma - s_o)}{1 - c \cdot (\Sigma - s_o)}\right)^{\frac{1}{3}} \tag{H.3}$$

where

$$\Sigma = \left[3 \cdot (t - t_o) \cdot A \cdot \exp\left(-\frac{Q_1}{RT_o}\right) + s_o^3\right]^{\frac{1}{3}} \tag{H.4}$$

$$c = \frac{Q_1 \cdot f}{RT_o^2} \tag{H.5}$$

The transition occurs at time t_a (days), given by

$$t_a = k_a \cdot \exp\left(\frac{Q_a}{RT}\right) \tag{H.6}$$

where k_a and Q_a are constants given in Table H.1.

Post-transition oxidation

The growth rate in the post-transition region is described by

$$\frac{ds}{dt} = B \cdot \exp\left(-\frac{Q_2}{RT}\right) \tag{H.7}$$

where Q_2 is constant. For films of moderate thickness, B is a constant but after the oxide thickness reaches a critical value, s_c, B becomes a function of both the fast neutron flux and the oxide layer thickness.

$$B = C \cdot E, \qquad E = 1 + u \cdot \phi \cdot \delta \cdot (s - s_c), \tag{H.8}$$

where C is a constant, s_c is the threshold thickness (μm) for which the second transition occurs, δ is either 1 or 0 depending on the oxide thickness, φ (n cm^{-2} s^{-1}) is the fast flux over 1MeV and u is a constant determined by in-reactor corrosion measurements. At long residence times the enhancements in oxidation rate due to neutron flux and oxide thickness level off, which is represented by setting $E = Min[1 + u \cdot \phi \cdot \delta \cdot (s - s_c), E_{max}]$, where E_{max} is an experimentally adjusted value.

For constant temperature, the analytical solution to equations H.7 and H.8 is

$$s = \left(s_o + \frac{\exp(FG) - 1}{G}\right) \tag{H.9}$$

where

$$G = \frac{Q_2 \cdot f}{R \cdot T_o^2} + \frac{u \cdot \phi \cdot \delta}{1 + u \cdot \phi \cdot \delta \cdot (s - s_c)} \tag{H.10}$$

$$F = C[1 + u \cdot \phi \cdot \delta \cdot (s - s_c)] \cdot \exp\left(-\frac{Q_2}{RT_o}\right) \cdot (t - t_o) \tag{H.11}$$

Thermal-hydraulic model

Consider for simplicity a single, closed subchannel, that does not account for cross flows. The bulk coolant temperature $T_b(z)$ at a given axial position z is

$$T_b(z) = T_{in} + \frac{4}{2\pi D_e} \int_z \frac{q'(z)}{GC_p r} dz \tag{H.12}$$

where T_{in} (K) is the inlet coolant temperature, q' (W m^{-1}) is the linear heat generation rate, C_p (J $kg^{-1}K^{-1}$) is the heat capacity of the coolant, G(kg m^{-2} s^{-1}) is the coolant mass flux, r (m) is the cladding outer radius including crud and oxide layer thickness, and D_e (m) is the hydraulic diameter, given by

$$D_e = \frac{4 \cdot (P^2 - \pi \cdot r^2)}{2 \cdot \pi \cdot r}, \tag{H.13}$$

wher P (m) is the pin pitch in the assembly.

Heat may be transferred from cladding to coolant by either forced convection or nucleate boiling. The cladding surface temperature at the outermost surface is taken as the minimum of the temperatures under forced convection, T_{fc}, and nucleate boiling, T_{nb}:

$$T_{cr}(z) = Min(T_{fc}, T_{nb}) \tag{H.14}$$

In the forced convection regime, the metal-oxide interface temperature is given by

$$T_{fc}(z) = T_b(z) + \frac{q'}{2\pi r} \cdot \frac{1}{h_{film}} + \Delta T_{crud}(z) \tag{H.15}$$

where ΔT_{crud} is the temperature drop in the crud layer, and h_{film} is the heat transfer coefficient for turbulent flow:

$$h_{film} = f_F \cdot \frac{k}{D_e} Re^{0.8} \cdot Pr^{0.4} \tag{H.16}$$

where Re and Pr are the Reynolds and Prandtl numbers, respectively, and

$$f_F = 0.042 \cdot \left(\frac{P}{2r}\right)^{-0.024} \tag{H.17}$$

The temperature drop across the crud layer is

$$\Delta T_{crud}(z) = \frac{q'}{2\pi\lambda_{cr}} \cdot \frac{s_{cr}}{r' + s} \tag{H.18}$$

where $\lambda_{cr,}$ thermal conductivity of the crud, is taken as 0.7 W m^{-1} K^{-1}, r‘ is the clad outer radius and s_{cr} is the crud layer thickness.

In the nucleate boiling regime, the temperature at the outer crud layer surface is

$$T_{nb}(z) = T_{sat} + 0.02265 \cdot \left(\frac{q'}{2 \cdot \pi \cdot r}\right)^{\frac{1}{2}} \cdot \exp\left(-\frac{P}{8687000}\right) \quad \text{(H.19)}$$

where P (Pa) is the coolant pressure.

Once T_{cr} in eq. H.14 is calculated, the metal-oxide interface temperature, T_{co}, can be obtained as

$$T_{co}(z) = T_{cr}(z) + \Delta T_{ox}(z) \quad \text{(H.20)}$$

where the temperature drop across the oxide layer, ΔT_{ox} is given by

$$\Delta T_{ox}(z) = \frac{q'}{2\pi\lambda_{ox}} \cdot \frac{s}{r'} \quad \text{(H.21)}$$

Constants and properties

The constants in equations H.1 through H.11 are given in Table H.1. The constants A and C depend on the cladding material. In this case they are tuned from in-reactor corrosion data for low tin Zircaloy-4 with 1.3 $^{w}/_{o}$ Sn.

Table H.1: Constants used in the Zircaloy oxidation model

Constant	Value
Q_1	32289 cal mol^{-1}
Q_2	27354 cal mol^{-1}
Q_a	26130 cal mol^{-1}
E_{max}	2.42
k_a	7.98 x10^{-8} days
u	1.7 x 10^{-16} cm^2 sec $neutron^{-1}$ μm^{-1}
s_c	6.0 μm
A	1.65 x10^{10} μm^3 day^{-1}
C	1.6 x10^8 μm^3 day^{-1}

For simplicity in the calculations, coolant properties are taken at an approximate core average temperature of 307.7 °C. The values are obtained by interpolation in the steam tables [K-3], and listed in Table H.2. It should be noted that the properties are temperature dependent, and, therefore, vary along the channel. In particular, changes in the heat capacity with temperature are significant in the range of conditions of the reactor.

Table H.2: Average properties of the coolant fluid

Parameter	Value
Density	721.0 kg m^{-3}
Viscosity	88.9×10^{-6} N s m^{-2}
Heat capacity	6100.0 J kg^{-1} K^{-1}
Thermal conductivity	0.546 W m^{-1} K^{-1}
Prandtl number	1.48

The rod and assembly dimensions are taken from Table 2.1 (Chapter 2), except for the coolant mass flux, which is taken as 3600 kg m^{-2} s^{-1}. Note that the value given in Table 2.1 considers the total core cross sectional area, including the rods, whereas the value given here only considers the free flow area.

Appendix I. FORTRAN Code for the Cladding Corrosion Model

```
c=====================================================================
c Clad corrosion model for PWR cores
c     Based on paper: K.Forsberg, M.Limback,A.R.Massih, "A model
c           for uniform Zircaloy clad corrosion in pressurized
c           water reactors", Nuc. Eng&Des. 154 (1995) pp 157-168.
c     Comments:
c       1. Calculates Tco with incremental steps from the corrosion
c          model. Only uses thermal hydraulic model in each change of
c          power conditions.
c
c     Luis Garcia Delgado
c     April 1st, 1998
c     Massachusetts Institute of Technology
c
c     to compile this program:
c     f77 -C corrmod.f -o corrmod
c     to run this program:
c     corrmod
c=====================================================================

      program corrmod

      real q1,q2,qa,emax,ka,u,sc,A,C,lambdaox,lambdacr,R
      real Pres,Tsat,Gmass,Tin,Pitch
      real dens,visc,Cp,k
      real Re,Pr,fF,hfilm
      real rad,rprim,s
      real De,Tb,DTfilm,DTcrud,Tfc,DTnb,Tnb,Tcr,Tco,DTox,Tcoin
      real scr,qinteg,qloc
      real t,ta,sigma1,sigma,dtime,tcycle,soin,ced,f
      real E,psi,delta,B,Fc,Gc,e1,D
      real tlimit(6), qlocal(6),qintegral(6),flux(6)
      integer n,i

c constant values in corrosion model
      DATA q1,q2,qa,emax,ka/32289,27354,26130,2.42,7.98e-8/
      DATA u,sc,A,C,pi,R/1.7e-16,6.0,1.65e10,1.6e8,3.1416,1.98/
      DATA lambdaox,lambdacr,psi,n/2.0,0.7,0.0,1/
c data to modify in each run
      DATA (qintegral(i),i=1,3)/74959,66300,50809/
      DATA (qlocal(i),i=1,3)/27466,24674,19418/
      DATA (tlimit(i),i=1,3)/439,878,1317/
      DATA (flux(i),i=1,3)/1.96e13,1.76e13,1.38e13/
      DATA dtime,tcycle/8,1317/
      DATA scr/0.0/
c reactor data
      DATA Pres,Tsat,Gmass,Tin/15.51e6,617.9,3600.00,565.7/
      DATA Pitch,rprim/ 12.6e-3,4.75e-3/
```

```
c coolant properties at T=617.9 K (652.8F)
c     density(kg/m3),viscosity(Ns/m2),sp. heat(J/kg/K),conduc(W/m/K)
      dens=721.0
      visc=88.9e-6
      Cp=6100.0
      k=0.546
      Pr=1.48

      open(2,file='output',status='new')
c initial values
      t=dtime
      soin=0
      n=1
      i=0
      s=0.0
      f=0.0

 30   i=i+1
      psi=flux(i)
      qloc=qlocal(i)
      qinteg=qintegral(i)
      write(2,*)'qintegral=',qinteg
      write(2,*)'qlocal=',qloc
      write(2,*)'fast flux=',psi
      write(2,*)

c Thermal and hydraulic model
      rad=rprim+(s+scr)*1.0e-6
      De=4.0*(Pitch**2-pi*rad**2)/(2.0*pi*rad)
      Tb=Tin+(4.0/(2.0*pi*De))*(1.0/(Gmass*Cp*rad))*qinteg
      if (Tb.gt.Tsat) then
         Tb=Tsat
         endif
      Re=Gmass*De/visc
      Pr=visc*Cp/k
      fF=0.042*(Pitch/(2.0*rad))**-0.024
      hfilm=fF*k/De*(Re**0.8)*(Pr**0.4)
      DTfilm=qloc/(2.0*pi*rad*hfilm)
      DTcrud=(qloc/(2.0*pi*lambdacr))*(scr*1.0e-6/(rprim+s*1.0e-6))
      Tfc=Tb+DTfilm+DTcrud

      DTnb=0.02265*(qloc/(2.0*pi*rad))**0.5*exp(-Pres/8687000.0)
      Tnb=Tsat+DTnb

      Tcr=MIN(Tfc,Tnb)
      DTox=qloc/(2.0*pi*lambdaox)*(s*1.0e-6/rprim)
      Tco=Tcr+DTox
      write(2,*) Tco
      Tcoin=Tco

 50   if (t.lt.tcycle) then
c Oxidation model
      if (t.ge.tlimit(i))then
        goto 30
```

```
      endif

      if (n.eq.1) then
      ta=ka*exp(qa/(R*Tco))
      n=n+1
      endif
      Tcoin=Tcoin+f*1.0e-6*(s-soin)
      soin=s
      if (t.lt.ta) then
         sigma1=(3.0*dtime*A*exp(-q1/(R*Tcoin))+soin**3)
         sigma=sigma1**(0.333333)
         qflux=qloc/(2.0*pi*rad)
         f=qflux/lambdaox
         ced=q1*f*1.0e-6/(R*Tcoin**2)
         s=(sigma1-soin**3*ced*(sigma-soin))/(1.0-ced*(sigma-soin))
         s=s**(1.0/3.0)
         sfirst=s
      else
         if (s.lt.sc) then
            delta=0
         else
            delta=1
         endif
         e1=1.0+u*psi*delta*(s-sc)
         E=MIN(e1,emax)
         B=C*E
         D=u*psi*delta
         Fc=C*E*exp(-q2/(R*Tcoin))*dtime
         qflux=qloc/(2.0*pi*rad)
         f=qflux/lambdaox
         Gc=(q2*f*1.0e-6/(R*Tcoin**2))+(D/E)
         s=soin+(exp(Fc*Gc)-1.0)/Gc
      endif
      write(2,1000) t
      write(2,1010)
      write(2,1020) Tb,Tcoin
      write(2,1030) s
      write(2,*)
      t=t+dtime

      goto 50

      endif

200   continue

1000  format ('time=',f6.1,' days')
1010  format ('   Temperature distribution (K)')
1020  format ('Tbulk='f7.2, ' Tmet_ox=',f7.2)
1030  format ('Oxide thickness:', f9.3)
      write (2,*) 'sfirst=', sfirst, ' ta=',ta
      close (2)
      write (*,*) 'done'
      end
```

Appendix J. Equations for the Fission Gas Release Model

Let t_i denote the time at the end of the i^{th} step, (i=1..I), with $\Delta t_i = t_i - t_{i-1}$;

Let j denote the j^{th} axial node limited by z_{j-1} and z_j, with j=1..J, and $z_o=0$, $z_J=L$;

Let k denote the k^{th} radial node limited by R_{k-1} and R_k, with k=1..K, and $R_o=0$, $R_K=R_{fo}$.

The rate of gas production, P_i^j(moles/sec) in an axial node of length L^j(m) during the time step i is given by

$$P_i^j = 6.244E15 \cdot \frac{\gamma \cdot q'^j_i \cdot L^j}{NA \cdot E_{fiss}} \tag{J.1}$$

where γ is the gas atoms produced per fission, $\gamma=\gamma_{Kr}+\gamma_{Xe}=0.047+0.344=0.391$

E_{fiss} is the energy deposited in the rod per fission,

E_{fiss}= 97.3% x 197.5 MeV/fission = 192.2 MeV

NA is the Avogadro number,

q'^j_i is the linear heat rate (kW/m) in the axial node j during the time step i, and the constant in the numerator is introduced to adjust the units in the equation.

The rate of gas produced in a radial ring in an axial node, $PR^j_{k,i}$, (moles/sec) is

$$PR^j_{k,i} = \frac{P_i^j \cdot (R_k^2 - R_{k-1}^2)}{R_{fo}^2} \tag{J.2}$$

where P_i^j is the rate of gas produced in the axial node j during time step i as given by equation J.1.

The number of moles produced in a node during a time step Δt_i is $PR^j_{k,i} \cdot \Delta t_i$.

The number of moles released from the node, $\Delta r^j_{k,i}$, during the ith time interval, Δt_i, is given by the following empirical correlation

$$\Delta r^j_{k,i} = PR^j_{k,i}\left\{\Delta t_i - \frac{1-K_1}{K_2} \cdot [1-\exp(-K_2 \cdot \Delta t_i)]\right\} + C^j_{k,i-1} \cdot [1-\exp(-K_2 \cdot \Delta t_i)] \tag{J.3}$$

where $PR^j_{k,i}$ is the gas production rate in moles/sec,

$$K_1 = \exp\left(-\frac{12450}{T} + 1.84\right)$$

$$K_2 = 0.25 \cdot \frac{1}{3600} \cdot \exp\left(-\frac{21410}{T}\right)$$, where T is in ^oR and K_2 is 1/sec

Δt_i is the time interval in sec,

$C^j_{k,i-1}$ is the gas retained in the node at the beginning of the time step i.

The total gas trapped in the node at the end of the time step i is

$$C^j_{k,i} = (PR^j_{k,i} \cdot \Delta t_i + C^j_{k,i-1}) - \Delta r^j_{k,i} \tag{J.4}$$

where all the terms have already been defined.

The above calculations are repeated for all the radial rings (k=1..K) in each axial node (j=1..J), then for all the nodes in each time step, and finally for all the time steps.

The total gas release from time zero is $\sum_i \sum_j \sum_k \Delta r^j_{k,i}$, and the fraction of gas released out of the total produced is

$$FGR = \frac{\sum_i \sum_j \sum_k \Delta r^j_{k,i}}{\sum_i \sum_j \sum_k PR^j_{k,i} \cdot \Delta t_i} \tag{J.5}$$

Appendix K. FORTRAN Code for the Fission Gas Release Model

```
c=====================================================================
c Fission Gas release model
c   Based on equations in Fredom, by Loftus and Hochreiter.
c   Fuel centerline temperature from combination of Maki and Garner.
c   Fuel outside temperature from Maki.
c   Temperature distribution in fuel pellet by fitting a
c      parabola to the two previous values.
c    Vectors yo(j), wo(j,k) are calculated by:
c       taking the values from Tree-1268, figure 1, at 0 GWd/MTU
c       linking these points with Maki's values at 20GWd/MTU
c       interpolating the values in between.
c
c     Luis Garcia Delgado
c     April 28th, 1998
c     Massachusetts Institute of Technology
c
c     to compile this program:
c     f77 -C fgr.f -o fgr
c     to run this program:
c     fgr
c=====================================================================
      program GasRelease

c  define variables
      real Rfo,drad,rad(51),Lnode,Mnode
      real yo(11), wo(13,4),qpavg, qp(24,10)
      real TSTEP(10),time,dtimed,dtimes,dtimeh,B(24,2100)
      real gamma,NA,efiss,P(24,2100),PT(24,2100),PR(51,2100)
      real Tfo(24,2100),Tfi(24,2100),val2,val1,temp(51),dq,qref
      real K1(51),k2(51),Co(24,51)
      real Pac(2100),Rel(24,2100),FGR(2100),Relac(2100),PTz(2100)
      real func1(51),func2(51),drel(51,2100),TGrel(24,2100),Grel(2100)
      integer STEPS,n,nnodes,zi,ti,ql,qup,Bl,Bup
      integer ri,rnodes,j
c      maxt=2100                          !maximum # of time steps

c  constant values in the model
      DATA nnodes,rnodes,dtimed/24,25,1.0/      !dtimed is in days
      DATA Mnode,Rfo,qpavg,Lnode/0.0725,4.095e-3,18.25,0.1524/
      DATA gamma,NA,efiss/0.391,6.022e23,192.2/
c  input data from Figures in Maki and Garner
      DATA (yo(j),j=1,11)/282,304,326,347,369,391,396,401,406,411,416/
      DATA (wo(j,1),j=1,6)/282,282,282,282,282,282/
      DATA (wo(j,1),j=7,13)/281,281,280,280,279,279,278/
      DATA (wo(j,2),j=1,6)/502,508,514,520,526,531/
      DATA (wo(j,2),j=7,13)/536,541,546,551,556,561,566/
      DATA (wo(j,3),j=1,6)/1057,1065,1073,1082,1090,1108/
      DATA (wo(j,3),j=7,13)/1125,1143,1160,1178,1195,1213,1230/
```

```
      DATA (wo(j,4),j=1,6)/1627,1661,1695,1728,1762,1778/
      DATA (wo(j,4),j=7,13)/1794,1810,1826,1842,1858,1874,1890/

c initialize values
      N=1
      time=dtimed
      ti=1
      dtimeh=dtimed*24.0        ! time in hours
      dtimes=dtimeh*3600.0      ! time in seconds
      do 5 zi=1,nnodes
         do 10 ri=1,rnodes
 10         Co(zi,ri)=0.0
 5          continue

c read power histories from external file
      open(1,file='input',status='old')
      open(2,file='output',status='new')
      read(1,1000) STEPS                    !read # of steps
      read(1,*)                             !read blank line
 20   if (N.le.STEPS) then
       read(1,1010) TSTEP(N)
       N=N+1
       goto 20
       endif
       N=1
 30   if (N.le.STEPS) then
         zi=1
         read(1,*)                           !read blank line
 50    if (zi.le.nnodes) then
            read(1,1020) qp(zi,N)
            qp(zi,N)=qp(zi,N)*qpavg
            zi=zi+1
            goto 50
            endif
          N=N+1
          goto 30
         endif
         write(*,*) 'read OK'

c     Initialize values
         zi=1
 60    if (zi.le.nnodes) then
         B(zi,1)=0
         zi=zi+1
         goto 60
        endif
      Pac(1)=0
      Relac(1)=0

c Time iteration
      N=1
      ti=2
 70   if (time.gt.TSTEP(N)) then
         N=N+1
```

```
         endif
      if (N.gt.STEPS) then
         goto 150
         endif
      if (time.le.TSTEP(N)) then
         Grel(ti)=0
         PTz(ti)=0
         do 80 zi=1,nnodes
 80         TGrel(zi,ti)=0

c     Spatial iteration
         zi=1
         PTz(ti)=0
 90      if (zi.le.nnodes) then
            B(zi,ti)=B(zi,ti-1)+dtimed*qp(zi,N)*Lnode*1.0e-3/Mnode
            P(zi,ti)=gamma*6.244e15/(NA*efiss)*qp(zi,N)*Lnode
            PT(zi,ti)=P(zi,ti)*dtimes

c     Interpolation of Tfo
        ql=int((qp(zi,N)/5.0)+1)
        qup=ql+1
        Tfo(zi,ti)=yo(ql)+((yo(qup)-yo(ql))/5.0)*(qp(zi,N)-5.0*(ql-1))

c     Interpolation of Tfi
        if (B(zi,ti).ge.60) then
           Bl=12
           goto 100
           endif
        Bl=int((B(zi,ti)/5.0)+1)
 100    Bup=Bl+1
c     give values for dq and qref
            if (qp(zi,N).le.10) then
               ql=1
               dq=10
               qref=0
              elseif (qp(zi,N).le.30) then
                  ql=2
                  dq=20
                  qref=10
              elseif (qp(zi,N).le.50) then
                  ql=3
                  dq=20
                  qref=30
            endif
            qup=ql+1

         val1=wo(Bl,ql)+((wo(Bl,qup)-wo(Bl,ql))/dq)*(qp(zi,N)-qref)
         val2=wo(Bup,ql)+((wo(Bup,qup)-wo(Bup,ql))/dq)*(qp(zi,N)-qref)

         Tfi(zi,ti)=val1+((val2-val1)/5.0)*(B(zi,ti)-5.0*(Bl-1))

c     calculation in radial nodes
            temp(1)=1.8*Tfi(zi,ti)+32.0+460.0
            rad(1)=0.0
```

```
            ri=2
            drad=Rfo/(rnodes-1)

          do 110 ri=2,rnodes,1
c       if (ri.le.rnodes) then
            rad(ri)=drad*(ri-1)
         temp(ri)=Tfi(zi,ti)+((Tfo(zi,ti)-Tfi(zi,ti))/Rfo**2)*rad(ri)**2
c       those temperatures are in C and have to be converted to R
            temp(ri)=1.8*temp(ri)+32.0+460.0

             K1(ri)=exp((-12450.0/temp(ri))+1.84)
             k2(ri)=0.25*exp(-21410.0/temp(ri))

           PR(ri,ti)=P(zi,ti)*(rad(ri)**2-rad(ri-1)**2)/Rfo**2
         func1(ri)=(1.0-K1(ri))*(1.0-exp(-k2(ri)*dtimeh))/(k2(ri)/3600.0)
c       the following is done to avoid truncature problems
            if (func1(ri).ge.dtimes) then
               func1(ri)=dtimes
               endif
            if (temp(ri).le.1430) then
               func1(ri)=dtimes
               endif
            func2(ri)=(1-exp(-k2(ri)*dtimeh))
           drel(ri,ti)=PR(ri,ti)*(dtimes-func1(ri))+Co(zi,ri)*func2(ri)
            Co(zi,ri)=PR(ri,ti)*dtimes+Co(zi,ri)-drel(ri,ti)
            TGrel(zi,ti)=TGrel(zi,ti)+drel(ri,ti)
 110        continue

             PTz(ti)=PTz(ti)+PT(zi,ti)
             Grel(ti)=Grel(ti)+TGrel(zi,ti)
             zi=zi+1
             goto 90
             endif

             Pac(ti)=Pac(ti-1)+PTz(ti)
             Relac(ti)=Relac(ti-1)+GRel(ti)
             FGR(ti)=Relac(ti)/Pac(ti)
             write(2,*) 'ti=',ti,' time(days)=',time,' FGR=',FGR(ti)
             write(2,*) 'Accum=',Pac(ti),'Total released=',Relac(ti)
             write(2,*)
             time=time+dtimed
             ti=ti+1
             goto 70
             endif

 150         continue

 1000 format(i2)
 1010 format(f6.0)
 1020 format(f6.3)
      close(1)
      write(*,*) 'done'
      end
```

Appendix L. Temperature Data for the Fission Gas Release Model

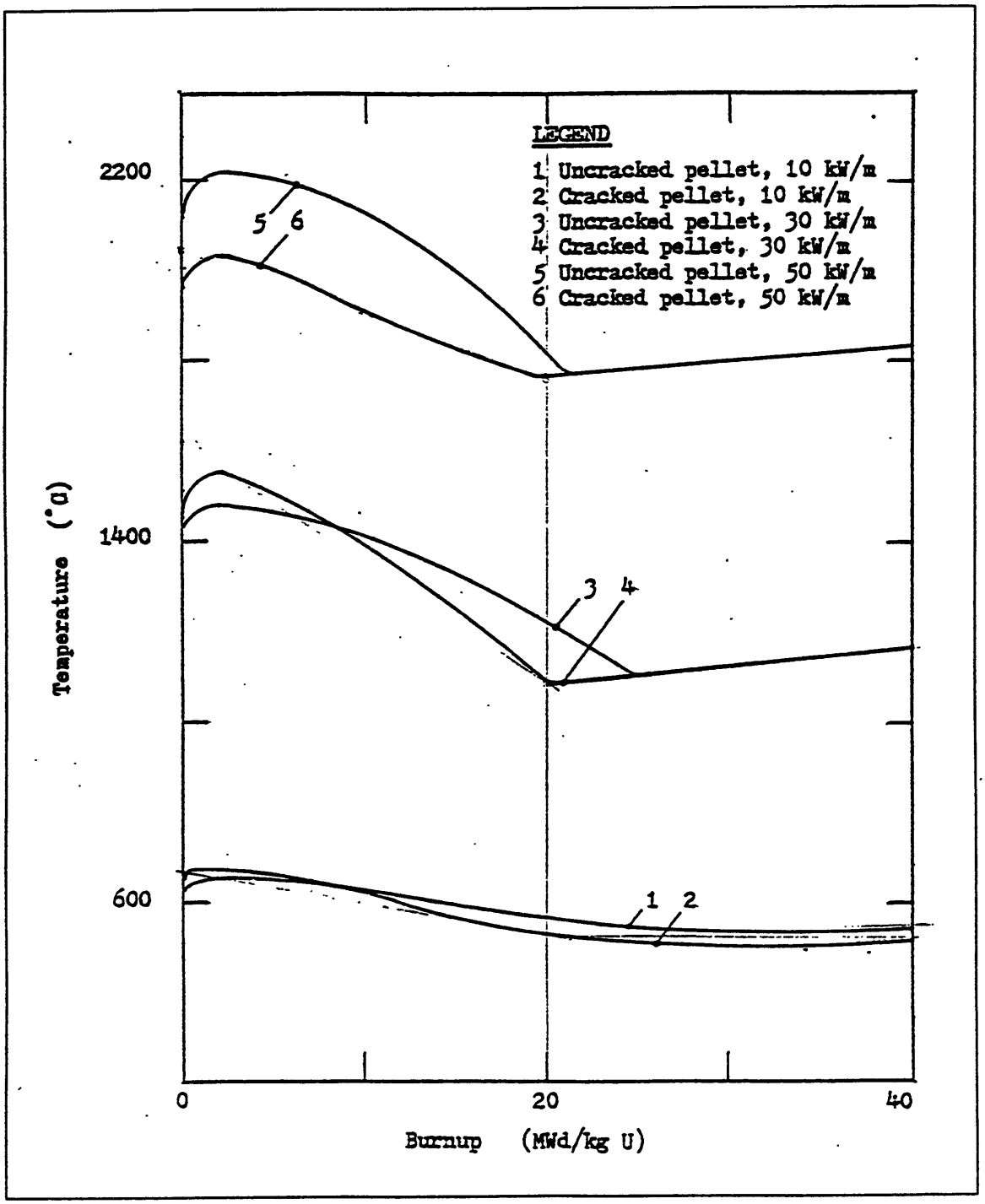

Figure L.1: Comparison of cracked and uncracked fuel pellet centerline temperatures at 10, 30, and 50 kW/m. (from [M-8]).

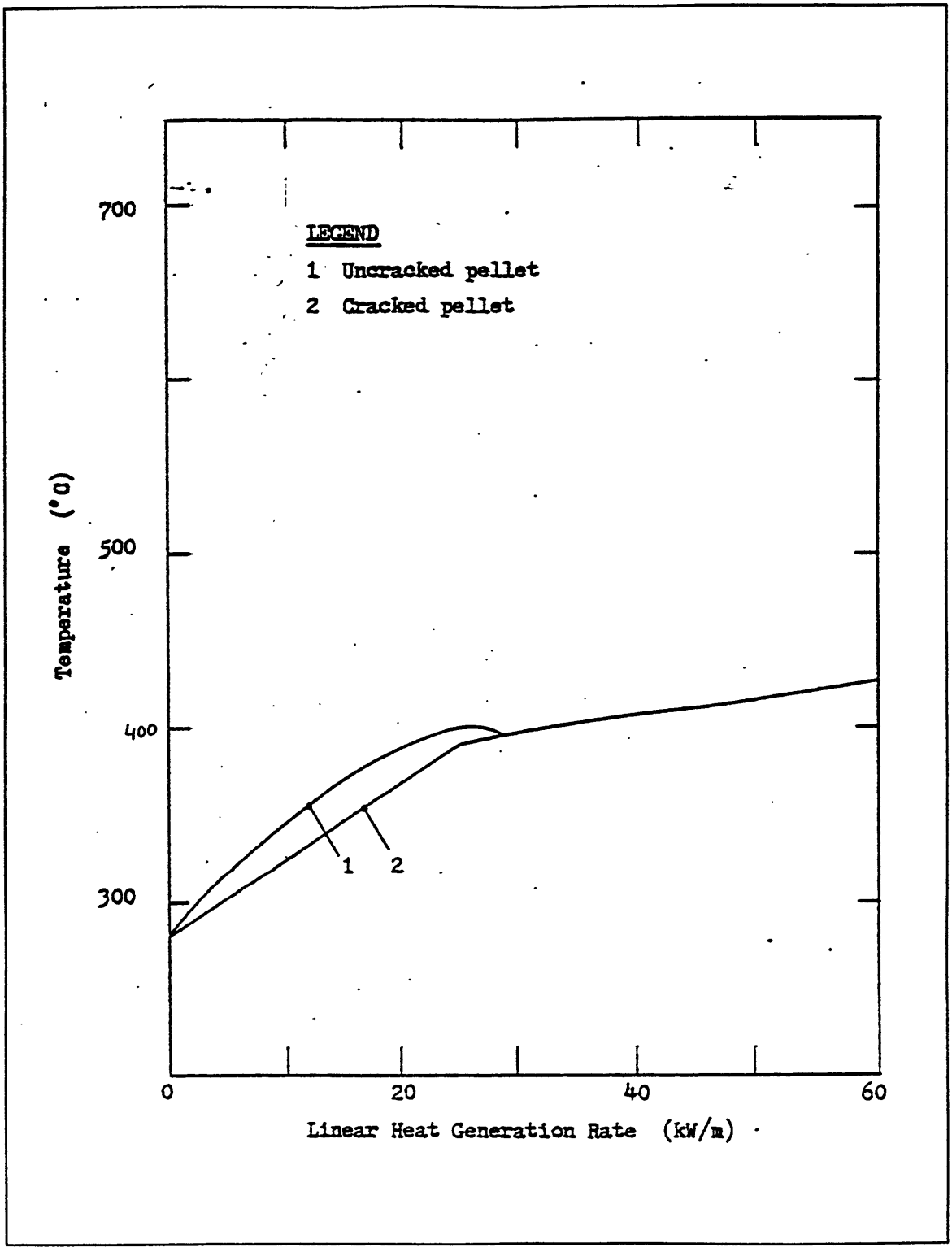

Figure L.2: Fuel surface temperature as a function of rod power (from [M-8])

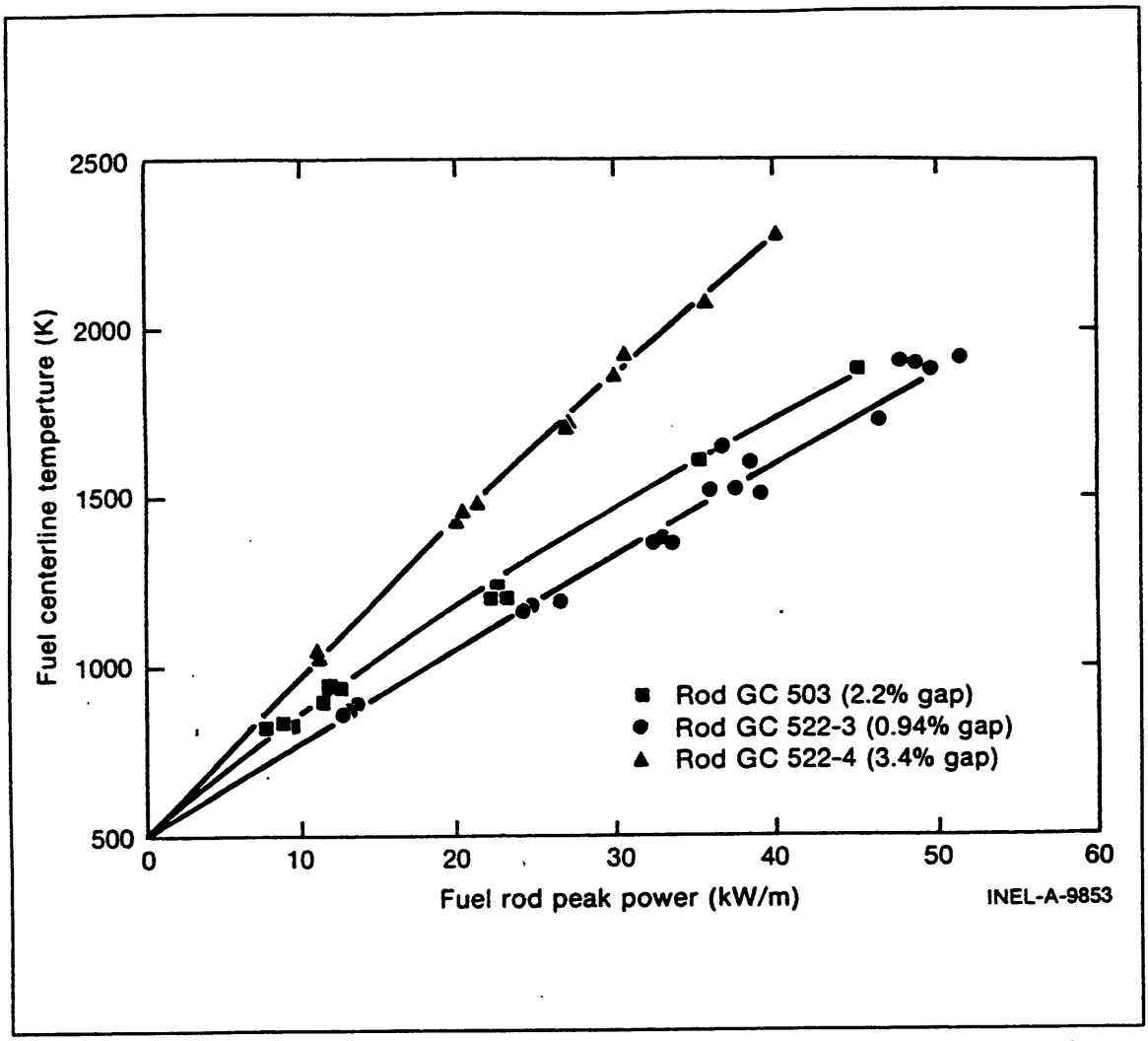

Figure L.3: Fuel centerline temperature measurements showing the effect of initial gap width in helium filled rods (from [G-5]).

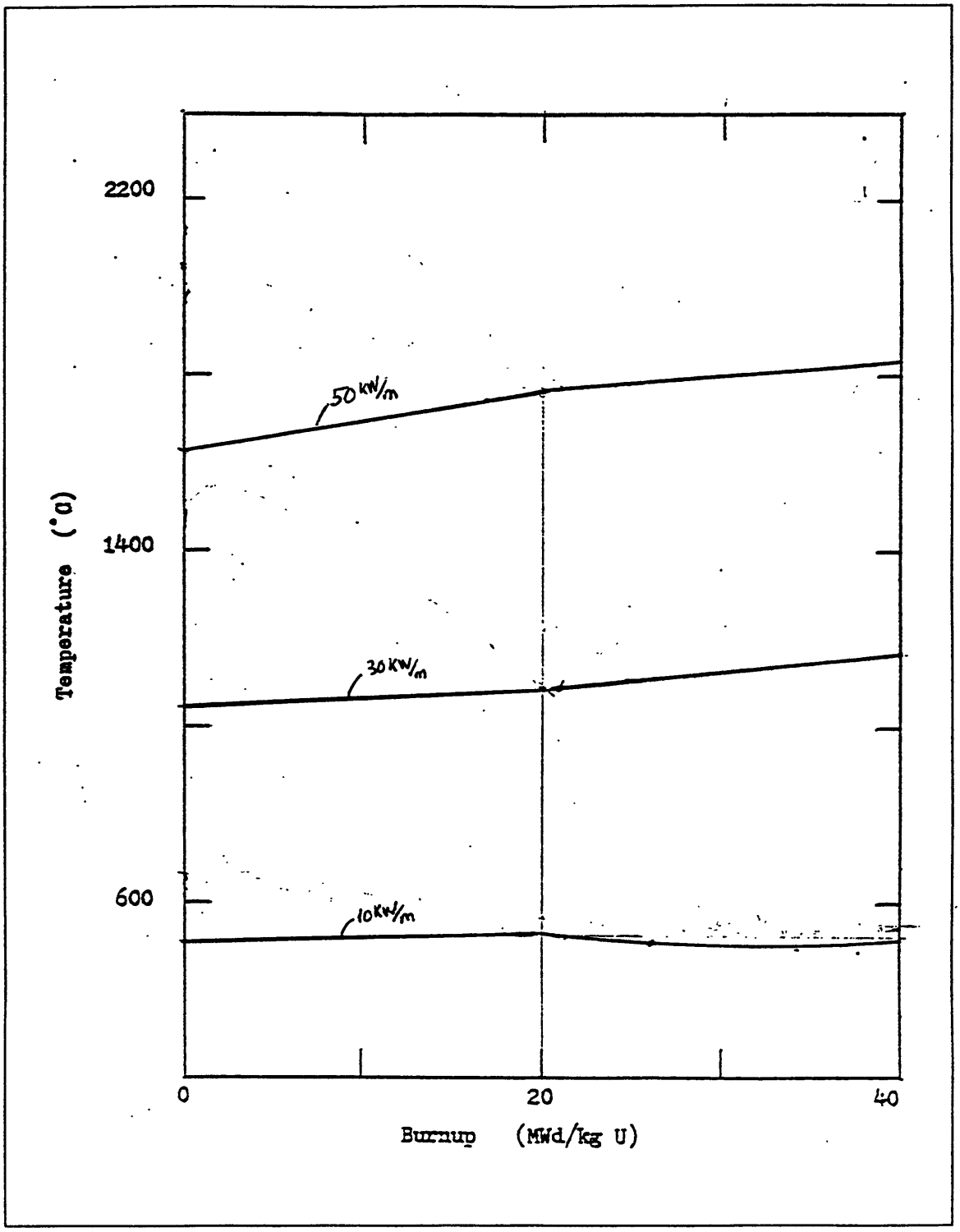

Figure L.4: Adjusted fuel centerline temperatures as a function of rod power and burnup